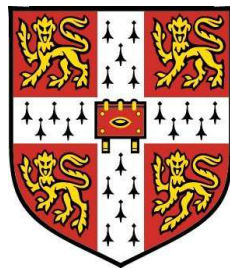


Modern PDE Techniques for Image Inpainting



Carola-Bibiane Schönlieb
Girton College
DAMTP, Centre for Mathematical Sciences
University of Cambridge

A thesis submitted for the degree of

Doctor of Philosophy

15th of June 2009

I would like to dedicate this thesis to my mother, who gave me the will to
be independent and always believed in me.

Declaration

This dissertation is the result of my own work and includes nothing which is the outcome of work done in collaboration except where specifically indicated in the text.

Carola-Bibiane Schönlieb

Acknowledgements

First I would like to thank my supervisor Peter A. Markowich for his support, his mentorship, his belief in me, and his friendship. Moreover, I owe thanks to my two co-supervisors, Martin Burger and Massimo Fornasier. They were always there for me, introduced me to interesting and challenging problems, and motivated me in my own creative thinking.

Further, I would like to thank all my collaborators, for numerous discussions, for our fruitful work together, and for all they have taught me (alphabetically ordered): Andrea Bertozzi, Julian Fernandez Bonder, Martin Burger, Shun-Yin Chu, Massimo Fornasier, Marzena Franek, Lin He, Andreas Langer, Peter A. Markowich and Julio D. Rossi.

Also, I would like to emphasize that I really enjoyed working alongside everyone in the Applied PDE (APDE) group of my supervisor. In particular, I would like to point out Marcus Wunsch, who welcomed me at the institute in Vienna and always believed in my academical excellence, Rada-Maria Weishäupl for preparing the way for other female PhD students in Peter's group to follow her, Alexander Lorz for his humanity and common love of dogs, Marie-Therese Wolfram for her friendship and her sympathy during the last six months of my PhD studies, and Clemens Fellner and Christof Sparber for playing the "older brothers" role. The other members of the APDE group (alphabetically ordered) - Gonca Aki, Paolo Antonelli, Marco DiFrancesco, Guillaume Dujardin, Norayr Matevosyan and Jan-Frederik Pietschmann - have also been very helpful, supportive, and reliable mates. Leaving this group now, I know that I will miss you all very much!

Moreover, I would like to thank the assistant of my supervisor, and very good friend of mine, Renate Feikes, for her honest and critical personality,

her caring and friendship (no matter on which part of the globe I was), and for her very efficient and reliable management of projects and paperwork.

There are also a couple of people outside of the APDE group, I owe thanks to. Practically, all the academic people in Vienna, Linz and Cambridge with whom I shared some time together. Among them, I especially would like to thank Carlota Cuesta and Vera Miljanovic, who showed me how women are able to make an excellent career, while still preserving their female qualities and their happiness, Helen Lei, who taught me that life barely stays between the lines, and Massimo Fornasier, for always believing in me and my qualities, for his coaching, his friendship, and his wonderful pasta al ragù. Many thanks as well to the whole Numerical Analysis group in Cambridge, in particular Tanya Shingel, with whom I shared the last steps of the PhD course, and Arieh Iserles for the warm and caring welcome he showed to our whole group when arriving at DAMTP.

During my research stays in Buenos Aires and Los Angeles, I received great hospitality. For someone who is used to a protected nest at home, it is not always easy to overcome one's inhibitions and leave for the unknown. I am glad I did it though, and I want to thank the following people for making these stays one of the most joyful times in my present life (in alphabetical order): Andrea Bertozzi, Julián Fernández Bonder, Lincoln Chayes, Irene Drelichman, Ricardo Durán, Dimitris Giannakis, Fredrik Johansson, Helen Lei, Sandra Martínez, Pierre Nolin, Jan-Frederik Pietschmann, Mariana Prieto, Jesus Rosado, Julio D. Rossi, Noemí Wolanski, Marie-Therese Wolfram and Marcus Wunsch.

For carefully proofreading parts of this thesis, I would like to thank (alphabetically ordered): Bertram Düring, Renate Feikes, Helen Lei and Marie-Therese Wolfram.

My whole family has been very supportive, especially my mother Karin Schönlieb. In my lows she encouraged me to look on the bright side of life and helped me to get up again. In my highs she was so proud of me and motivated me to keep it up. In addition, she made all my research

stays abroad possible by taking care of my beloved dog Eureka-Carissima von Salmannsdorf, short Reka. Mama, I love you very much! I also would like to thank a couple of important other people in my life in particular. My sister Charlotte Schönlieb for always keeping a place for me in her infinitely big heart. My nephew Manuel Michl for always viewing me as a mathematical genius. My best friend Isabella Wirth, who accompanied me from the beginnig of my mathematical studies, and always reminded me that there is something beyond work. My boyfriend and "father" of Reka, Herwig Rittsteiger, who always tried to give Reka additional love and care during my absence. My dear friend and breeder of Reka, Elfriede Wilfinger, who gave me a warm home in Vienna, and the best dog in the world. My current landlady Dorothea Heller, and her son Nicholas Heller, for making it possible for Reka and myself to be together in Cambridge, and for accepting me as a member of their family. And last but by no means least within this list, I thank Hannelore and Hans Liszt, Elisabeth Beranek, and Ingeborg Schön, for their company and support during the whole time since my birth. In the end, I would like to address Reka separately: Without her, my PhD time would have been half as much fun as it has been.

I also acknowledge the financial support provided by the following institutions and funds: the Wissenschaftskolleg (Graduiertenkolleg, Ph.D. program) of the Faculty for Mathematics at the University of Vienna (funded by the Austrian Science Fund FWF), the project WWTF Five senses-Call 2006, *Mathematical Methods for Image Analysis and Processing in the Visual Arts*, the FFG project no. 813610 *Erarbeitung neuer Algorithmen zum Image Inpainting*. Further, this publication is based on work supported by Award No. KUK-I1-007-43 , made by King Abdullah University of Science and Technology (KAUST). For the hospitality and the financial support during parts of the preparation of this work, I thank the Institute for Pure and Applied Mathematics (IPAM), UCLA. I also acknowledge the financial support of the US Office of Naval Research grant N000140810363, and the Department of Defense, National Science Foundation Grant ACI-0321917, during my visits to UCLA. Further the author would like to thank the UCLA

Mathematics Department, and Alan Van Nevel and Gary Hewer from the Naval Air Weapons Station in China Lake, CA for providing the road data in Section [5.2](#).

Abstract

Partial differential equations (PDEs) are expressions involving an unknown function in many independent variables and their partial derivatives up to a certain order (which is then called the order of the PDE). Since PDEs express continuous change, they have long been used to formulate a myriad of dynamical physical and biological phenomena: heat flow, optics, electrostatics and -dynamics, elasticity, fluid flow and much more. In this globalized and technologically advanced age, PDEs are also extensively used for modeling social situations (e.g., models for opinion formation) and tasks in engineering (like models for semiconductors, networks, and signal and image processing tasks). In my Ph.D. thesis I study nonlinear PDEs of higher-order appearing in image processing with specialization to inpainting (i.e., image interpolation). Digital image interpolation is an important challenge in our modern computerized society: From the reconstruction of crucial information in satellite images of our earth, restoration of CT- or PET images in molecular imaging to the renovation of digital photographs and ancient artwork, digital image interpolation is ubiquitous. Motivated by these applications, I investigate certain PDEs used for these tasks. I am concerned with the mathematical analysis and the efficient numerical solution of these equations as well as the concrete real world applications (like the restoration of ancient Viennese frescoes).

Keywords: Partial Differential Equations, Variational Calculus, Image Processing, Numerical Analysis.

Contents

Notation and Symbols	xi
1 Introduction	1
1.1 The Role of Image Processing in our Modern Society	3
1.2 What is a Digital Image?	4
1.3 Image Inpainting	5
1.3.1 Energy-Based and PDE Methods for Image Inpainting	7
1.3.2 Second- Versus Higher-Order Approaches	16
1.3.3 Numerical Solution of Higher-Order Inpainting Approaches . . .	19
2 Image Inpainting With Higher-Order Equations	24
2.1 Cahn-Hilliard Inpainting	24
2.1.1 Existence of a Stationary Solution	26
2.1.2 Numerical Results	37
2.1.3 Neumann Boundary Conditions and the Space $H_\partial^{-1}(\Omega)$	38
2.2 TV-H ⁻¹ Inpainting	41
2.2.1 Γ -Convergence of the Cahn-Hilliard Energy	46
2.2.2 Existence of a Stationary Solution	48
2.2.3 Characterization of Solutions	51
2.2.4 Error Estimation and Stability Analysis With the Bregman Distance	54
2.2.5 Numerical Results	58
2.3 Inpainting with LCIS	60
2.3.1 Numerical Results	61
2.4 The Inpainting Mechanisms of Transport and Diffusion - A Comparison	62

3 Analysis of Higher-Order Equations	70
3.1 Instabilities in the Cahn-Hilliard Equation	70
3.1.1 Asymptotic Behavior	77
3.1.2 Linear Stability / Instability	81
3.1.3 Nonlinear Stability / Instability	85
3.1.4 Consequences	92
3.2 Nonlocal Higher-Order Evolution Equations	93
3.2.1 Existence and Uniqueness	97
3.2.2 Asymptotic Behavior	98
3.2.3 Scaling the Kernel	103
4 Numerical Solution of Higher-Order Inpainting Approaches	104
4.1 Unconditionally Stable Solvers	105
4.1.1 The Convexity Splitting Idea	106
4.1.2 Cahn-Hilliard Inpainting	109
4.1.3 TV-H ⁻¹ Inpainting	120
4.1.4 LCIS Inpainting	128
4.1.5 Numerical Discussion	133
4.2 A Dual Solver for TV-H ⁻¹ Minimization	135
4.2.1 Introduction and Motivation	135
4.2.2 The Algorithm	140
4.2.3 Applications	150
4.3 Domain Decomposition for TV Minimization	153
4.3.1 Preliminary Assumptions	159
4.3.2 A Convex Variational Problem and Subspace Splitting	162
4.3.3 Local Minimization by Lagrange Multipliers	165
4.3.4 Convergence of the Sequential Alternating Subspace Minimization	174
4.3.5 A Parallel Alternating Subspace Minimization and its Convergence	180
4.3.6 Domain Decomposition for TV-L ² Minimization	182
4.3.7 Domain Decomposition for TV-H ⁻¹ Minimization	197

CONTENTS

5 Applications	202
5.1 Restoration of Medieval Frescoes	202
5.1.1 Neidhart Frescoes	203
5.1.2 Methods	204
5.2 Road Reconstruction	211
5.2.1 Bitwise Cahn-Hilliard Inpainting	212
6 Conclusion	214
A Mathematical Preliminaries	217
A.1 Distributional Derivatives	217
A.2 Subgradients and Subdifferentials	217
A.3 Functional Analysis	218
A.4 The Space H^{-1} and the Inverse Laplacian Δ^{-1}	218
A.5 Functions of Bounded Variation	219
References	241

Notation and Symbols

Function Spaces and Norms

For Ω an open and bounded subset of \mathbb{R}^d we define the following real-valued function spaces.

\mathbb{R}^d	The Euclidean space of dimension d with the Euclidean norm $ \cdot $.
\mathbb{R}_+	the non-negative real numbers.
$BV(\Omega)$	Space of functions of bounded variation with seminorm $ Df (\Omega)$, the total variation of f in Ω .
$BV - w^*$	The weak* topology of $BV(\Omega)$.
$C^m(\Omega)$	The space of functions on Ω , which are m -times continuously differentiable.
$L^p(\Omega)$	With $1 \leq p < \infty$: Space of Lebesgue measurable functions f such that $\int_{\Omega} f ^p dx < \infty$. The space $L^p(\Omega)$ is a Banach space with corresponding norm $\ f\ _{L^p(\Omega)} = (\int_{\Omega} f ^p dx)^{1/p}$. In the case $p = 2$ it is a Hilbert space with corresponding inner product $\langle f, g \rangle_{L^2(\Omega)} = \int_{\Omega} f \cdot g dx$.
$\langle \cdot, \cdot \rangle_2$	$:= \langle \cdot, \cdot \rangle_{L^2(\Omega)}$
$\ \cdot\ _2$	$:= \ \cdot\ _{L^2(\Omega)}$ for the norm in $L^2(\Omega)$
$L^\infty(\Omega)$	Space of Lebesgue measurable functions f such that there exists a constant C with $ f(x) \leq C$, a.e. $x \in \Omega$. The space $L^\infty(\Omega)$ is a Banach space with corresponding norm $\ f\ _{L^\infty(\Omega)} = \sup_{x \in \Omega} \{ f(x) \}$.
$L^p_{loc}(\Omega)$	$L^p_{loc}(\Omega) = \{f : \Omega \rightarrow \mathbb{R} : f \in L^p(D) \text{ for each } D \Subset \Omega\}$.
$W^{p,q}(\Omega)$	With $1 \leq p, q \leq \infty$: Sobolev space of functions $f \in L^q(\Omega)$ such that all derivatives up to order p belong to $L^q(\Omega)$. The space $W^{p,q}(\Omega)$ is a Banach space with norm $\ f\ _{W^{p,q}(\Omega)} = (\sum_{k=1}^p \int_{\Omega} D^k f ^q dx)^{1/q}$, where $D^k f$ denotes the k -th distributional derivative of f , cf. Appendix A.1
$W_0^{p,q}(\Omega)$	$\{f \in W^{p,q}(\Omega) : f _{\partial\Omega} = 0\}$.

$H^p(\Omega)$	$W^{p,2}(\Omega)$. This is a Hilbert space with corresponding inner product $\langle f, g \rangle_{H^p(\Omega)} = \sum_{k=1}^p \int_{\Omega} D^k f \cdot D^k g \, dx$. For this special Sobolev space we write $\ \cdot\ _{H^p(\Omega)} := \ \cdot\ _{W^{p,2}(\Omega)}$ for its corresponding norm.
$\ \cdot\ _1$	$:= \ \cdot\ _{H^1(\Omega)}$
$H_0^p(\Omega)$	$W_0^{p,2}(\Omega)$.
$H^{-1}(\Omega)$	$(H_0^1(\Omega))^*$, i.e., the dual space of $H_0^1(\Omega)$ with corresponding norm $\ \cdot\ _{H^{-1}(\Omega)} = \ \nabla \Delta^{-1} \cdot\ _2$ and inner product $\langle \cdot, \cdot \rangle_{H^{-1}(\Omega)} = \langle \nabla \Delta^{-1} \cdot, \nabla \Delta^{-1} \cdot \rangle_2$. Thereby Δ^{-1} is the inverse of the negative Laplacian $-\Delta$ with zero Dirichlet boundary conditions, cf. Appendix A.4.
$\ \cdot\ _{-1}$	$:= \ \cdot\ _{H^{-1}(\Omega)}$
$\langle \cdot, \cdot \rangle_{-1}$	$:= \langle \cdot, \cdot \rangle_{H^{-1}(\Omega)}$
$H_\partial^{-1}(\Omega)$	This is a nonstandard space, i.e., $H_\partial^{-1}(\Omega)$ is a subspace of the space $\{\psi \in H^1(\Omega) : \int_{\Omega} \psi \, dx = 0\}^*$. The norm and the inner product are defined as for $H^{-1}(\Omega)$ above, with the only difference, that Δ^{-1} is the inverse of the negative Laplacian $-\Delta$ with zero Neumann boundary conditions, cf. Section 2.1.3 for details.

For X a Banach space with a norm $\|\cdot\|_X$ and $v : (0, T) \rightarrow X$ we denote

$C^m(0, T; X)$	With $m \geq 0$, $0 < T < \infty$: Space of functions from $[0, T]$ to X , which are m -times continuously differentiable. It is a Banach space with the norm $\ v\ _{C^m(0, T; X)} = \max_{0 \leq l \leq m} \left(\sup_{0 \leq t \leq T} \left\ \frac{\partial^l v}{\partial t^l}(t) \right\ _X \right)$.
$L^p(0, T; X)$	With $1 \leq p < \infty$: Space of functions $v \rightarrow v(t)$ measurable on $(0, T)$ for the measure dt (i.e., the scalar functions $t \rightarrow \ v\ _X$ are dt -measurable). It is a Banach space with the norm $\ v\ _{L^p(0, T; X)} = \left(\int_0^T \ v\ _X^p \, dt \right)^{1/p} < +\infty$.

For a functional $\mathcal{J} : X \rightarrow (-\infty, +\infty]$ where X is a Banach space we write

$\operatorname{argmin} \{\mathcal{J}\}$	$:= \{u \in X : \mathcal{J}(u) = \inf_X \mathcal{J}\}$
l.s.c. (sequen- tially)	Lower semicontinuous: \mathcal{J} is called l.s.c. if for every sequence (u^n) converging to u we have $\liminf_{n \rightarrow \infty} \mathcal{J}(u^n) \geq \mathcal{J}(u)$.

About Functions

For a function $f : \Omega \subset \mathbb{R}^d \rightarrow \mathbb{R}$ and a sequence of functions $(f^n)_{n \in \mathbb{N}}$ belonging to a Banach space X we have

$f^n \rightarrow f$ in X	The sequence (f^n) converges strongly to f in X .
$f^n \rightharpoonup f$ in X	The sequence (f^n) converges weakly to f in X .
$f^n \xrightarrow{*} f$ in X	The sequence (f^n) converges to f in the weak* topology of X .
$\ f\ _X$	The norm of f in X ; for specific norm definitions compare the notations in “Function Spaces and Norms”.
$\text{supp } \{f\}$	For a measurable function $f : \Omega \subset \mathbb{R}^d \rightarrow \mathbb{R}$, let $(w_i)_{i \in I}$ be the family of all open subsets such that $w_i \subseteq \Omega$ and for each $i \in I$, $f = 0$ a.e. on w_i . Then supp (the support of f) is defined by $\text{supp } \{f\} = \Omega \setminus \bigcup_i w_i$.
Df	Distributional derivative of f , cf. Appendix A.1.
∇f	Gradient of f .
$\nabla \cdot f$	Divergence of f , i.e., $\nabla \cdot f = \sum_{i=1}^d \frac{\partial f}{\partial x_i}$.
Δf	Laplacian operator, i.e., $\Delta f = \sum_{i=1}^d \frac{\partial^2 f}{\partial x_i^2}$.
v_t	Time derivative of a function $v : (0, T) \rightarrow X$ for $t > 0$.
f_Ω	Mean value of f over Ω , i.e., $f_\Omega = \frac{1}{ \Omega } \int_\Omega f \, dx$.

Let \mathcal{H} be a real separable Hilbert space. For a function $\psi : \mathcal{H} \rightarrow \mathbb{R} \cup \{+\infty\}$ we write

$\psi^*(\cdot)$	The Legendre-Fenchel transform, i.e., convex conjugate $\psi^* : \mathcal{H}^* \rightarrow \mathbb{R} \cup \{+\infty\}$ is defined by $\psi^*(u) = \sup_{v \in \mathcal{H}} \{\langle v, u \rangle - \psi(v)\}$.
-----------------	---

Miscellaneous Notation

Let A, B and R be bounded and open sets in \mathbb{R}^d .

$\Omega \subset \mathbb{R}^d$	An open and bounded set with Lipschitz boundary.
$A \hookrightarrow B$	A is continuously embedded into B .
$A \hookrightarrow\hookleftarrow B$	A is compactly embedded into B .
$T \in \mathcal{L}(\mathcal{H})$	T is a bounded linear operator in a Hilbert space \mathcal{H} .
T^*	The adjoint operator of T in \mathcal{H} , i.e., $\langle T^*u, v \rangle = \langle u, Tv \rangle$, where $\langle \cdot, \cdot \rangle$ denotes the inner product in \mathcal{H} .
$\ T\ $	The operator norm of T .
$ \cdot $	Euclidean norm in \mathbb{R}^d .
V^*	The topological dual for a topological vector space V .
\mathcal{H}_d	d-dimensional Hausdorff measure.

$\text{sign}(s)$	Sign function, i.e., $\text{sign}(s) = \begin{cases} 1 & s > 0 \\ 0 & s = 0 \\ -1 & s < 0. \end{cases}$
χ_R	Characteristic function of a bounded and open set R , i.e., $\chi_R(x) = \begin{cases} 1 & x \in R \\ +\infty & \text{otherwise.} \end{cases}$
$\mathbf{1}_R$	Indicator function of a bounded and open set R , i.e., $\mathbf{1}_R(x) = \begin{cases} 1 & x \in R \\ 0 & \text{otherwise.} \end{cases}$

Where needed, notations and definitions might be extended in the introductory part of a new chapter or section.

Chapter 1

Introduction

My Ph.D. thesis is concerned with modern techniques which use partial differential equations (PDEs) for image processing. I am especially interested in the analysis and numerical solution of higher-order flows such as the Cahn-Hilliard equation, and singular flows such as total variation minimizations, appearing in image inpainting (interpolation) tasks as well as concrete real world applications.

Now, inpainting is an artistic word for virtual image restoration or image interpolation, whereby missing parts of damaged images are filled in, based on the information obtained from the surrounding areas. Virtual image restoration is an important challenge in our modern computerized society: From the reconstruction of crucial information in satellite images of our earth to the renovation of digital photographs and ancient artwork, virtual image restoration is ubiquitous.

Inpainting methods based on higher-order flows, i.e., PDEs of third-or fourth differential order, stirred growing interest in the image processing community in recent years. This is because of the high-quality visual results produced by these methods, which are superior to the ones produced via second-order PDEs. Current research in this area mainly concentrates on three issues.

The first one, being the development of simple but effective higher-order inpainting models, is also the first big topic of this thesis. Therein I aim to replace curvature driven models, like Euler's elastica inpainting, by higher-order, diffusion-like models such as Cahn-Hilliard- and $\text{TV}-\text{H}^{-1}$ inpainting. The diffusion-like inpainting approaches have the advantage that their numerical solution is in general easier and faster, while preserving the good visual results produced by the curvature driven approaches.

The second issue is a derivation of rigorous analytic properties and geometric interpretation of these equations. This is a challenging task in its own right, since higher-order equations are very new and little is known about them. Often higher-order equations do not possess a maximum or comparison principle, hence their analysis, like proofs of existence, uniqueness and convergence of solutions to these equations, is very involved and has not been established yet for all cases. A large part of my thesis provides answers to some of these open questions. In particular I shall present results for the Cahn-Hilliard equation, for a fourth-order total variation flow, and for a nonlocal higher-order diffusion equation.

The third issue is the effective and fast numerical solution of inpainting approaches, and constitutes the third main topic of this work. Although higher-order inpainting approaches produce very good visual results, in general they suffer from high computational complexity. This means that the computational effort for producing an inpainted image from one of these methods can be big. This high complexity makes such inpainting approaches less attractive for interactive image manipulation and thus less popular in real-world applications. Hence the focus is on the development of fast and efficient numerical algorithms for their solution.

Finally, I am also interested in applications of these inpainting methods in real life. A particular example for this is the recently found Neidhart frescoes in Vienna: Advanced mathematical inpainting tools can restorate the frescoes digitally. The virtually restored frescoes then serve as a virtual template for museums artists who work on the physical restoration of the frescoes. Another real world application is the restoration of satellite images of roads in urban areas in the United States: Here the problem is that the roads are partly covered by trees or buildings and the goal is to remove these obstacles and receive a picture of just the road. For this task PDEs turned out to be the method of choice, not only due to the high quality visual results but also due to the fact that this enables automated restoration of whole databases of roads. In other words, combined with *a-priori* segmentation algorithms for the trees (providing an initial condition), PDEs inpaint the road images unsupervised, i.e., no user action is required.

In the present chapter, in Section 1.1, I start the discussion with some general remarks about the importance of digital image processing methods. Section 1.2 shall explain the term *digital image* for a general audience. Then in Section 1.3 the task

1.1 The Role of Image Processing in our Modern Society

of image inpainting is explained in more detail and an overview of existing work in this area is given, in particular in the range of PDE- and energy-based approaches in Section 1.3.1. Further the use of third- and fourth-order partial differential equations instead of second-order flows in image inpainting is motivated in Section 1.3.2, and an overview of existing numerical methods for higher-order inpainting approaches is given in Section 1.3.3.

1.1 The Role of Image Processing in our Modern Society

In our modern society we encounter digital images in a lot of different situations: from everyday life, where analogue cameras have long been replaced by digital ones, to their professional use in medicine, earth sciences, arts, and security applications. The images produced in these situations usually have to be organized and possibly postprocessed. The organization and processing of digital images is known under the name of image processing or computer vision.

We often have to deal with the processing of images, e.g., the restoration of images corrupted by noise, blur, or intentional scratching. The idea behind image processing is to provide methods that improve the quality of these images by postprocessing them. Examples of damaged images come from medical imaging tools such as brain imaging with MRI (Magnetic Resonance Imaging), PET (Positron Emission Tomography) imaging of inner organs like the human heart, and X-ray imaging of our skeleton. These imaging tools usually produce noisy or incomplete image data. Other examples include satellite images of our earth, which are often blurred. Further, digital image restoration is used in art preservation and restoration, where digital photographs are taken from ancient artwork and are digitally restorated and stored. As such they can serve as templates for restorators and can be kept in a databank for preservation. In sum, digital image restoration provides effective tools to recover or complete lost image information. Keywords in this context are image denoising, image deblurring, image decomposition, image inpainting, and image synthesizing.

Another branch of image processing is object recognition and tracking. In these applications one is interested in certain objects in an image that one wants to extract and/or follow, e.g., in a video stream. Keywords here are image segmentation, object recognition, object tracking, and remote sensing.

Finally, there is also the important issue of organizing image data in an efficient way. To do so we have to think about the classification of images, e.g., depending on their contents, and an optimal way of storing them in terms of minimizing the storage place.

For a more complete introduction to digital image processing we refer to [AK06].

Considering this huge – but by no means complete – amount of image processing applications listed above and the fact that there are still problems in this area which have not been completely and satisfactorily solved, it is not surprising that this is a very active and broad field of research. From engineers to computer scientists and mathematicians, a large group of people have been and are still working in this area. In the following we focus on the first branch of applications, namely image restoration and in particular on so-called image inpainting techniques, cf. Section 1.3.

1.2 What is a Digital Image?

In order to appreciate the following theory and the image inpainting applications, we first need to understand what a digital image really is. Roughly speaking a digital image is obtained from an analogue image (representing the continuous world) by sampling and quantization. Basically this means that the digital camera superimposes a regular grid on an analogue image and assigns a value, e.g., the mean brightness in this field, to each grid element, cf. [AK06]. In the terminology of digital images these grid elements are called pixels. The image content is then described by grayvalues or colour values prescribed in each pixel. The grayvalues are scalar values ranging between 0 (black) and 255 (white). The colour values are vector values, e.g., (r, g, b) , where each channel r, g and b represents the red, green, and blue component of the colour and ranges, as the grayvalues, from 0 to 255. The mathematical representation of a digital image is a so-called image function u defined on a two dimensional (in general rectangular) image domain, the grid. This function is either scalar valued in the case of a grayvalue image, or vector valued in the case of a colour image. Here the function value $u(x, y)$ denotes the grayvalue, i.e., colourvalue, of the image in the pixel (x, y) of the image domain. Figure 1.1 visualizes the connection between the digital image and its image function for the case of a grayvalue image.

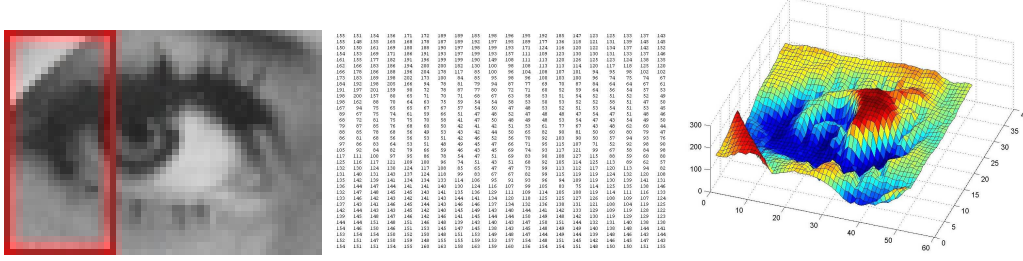


Figure 1.1: Digital image versus image function: On the very left a zoom into a digital photograph where the image pixels (small squares) are clearly visible is shown; in the middle the grayvalues of the red selection in the digital photograph are displayed in matrix form; on the very right the image function of the digital photograph is shown where the grayvalue $u(x, y)$ is plotted as the height over the x, y -plane.

Typical sizes of digital images range from 2000×2000 pixels in images taken with a simple digital camera, to 10000×10000 pixels in images taken with high-resolution cameras used by professional photographers. The size of images in medical imaging applications depends on the task at hand. PET for example produces three dimensional image data, where a full-length body scan has a typical size of $175 \times 175 \times 500$ pixels.

Now, since the image function is a mathematical object we can treat it as such and apply mathematical operations to it. These mathematical operations are summarized by the term *image processing techniques*, and range from statistical methods, morphological operations, to solving a partial differential equation for the image function, cf. Section 1.1. We are especially interested in the last, i.e., PDE- and variational methods used in imaging and in image inpainting in particular.

1.3 Image Inpainting

An important task in image processing is the process of filling in missing parts of damaged images based on the information obtained from the surrounding areas. It is essentially a type of interpolation and is called inpainting.

Let f represent some given image defined on an image domain Ω . Loosely speaking, the problem is to reconstruct the original image u in the (damaged) domain $D \subset \Omega$, called inpainting domain or a hole/gap (cf. Figure 1.2).

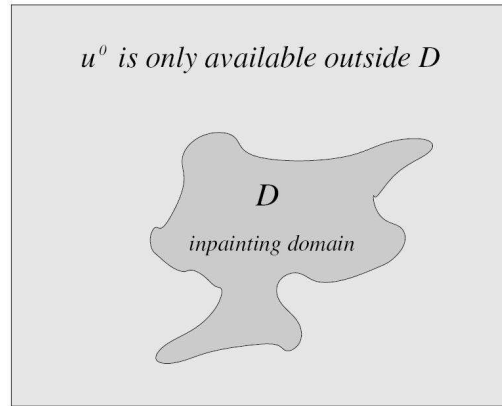


Figure 1.2: The inpainting task. Figure from [CS05]

The term *inpainting* was invented by art restoration workers, cf. [Em76, Wa85], and first appeared in the framework of digital restoration in the work of Bertalmio et al. [BSCB00]. Therein the authors design a discrete partial differential equation, which intends to imitate the restoration work of museum artists. Their method shall be explained in more detail in the subsequent section.

Applications

Applications of digital image inpainting are automatic scratch removal in old photographs and films [BSCB00, CS01a, KMFR95b], digital restoration of ancient paintings for conservation purposes [BFMS08], text erasing, like the removal of dates, subtitles, or publicity from a photograph [BSCB00, BBCSV01, CS01a, CS01c], special effects like object disappearance [BSCB00, CS01c], disocclusion [NMS93, MM98], spatial/temporal zooming and super-resolution [BBCSV01, CS01a, Ma00, MG01, TYW01], error concealment [WZ98], lossy perceptual image coding [CS01a], removal of the laser dazzling effect [CCB03], and sinogram inpainting in X-ray imaging [GZYXC06], only to name a few.

The beginnings of digital image inpainting

The history of digital image inpainting has its beginning in the works of engineers and computer scientists. Their methods were based on statistical and algorithmic

approaches in the context of image interpolation [AKR97, KMFR95a, KMFR95b], image replacement [IP97, WL00], error concealment [JCL94, KS93], and image coding [Ca96, FL96, RF95]. In [KMFR95b], for example, the authors present a method for video restoration. Their algorithm uses intact information from earlier and later frames to restore the current one and is therefore not applicable to still images. In interpolation approaches for “perceptually motivated” image coding [Ca96, FL96, RF95] the underlying image model is based on the concept of “raw primal sketch” [Ma82]. More precisely this method assumes that the image consists of mainly homogeneous regions, separated by discontinuities, i.e., edges. The coded information then just consists of the geometric structure of the discontinuities and the amplitudes at the edges. Some of these coding techniques already used PDEs for this task, see e.g., [Ca88, Ca96, CT94].

Initiated by the pioneering works of [NMS93, MM98, CMS98, BSCB00], and [CS01a] also the mathematics community got involved in image restoration, using partial differential equations and variational methods for this task. Their approach and some of their methods shall be presented in the following section.

1.3.1 Energy-Based and PDE Methods for Image Inpainting

In this section I present the general energy-based, and PDE approach used in image inpainting. After a derivation of both methods in the context of inverse problems and prior image models, I give an overview of the most important contributions within this area. To keep to chronological order, I start with the energy-based approach, also called variational approach, or image prior model.

Energy-based methods

Energy-based methods can be best explained from the point of view of inverse problems. In a wide range of image processing tasks one encounters the situation that the observed image f is corrupted, e.g., by noise or blur. The goal is to recover the original image u from the observed datum f . In mathematical terms this means that one has to solve an inverse problem $Tu = f$, where T models the process through which the image u went before observation. In the case of an operator T with unbounded inverse, this problem is ill-posed. In such cases one modifies the problem by introducing some additional *a-priori* information on u , usually in terms of a regularizing term involving, e.g., the total variation of u . This results in a minimization problem for the fidelity $Tu - f$ plus

the *a-priori* information modeled by the regularizing term $R(u)$. In the terminology of prior image models, the regularizing term is the so-called prior image model, and the fidelity term is the data model. The concept of image prior models has been introduced by Mumford, cf. [Mu94]. For a general overview on this topic see also [AK06].

Inpainting approaches can also be formulated within this framework. More precisely let $\Omega \subset \mathbb{R}^2$ be an open and bounded domain with Lipschitz boundary, and let B_1, B_2 be two Banach spaces with $B_2 \subseteq B_1$, $f \in B_1$ denoting the given image, and $D \subset \Omega$ the missing domain. A general variational approach in image inpainting is formulated mathematically as a minimization problem for a regularized cost functional $\mathcal{J} : B_2 \rightarrow \mathbb{R}$,

$$\mathcal{J}(u) = R(u) + \frac{1}{2} \|\lambda(f - u)\|_{B_1}^2 \rightarrow \min_{u \in B_2}, \quad (1.1)$$

where $R : B_2 \rightarrow \mathbb{R}$ and

$$\lambda(x) = \begin{cases} \lambda_0 & \Omega \setminus D \\ 0 & D, \end{cases} \quad (1.2)$$

is the indicator function of $\Omega \setminus D$ multiplied by a constant $\lambda_0 \gg 1$. This constant is the tuning parameter of the approach. As before $R(u)$ denotes the regularizing term and represents a certain *a-priori* information from the image u , i.e., it determines in which space the restored image lies in. In the context of image inpainting, i.e., in the setting of (1.1)-(1.2), it plays the main role of filling in the image content into the missing domain D , e.g., by diffusion and/or transport. The fidelity term $\|\lambda(f - u)\|_{B_1}^2$ of the inpainting approach forces the minimizer u to stay close to the given image f outside of the inpainting domain (how close is dependent on the size of λ_0). In this case the operator T from the general approach equals the indicator function of $\Omega \setminus D$. In general we have $B_2 \subset B_1$, which signifies the smoothing effect of the regularizing term on the minimizer $u \in B_2(\Omega)$.

Note that the variational approach (1.1)-(1.2) acts on the whole image domain Ω (global inpainting model), instead of posing the problem on the missing domain D only. This has the advantage of simultaneous noise removal in the whole image and makes the approach independent of the number and shape of the holes in the image. In this global model the boundary condition for D is superimposed by the fidelity term.

Before the development of inpainting algorithms one has to understand what an image really is. In the framework of image prior models this knowledge is encoded in the regularizing term $R(u)$. As a consequence different image prior models result in different

inpainting methods. As pointed out in [CS01a], the challenge of inpainting lies in the fact that image functions are complex and mostly lie outside of usual Sobolev spaces. Natural images for example are modeled by Mumford as distributions, cf. [Mu94]. Texture images contain oscillations and are modeled by Markov random fields, see e.g., [GG84, Br98], or by functions in negative Sobolev spaces, see e.g., [OSV03, LV08]. Most nontexture images are modeled in the space of functions of bounded variation ([ROF92, CL97]), and in the Mumford-Shah object-boundary model, cf. [MS89].

Note also that despite its similarity to usual image enhancement methods such as denoising or deblurring, inpainting is very different from these approaches. This is because the missing regions are usually large, i.e., larger than the type of noise treated by common image enhancement algorithms. Additionally, in image enhancement the pixels contain both noise and original image information whereas in inpainting there is no significant information inside the missing domain. Hence reasonable energy-based approaches in denoising do not necessarily make sense for inpainting. An example for this discrepancy between inpainting approaches and existing image enhancement methods is given in the work of Chan and Shen [CS05]. Therein the authors pointed out that the extension of existing texture modeling approaches in denoising, deblurring and decomposition to inpainting, is not straightforward. In fact the authors showed that the Meyer model [Me01] modified for inpainting, where the fidelity term modeled in Meyer's norm only acts outside of the missing domain, is not able to reconstruct interesting texture information inside of the gap: For every minimizer pair (u, g) (where g represents the texture in the image) of the modified Meyer model, it follows that g is identically zero inside the gap D .

PDE methods

To segue into the PDE-based approach for image inpainting, we first go back to the general variational model in (1.1)-(1.2). Under certain regularity assumptions on a minimizer u of the functional \mathcal{J} , the minimizer fulfills a so-called optimality condition on (1.1), i.e., the corresponding Euler-Lagrange equation. In other words, for a minimizer u the first variation, i.e., the Fréchet derivative of \mathcal{J} , has to be zero. In the case $B_1 = L^2(\Omega)$, in mathematical terms this reads

$$-\nabla R(u) + \lambda(f - u) = 0 \quad \text{in } \Omega, \tag{1.3}$$

which is a partial differential equation with certain boundary conditions on $\partial\Omega$. Here ∇R denotes the Fréchet derivative of R over $B_1 = L^2(\Omega)$, or more general an element from the subdifferential of $R(u)$. The dynamic version of (1.3) is the so-called steepest-descent or gradient flow approach. More precisely, a minimizer u of (1.1) is embedded in an evolution process. We denote it by $u(\cdot, t)$. At time $t = 0$, $u(\cdot, t = 0) = f \in B_1$ is the original image. It is then transformed through a process that is characterized by

$$u_t = -\nabla R(u) + \lambda(f - u) \quad \text{in } \Omega. \quad (1.4)$$

Given a variational formulation (1.1)-(1.2), the steepest-descent approach is used to numerically compute a minimizer of \mathcal{J} , whereby (1.4) is iteratively solved until one is close enough to a minimizer of \mathcal{J} .

In other situations we will encounter equations that do not come from variational principles, such as CDD inpainting [CS01c], Cahn-Hilliard-, and TV-H⁻¹inpainting in Section 2.1 and 2.2. Then the inpainting approach is directly given as an evolutionary PDE, i.e.,

$$u_t = F(x, u, Du, D^2u, \dots) + \lambda(f - u), \quad (1.5)$$

where $F : \Omega \times \mathbb{R} \times \mathbb{R}^2 \times \mathbb{R}^4 \times \dots \rightarrow \mathbb{R}$, and belongs to the class of PDE-based inpainting approaches.

State of the art

Depending on the choice of the regularizing term R and the Banach spaces B_1, B_2 , i.e., the flow $F(x, u, Du, \dots)$, various inpainting approaches have been developed. These methods can be divided into two categories: texture inpainting that is mainly based on synthesizing the texture and filling it in, and nontexture (or geometric/structure) inpainting that concentrates on the recovery of the geometric part of the image inside the missing domain. In the following we shall only concentrate on nontexture images. In fact the usual variational/PDE approach in inpainting uses local PDEs (in contrast to nonlocal PDEs cf. Section 3.2), which smooth out every statistical fluctuation, i.e., do not see a global pattern such as texture in an image. In [CS01a] the authors call this kind of image restoration low-level inpainting since it does not take into account global features, like patterns and textures. For now, let us start with the presentation of existing nontexture inpainting models.

Pioneering works The terminology of digital inpainting first appeared in the work of Bertalmio et al. [BSCB00]. Their model is based on observations about the work of museum artists, who restorate old paintings. Their approach follows the principle of prolongating the image intensity in the direction of the level lines (sets of image points with constant grayvalue) arriving at the hole. This results in solving a discrete approximation of the PDE

$$u_t = \nabla^\perp u \cdot \nabla \Delta u, \quad (1.6)$$

solved within the hole D extended by a small strip around its boundary. This extension of the computational domain about the strip serves as the intact source of the image. It is implemented in order to fetch the image intensity and the direction of the level lines which are to be continued. Equation (1.6) is a transport equation for the image smoothness modeled by Δu along the level lines of the image. Here $\nabla^\perp u$ is the perpendicular gradient of the image function u , i.e., it is equal to $(-u_y, u_x)$. To avoid the crossing of level lines, the authors additionally apply intermediate steps of anisotropic diffusion, which may result in the solution of a PDE like

$$u_t = \nabla^\perp u \cdot \nabla \Delta u + \nu \nabla \cdot (g(|\nabla u|) \nabla u),$$

where $g(s)$ defines the diffusivity coefficient and $\nu > 0$ a small parameter. In [BBS01] the authors interpret a solution of the latter equation as a direct solution of the Navier-Stokes equation for an incompressible fluid, where the image intensity function plays the role of the stream function whose level lines define the stream lines of the flow. Note that the advantage of this viewpoint is that one can exploit a rich and well-developed history of fluid problems, both analytically and numerically. Also note that Bertalmio et al.'s model actually is a third-order nonlinear partial differential equation. In the next section we shall see why higher-order PDEs are needed to solve the inpainting task satisfactorily.

In a subsequent work of Ballester et al. [BBCSV01] the authors adapt the ideas of [BSCB00] about the simultaneous graylevel- and gradient-continuation to define a formal variational approach to the inpainting problem. Their variational approach is solved via its steepest descent, which leads to a set of two coupled second-order PDEs, one for the graylevels and one for the gradient orientations.

An axiomatic approach and elastica curves Chronologically earlier Caselles, Morel and Sbert in [CMS98] and Masnou and Morel in [MM98] initiated the variational/PDE approach for image interpolation. In [CMS98] the authors show that any operator that interpolates continuous data given on a set of curves can be computed as a viscosity solution (cf. [Ev98]) of a degenerate elliptic PDE. This equation is derived via an axiomatic approach, in which the basic interpolation model, i.e., the PDE, results from a series of assumptions about the image function and the interpolation process. We note that this inpainting approach is only able to continue smooth image contents and cannot be used for the continuation of edges.

The approach of Masnou and Morel [MM98] belongs to the class of variational approaches and is based on Nitzberg et al.'s work on segmentation [NMS93]. In [NMS93] Nitzberg et al. presented a variational technique for removing occlusions of objects with the goal of image segmentation. Therein the basic idea is to connect T-junctions at the occluding boundaries of objects with Euler elastica minimizing curves. A curve is said to be Eulers elastica if it is the equilibrium curve of the Euler elastica energy

$$E(\gamma) = \int_{\gamma} (a + b\kappa^2) ds,$$

where ds denotes the arc length element, $\kappa(s)$ the scalar curvature, and a, b two positive constants. These curves have been originally obtained by Euler in 1744, cf. [Lo27], and were first introduced in computer vision by Mumford in [Mu94]. The basic principle of the elastica curves approach is to prolongate edges by minimizing their length and curvature, In [Mu94, NMS93] it is based on *a-priori* edge detection. Hence, this approach is only applicable to highly segmented images with few T-junctions and is not applicable to natural images. Moreover, edges alone are not reliable information since they are sensitive to noise. In [MM98] Masnou and Morel extend Mumford's idea of length and curvature minimization from edges to all the level lines of the image function. Their approach is based on the global minimization of a discrete version of a constrained Euler elastica energy for all level lines. This level line approach has the additional advantage that it is contrast invariant; this is different from the edge-approach of Nitzberg et al. [NMS93] which depends on the difference of grayvalues. The discrete version of the Euler elastica energy is connected to the human vision approach of Gestalt theory, in particular Kanizsa's amodal completion theory [Ka96]. Gestalt theory tries to explain how the human visual system understands partially occluded objects. This gave the

approach in [MM98] its name disocclusion instead of image inpainting. Details of the theoretical justification of the model in [MM98] and the algorithm itself were much later published by Masnou [Ma02]. Note that the Euler elastica energy was used for inpainting later by Chan and Shen in a functionalized form, cf. [CKS02] and later remarks within this section.

Anisotropic diffusion: total variation inpainting and CDD Another variational inpainting approach constitutes the work of Chan and Shen in [CS01a]. Their approach is chronologically in between the two works of Bertalmio et al. i.e., [BSCB00, BBCSV01]. The motivation was to create a scheme which is motivated by existing denoising/segmentation methods and is mathematically easier to understand and to analyze. Their approach is based on the most famous model in image processing, the total variation (TV) model, where $R(u) = |Du|(\Omega) \approx \int_{\Omega} |\nabla u| dx$ denotes the total variation of u , $B_1 = L^2(\Omega)$ and $B_2 = BV(\Omega)$ the space of functions of bounded variation, cf. also [CS01d, CS01a, RO94, ROF92]. It results in the action of anisotropic diffusion inside the inpainting domain, which preserves edges and diffuses homogeneous regions and small oscillations like noise. More precisely the corresponding steepest descent equation reads

$$u_t = \nabla \cdot \left(\frac{\nabla u}{|\nabla u|} \right) + \lambda(f - u).$$

The disadvantage of the total variation approach in inpainting is that the level lines are interpolated linearly, cf. Section 1.3.2. This means that the direction of the level lines is not preserved, since they are connected by a straight line across the missing domain. A straight line connection might still be pleasant for small holes, but very unpleasant in the presence of larger gaps, even for simple images. Another consequence of the linear interpolation is that level lines might not be connected across large distances, cf. Section 1.3.2. A solution for this is the use of higher-order PDEs such as the first works of Bertalmio et al. [BSCB00], Ballester et al. [BBCSV01], and the elastica approach of Masnou and Morel [MM98], and also some PDE/variational approaches proposed later on.

Within this context, the authors in [CS01c] proposed a new TV-based inpainting method. In their model the conductivity coefficient of the anisotropic diffusion depends on the curvature of level lines and it is possible to connect the level lines across large

distances. This new approach is a third-order diffusion equation and is called inpainting with Curvature Driven Diffusions (CDD). The CDD equation reads

$$u_t = \nabla \cdot \left(\frac{g(\kappa)}{|\nabla u|} \nabla u \right) + \lambda(f - u),$$

where $g : B \rightarrow [0, +\infty)$ is a continuous function, which penalizes large curvatures, and encourages diffusion when the curvature is small. Here B is an admissible class of functions for which the curvature κ is well defined, e.g., $B = C^2(\Omega)$. It is of similar type as other diffusion driven models in imaging such as the Perona-Malik equation [PM90, MS95], and like the latter does not (in general) follow a variational principle. To give a more precise motivation for the CDD inpainting model, let us recall that a problem of the usual total variation model is that the diffusion strength only depends on the contrast or strength of the level lines. In other words the anisotropic diffusion of the total variation model diffuses with conductivity coefficient $1/|\nabla u|$. Hence the diffusion strength does not depend on geometric properties of the level line, given by its curvature. In the CDD model the conductivity coefficient is therefore changed to $g(|\kappa|)/|\nabla u|$, where g annihilates large curvatures and stabilizes small ones. Interestingly enough CDD performs completely orthogonally to the transport equation of Bertalmio et al. [BSCB00]. Bertalmio et al.'s equation transports the smoothness along the level lines, whereas the CDD equation diffuses image pixel information perpendicularly to the level lines.

Euler's elastica inpainting This observation gave Chan, Kang, and Shen the idea to combine both methods, which resulted in the Euler's elastica inpainting model, cf. [CKS02, CS01b]. Their approach is based on the earlier work of Masnou and Morel [MM98], with the difference that the new approach poses a functionalized model. This means that instead of an elastica curve model for the level lines of the image, they rewrote the elastica energy in terms of the image function u . Then the regularizing term reads $R(u) = \int_{\Omega} (a + b(\nabla \cdot (\frac{\nabla u}{|\nabla u|}))^2)|\nabla u| dx$ with positive weights a and b , $B_1 = L^2(\Omega)$, and $B_2 = BV(\Omega)$. In fact in [CKS02] the authors verified that the Euler elastica inpainting model combines both transportation processes [BSCB00] and [CS01c]. They also presented a very useful geometric interpretation for all three models. We shall discuss this issue in a little more detail in Section 2.4, where I compare this geometric

interpretation with the newly proposed higher-order inpainting schemes from Section 2.1-2.3.

Active contour models Other examples to be mentioned for (1.1) are the active contour model based on Mumford and Shah’s segmentation [MS89, CS01a, TYW01, ES02], and its high-order correction the Mumford-Shah-Euler image model [ES02]. The latter improves the former by replacing the straight-line curve model by the elastica energy. The Mumford and Shah image model reads

$$R(u, \Gamma) = \frac{\gamma}{2} \int_{\Omega \setminus \Gamma} |\nabla u|^2 dx + \alpha \mathcal{H}_1(\Gamma), \quad (1.7)$$

where Γ denotes the edge collection and \mathcal{H}_1 the one dimensional Hausdorff measure (generalization of the length for regular curves). The corresponding inpainting approach minimizes the Mumford Shah image model plus the usual L^2 fidelity on $\Omega \setminus D$. The idea to consider this model for inpainting goes back to Chan and Shen [CS01a] as an alternative to TV inpainting, and to Tsai et al. [TYW01]. The Mumford-Shah-Euler image model differs from (1.7) in the replacement of the straight line model by Euler’s elastica curve model

$$R(u, \Gamma) = \frac{\gamma}{2} \int_{\Omega \setminus \Gamma} |\nabla u|^2 dx + \int_{\Gamma} (a + b\kappa^2) ds,$$

where κ denotes the curvature of a level line inside the edge collection Γ , and a and b are positive constants as before.

...and more More recently Bertozzi, Esedoglu, and Gillette [BEG07a, BEG07b] proposed a modified Cahn-Hilliard equation for the inpainting of binary images (also cf. Section 2.1), and in a separate work Grossauer and Scherzer [GS03] proposed a model based on the complex Ginzburg-Landau energy. A generalization of Cahn-Hilliard inpainting for grayvalue images, called TV-H⁻¹inpainting was proposed in [BHS08], also cf. Section 2.2.

To finish this overview let us just list some more inpainting approaches in the literature: total variation wavelet inpainting [CSZ06], fast image inpainting based on coherence transport [BM07], landmark based inpainting [KCS02], inpainting via correspondence map [DSC03], texture inpainting with nonlocal PDEs [GO07], simultaneous

structure and texture inpainting [BVSO03], cartoon and texture inpainting via morphological component analysis [ESQD05]. For a very good introduction to image inpainting I also refer to [CS05].

The scope of the present work are inpainting methods, which use third- and fourth-order PDEs to fill in missing image contents into gaps in the image domain. In the following section I shall, once again, motivate the choice of higher-order flows for image inpainting.

1.3.2 Second- Versus Higher-Order Approaches

In this section I want to emphasize the difference between second- and higher-order models in inpainting. Now, second-order variational inpainting methods (where the order of the method is determined by the derivatives of highest order in the corresponding Euler-Lagrange equation), like TV inpainting, have drawbacks when it comes to the connection of edges over large distances (*Connectivity Principle*, cf. Figure 1.3) and the smooth propagation of level lines into the damaged domain (*Curvature Preservation*, cf. Figure 1.4). This is due to the penalization of the length of the level lines within the minimizing process with a second-order regularizer, thus connecting level lines from the boundary of the inpainting domain via the shortest distance (linear interpolation). The regularizing term $R(u) \approx \int_{\Omega} |\nabla u| dx$ in the TV inpainting approach for example can be interpreted via the coarea formula which gives

$$\min_u \int_{\Omega} |\nabla u| dx \iff \min_{\Gamma_\lambda} \int_{-\infty}^{\infty} \text{length}(\Gamma_\lambda) d\lambda,$$

where $\Gamma_\lambda = \{x \in \Omega : u(x) = \lambda\}$ is the level line for the grayvalue λ . If we consider on the other hand the regularizing term in the Euler elastica inpainting approach the coarea formula reads

$$\begin{aligned} & \min_u \int_{\Omega} \left(a + b \left(\nabla \cdot \left(\frac{\nabla u}{|\nabla u|} \right) \right)^2 \right) |\nabla u| dx \\ & \iff \min_{\Gamma_\lambda} \int_{-\infty}^{\infty} a \text{length}(\Gamma_\lambda) + b \text{curvature}^2(\Gamma_\lambda) d\lambda. \end{aligned} \tag{1.8}$$

Hence, not only the length of the level lines but also their curvature is penalized (the penalization of each depends on the ratio b/a). This results in a smooth continuation of level lines over the inpainting domain also over large distances, compare Figure 1.3 and 1.4.

The performance of higher-order inpainting methods, such as Euler elastica inpainting, can also be interpreted via the second boundary condition, necessary for the well-posedness of the corresponding Euler-Lagrange equation of fourth order. As an example, Bertozzi et al. showed in [BEG07b] that the Cahn-Hilliard inpainting model in fact favors the continuation of the image gradient into the inpainting domain. More precisely, the authors proved that in the limit $\lambda_0 \rightarrow \infty$ a stationary solution of the Cahn-Hilliard inpainting equation fulfills

$$\begin{aligned} u &= f && \text{on } \partial D \\ \nabla u &= \nabla f && \text{on } \partial D, \end{aligned}$$

for a given image f regular enough ($f \in C^2$). This means that not only the grayvalues of the image are specified on the boundary of the inpainting domain but also the gradient of the image function, namely the direction of the level lines are given.

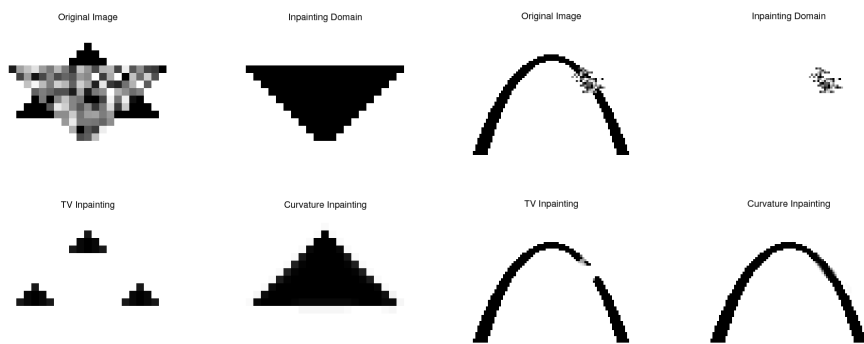


Figure 1.3: Two examples of Euler elastica inpainting compared with TV inpainting. In the case of large aspect ratios the TV inpainting fails to comply with the *Connectivity Principle*. Figure from [CS05].

In an attempt to fulfill both the connectivity principle and the curvature preservation a number of third and fourth-order diffusions has been suggested for image inpainting, most of which have already been discussed in the previous section. Let us recall the main higher-order approaches within this group in the following short summary. The first work connecting image inpainting to a third-order PDE (partial

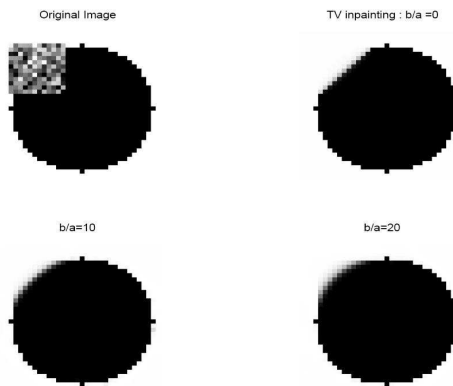


Figure 1.4: An example of Euler elastica inpainting compared with TV inpainting. Despite the presence of high curvature TV inpainting truncates the circle inside the inpainting domain (linear interpolation of level lines). Depending on the weights a and b Eulers elastica inpainting returns a smoothly restored object, taking the curvature of the circle into account (*Curvature Preservation*). Figure from [CKS02].

differential equation) is the transport process of Bertalmio et al. [BSCB00]. A variational third-order approach to image inpainting is CDD (Curvature Driven Diffusion) [CS01c]. Although solving the problem of connecting level lines over large distances (connectivity principle), the level lines are still interpolated linearly and thus curvature is not preserved. The drawbacks of the third-order inpainting models [BSCB00, CS01c] have driven Chan, Kang and Shen [CKS02] to a reinvestigation of the earlier proposal of Masnou and Morel [MM98] on image interpolation based on the Euler elastica energy, compare (1.8). The fourth-order elastica inpainting PDE combines CDD [CS01c] and the transport process of Bertalmio et al. [BSCB00] and is as such able to fulfill both the connectivity principle and curvature preservation. Other recently proposed higher-order inpainting algorithms are inpainting with the Cahn-Hilliard equation (cf. [BEG07a, BEG07b] and Section 2.1), TV- H^{-1} inpainting (cf. [BHS08] and Section 2.2), inpainting with LCIS (cf. [SB09] and Section 2.3), and combinations of second and higher-order methods, e.g. [LT06].

1.3.3 Numerical Solution of Higher-Order Inpainting Approaches

As correctly remarked in [CS05], the main challenge in digital inpainting is the fast and efficient numerical solution of energy- and PDE-based approaches. Especially high-quality, and thus higher-order, approaches, such as Bertalmio's inpainting approach [BSCB00], inpainting with CDD [CS01c], Euler's elastica inpainting [CKS02], and the recently proposed Cahn-Hilliard inpainting - and TV-H⁻¹ inpainting - model [BEG07a, BEG07b, BHS08], despite their superior visual results, demand sophisticated numerical algorithms in order to provide acceptable computation times for large images. In this presentation I will concentrate on numerical methods for higher-order approaches only, since they are the ones we are particularly interested in within this work.

Numerical methods for higher-order equations The numerical solution of higher-order equations, like thin films, phase field models, surface diffusion equations, and much more, occupied a big part of research in numerical analysis in the last decades. In [DD71] the authors propose a semi-implicit finite difference scheme for the solution of second-order parabolic equations. In order to suppress unstable modes a diffusion term was added and subtracted to the numerical scheme, i.e., added implicitly and subtracted explicitly in time. Smereka picked up their idea and used it to solve the fourth-order surface diffusion equation, cf. [Sm03]. The same idea was rediscovered by Glasner and applied to a phase field approach for the Hele-Shaw interface model, cf. [Gl03]. Besides the finite difference approximations, there also exist a lot of finite element algorithms for fourth-order equations. Barrett, Blowey, and Garcke published a series of papers on the solution of various Cahn-Hilliard equations, cf. [BB98, BB99a, BB99b]. For the sharp interface limit of Cahn-Hilliard, i.e., the Hele-Shaw model, Feng and Prohl analyzed finite element methods in [FP04, FP05]. Finite element methods for thin film equations have been studied, for instance, in [GR00, BGLR02].

In inpainting, efficient numerical schemes for higher-order approaches are still a mostly open issue. Most existing numerical schemes for their solution are iterative by nature. PDE based approaches are approximately solved via fixed-point or time-stepping schemes. For energy-based methods the minimizer is usually computed iteratively via the corresponding steepest descent equation.

Iterative methods for curvature driven approaches For curvature driven inpainting approaches, such as [CS01c] and [CKS02], explicit time stepping schemes have been used until recently. Solving a fourth-order nonlinear evolution equation explicitly in time may restrict the time steps to an order $(\Delta x)^4$ of the spatial grid size Δx . Hence this may result in the need of a huge amount of iterations until the inpainted image is obtained. The performance of these schemes could be accelerated by, e.g., the method of Marquina and Osher [MO00]. But still the CPU time required is not appropriate for large images. This computational complexity makes such inpainting approaches less attractive for interactive image manipulation and thus less popular in real-life applications.

A very recent advance in the design of fast numerical solvers for these inpainting approaches was made in [BC08], where the authors propose a nonlinear multigrid approach for inpainting with CDD [CS01c]. In order to get a non-singular smoother, i.e., fixed-point algorithm, for the multigrid approach, the authors modify the CDD equation by changing the definition of the curvature-dependent diffusivity coefficient g . Numerical results confirm that the modified method retains the desirable properties of the original CDD inpainting model while accelerating its numerical computation tremendously. In comparison with the explicit time marching of [CS01c] the multigrid method in [BC08] is four orders of magnitude faster. A matter of future research will be the construction of multigrid solvers for other higher-order inpainting approaches, such as Euler's elastica inpainting [CKS02], and the recently proposed inpainting methods [BEG07b, BEG07a, GS03, BHS08]. In this regard, the crucial point will be to construct an appropriate non-singular smoother for the respective multigrid algorithm.

Numerical methods for diffusion-like inpainting models A fast noniterative method for image inpainting was proposed by Bornemann and M  rz in [BM07]. Their method aims to preserve the visually qualitative results of Bertalmio et al. while performing its numerical solution with a computational speed comparable with the one of Telea's method [Te04]. In their numerical experiments Bornemann and M  rz showed that their method is in fact at least one order of magnitude faster than Bertalmio's method.

One motivation for the proposal of the Cahn-Hilliard equation for inpainting was its superior computational performance in comparison with curvature driven methods.

As pointed out in [BEG07a, BEG07b] Cahn-Hilliard inpainting beats Euler's elastica inpainting by one order of magnitude in its computational complexity. Therein the authors use a certain kind of semi-implicit solver, called convexity splitting, for its numerical solution. The same method was used for TV- H^{-1} inpainting [BHS08, SB09] and for inpainting with LCIS [SB09]. In [SB09] the authors prove rigorous estimates for their numerical scheme, among them the unconditional stability of the scheme, cf. also Section 4.1. Despite this unconditional stability, these numerical schemes still converge slowly due to a damping on the iterates resulting from the method. For more details on convexity splitting and its application to higher-order inpainting methods, cf. [SB09] and Section 4.1.

Further, for TV- H^{-1} minimization in the case of denoising and cartoon/texture decomposition, Elliott and Smitheman proposed a finite element method for its numerical solution, cf. [ES07, ES08]. Their scheme is inspired by a work of Feng and Prohl [FP03], who proposed a finite element method for the ROF model, i.e., the TV- L^2 minimization problem. Therein the authors also proved rigorous mathematical results about the approximation and convergence properties of their scheme. An extension of their approach to TV- H^{-1} inpainting would be interesting. Note that, however, the difference of the inpainting approach from denoising and decomposition is that the former does not follow a variational principle and the fidelity term is locally dependent on the spatial position.

A dual approach for TV- H^{-1} minimization was proposed by the author in [Sc09], also compare Section 4.2 of this work. This work generalizes the algorithm of Chambolle [Ch04] and Bect et al. [BBAC04] from an L^2 fidelity term to an H^{-1} fidelity. The main motivation for the work in [Sc09] is that with the proposed algorithm the domain decomposition approach developed in [FS07], also cf. Section 4.3, can be applied to the higher-order total variation case. Being able to apply domain decomposition methods to TV- H^{-1} minimization can result in a tremendous acceleration of computational speed due to the ability to parallelize the computation, cf. Section 4.3, and in particular Subsection 4.3.7.

Another promising approach within the design of fast numerical solvers in image processing is the Bregman split method proposed by Goldstein and Osher in 2008, [GO08]. In [GBO09] the authors consider the application of this method to image

segmentation and surface reconstruction. The latter application is about the reconstruction of surfaces from unorganized data points, which is used for constructing level set representations in three dimensions. The Bregman split method, originally designed to accelerate the computation of ℓ_1 regularized minimization problems in general, is thereby used to solve a minimization problem regularized with total variation, i.e., the ℓ_1 norm of the gradient of the image function. The computational speed of the Bregman split method in this case is comparable with the one using graph cuts [CD08, DS05], with the additional advantage that it is also able to compute the isotropic total variation. The nature of this application, i.e., surface reconstruction interpreted as an interpolation problem for the given data points, already suggests its possible effectiveness for image inpainting. This is certainly something worthwhile to be considered in a future project.

In the following chapters I will summarize my main research directions and present applications of the methods we have developed.

Organization of the Thesis

Chapter 2 is concerned with mathematical models consisting of (higher-order) partial differential equations used for the task of image inpainting. In Section 2.1 a binary inpainting approach based on a modified Cahn-Hilliard equation is presented. This inpainting method has been proposed by Bertozzi et al. in [BEG07a, BEG07b], where the latter paper contains a rigorous analysis of the modified Cahn-Hilliard equation. We extend this analysis by providing the proof of existence of a stationary solution for the equation. A generalization of this approach for grayvalue images is proposed in Section 2.2. This new inpainting approach is called TV-H⁻¹inpainting. I state analytical results and present numerical examples. Both sections, i.e., Section 2.1 and Section 2.2, have been obtained in a joint work with Martin Burger and Lin He, cf. [BHS08]. In Section 2.3 I present a new inpainting approach based on *Low Curvature Image Simplifiers* (LCIS), first proposed in a joint work with Andrea Bertozzi in [SB09]. Finally, Section 2.4 contains an interpretation of TV-H⁻¹inpainting and inpainting with LCIS in terms of transport and diffusion of grayvalues into the missing domain. This interpretation was inspired by [CKS02], where the authors discuss this issue for Euler's elastica inpainting, and by discussions with Massimo Fornasier. The results

from [CKS02] are also briefly presented in this section, and are further used as a basis for comparison with our two inpainting models.

Chapter 3 is dedicated to theoretical results about higher-order flows arising in image inpainting. In Section 3.1 I discuss the Cahn-Hilliard equation as a model for phase separation and coarsening of binary alloys – the original motivation for the equation. In particular, I present the results we achieved in [BCMS08], in collaboration with Martin Burger, Shun-Jin Chu, and Peter A. Markowich, about finite-time instabilities of the Cahn-Hilliard equation and their connection to the Willmore functional. Additionally, in Section 3.2 I present asymptotic results for nonlocal higher-order evolution equations. The latter section is joint work with Julio D. Rossi and is contained in [RS09].

In Chapter 4, numerical methods, which have been especially designed for higher-order inpainting approaches, are presented. In Section 4.1 I start with the discussion of unconditionally stable numerical schemes for higher-order inpainting approaches proposed together with Andrea Bertozzi in [SB09]. Then, in Section 4.2 I present a dual solver for $\text{TV}-\text{H}^{-1}$ minimization problems, cf. [Sc09]. In particular, I show that this dual solver can be applied to solve the $\text{TV}-\text{H}^{-1}$ inpainting approach from Section 2.2. Finally, in Section 4.3 a domain decomposition method, which is applicable for minimizing functionals with total variation constraints, is presented. This is joint work with Massimo Fornasier and is contained in [FS07]. The main motivations for such an approach are given, and the results achieved in [FS07] are discussed. With the help of the dual solver proposed in Section 4.2, I further show how the theory developed in [FS07] can be applied to solve $\text{TV}-\text{H}^{-1}$ inpainting in a computationally efficient way.

Finally, in Chapter 5 I present two applications of the higher-order inpainting methods discussed in Chapter 2. The first is the restoration of ancient frescoes in Section 5.1, which evolved from an ongoing project at the University of Vienna in joint work with Wolfgang Baatz, Massimo Fornasier, and Peter Markowich (cf. also [BFMS08]). The second is the reconstruction of roads in satellite images in Section 5.2 and is based on joint work with Andrea Bertozzi.

The Appendix contains mathematical preliminaries necessary for the understanding of the presented work.

Chapter 2

Image Inpainting With Higher-Order Equations

This chapter is dedicated to the presentation and the analysis of three fourth-order PDEs used for image inpainting. Thereby Section 2.1 and Section 2.2 about Cahn-Hilliard- and TV-H⁻¹inpainting have been mainly developed in collaboration with Martin Burger and Lin He and appeared in [BHS08]. The idea of inpainting with LCIS in Section 2.3 arose in a joint work with Andrea Bertozzi [SB09]. The last section, Section 2.4, about the inpainting mechanism of transport and diffusion is inspired by the work of Chan, Kang and Shen [CKS02] and discussions with Massimo Fornasier.

2.1 Cahn-Hilliard Inpainting

The Cahn-Hilliard equation is a nonlinear fourth-order diffusion equation originating in material science for modeling phase separation and phase coarsening in binary alloys. A new approach in the class of fourth-order inpainting algorithms is inpainting of binary images using a modified Cahn-Hilliard equation, as proposed in [BEG07a] by Bertozzi, Esedoglu and Gillette. The inpainted version u of $f \in L^2(\Omega)$ assumed with any (trivial) extension to the inpainting domain is constructed by following the evolution of

$$u_t = \Delta \left(-\epsilon \Delta u + \frac{1}{\epsilon} F'(u) \right) + \lambda(f - u) \quad \text{in } \Omega, \quad (2.1)$$

where $F(u)$ is a so-called double-well potential, e.g., $F(u) = u^2(u - 1)^2$, and as before

$$\lambda(x) = \begin{cases} \lambda_0 & \Omega \setminus D \\ 0 & D \end{cases}$$

is the indicator function of $\Omega \setminus D$ multiplied by a constant $\lambda_0 \gg 1$. The two wells of F correspond to values of u that are taken by most of the grayscale values. Choosing a potential with wells at the values 0 (black) and 1 (white), equation (2.1) therefore provides a simple model for the inpainting of binary images. The parameter ϵ determines the steepness of the transition between 0 and 1.

The Cahn-Hilliard equation is a relatively simple fourth-order PDE used for this task rather than more complex models involving curvature terms, cf. also Section 3.1 for more details on the equation. In fact the numerical solution of (2.1) was shown to be of at least an order of magnitude faster than competing inpainting models, cf. [BEG07a]. Still the Cahn-Hilliard inpainting model has many of the desirable properties of curvature based inpainting models such as the smooth continuation of level lines into the missing domain. In fact the mainly numerical paper [BEG07a] was followed by a very careful analysis of (2.1) in [BEG07b]. Therein the authors prove that in the limit $\lambda_0 \rightarrow \infty$ a stationary solution of (2.1) solves

$$\begin{aligned} \Delta \left(\epsilon \Delta u - \frac{1}{\epsilon} F'(u) \right) &= 0 && \text{in } D \\ u &= f && \text{on } \partial D \\ \nabla u &= \nabla f && \text{on } \partial D, \end{aligned} \tag{2.2}$$

for f regular enough ($f \in C^2$). This, once more, supports the claim, that fourth-order methods are superior over second-order methods with respect to a smooth continuation of the image contents into the missing domain.

In [BEG07b] the authors further proved global existence of a unique weak solution of the evolution equation (2.1). More precisely the solution u was proven to be an element in $C([0, T]; L^2(\Omega)) \cap L^2(0, T; V)$, where $V = \{\phi \in H^2(\Omega) \mid \partial\phi/\partial\nu = 0 \text{ on } \partial\Omega\}$, and ν is the outward pointing normal on $\partial\Omega$. Nevertheless the existence of a solution of the stationary equation

$$\Delta \left(-\epsilon \Delta u + \frac{1}{\epsilon} F'(u) \right) + \lambda(f - u) = 0 \quad \text{in } \Omega, \tag{2.3}$$

remains unaddressed. The difficulty in dealing with the stationary equation is the lack of an energy functional for (2.1), i.e., the modified Cahn-Hilliard equation (2.1) cannot be represented by a gradient flow of an energy functional over a certain Banach space. This is because the fidelity term $\lambda(f - u)$ is not symmetric with respect to the H^{-1}

inner product, whereby H^{-1} is defined in the prefix of the thesis. In fact the most evident variational approach would be to minimize the functional

$$\int_{\Omega} \left(\frac{\epsilon}{2} |\nabla u|^2 + \frac{1}{\epsilon} F(u) \right) dx + \frac{1}{2} \|\lambda(u - f)\|_{-1}^2. \quad (2.4)$$

This minimization problem exhibits the optimality condition

$$0 = -\epsilon \Delta u + \frac{1}{\epsilon} F'(u) + \lambda \Delta^{-1}(\lambda(u - f)),$$

which splits into

$$\begin{aligned} 0 &= -\epsilon \Delta u + \frac{1}{\epsilon} F'(u) && \text{in } D \\ 0 &= -\epsilon \Delta u + \frac{1}{\epsilon} F'(u) + \lambda_0^2 \Delta^{-1}(u - f) && \text{in } \Omega \setminus D. \end{aligned}$$

Hence the minimization of (1.4) translates into a second-order diffusion inside the inpainting domain D , whereas a stationary solution of (1.1) fulfills

$$\begin{aligned} 0 &= \Delta \left(-\epsilon \Delta u + \frac{1}{\epsilon} F'(u) \right) && \text{in } D \\ 0 &= \Delta \left(-\epsilon \Delta u + \frac{1}{\epsilon} F'(u) \right) + \lambda_0(f - u) && \text{in } \Omega \setminus D. \end{aligned}$$

One challenge of our work in [BHS08] is to extend the analysis from [BEG07b] by partial answers to questions concerning the stationary equation (2.3) using alternative methods, namely by fixed point arguments. In [BHS08] we prove

Theorem 2.1.1. *Equation (2.3) admits a weak solution in $H^1(\Omega)$ provided $\lambda_0 \geq \frac{C}{\epsilon^3}$ for a positive constant C depending on $|\Omega|$, $|D|$, and F only.*

In our numerical examples in [BHS08] we can see that the condition $\lambda_0 \geq \frac{C}{\epsilon^3}$ in Theorem 2.1.1 is naturally fulfilled, since in order to obtain good visual results in inpainting approaches λ_0 has to be chosen rather large in general, cf. Figure 2.2. Note that the same condition also appears in [BEG07b] where it is needed to prove the global existence of solutions of (2.1).

2.1.1 Existence of a Stationary Solution

In this section we prove the existence of a weak solution of the stationary equation (2.3), i.e., we shall verify Theorem 2.1.1. Let $\Omega \subset \mathbb{R}^2$ be a bounded Lipschitz domain and

$f \in L^2(\Omega)$ given. In order to be able to impose boundary conditions in the equation, we assume f to be constant in a small neighborhood of $\partial\Omega$. This assumption is for technical purposes only and does not influence the inpainting process as long as the inpainting domain D does not touch the boundary of the image domain Ω . Instead of Neumann boundary data as in the original Cahn-Hilliard inpainting approach (cf. [BEG07b]) we use Dirichlet boundary conditions for our analysis, i.e., we consider

$$\begin{cases} u_t = \Delta \left(-\epsilon \Delta u + \frac{1}{\epsilon} F'(u) \right) + \lambda(f - u) & \text{in } \Omega \\ u = f, -\epsilon \Delta u + \frac{1}{\epsilon} F'(u) = 0 & \text{on } \partial\Omega. \end{cases} \quad (2.5)$$

This change from a Neumann- to a Dirichlet problem makes it easier to deal with the boundary conditions in our proofs but does not have a significant impact on the inpainting process as long as we assume that $\bar{D} \subset \Omega$. In Appendix 2.1.3 we nevertheless propose a setting to extend the presented analysis for (2.1) to the originally proposed model with Neumann boundary data. In our new setting we define a weak solution of equation (2.3) as a function $u \in H = \{u \in H^1(\Omega), u|_{\partial\Omega} = f|_{\partial\Omega}\}$ that fulfills

$$\langle \epsilon \nabla u, \nabla \phi \rangle_2 + \left\langle \frac{1}{\epsilon} F'(u), \phi \right\rangle_2 - \langle \lambda(f - u), \phi \rangle_{-1} = 0, \quad \forall \phi \in H_0^1(\Omega). \quad (2.6)$$

Remark 2.1.2. With $u \in H^1(\Omega)$ and the compact embedding $H^1(\Omega) \hookrightarrow \hookrightarrow L^q(\Omega)$ for every $1 \leq q < \infty$ and $\Omega \subset \mathbb{R}^2$ the weak formulation is well defined.

To see that (2.6) defines a weak formulation for (2.3) with Dirichlet boundary conditions we integrate by parts in (2.6) and get

$$\begin{aligned} & \int_{\Omega} \left(-\epsilon \Delta u + \frac{1}{\epsilon} F'(u) - \Delta^{-1}(\lambda(f - u)) \right) \phi \, dx \\ & - \int_{\partial\Omega} \Delta^{-1}(\lambda(f - u)) \nabla \Delta^{-1} \phi \cdot \nu \, d\mathcal{H}_1 = 0, \quad \forall \phi \in H_0^1(\Omega), \end{aligned}$$

where \mathcal{H}_1 denotes the one dimensional Hausdorff measure. Since the above equality holds for all $\phi \in H_0^1(\Omega)$ it holds in particular for all ϕ in the subset $H_0^1(\Omega) \cap \{\nabla \Delta^{-1} \phi \cdot \nu = 0 \text{ on } \partial\Omega\}$. This yields

$$\begin{cases} \epsilon \Delta u - \frac{1}{\epsilon} F'(u) + \Delta^{-1}(\lambda(f - u)) = 0 & \text{in } \Omega \\ \Delta^{-1}(\lambda(f - u)) = 0 & \text{on } \partial\Omega. \end{cases} \quad (2.7)$$

2.1 Cahn-Hilliard Inpainting

Assuming sufficient regularity on u we can use the definition of Δ^{-1} to see that u solves

$$\begin{cases} -\epsilon \Delta \Delta u + \frac{1}{\epsilon} \Delta F'(u) + \lambda(f - u) = 0 & \text{in } \Omega \\ \Delta^{-1}(\lambda(f - u)) = -\epsilon \Delta u + \frac{1}{\epsilon} F'(u) = 0 & \text{on } \partial\Omega, \end{cases}$$

Since additionally $u|_{\partial\Omega} = f|_{\partial\Omega}$, the function u solves (2.3) with Dirichlet boundary conditions.

For the proof of existence of a solution to (2.6) we follow the following strategy. We consider the fixed point operator $\mathcal{A} : L^2(\Omega) \rightarrow L^2(\Omega)$ where $\mathcal{A}(v) = u$ fulfills for a given $v \in L^2(\Omega)$ the equation

$$\begin{cases} \frac{1}{\tau} \Delta^{-1}(u - v) = \epsilon \Delta u - \frac{1}{\epsilon} F'(u) + \Delta^{-1}[\lambda(f - u) + (\lambda_0 - \lambda)(v - u)] & \text{in } \Omega, \\ u = f, \quad \Delta^{-1}\left(\frac{1}{\tau}(u - v) - \lambda(f - u) - (\lambda_0 - \lambda)(v - u)\right) = 0 & \text{on } \partial\Omega, \end{cases} \quad (2.8)$$

where $\tau > 0$ is a parameter. The boundary conditions of \mathcal{A} are given by the second equation in (2.8). Note that actually the solution u will be in $H^1(\Omega)$ and hence the boundary condition is well-defined in the trace sense, the operator \mathcal{A} into $L^2(\Omega)$ is then obtained with further embedding. We define a weak solution of (2.8) as before by a function $u \in H = \{u \in H^1(\Omega), u|_{\partial\Omega} = f|_{\partial\Omega}\}$ that fulfills

$$\begin{aligned} & \left\langle \frac{1}{\tau}(u - v), \phi \right\rangle_{-1} + \langle \epsilon \nabla u, \nabla \phi \rangle_2 + \left\langle \frac{1}{\epsilon} F'(u), \phi \right\rangle_2 \\ & \quad - \langle \lambda(f - u) + (\lambda_0 - \lambda)(v - u), \phi \rangle_{-1} = 0 \quad \forall \phi \in H_0^1(\Omega). \end{aligned} \quad (2.9)$$

A fixed point of the operator \mathcal{A} , provided it exists, then solves the stationary equation with Dirichlet boundary conditions as in (2.7).

Note that in (2.8) the indicator function λ in the fitting term $\lambda(f - u) + (\lambda_0 - \lambda)(v - u) = \lambda_0(v - u) + \lambda(f - v)$ only appears in combination with given functions f, v and is not combined with the solution u of the equation. For equation (2.8), i.e., (2.9), we can therefore state a variational formulation. This is, for a given $v \in L^2(\Omega)$ equation (2.8) is the Euler-Lagrange equation of the minimization problem

$$u^* = \operatorname{argmin}_{u \in H^1(\Omega), u|_{\partial\Omega} = f|_{\partial\Omega}} \mathcal{J}^\epsilon(u, v) \quad (2.10)$$

with

$$\mathcal{J}^\epsilon(u, v) = \int_{\Omega} \left(\frac{\epsilon}{2} |\nabla u|^2 + \frac{1}{\epsilon} F(u) \right) dx + \frac{1}{2\tau} \|u - v\|_{-1}^2 + \frac{\lambda_0}{2} \left\| u - \frac{\lambda}{\lambda_0} f - \left(1 - \frac{\lambda}{\lambda_0}\right) v \right\|_{-1}^2. \quad (2.11)$$

We are going to use the variational formulation (2.11) to prove that (2.8) admits a weak solution in $H^1(\Omega)$. This solution is unique under additional conditions.

Proposition 2.1.3. *Equation (2.8) admits a weak solution in $H^1(\Omega)$ in the sense of (2.9). For $\tau \leq C\epsilon^3$, where C is a positive constant depending on $|\Omega|, |D|$, and F only, the weak solution of (2.8) is unique.*

Further we prove that the operator \mathcal{A} admits a fixed point under certain conditions.

Proposition 2.1.4. *Set $\mathcal{A} : L^2(\Omega) \rightarrow L^2(\Omega)$, $\mathcal{A}(v) = u$, where $u \in H^1(\Omega)$ is the unique weak solution of (2.8). Then \mathcal{A} admits a fixed point $\hat{u} \in H^1(\Omega)$ if $\tau \leq C\epsilon^3$ and $\lambda_0 \geq \frac{C}{\epsilon^3}$ for a positive constant C depending on $|\Omega|, |D|$, and F only.*

Hence the existence of a stationary solution of (2.1) follows under the condition $\lambda_0 \geq C/\epsilon^3$.

We begin with considering the fixed point equation (2.8), i.e., the minimization problem (2.10). In the following we prove the existence of a unique weak solution of (2.8) by showing the existence of a unique minimizer for (2.11).

Proof of Proposition 2.1.3. We want to show that $\mathcal{J}^\epsilon(u, v)$ has a minimizer in $H = \{u \in H^1(\Omega), u|_{\partial\Omega} = f|_{\partial\Omega}\}$. For this we consider a minimizing sequence $u^n \in H$ of $\mathcal{J}^\epsilon(u, v)$. To see that u^n is uniformly bounded in $H^1(\Omega)$ we show that $\mathcal{J}^\epsilon(u, v)$ is coercive in $H^1(\Omega)$. With $F(u) \geq C_1 u^2 - C_2$ for two positive constants $C_1, C_2 > 0$ and the triangular inequality in the $H^{-1}(\Omega)$ space, we obtain

$$\begin{aligned} \mathcal{J}^\epsilon(u, v) &\geq \frac{\epsilon}{2} \|\nabla u\|_2^2 + \frac{C_1}{\epsilon} \|u\|_2^2 - \frac{C_2}{\epsilon} + \frac{1}{2\tau} \left(\frac{1}{2} \|u\|_{-1}^2 - \|v\|_{-1}^2 \right) \\ &\quad + \frac{\lambda_0}{2} \left(\frac{1}{2} \|u\|_{-1}^2 - \left\| \frac{\lambda}{\lambda_0} f + \left(1 - \frac{\lambda}{\lambda_0} \right) v \right\|_{-1}^2 \right) \\ &\geq \frac{\epsilon}{2} \|\nabla u\|_2^2 + \frac{C_1}{\epsilon} \|u\|_2^2 + \left(\frac{\lambda_0}{4} + \frac{1}{4\tau} \right) \|u\|_{-1}^2 - C_3(v, f, \lambda_0, \epsilon, \Omega, D). \end{aligned}$$

Therefore a minimizing sequence u^n is bounded in $H^1(\Omega)$ and it follows that $u^n \rightharpoonup u^*$ in $H^1(\Omega)$. To finish the proof of existence for (2.8) we have to show that $\mathcal{J}^\epsilon(u, v)$ is weakly lower semicontinuous in $H^1(\Omega)$. For this we divide the sequence $\mathcal{J}^\epsilon(u^n, v)$ of (2.11) in two parts. We denote the first term by

$$a^n = \underbrace{\int_{\Omega} \left(\frac{\epsilon}{2} |\nabla u^n|^2 + \frac{1}{\epsilon} F(u^n) \right) dx}_{CH(u^n)}$$

2.1 Cahn-Hilliard Inpainting

and the second term by

$$b^n = \underbrace{\frac{1}{2\tau} \|u^n - v\|_{-1}^2}_{D(u^n, v)} + \underbrace{\frac{\lambda_0}{2} \left\| u^n - \frac{\lambda}{\lambda_0} f - \left(1 - \frac{\lambda}{\lambda_0}\right) v \right\|_{-1}^2}_{FIT(u^n, v)}.$$

Since $H^1 \hookrightarrow L^2$ it follows $u^n \rightarrow u^*$ in $L^2(\Omega)$. Further we know that if b^n converges strongly, then

$$\liminf (a^n + b^n) = \liminf a^n + \lim b^n. \quad (2.12)$$

We begin with the consideration of the last term in (2.11). We denote $\tilde{f} := \frac{\lambda}{\lambda_0} f + (1 - \frac{\lambda}{\lambda_0})v$. We want to show

$$\|u^n - \tilde{f}\|_{-1}^2 \longrightarrow \|u^* - \tilde{f}\|_{-1}^2,$$

or equivalently

$$\langle \Delta^{-1}(u^n - \tilde{f}), u^n - \tilde{f} \rangle_2 \longrightarrow \langle \Delta^{-1}(u^* - \tilde{f}), u^* - \tilde{f} \rangle_2.$$

For this we consider the absolute difference of the two terms,

$$\begin{aligned} & |\langle \Delta^{-1}(u^n - \tilde{f}), u^n - \tilde{f} \rangle_2 - \langle \Delta^{-1}(u^* - \tilde{f}), u^* - \tilde{f} \rangle_2| \\ &= |\langle \Delta^{-1}(u^n - u^*), u^n - \tilde{f} \rangle_2 - \langle \Delta^{-1}(u^* - \tilde{f}), u^n - u^* \rangle_2| \\ &\leq |\langle u^n - u^*, \Delta^{-1}(u^n - \tilde{f}) \rangle_2| + |\langle \Delta^{-1}(u^* - \tilde{f}), u^* - u^n \rangle_2| \\ &\leq \underbrace{\|u^n - u^*\|_2}_{\rightarrow 0} \cdot \underbrace{\|\Delta^{-1}(u^n - \tilde{f})\|_2}_{\rightarrow 0} + \underbrace{\|u^n - u^*\|_2}_{\rightarrow 0} \cdot \underbrace{\|\Delta^{-1}(u^* - \tilde{f})\|_2}_{\rightarrow 0} \end{aligned}$$

Since the operator $\Delta^{-1} : H^{-1}(\Omega) \rightarrow H_0^1(\Omega)$ is linear and continuous it follows that

$$\|\Delta^{-1}F\|_2 \leq \|\Delta^{-1}\| \cdot \|F\|_2 \quad \text{for all } F \in H^{-1}(\Omega).$$

Thus

$$\begin{aligned} & |\langle \Delta^{-1}(u^n - \tilde{f}), u^n - \tilde{f} \rangle_2 - \langle \Delta^{-1}(u^* - \tilde{f}), u^* - \tilde{f} \rangle_2| \\ &\leq \underbrace{\|u^n - u^*\|_2}_{\rightarrow 0} \underbrace{\|\Delta^{-1}\|}_{const} \underbrace{\|u^n - \tilde{f}\|_2}_{bounded} + \underbrace{\|u^n - u^*\|_2}_{\rightarrow 0} \underbrace{\|\Delta^{-1}\|}_{const} \underbrace{\|u^* - \tilde{f}\|_2}_{const} \\ &\longrightarrow 0 \text{ as } n \rightarrow \infty, \end{aligned}$$

2.1 Cahn-Hilliard Inpainting

and we conclude that $FIT(u^n, v)$ converges strongly to $FIT(u^*, v)$. With the same argument it follows that $D(u^n, v)$ converges strongly and consequently that the sequence b^n converges strongly in $L^2(\Omega)$. Further $CH(\cdot)$ is weakly lower semicontinuous, which follows from the lower semicontinuity of the Dirichlet integral and from the continuity of F by applying Fatou's Lemma. Hence we obtain

$$\mathcal{J}^\epsilon(u^*, v) \leq \liminf \mathcal{J}^\epsilon(u^n, v).$$

Therefore \mathcal{J}^ϵ has a minimizer in H^1 , i.e.,

$$\exists u^* \text{ with } u^* = \operatorname{argmin}_{u \in H^1(\Omega)} \mathcal{J}^\epsilon(u, v).$$

We next assert that u^* fulfills the boundary condition $u^*|_{\partial\Omega} = f|_{\partial\Omega}$. To see this, note that for an admissible function $w \in H$, $u^n - w \in H_0^1(\Omega)$. Now $H_0^1(\Omega)$ is a closed, linear subspace of $H^1(\Omega)$, and so, by Mazur's theorem (cf. [Ev98] D.4 for example), is weakly closed. Hence $u^* - w \in H_0^1(\Omega)$ and consequently the trace of u^* on $\partial\Omega$ is equal to f .

For simplicity let in the following $u = u^*$. To see that the minimizer u is a weak solution of (2.8) we compute the corresponding Euler-Lagrange equation to the minimization problem. For this sake we choose any test function $\phi \in H_0^1(\Omega)$ and compute the first variation of \mathcal{J}^ϵ , i.e.,

$$\left(\frac{d}{d\delta} \mathcal{J}^\epsilon(u + \delta\phi, v) \right)_{\delta=0},$$

which has to be zero for a minimizer u . Thus we have

$$\epsilon \langle \nabla u, \nabla \phi \rangle_2 + \frac{1}{\epsilon} \langle F'(u), \phi \rangle_2 + \left\langle \frac{1}{\tau}(u - v) + \lambda_0 \left[u - \frac{\lambda}{\lambda_0} f - \left(1 - \frac{\lambda}{\lambda_0}\right) v \right], \phi \right\rangle_{-1} = 0.$$

Integrating by parts in both terms we get

$$\begin{aligned} & \left\langle -\epsilon \Delta u + \frac{1}{\epsilon} F'(u) - \Delta^{-1} \left(\frac{1}{\tau}(u - v) + \lambda_0 \left[u - \frac{\lambda}{\lambda_0} f - \left(1 - \frac{\lambda}{\lambda_0}\right) v \right] \right), \phi \right\rangle_2 \\ & + \int_{\partial\Omega} \nabla u \cdot \nu \phi \, ds + \int_{\partial\Omega} \Delta^{-1} \left(\frac{1}{\tau}(u - v) + \lambda_0 \left[u - \frac{\lambda}{\lambda_0} f - \left(1 - \frac{\lambda}{\lambda_0}\right) v \right] \right) \nabla \Delta^{-1} \phi \cdot \nu \, ds = 0. \end{aligned}$$

Since ϕ is an element in $H_0^1(\Omega)$, the first boundary integral vanishes. Further, a minimizer u fulfills the boundary condition $u = f$ on the boundary $\partial\Omega$. Hence, we obtain that u fulfills the weak formulation (2.9) of (2.8).

For the uniqueness of the minimizer, we need to prove that \mathcal{J}^ϵ is strictly convex. To do so, we prove that for any $u_1, u_2 \in H^1(\Omega)$,

$$\mathcal{J}^\epsilon(u_1, v) + \mathcal{J}^\epsilon(u_2, v) - 2\mathcal{J}^\epsilon\left(\frac{u_1 + u_2}{2}, v\right) > 0, \quad (2.13)$$

based on an assumption that $F(\cdot)$ satisfies $F(u_1) + F(u_2) - 2F(\frac{u_1+u_2}{2}) > -C(u_1 - u_2)^2$, for a constant $C > 0$. An example is when $F(u) = \frac{1}{8}(u^2 - 1)^2$, $C = \frac{1}{8}$. Denoting $u = u_1 - u_2$, we have

$$\mathcal{J}^\epsilon(u_1, v) + \mathcal{J}^\epsilon(u_2, v) - 2\mathcal{J}^\epsilon\left(\frac{u_1 + u_2}{2}, v\right) > \frac{\epsilon}{4}\|u\|_1^2 + \left(\frac{1}{4\tau} + \frac{\lambda_0}{4}\right)\|u\|_{-1}^2 - \frac{C}{\epsilon}\|u\|_2^2.$$

By using the inequality

$$\|u\|_2^2 \leq \|u\|_1\|u\|_{-1} \quad (2.14)$$

and the Cauchy-Schwarz inequality, for (2.13) to be fulfilled, we need

$$2\sqrt{\frac{\epsilon}{4}\left(\frac{1}{4\tau} + \frac{\lambda_0}{4}\right)} \geq \frac{C}{\epsilon},$$

i.e.,

$$\epsilon^3\left(\lambda_0 + \frac{1}{\tau}\right) \geq C^2.$$

Therefore $\mathcal{J}^\epsilon(u, v)$ is strictly convex in u and our minimization problem has a unique minimizer if τ is chosen smaller than $C\epsilon^3$ for a constant C depending on $|\Omega|, |D|$, and F only. Because of the convexity of \mathcal{J}^ϵ in ∇u and u , every weak solution of the Euler-Lagrange equation (2.8) is in fact a minimizer of \mathcal{J}^ϵ . This proves the uniqueness of a weak solution of (2.8) provided $\tau < C\epsilon^3$. \square

Next we want to prove Proposition 2.1.4, i.e., the existence of a fixed point of (2.8) and with this the existence of a stationary solution of (2.1). To do so we are going to apply Schauder's fixed point theorem.

Proof of Proposition 2.1.4. We consider a solution $\mathcal{A}(v) = u$ of (2.8) with $v \in L^2(\Omega)$ given. In the following we will prove the existence of a fixed point by using Schauder's fixed point theorem. We start with proving that

$$\|\mathcal{A}(v)\|_2^2 = \|u\|_2^2 \leq \beta\|v\|_2^2 + \alpha \quad (2.15)$$

for constants $\beta < 1$ and $\alpha > 0$. Having this, we have shown that \mathcal{A} is a map from the closed ball $K = B(0, M) = \{u \in L^2(\Omega) : \|u\|_2 \leq M\}$ into itself for an appropriate constant $M > 0$. We conclude the proof with showing the compactness of K and the continuity of the fixed point operator \mathcal{A} . From Schauder's theorem the existence of a fixed point follows.

2.1 Cahn-Hilliard Inpainting

Let us, for the time being, additionally assume that ∇u and Δu are bounded in $L^2(\Omega)$. Hence we can multiply (2.8) with $-\Delta u$ and integrate over Ω to obtain

$$\begin{aligned} - \int_{\Omega} \Delta u \Delta^{-1} \left[\frac{1}{\tau} (u - v) - \lambda(f - u) - (\lambda_0 - \lambda)(v - u) \right] dx \\ = -\epsilon \langle \Delta u, \Delta u \rangle_2 + \frac{1}{\epsilon} \int_{\Omega} F'(u) \Delta u dx \end{aligned}$$

After integration by parts we find with the short-hand notation

$$w := \frac{1}{\tau} (u - v) - \lambda(f - u) - (\lambda_0 - \lambda)(v - u)$$

that

$$\begin{aligned} \int_{\Omega} uw dx - \int_{\partial\Omega} \left[\nabla u \cdot \nu (\Delta^{-1} w + \frac{1}{\epsilon} F'(u)) - u \nabla (\Delta^{-1} w) \cdot \nu \right] d\mathcal{H}_1 \\ = -\epsilon \|\Delta u\|_2^2 - \frac{1}{\epsilon} \int_{\Omega} F''(u) |\nabla u|^2 dx. \end{aligned}$$

Now we insert the boundary conditions $\Delta^{-1} w = 0$, $u = f =: f_1$ and $F'(u) = F'(f) = f_2$ on $\partial\Omega$ with constants f_1 and f_2 on the left-hand side, i.e.

$$\int_{\Omega} uw dx - \int_{\partial\Omega} \left[\frac{f_2}{\epsilon} \nabla u \cdot \nu - f_1 \nabla (\Delta^{-1} w) \cdot \nu \right] d\mathcal{H}_1 = -\epsilon \|\Delta u\|_2^2 - \frac{1}{\epsilon} \int_{\Omega} F''(u) |\nabla u|^2 dx.$$

An application of Gauss' Theorem to the boundary integral implies

$$\int_{\partial\Omega} \left[\frac{f_2}{\epsilon} \nabla u \cdot \nu - f_1 \nabla (\Delta^{-1} w) \cdot \nu \right] d\mathcal{H}_1 = \frac{f_2}{\epsilon} \int_{\Omega} \Delta u dx + f_1 \int_{\Omega} w dx,$$

and we get

$$\int_{\Omega} uw dx = -\epsilon \|\Delta u\|_2^2 - \frac{1}{\epsilon} \int_{\Omega} F''(u) |\nabla u|^2 dx + \frac{f_2}{\epsilon} \int_{\Omega} \Delta u dx + f_1 \int_{\Omega} w dx.$$

By further applying Young's inequality to the last two terms we get

$$\int_{\Omega} uw dx \leq \left(\frac{f_2 \delta}{2\epsilon} - \epsilon \right) \|\Delta u\|_2^2 - \frac{1}{\epsilon} \int_{\Omega} F''(u) |\nabla u|^2 dx + \frac{f_1 \delta}{2} \|w\|_2^2 + C(f_1, f_2, |\Omega|, \epsilon, \delta).$$

Using the identity $\lambda(f - u) + (\lambda_0 - \lambda)(v - u) = \lambda(f - v) + \lambda_0(v - u)$ in the definition of w yields

$$\begin{aligned} \int_{\Omega} u \cdot \frac{1}{\tau} (u - v) dx &\leq \left(\frac{f_2 \delta}{2\epsilon} - \epsilon \right) \|\Delta u\|_2^2 - \frac{1}{\epsilon} \int_{\Omega} F''(u) |\nabla u|^2 dx + \frac{f_1 \delta}{2} \|w\|_2^2 \\ &\quad + \lambda_0 \left(\int_{\Omega \setminus D} u(f - u) dx + \int_D u(v - u) dx \right) + C(f_1, f_2, |\Omega|, \epsilon, \delta). \end{aligned}$$

By applying the standard inequality $(a + b)^2 \leq 2(a^2 + b^2)$ to the L^2 norm of $w = (\frac{1}{\tau} + \lambda_0)u - (\frac{1}{\tau} + \lambda_0 - \lambda)v - \lambda f$ and by using $(1 - \lambda/\lambda_0) \leq 1$ in the resulting L^2 norm of v we get

$$\begin{aligned} \int_{\Omega} u \cdot \frac{1}{\tau}(u - v) dx &\leq \left(\frac{f_2 \delta}{2\epsilon} - \epsilon \right) \|\Delta u\|_2^2 - \frac{1}{\epsilon} \int_{\Omega} F''(u) |\nabla u|^2 dx + f_1 \delta \left(\frac{1}{\tau} + \lambda_0 \right)^2 \|u\|_2^2 \\ &\quad + 2f_1 \delta \left(\frac{1}{\tau} + \lambda_0 \right)^2 \|v\|_2^2 + \lambda_0 \left(\int_{\Omega \setminus D} u(f - u) dx + \int_D u(v - u) dx \right) \\ &\quad + C(f, f_1, f_2, |\Omega|, \epsilon, \delta, \lambda_0). \end{aligned}$$

With $F''(u) \geq C_1 u^2 - C_2$ for some constants $C_1, C_2 > 0$ and for all $u \in \mathbb{R}$, and by further applying the Cauchy-Schwarz inequality to the last two integrals we obtain

$$\begin{aligned} \int_{\Omega} u \cdot \frac{1}{\tau}(u - v) dx &\leq \left(\frac{f_2 \delta}{2\epsilon} - \epsilon \right) \|\Delta u\|_2^2 - \frac{C_1}{\epsilon} \|u |\nabla u|\|_2^2 + \frac{C_2}{\epsilon} \|\nabla u\|_2^2 \\ &\quad + f_1 \delta \left(\frac{1}{\tau} + \lambda_0 \right)^2 \|u\|_2^2 + 2f_1 \delta \left(\frac{1}{\tau} + \lambda_0 \right)^2 \|v\|_2^2 + \lambda_0 \left[- \left(1 - \frac{\delta_2}{2} \right) \int_{\Omega \setminus D} u^2 dx \right. \\ &\quad \left. + \left(\frac{\delta_1}{2} - 1 \right) \int_D u^2 dx + \frac{1}{2\delta_1} \int_D v^2 dx \right] + C(f, f_1, f_2, |\Omega|, |D|, \epsilon, \lambda_0, \delta, \delta_2). \end{aligned}$$

Setting $\delta_2 = 1$ and $\delta_1 = 2$ we see that

$$\begin{aligned} \int_{\Omega} u \cdot \frac{1}{\tau}(u - v) dx &\leq \left(\frac{f_2 \delta}{2\epsilon} - \epsilon \right) \|\Delta u\|_2^2 - \frac{C_1}{\epsilon} \|u |\nabla u|\|_2^2 + \frac{C_2}{\epsilon} \|\nabla u\|_2^2 \\ &\quad + f_1 \delta \left(\frac{1}{\tau} + \lambda_0 \right)^2 \|u\|_2^2 + 2f_1 \delta \left(\frac{1}{\tau} + \lambda_0 \right)^2 \|v\|_2^2 + \lambda_0 \left[- \frac{1}{2} \int_{\Omega \setminus D} u^2 dx + \frac{1}{4} \int_D v^2 dx \right] \\ &\quad + C(f, f_1, f_2, |\Omega|, |D|, \epsilon, \delta, \lambda_0). \end{aligned}$$

We follow the argument used in the proof of existence for (2.1) in [BEG07b] by observing the following property: A standard interpolation inequality for ∇u reads

$$\|\nabla u\|_2^2 \leq \delta_3 \|\Delta u\|_2^2 + \frac{C_3}{\delta_3} \|u\|_2^2. \quad (2.16)$$

The domain of integration in the second integral of the equation above can be taken to be smaller than Ω by taking a larger constant C_3 . Further we use the L^1 version of Poincare's inequality applied to the function u^2 . We recall this inequality in the following theorem.

Theorem 2.1.5. (*Poincare's inequality in L^1*). *Assume that Ω is a precompact open subset of the n -dimensional Euclidean space \mathbb{R}^n having Lipschitz boundary (i.e., Ω is*

2.1 Cahn-Hilliard Inpainting

an open, bounded Lipschitz domain). Then there exists a constant C , depending only on Ω , such that, for every function u in the Sobolev space $W^{1,1}(\Omega)$,

$$\|u - u_\Omega\|_{L^1(\Omega)} \leq C\|\nabla u\|_{L^1(\Omega)},$$

where $u_\Omega = \frac{1}{|\Omega|} \int_\Omega u(y) dy$ is the average value of u over Ω , with $|\Omega|$ denoting the Lebesgue measure of the domain Ω .

Then, assuming that $u \neq 0$ in $\Omega \setminus D$, we choose the constant C_4 (which depends on the size of D compared to Ω) large enough such that

$$\int_\Omega u^2 dx - C_4 \int_{\Omega \setminus D} u^2 dx \leq \int_\Omega |u^2 - u_\Omega^2| dx \leq C_4 \int_\Omega |\nabla u^2| dx,$$

or in other words

$$\|u\|_2^2 \leq C_4 \|\nabla u^2\|_{L^1(\Omega)} + C_4 \int_{\Omega \setminus D} u^2 dx. \quad (2.17)$$

By Hölder's inequality we also have

$$\|\nabla u^2\|_{L^1(\Omega)} \leq \frac{\alpha}{2} \|u \nabla u\|_2^2 + \frac{C_5}{2\alpha}. \quad (2.18)$$

Putting the last three inequalities (2.16)-(2.18) together we obtain

$$\|\nabla u\|_2^2 \leq \delta_3 \|\Delta u\|_2^2 + \frac{C_3 C_4 \alpha}{2\delta_3} \|u \nabla u\|_2^2 + \frac{C_3 C_4}{\delta_3} \int_{\Omega \setminus D} u^2 dx + \frac{C_3 C_4 C_5}{2\alpha \delta_3}.$$

We now use the last inequality to bound the gradient term in our estimates from above to get

$$\begin{aligned} \int_\Omega u \cdot \frac{1}{\tau} (u - v) dx &\leq \left(\frac{f_2 \delta + 2C_2 \delta_3}{2\epsilon} - \epsilon \right) \|\Delta u\|_2^2 + \left(\frac{C_2 C_3 C_4 \alpha}{2\delta_3 \epsilon} - \frac{C_1}{\epsilon} \right) \|u \nabla u\|_2^2 \\ &\quad + \left(f_1 \delta \left(\frac{1}{\tau} + \lambda_0 \right)^2 + \frac{C_2 C_3 C_4}{\delta_3 \epsilon} - \frac{C_4 \lambda_0}{2} \right) \|u\|_2^2 \\ &\quad + \left(\frac{\lambda_0}{4} + 2f_2 \delta \left(\frac{1}{\tau} + \lambda_0 \right)^2 \right) \|v\|_2^2 + C(f, f_1, f_2, |\Omega|, |D|, \epsilon, \delta, \lambda_0). \end{aligned} \quad (2.19)$$

With $\delta_3 < \frac{2\epsilon^2 - f_2 \delta}{2C_2}$ and α, δ small enough, the first two terms can be estimated from above by zero. Applying the Cauchy-Schwarz inequality on the left-hand side and rearranging the terms on both sides of the inequality we conclude that

$$\begin{aligned} &\left(\frac{1}{2\tau} + \frac{C_4 \lambda_0}{2} - f_1 \delta \left(\frac{1}{\tau} + \lambda_0 \right)^2 - \frac{C_2 C_3 C_4}{\delta_3 \epsilon} \right) \|u\|_2^2 \\ &\leq \left(\left(\frac{\lambda_0}{4} + \frac{1}{2\tau} \right) + 2f_2 \delta \left(\frac{1}{\tau} + \lambda_0 \right)^2 \right) \|v\|_2^2 + C(f, f_1, f_2, |\Omega|, |D|, \epsilon, \delta, \lambda_0). \end{aligned}$$

Choosing δ small enough, C_4 large enough, and $\lambda_0 \geq CC_4\frac{1}{\epsilon^3}$, the solutions u and v fulfill

$$\|u\|_2^2 \leq \beta \|v\|_2^2 + C, \quad (2.20)$$

with $\beta < 1$ and a constant C independent of v . Hence u is bounded in $L^2(\Omega)$.

To see that our regularity assumptions on u from the beginning of the proof are automatically fulfilled we consider (2.19) with appropriate constants δ_3 , δ , and α as specified in the paragraph below (2.19). But now we only estimate the second term on the right side by zero and keep the first term. By applying the Cauchy-Schwarz inequality and rearranging the terms as before we obtain

$$\begin{aligned} & \left(\frac{1}{2\tau} + \frac{C_4\lambda_0}{2} - f_1\delta \left(\frac{1}{\tau} - \lambda_0 \right)^2 - \frac{C_2C_3C_4}{\delta_3\epsilon} \right) \|u\|_2^2 + \left(\epsilon - \frac{f_2\delta + 2C_2\delta_3}{2\epsilon} \right) \|\Delta u\|_2^2 \\ & \leq \left(\left(\frac{\lambda_0}{4} + \frac{1}{2\tau} \right) + 2f_2\delta \left(\frac{1}{\tau} + \lambda_0 \right)^2 \right) \|v\|_2^2 + C(f, f_1, f_2, |\Omega|, |D|, \epsilon, \delta, \lambda_0), \end{aligned}$$

with the coefficient $\epsilon - \frac{f_2\delta + 2C_2\delta_3}{2\epsilon} > 0$ due to our choice of δ_3 . Therefore not only the L^2 -norm of u is uniformly bounded but also the L^2 -norm of Δu . By the standard interpolation inequality (2.16) the boundedness of u in $H^1(\Omega)$ follows. From the last result we additionally get that the operator \mathcal{A} is a compact map since $\mathcal{A} : L^2(\Omega) \rightarrow H^1(\Omega) \hookrightarrow L^2(\Omega)$. Therefore K is a compact and convex subset of $L^2(\Omega)$.

It remains to show that the operator \mathcal{A} is continuous. Indeed if $v_k \rightarrow v$ in $L^2(\Omega)$ then $\mathcal{A}(v_k) = u_k$ is bounded in $H^1(\Omega)$ for all $k = 0, 1, 2, \dots$. Thus, we can consider a weakly convergent subsequence $u_{k_j} \rightharpoonup u$ in $H^1(\Omega)$. Because $H^1(\Omega) \hookrightarrow L^q(\Omega)$, $1 \leq q < \infty$ the sequence u_{k_j} converges also strongly to u in $L^q(\Omega)$. Hence, a weak solution $\mathcal{A}(v_k) = u_k$ of (2.8) weakly converges to a weak solution u of

$$\frac{1}{\tau}(-\Delta^{-1})(u - v) = \epsilon\Delta u - \frac{1}{\epsilon}F'(u) - \Delta^{-1}[\lambda(f - u) + (\lambda_0 - \lambda)(v - u)],$$

where u is the weak limit of $\mathcal{A}(v_k)$ as $k \rightarrow \infty$. Because the solution of (2.8) is unique provided $\tau \leq C\epsilon^3$ (cf. Proposition 2.1.3), $u = \mathcal{A}(v)$, and therefore \mathcal{A} is continuous. Applying Schauder's Theorem we have shown that the fixed point operator \mathcal{A} admits a fixed point \hat{u} in $L^2(\Omega)$ which fulfills

$$\langle \epsilon\nabla\hat{u}, \nabla\phi \rangle_2 + \left\langle \frac{1}{\epsilon}F'(\hat{u}), \phi \right\rangle_2 - \langle \lambda(f - \hat{u}), \phi \rangle_{-1} + \int_{\partial\Omega} \Delta^{-1}(\lambda(f - \hat{u})) \nabla\Delta^{-1}\phi \cdot \nu \, d\mathcal{H}_1 = 0$$

for all $\phi \in H_0^1(\Omega)$. Because the solution of (2.8) is an element of H also the fixed point \hat{u} belongs to H . \square

Following the arguments from the beginning of this section we conclude with the existence of a stationary solution for (2.1).

By modifying the setting and the above proof in an appropriate way one can prove the existence of a stationary solution for (2.1) also under Neumann boundary conditions, i.e.,

$$\nabla u \cdot \nu = \nabla \Delta u \cdot \nu = 0, \quad \text{on } \partial\Omega.$$

A corresponding reformulation of the problem is given in Subsection 2.1.3.

2.1.2 Numerical Results

In this section numerical results for the Cahn-Hilliard inpainting approach (2.1) are presented. The numerical scheme used is discussed in detail in Section 4.1, and in particular in Section 4.1.2 (cf. also [SB09, BHS08]).

In Figures 2.1-2.2 Cahn-Hilliard inpainting was applied to two different binary images. In all of the examples we follow the procedure of [BEG07a], i.e., the inpainted image is computed in a twostep process. In the first step Cahn-Hilliard inpainting is solved with a rather large value of ϵ , e.g., $\epsilon = 0.1$, until the numerical scheme is close to steady state. In this step the level lines are continued into the missing domain. In a second step the result of the first step is put as an initial condition into the scheme for a small ϵ , e.g., $\epsilon = 0.01$, in order to sharpen the contours of the image contents. The reason for this two step procedure is twofold. First of all in [BEG07b] the authors give numerical evidence that the steady state of the modified Cahn-Hilliard equation (2.1) is not unique, i.e., it is dependent on the initial condition for the equation. As a consequence, computing the inpainted image by the application of Cahn-Hilliard inpainting with a small ϵ only, might not prolongate the level lines into the missing domain as desired. See also [BEG07b] for a bifurcation diagram based on the numerical computations of the authors. The second reason for solving Cahn-Hilliard inpainting in two steps is that it is computationally less expensive. Solving the above time-marching scheme for, e.g., $\epsilon = 0.1$ is faster than solving it for $\epsilon = 0.01$. This is because of a damping introduced by ϵ into the scheme, cf. Section 4.1.2 for details.

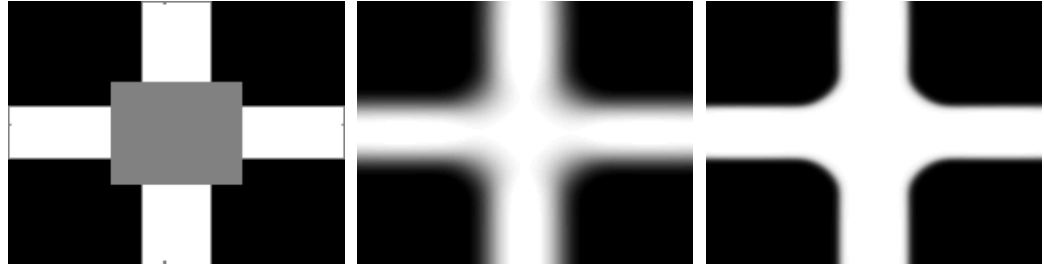


Figure 2.1: Destroyed binary image and the solution of Cahn-Hilliard inpainting with switching ϵ value: $u(1200)$ with $\epsilon = 0.1$, $u(2400)$ with $\epsilon = 0.01$



Figure 2.2: Destroyed binary image and the solution of Cahn-Hilliard inpainting with $\lambda_0 = 10^9$ and switching ϵ value: $u(800)$ with $\epsilon = 0.8$, $u(1600)$ with $\epsilon = 0.01$

2.1.3 Neumann Boundary Conditions and the Space $H_\partial^{-1}(\Omega)$

In this section we want to pose the Cahn-Hilliard inpainting problem with Neumann boundary conditions in a way such that the analysis from Section 2.1.1 can be carried out in a similar way. Namely we consider

$$\begin{cases} u_t = \Delta(-\epsilon\Delta u + \frac{1}{\epsilon}F'(u)) + \lambda(f - u) & \text{in } \Omega, \\ \frac{\partial u}{\partial \nu} = \frac{\partial \Delta u}{\partial \nu} = 0 & \text{on } \partial\Omega, \end{cases}$$

For the existence of a stationary solution of this equation we consider again a fixed point approach similar to (2.8) in the case of Dirichlet boundary conditions, i.e.,

$$\begin{cases} \frac{u - v}{\tau} = \Delta(-\epsilon\Delta u + \frac{1}{\epsilon}F'(u)) + \lambda(f - u) + (\lambda_0 - \lambda)(v - u) & \text{in } \Omega, \\ \frac{\partial u}{\partial \nu} = \frac{\partial (\epsilon\Delta u - \frac{1}{\epsilon}F'(u))}{\partial \nu} = 0 & \text{on } \partial\Omega. \end{cases} \quad (2.21)$$

To reformulate the above equation in terms of the operator Δ^{-1} with Neumann boundary conditions we first have to introduce the space $H_\partial^{-1}(\Omega)$ in which the operator Δ^{-1} is now the inverse of $-\Delta$ with Neumann boundary conditions.

Thus we define the non-standard Hilbert space

$$H_\partial^{-1}(\Omega) = \left\{ F \in H^1(\Omega)^* \mid \langle F, 1 \rangle_{(H^1)^*, H^1} = 0 \right\}.$$

Since Ω is bounded we know that $1 \in H^1(\Omega)$, hence $H_\partial^{-1}(\Omega)$ is well defined. Before we define a norm and an inner product on $H_\partial^{-1}(\Omega)$ we have to define more spaces. Let

$$H_\phi^1(\Omega) = \left\{ \psi \in H^1(\Omega) : \int_\Omega \psi \, dx = 0 \right\},$$

with norm $\|u\|_{H_\phi^1} := \|\nabla u\|_2$ and inner product $\langle u, v \rangle_{H_\phi^1} := \langle \nabla u, \nabla v \rangle_2$. This is a Hilbert space and the norms $\|\cdot\|_1$ and $\|\cdot\|_{H_\phi^1}$ are equivalent (up to constants) on $H_\phi^1(\Omega)$. Let $(H_\phi^1(\Omega))^*$ denote the dual of $H_\phi^1(\Omega)$. We will use $(H_\phi^1(\Omega))^*$ to induce an inner product on $H_\partial^{-1}(\Omega)$. Given $F \in (H_\phi^1(\Omega))^*$ with associate $u \in H_\phi^1(\Omega)$ (from the Riesz representation theorem) we have by definition

$$\langle F, \psi \rangle_{(H_\phi^1)^*, H_\phi^1} = \langle u, \psi \rangle_{H_\phi^1} = \langle \nabla u, \nabla \psi \rangle_2 \quad \forall \psi \in H_\phi^1(\Omega).$$

Let us now define a norm and an inner product on $H_\partial^{-1}(\Omega)$.

Definition 2.1.6.

$$\begin{aligned} H_\partial^{-1}(\Omega) &:= \left\{ F \in H^1(\Omega)^* \mid \langle F, 1 \rangle_{(H^1)^*, H^1} = 0 \right\} \\ \|F\|_{H_\partial^{-1}} &:= \|F| H_\phi^1\|_{(H_\phi^1)^*} \\ \langle F_1, F_2 \rangle_{H_\partial^{-1}} &:= \langle \nabla u_1, \nabla u_2 \rangle_2, \end{aligned}$$

where $F_1, F_2 \in H_\partial^{-1}(\Omega)$ and where $u_1, u_2 \in H_\phi^1(\Omega)$ are the associates of $F_1| H_\phi^1$, $F_2| H_\phi^1 \in (H_\phi^1(\Omega))^*$.

At this point it is not entirely obvious that $H_\partial^{-1}(\Omega)$ is a Hilbert space. That this is the case though is verified in the following theorem.

Theorem 2.1.7. 1. $H_\partial^{-1}(\Omega)$ is closed in $(H^1(\Omega))^*$.

2. The norms $\|\cdot\|_{H_\partial^{-1}}$ and $\|\cdot\|_{(H^1)^*}$ are equivalent on $H_\partial^{-1}(\Omega)$.

Theorem 2.1.7 can be easily checked just by the application of the definitions and the fact that the norms $\|\cdot\|_1$ and $\|\cdot\|_{H_\phi^1}$ are equivalent on $H_\phi^1(\Omega)$. From point 1. of Theorem 2.1.7 we have that $H_\partial^{-1}(\Omega)$ is a Hilbert space w.r.t. the $(H^1(\Omega))^*$ norm and point 2. tells us that the norms $\|\cdot\|_{H_\partial^{-1}}$ and $\|\cdot\|_{(H^1)^*}$ are equivalent on $H_\partial^{-1}(\Omega)$.

Therefore the norm in Definition 2.1.6 is well defined and $H_\partial^{-1}(\Omega)$ is a Hilbert space w.r.t. $\|.\|_{H_\partial^{-1}}$.

In the following we want to characterize elements $F \in H_\partial^{-1}(\Omega)$. By the above definition we have for each $F \in H_\partial^{-1}(\Omega)$ that there exists a unique element $u \in H_\phi^1(\Omega)$ such that

$$\langle F, \psi \rangle_{(H^1)^*, H^1} = \int_{\Omega} \nabla u \cdot \nabla \psi \, dx, \quad \forall \psi \in H_\phi^1(\Omega). \quad (2.22)$$

We define

$$\Delta^{-1} F := u \quad (2.23)$$

the unique solution to (2.22).

Now let $F \in L^2(\Omega)$ and assume $u \in H^2(\Omega)$. Set $\langle F, \psi \rangle_{(H^1)^*, H^1} := \int_{\Omega} F \psi \, dx$. Because $L^2(\Omega) \subset H_\partial^{-1}(\Omega)$ an element F is also an element in $H_\partial^{-1}(\Omega)$. Thus there exists a unique element $u \in H_\phi^1(\Omega)$ such that

$$\int_{\Omega} (-\Delta u - F) \psi \, dx + \int_{\partial\Omega} \nabla u \cdot \nu \psi \, d\mathcal{H}_1 = 0, \quad \forall \psi \in H_\phi^1(\Omega).$$

Since $\langle F, 1 \rangle_{(H^1)^*, H^1} = 0$, we see that $\langle F, \psi + K \rangle_{(H^1)^*, H^1} = \langle F, \psi \rangle_{(H^1)^*, H^1}$ for all constants $K \in \mathbb{R}$ and therefore (2.22) extends to all $\psi \in H^1(\Omega)$. Therefore $u \in H_\phi^1(\Omega)$ is the unique weak solution of the following problem:

$$\begin{cases} -\Delta u - F = 0 & \text{in } \Omega \\ \nabla u \cdot \nu = 0 & \text{on } \partial\Omega. \end{cases} \quad (2.24)$$

Remark 2.1.8. With the above characterization of elements $F \in H_\partial^{-1}(\Omega)$ and the notation (2.23) for its associates the inner product and the norm in H_∂^{-1} can be written as

$$\langle F_1, F_2 \rangle_{H_\partial^{-1}} := \int_{\Omega} \nabla \Delta^{-1} F_1 \cdot \nabla \Delta^{-1} F_2 \, dx, \quad \forall F_1, F_2 \in H_\partial^{-1}(\Omega),$$

and norm

$$\|F\|_{H_\partial^{-1}} := \sqrt{\int_{\Omega} (\nabla \Delta^{-1} F)^2 \, dx}.$$

Throughout the rest of this section we will write the short forms $\langle ., . \rangle_{-1}$ and $\|.\|_{-1}$ for the inner product and the norm in $H_\partial^{-1}(\Omega)$ respectively. Note that this notation is only valid within this section.

It is important to notice that in order to rewrite (2.21) in terms of Δ^{-1} we require the "right hand side" of the equation, i.e., $\frac{u-v}{\tau} + \lambda(u-f) + (\lambda_0 - \lambda)(u-v)$ to be an

element of our new space $H_\partial^{-1}(\Omega)$ (cf. Definition 2.1.6). In other words the "right hand side" has to have zero mean over Ω . Because we cannot guarantee this property for solutions of the fixed point equation (2.21) we are going to modify the right hand side by subtracting its mean. Let

$$\begin{aligned} F_\Omega &= \frac{1}{\tau} F_\Omega^1 + \lambda_0 F_\Omega^2 \\ F_\Omega^1 &= \frac{1}{|\Omega|} \int_\Omega (u - v) \, dx \\ F_\Omega^2 &= \frac{1}{|\Omega|} \int_\Omega \frac{\lambda}{\lambda_0} (u - f) + \left(1 - \frac{\lambda}{\lambda_0}\right) (u - v) \, dx, \end{aligned}$$

and consider instead of (2.21) the equation

$$\begin{cases} \epsilon \Delta u - \frac{1}{\epsilon} F'(u) = \Delta^{-1} \left(\frac{u - v}{\tau} - \lambda(f - u) - (\lambda_0 - \lambda)(v - u) - F_\Omega \right) & \text{in } \Omega, \\ \frac{\partial u}{\partial \nu} = 0 & \text{on } \partial\Omega, \end{cases}$$

where the second Neumann boundary condition $\frac{\partial(\epsilon \Delta u - \frac{1}{\epsilon} F'(u))}{\partial \nu} = 0$ on $\partial\Omega$ is included in the definition of Δ^{-1} . The functional of the corresponding variational formulation then reads

$$\begin{aligned} J^\epsilon(u, v) &= \int_\Omega \left(\frac{\epsilon}{2} |\nabla u|^2 + \frac{1}{\epsilon} F(u) \right) \, dx + \frac{1}{2\tau} \|(u - v) - F_\Omega^1\|_{-1}^2 \\ &\quad + \frac{\lambda_0}{2} \left\| \left(u - \frac{\lambda}{\lambda_0} f - \left(1 - \frac{\lambda}{\lambda_0}\right) v \right) - F_\Omega^2 \right\|_{-1}^2. \end{aligned}$$

With these definitions the proof for the existence of a stationary solution for the modified Cahn-Hilliard equation with Neumann boundary conditions can be carried out similarly to the proof in Section 2.1.1. Note that every solution of (2.1) fulfills $\frac{d}{dt} \int_\Omega u \, dx = \int_\Omega \lambda(f - u) \, dx$. This means that for a stationary solution \hat{u} the integral $C \int_\Omega \lambda(f - u) \, dx = 0$ for every constant $C \in \mathbb{R}$ (i.e., the "right hand side" has zero mean and therefore $F_\Omega^1 = F_\Omega^2 = 0$).

2.2 TV-H⁻¹Inpainting

Let $\Omega \subset \mathbb{R}^d$, for $d = 1, 2$ be a bounded open set with Lipschitz boundary, and $H = L^2(\Omega)$. We recall that for $u \in L^1_{loc}(\Omega)$

$$V(u, \Omega) := \sup \left\{ \int_\Omega u \nabla \cdot \varphi \, dx : \varphi \in [C_c^1(\Omega)]^d, \|\varphi\|_\infty \leq 1 \right\} \quad (2.25)$$

is the variation of u and that $u \in BV(\Omega)$ (the space of functions of bounded variation, [AFP00, EG92]) if and only if $V(u, \Omega) < \infty$, see [AFP00, Proposition 3.6]. In such a case, $|D(u)|(\Omega) = V(u, \Omega)$, where $|D(u)|(\Omega)$ is the total variation (TV) of the finite Radon measure Du , the derivative of u in the sense of distributions. For more details about the total variation and the space of functions of bounded variation we refer to Appendix A.5.

The minimization of energies with total variation constraints, i.e.,

$$\min_{u \in BV(\Omega)} \left\{ \|Tu - f\|_H^2 + 2\alpha|D(u)|(\Omega) \right\}, \quad (2.26)$$

for a given $f \in \mathcal{H}$, where \mathcal{H} is a suitable Hilbert space, e.g., $\mathcal{H} = L^2(\Omega)$, and $T \in \mathcal{L}(\mathcal{H})$ is a linear bounded operator in \mathcal{H} , traces back to the first uses of such a functional model in noise removal in digital images as proposed by Rudin, Osher, and Fatemi [ROF92]. There the operator T is just the identity. Extensions to more general operators T and numerical methods for the minimization of the functional appeared later in several important contributions [CL97, DV97, AV97, Ve01, Ch04]. From these pioneering and very successful results, the scientific output related to total variation minimization and its applications in signal and image processing increased dramatically in the last decade. For brevity we do not list here all the possible directions and contributions.

Now, after the result about a stationary solution for the Cahn-Hilliard inpainting approach (2.1) presented in Section 2.1, the second contribution of [BHS08] is to generalize the latter approach to grayvalue images. This is realized by using subgradients of the TV functional within the flow, which leads to structure inpainting with smooth curvature of level sets. In the present section the results about this new inpainting approach shall be reported.

We motivate this new approach by a Γ -convergence result for the Cahn-Hilliard energy. In fact we prove that the sequence of functionals for an appropriate time-discrete Cahn-Hilliard inpainting approach Γ -converges to a functional regularized with the total variation for binary arguments $u = \mathbf{1}_E$, where E is some Borel measurable subset of Ω . This is stated in more detail in the following Theorem.

Throughout this section we keep to the notation, and the definitions from Section 2.1, i.e., $\Omega \subset \mathbb{R}^2$ is a bounded open set with Lipschitz boundary, $D \subset \Omega$ denotes the inpainting domain, and λ is the indicator function of $\Omega \setminus D$ multiplied by a constant $\lambda_0 \gg 1$ as defined in (1.2).

Theorem 2.2.1. Let $f, v \in L^2(\Omega)$ be two given functions, and $\tau > 0$ a positive parameter. Let further $\|\cdot\|_{-1}$ be the norm in $H^{-1}(\Omega)$, defined in more detail in the Appendix A.4, and $\epsilon > 0$ a parameter. Then the sequence of functionals

$$\mathcal{J}^\epsilon(u, v) = \int_\Omega \left(\frac{\epsilon}{2} |\nabla u|^2 + \frac{1}{\epsilon} F(u) \right) dx + \frac{1}{2\tau} \|u - v\|_{-1}^2 + \frac{\lambda_0}{2} \left\| u - \frac{\lambda}{\lambda_0} f - \left(1 - \frac{\lambda}{\lambda_0}\right) v \right\|_{-1}^2$$

Γ -converges for $\epsilon \rightarrow 0$ in the topology of $L^1(\Omega)$ to

$$\mathcal{J}(u, v) = TV(u) + \frac{1}{2\tau} \|u - v\|_{-1}^2 + \frac{\lambda_0}{2} \left\| u - \frac{\lambda}{\lambda_0} f - \left(1 - \frac{\lambda}{\lambda_0}\right) v \right\|_{-1}^2,$$

where

$$TV(u) = \begin{cases} C_0 |Du|(\Omega) & \text{if } u = \mathbf{1}_E \text{ for some Borel measurable subset } E \subset \Omega \\ +\infty & \text{otherwise,} \end{cases}$$

$\mathbf{1}_E$ denoting the indicator function of E and $C_0 = 2 \int_0^1 \sqrt{F(s)} ds$.

Remark 2.2.2. Setting $v = u_k$ and a minimizer u of the functional $\mathcal{J}^\epsilon(u, v)$ to be $u = u_{k+1}$, the minimization of \mathcal{J}^ϵ can be seen as an iterative approach with stepsize τ to solve (2.1).

Remark 2.2.3. The Γ -convergence of the Ginzburg-Landau energy $\int_\Omega (\epsilon/2 |\nabla u|^2 + 1/\epsilon F(u)) dx$ to the total variation of an indicator function for a subset of Ω goes back to Modica and Mortola [MM77a, MM77b]. Their result can also be understood in terms of a sharp interface limit. In other words, the limit of the energy of a phase field model (the Ginzburg-Landau energy), where black (0) and white (1) regions are separated by a transition layer of order ϵ , was shown to be a model that describes the motion of the sharp interface between these regions without transition layer, i.e., $\epsilon = 0$. Similar results have been shown for the Cahn-Hilliard equation directly. Here, the corresponding sharp interface limit is known as the Mullins-Sekerka problem or Hele-Shaw problem, cf. [MS63, Pe89, ABC94, St96].

Now, by extending the validity of the total variation functional $TV(u)$ from functions $u = 0$ or 1 to functions $|u| \leq 1$ we receive an inpainting approach for grayvalue images rather than binary images. We shall call this new inpainting approach TV-H⁻¹inpainting and define it in the following way: The inpainted image u of $f \in L^2(\Omega)$, shall evolve via

$$u_t = \Delta p + \lambda(f - u), \quad p \in \partial TV(u), \tag{2.27}$$

with

$$TV(u) = \begin{cases} |Du|(\Omega) & \text{if } |u(x)| \leq 1 \text{ a.e. in } \Omega \\ +\infty & \text{otherwise.} \end{cases} \quad (2.28)$$

Here, $\partial TV(u)$ denotes the subdifferential of the functional $TV(u)$ (cf. Appendix A.2 for the definition). The L^∞ bound in the definition of the TV functional (2.28) is quite natural as we are only considering digital images u whose grayvalue can be scaled to $[-1, 1]$. It is further motivated by the Γ -convergence result of Theorem 2.2.1.

Remark 2.2.4. *Similar to the use of the functional \mathcal{J}^ϵ from Theorem 2.2.1 as an iterative approach to solve (2.1) (cf. Remark 2.2.2), the functional \mathcal{J} from Theorem 2.2.1 might serve as an iterative process to solve (2.27).*

A similar form of the TV-H⁻¹inpainting approach already appeared in the context of decomposition and restoration of grayvalue images, see for example [VO03, OSV03, LV08]. Different to the situation of TV-H⁻¹denoising / decomposition the TV-H⁻¹inpainting approach does not exhibit a variational formulation and hence, its analytical and numerical treatment is different. Further, in Bertalmio et al. [BVSO03] an application of the model from [VO03] to image inpainting has been proposed. In contrast to the inpainting approach (2.27) the authors in [BVSO03] only use a different form of the TV-H⁻¹approach for a decomposition of the image into cartoon and texture prior to the inpainting process, which is accomplished with the method presented in [BSCB00].

Using the same methodology as in the proof of Theorem 2.1.1 we obtain the following existence theorem,

Theorem 2.2.5. *Let $f \in L^2(\Omega)$. The stationary equation*

$$\Delta p + \lambda(f - u) = 0, \quad p \in \partial TV(u) \quad (2.29)$$

admits a solution $u \in BV(\Omega)$.

We shall also give a characterization of elements in the subdifferential $\partial TV(u)$ for $TV(u)$ defined as in (2.28), i.e., $TV(u) = |Du|(\Omega) + \chi_1(u)$, where

$$\chi_1(u) = \begin{cases} 0 & \text{if } |u| \leq 1 \text{ a.e. in } \Omega \\ +\infty & \text{otherwise.} \end{cases}$$

Namely, we shall prove the following theorem.

Theorem 2.2.6. Let $\tilde{p} \in \partial\chi_1(u)$. An element $p \in \partial TV(u)$ with $|u(x)| \leq 1$ in Ω , fulfills the following set of equations

$$\begin{aligned} p &= -\nabla \cdot \left(\frac{\nabla u}{|\nabla u|} \right) && \text{a.e. on } \text{supp}(\{|u| < 1\}) \\ p &= -\nabla \cdot \left(\frac{\nabla u}{|\nabla u|} \right) + \tilde{p}, \tilde{p} \leq 0 && \text{a.e. on } \text{supp}(\{u = -1\}) \\ p &= -\nabla \cdot \left(\frac{\nabla u}{|\nabla u|} \right) + \tilde{p}, \tilde{p} \geq 0 && \text{a.e. on } \text{supp}(\{u = 1\}). \end{aligned}$$

For (2.27) we additionally give error estimates for the inpainting error and stability information in terms of the Bregman distance. Let f_{true} be the original image and \hat{u} a stationary solution of (2.27). In our considerations we use the symmetric Bregman distance defined as

$$D_{TV}^{symm}(\hat{u}, f_{true}) = \langle \hat{u} - f_{true}, \hat{p} - \xi \rangle_2, \quad \hat{p} \in \partial TV(\hat{u}), \xi \in \partial TV(f_{true}).$$

We prove the following result

Theorem 2.2.7. Let f_{true} fulfill the so-called source condition, namely that

there exists $\xi \in \partial TV(f_{true})$ such that $\xi = \Delta^{-1}q$ for a source element $q \in H^{-1}(\Omega)$,

and $\hat{u} \in BV(\Omega)$ be a stationary solution of (2.27) given by $\hat{u} = u^s + u^d$, where u^s is a smooth function and u^d is a piecewise constant function. Then the inpainting error reads

$$D_{TV}^{symm}(\hat{u}, f_{true}) + \frac{\lambda_0}{2} \|\hat{u} - f_{true}\|_{-1}^2 \leq \frac{1}{\lambda_0} \|\xi\|_1^2 + C\lambda_0 |D|^{(r-2)/r} \text{err}_{\text{inpaint}},$$

with $2 < r < \infty$, constant $C > 0$ and

$$\text{err}_{\text{inpaint}} := K_1 + K_2 \left(|D| C(M(u^s), \beta) + 2 |R(u^d)| \right),$$

where K_1 and K_2 are appropriate positive constants, and C is a constant depending on the smoothness bound $M(u^s)$ for u^s and β that is determined from the shape of D . The error region $R(u^d)$ is determined by the level lines of u^d .

Finally we present numerical results for the proposed TV-H⁻¹inpainting approach and briefly explain the numerical implementation. Let us continue with the verification of the stated results in Theorems 2.2.1-2.2.7.

2.2.1 Γ-Convergence of the Cahn-Hilliard Energy

In the following we want to motivate our new inpainting approach (2.27) by considering the Γ-limit for $\epsilon \rightarrow 0$ of an appropriate time-discrete Cahn-Hilliard inpainting approach, i.e., the Γ-limit of the functionals from our fixed point approach in (2.11). More precisely we want to prove Theorem 2.2.1. Before starting our discussion let us recall the definition of Γ-convergence and its impact within the study of optimization problems. For more details on Γ-convergence we refer to [Ma93].

Definition 2.2.8. Let $X = (X, d)$ be a metric space and (F_h) , $h \in \mathbb{N}$ be family of functions $F_h : X \rightarrow [0, +\infty]$. We say that (F_h) **Γ-converges** to a function $F : X \rightarrow [0, +\infty]$ on X as $h \rightarrow \infty$ if $\forall x \in X$ we have

(i) for every sequence x_h with $d(x_h, x) \rightarrow 0$ we have

$$F(x) \leq \liminf_h F_h(x_h);$$

(ii) there exists a sequence \bar{x}_h such that $d(\bar{x}_h, x) \rightarrow 0$ and

$$F(x) = \lim_h F_h(\bar{x}_h)$$

(or, equivalently, $F(x) \geq \limsup_h F_h(\bar{x}_h)$).

Then F is the Γ-limit of (F_h) in X and we write: $F(x) = \Gamma - \lim_h F_h(x)$, $x \in X$.

The formulation of the Γ-limit for $\epsilon \rightarrow 0$ is analogous by defining a sequence ϵ_h with $\epsilon_h \rightarrow 0$ as $h \rightarrow \infty$.

The important property of Γ-convergent sequences of functions F_h is that their minima converge to minima of the Γ-limit F . In fact we have the following theorem

Theorem 2.2.9. Let (F_h) be like in Definition 2.2.8 and additionally equicoercive, that is there exists a compact set $K \subset X$ (independent of h) such that

$$\inf_{x \in X} \{F_h(x)\} = \inf_{x \in K} \{F_h(x)\}.$$

If F_h Γ-converges on X to a function F we have

$$\min_{x \in X} \{F(x)\} = \lim \inf_h \inf_{x \in X} \{F_h(x)\}.$$

After recalling these facts about Γ-convergence we continue this section with the proof of Theorem 2.2.1.

Proof of Theorem 2.2.1. Modica and Mortola have shown in [MM77a, MM77b] that the sequence of Cahn-Hilliard functionals

$$CH(u) = \int_{\Omega} \left(\frac{\epsilon}{2} |\nabla u|^2 + \frac{1}{\epsilon} F(u) \right) dx$$

Γ -converges in the topology $L^1(\Omega)$ to

$$TV(u) = \begin{cases} C_0 |Du|(\Omega) & \text{if } u = \mathbf{1}_E \text{ for some Borel measurable subset } E \subset \Omega \\ +\infty & \text{otherwise} \end{cases}$$

as $\epsilon \rightarrow 0$, where $C_0 = 2 \int_0^1 \sqrt{F(s)} ds$. (The space $BV(\Omega)$ and the total variation $|Du|(\Omega)$ are defined in the Appendix in Section A.5.)

Now, for a given function $v \in L^2(\Omega)$ the functional \mathcal{J}^ϵ from our fixed point approach (2.8), i.e.,

$$\mathcal{J}^\epsilon(u, v) = \underbrace{\int_{\Omega} \left(\frac{\epsilon}{2} |\nabla u|^2 + \frac{1}{\epsilon} F(u) \right) dx}_{:=CH(u)} + \underbrace{\frac{1}{2\tau} \|u - v\|_{-1}^2}_{:=D(u,v)} + \underbrace{\frac{\lambda_0}{2} \left\| u - \frac{\lambda}{\lambda_0} f - (1 - \frac{\lambda}{\lambda_0})v \right\|_{-1}^2}_{:=FIT(u,v)},$$

is the sum of the regularizing term $CH(u)$, the damping term $D(u, v)$ and the fitting term $FIT(u, v)$. We recall the following fact,

Theorem 2.2.10. [Ma93, Dal Maso, Proposition 6.21.] Let $G : X \rightarrow \mathbb{R}$ be a continuous function and (F_h) Γ -converges to F in X , then $(F_h + G)$ Γ -converges to $F + G$ in X .

Since the H^{-1} -norm is continuous in $H^{-1}(\Omega)$ and hence in particular in $L^1(\Omega)$, the two terms in \mathcal{J}^ϵ that are independent from ϵ , i.e., $D(u, v)$ and $FIT(u, v)$, are continuous in $L^1(\Omega)$. Together with the Γ -convergence result of Modica and Mortola for the Cahn-Hilliard energy, we have proven that the modified Cahn-Hilliard functional \mathcal{J}^ϵ can be seen as a regularized approximation in the sense of Γ -convergence of the TV-functional

$$\mathcal{J}(u, v) = TV(u) + D(u, v) + FIT(u, v),$$

for functions $u \in BV(\Omega)$ with $u(x) = \mathbf{1}_E$ for a Borel measurable subset $E \subset \Omega$. In fact we have gone from a smooth transition layer between 0 and 1 in the Cahn-Hilliard inpainting approach (depending on the size of ϵ) to a sharp interface limit in which the image function now jumps from 0 to 1. \square

This sharp interface limit motivates the extension of $\mathcal{J}(u, v)$ to grayvalue functions such that $|u| \leq 1$ on Ω and hence leads us from the Cahn-Hilliard inpainting approach for binary images to a generalization for grayvalue images, namely our so-called TV-H⁻¹inpainting method (2.27)-(2.28).

2.2.2 Existence of a Stationary Solution

Our strategy for proving the existence of a stationary solution for TV-H⁻¹inpainting (2.27) is similar to our existence proof for a stationary solution of the modified Cahn-Hilliard equation (2.1) in Section 2.1.1. Similarly as in our analysis for (2.1) in Section 2.1.1, we consider equation (2.27) with Dirichlet boundary conditions, namely

$$\begin{aligned} u_t &= \Delta p + \lambda(f - u) && \text{in } \Omega \\ u &= f && \text{on } \partial\Omega, \end{aligned}$$

for $p \in \partial TV(u)$.

Now let $f \in L^2(\Omega)$, $|f| \leq 1$ be the given grayvalue image. For $v \in L^r(\Omega)$, $1 < r < 2$, we consider the minimization problem

$$u^* = \arg \min_{u \in BV(\Omega)} \mathcal{J}(u, v),$$

with functionals

$$\mathcal{J}(u, v) := TV(u) + \underbrace{\frac{1}{2\tau} \|u - v\|_{-1}^2}_{D(u,v)} + \underbrace{\frac{\lambda_0}{2} \|u - \frac{\lambda}{\lambda_0} f - (1 - \frac{\lambda}{\lambda_0})v\|_{-1}^2}_{FIT(u,v)}, \quad (2.30)$$

with $TV(u)$ defined as in (2.28). Note that $L^r(\Omega)$ can be continuously embedded in $H^{-1}(\Omega)$. Hence the functionals in (2.30) are well defined.

First we will show that for a given $v \in L^r(\Omega)$ the functional $\mathcal{J}(\cdot, v)$ attains a unique minimizer $u^* \in BV(\Omega)$ with $|u^*(x)| \leq 1$ a.e. in Ω .

Proposition 2.2.11. *Let $f \in L^2(\Omega)$ be given with $|f(x)| \leq 1$ a.e. in Ω and $v \in L^r(\Omega)$. Then the functional $\mathcal{J}(\cdot, v)$ has a unique minimizer $u^* \in BV(\Omega)$ with $|u^*(x)| \leq 1$ a.e. in Ω .*

Proof. Let $(u^n)_{n \in \mathbb{N}}$ be a minimizing sequence for $\mathcal{J}(u, v)$, i.e.,

$$\mathcal{J}(u^n, v) \xrightarrow{n \rightarrow \infty} \inf_{u \in BV(\Omega)} \mathcal{J}(u, v).$$

Then $u^n \in BV(\Omega)$ and $|u^n(x)| \leq 1$ in Ω (because otherwise $TV(u^n)$ would not be finite). Therefore

$$|Du^n|(\Omega) \leq M, \quad \text{for an } M \geq 0 \text{ and for all } n \geq 1,$$

and, because of the uniform boundedness of $|u(x)|$ for every point $x \in \Omega$,

$$\|u^n\|_{L^p(\Omega)} \leq \tilde{M}, \text{ for an } \tilde{M} \geq 0, \forall n \geq 1, \text{ and } 1 \leq p \leq \infty.$$

Thus u^n is uniformly bounded in $L^p(\Omega)$ and in particular in $L^1(\Omega)$. Together with the boundedness of $|Du^n|(\Omega)$, the sequence u^n is also bounded in $BV(\Omega)$ and there exists a subsequence, still denoted u^n , and a $u \in BV(\Omega)$ such that $u^n \rightharpoonup u$ weakly in $L^p(\Omega)$, $1 \leq p \leq \infty$ and weakly* in $BV(\Omega)$. Because $L^2(\Omega) \subset L^2(\mathbb{R}^2) \subset H^{-1}(\Omega)$ (by zero extensions of functions on Ω to \mathbb{R}^2) $u^n \rightharpoonup u$ also weakly in $H^{-1}(\Omega)$. Because $|Du|(\Omega)$ is lower semicontinuous in $BV(\Omega)$ and by the lower semicontinuity of the H^{-1} norm we get

$$\begin{aligned} \mathcal{J}(u, v) &= TV(u) + D(u, v) + FIT(u, v) \\ &\leq \liminf_{n \rightarrow \infty} (TV(u_n) + D(u_n, v) + FIT(u_n, v)) \\ &= \liminf_{n \rightarrow \infty} \mathcal{J}(u_n, v). \end{aligned}$$

So u is a minimizer of $\mathcal{J}(u, v)$ over $BV(\Omega)$.

To prove the uniqueness of the minimizer we (similarly as in the proof of Theorem 2.1.3) show that \mathcal{J} is strictly convex. Namely we prove that for all $u_1, u_2 \in BV(\Omega)$, $u_1 \neq u_2$

$$\mathcal{J}(u_1, v) + \mathcal{J}(u_2, v) - 2\mathcal{J}\left(\frac{u_1 + u_2}{2}, v\right) > 0.$$

We have

$$\begin{aligned} &\mathcal{J}(u_1, v) + \mathcal{J}(u_2, v) - 2\mathcal{J}\left(\frac{u_1 + u_2}{2}, v\right) \\ &= \left(\frac{1}{2\tau} + \frac{\lambda_0}{2}\right) \left(\|u_1\|_{-1}^2 + \|u_2\|_{-1}^2 - 2 \left\| \frac{u_1 + u_2}{2} \right\|_{-1}^2 \right) \\ &\quad + TV(u_1) + TV(u_2) - 2TV\left(\frac{u_1 + u_2}{2}\right) \\ &\geq \left(\frac{1}{4\tau} + \frac{\lambda_0}{4}\right) \|u_1 - u_2\|_{-1}^2 > 0. \end{aligned}$$

This finishes the proof. \square

Next we shall prove the existence of stationary solution for (2.27). For this end we consider the corresponding Euler-Lagrange equation to (2.30), i.e.,

$$\Delta^{-1} \left(\frac{u - v}{\tau} \right) + p - \Delta^{-1} (\lambda(f - u) + (\lambda_0 - \lambda)(v - u)) = 0,$$

with weak formulation

$$\left\langle \frac{1}{\tau}(u - v), \phi \right\rangle_{-1} + \langle p, \phi \rangle_2 - \langle \lambda(f - u) + (\lambda_0 - \lambda)(v - u), \phi \rangle_{-1} = 0 \quad \forall \phi \in H_0^1(\Omega).$$

A fixed point of the above equation, i.e., a solution $u = v$, is then a stationary solution for (2.27). Thus, to prove the existence of a stationary solution of (2.27), i.e., to prove Theorem 2.2.5, as before we are going to use a fixed point argument. Let $\mathcal{A} : L^r(\Omega) \rightarrow L^r(\Omega)$, $1 < r < 2$, be the operator which maps a given $v \in L^r(\Omega)$ to $\mathcal{A}(v) = u$ under the condition that $\mathcal{A}(v) = u$ is the minimizer of the functional $\mathcal{J}(\cdot, v)$ defined in (2.30). The choice of the fixed point operator \mathcal{A} over $L^r(\Omega)$ was made in order to obtain the necessary compactness and continuity properties for the application of Schauder's theorem.

Since here the treatment of the boundary conditions is similar to that in Section 2.1.1, we will leave this part of the analysis in the upcoming proof to the reader and just carry out the proof without explicitly taking care of the boundary.

Proof of Theorem 2.2.5. Let $\mathcal{A} : L^r(\Omega) \rightarrow L^r(\Omega)$, $1 < r < 2$, be the operator that maps a given $v \in L^r(\Omega)$ to $\mathcal{A}(v) = u$, where u is the unique minimizer of the functional $\mathcal{J}(\cdot, v)$ defined in (2.30). Existence and uniqueness u follow from Proposition 2.2.11. Since u minimizes $\mathcal{J}(\cdot, v)$ we have $u \in L^\infty(\Omega)$ hence $u \in L^r(\Omega)$. Additionally we have $\mathcal{J}(u, v) \leq \mathcal{J}(0, v)$, i.e.,

$$\begin{aligned} \frac{1}{2\tau} \|u - v\|_{-1}^2 + \frac{\lambda_0}{2} \|u - \frac{\lambda}{\lambda_0} f - (1 - \frac{\lambda}{\lambda_0})v\|_{-1}^2 + TV(u) \\ \leq \frac{1}{2\tau} \|v\|_{-1}^2 + \frac{\lambda_0}{2} \|\frac{\lambda}{\lambda_0} f + (1 - \frac{\lambda}{\lambda_0})v\|_{-1}^2 \leq \frac{|\Omega|}{2\tau} + \lambda_0(|\Omega| + |D|). \end{aligned}$$

Here the last inequality was obtained since $L^r(\Omega) \hookrightarrow H^{-1}(\Omega)$ and hence $\|v\|_{-1} \leq C$ and $\|\lambda v\|_{-1} \leq C$ for a $C > 0$. (In fact, since $H^1(\Omega) \hookrightarrow L^{r'}(\Omega)$ for all $1 \leq r' < \infty$ it follows from duality that $L^r(\Omega) \hookrightarrow H^{-1}(\Omega)$ for $1 < r < \infty$.) By the last estimate we obtain $u \in BV(\Omega)$. Since $BV(\Omega) \hookrightarrow L^r(\Omega)$ compactly for $1 \leq r < 2$ and $\Omega \subset \mathbb{R}^2$ (cf. Theorem A.5.7), the operator \mathcal{A} maps $L^r(\Omega) \rightarrow BV(\Omega) \hookrightarrow L^r(\Omega)$, i.e., $\mathcal{A} : L^r(\Omega) \rightarrow K$, where K is a compact subset of $L^r(\Omega)$. Thus, for $v \in B(0, 1)$ (where $B(0, 1)$ denotes the ball in $L^\infty(\Omega)$ with center 0 and radius 1), the operator $\mathcal{A} : B(0, 1) \rightarrow B(0, 1) \cap K = \tilde{K}$, where \tilde{K} is a compact and convex subset of $L^r(\Omega)$.

Next we have to show that \mathcal{A} is continuous in $L^r(\Omega)$. Let $(v_k)_{k \geq 0}$ be a sequence which converges to v in $L^r(\Omega)$. Then $u_k = \mathcal{A}(v_k)$ solves

$$\Delta p_k = \frac{u_k - v_k}{\tau} - (\lambda(f - u_k) + (\lambda_0 - \lambda)(v_k - u_k)),$$

where $p_k \in \partial TV(u_k)$. Thus u_k is uniformly bounded in $BV(\Omega) \cap L^\infty(\Omega)$ (and hence in $L^r(\Omega)$) and, since the right-hand side of the above equation is uniformly bounded in $L^r(\Omega)$, also Δp_k is bounded in $L^r(\Omega)$. Thus there exists a subsequence p_{k_l} such that $\Delta p_{k_l} \rightharpoonup \Delta p$ in $L^r(\Omega)$ and a subsequence u_{k_l} that converges weakly * to a u in $BV(\Omega) \cap L^\infty(\Omega)$. Since $BV(\Omega) \hookrightarrow L^r(\Omega)$ we have $u_{k_l} \rightarrow u$ strongly in $L^r(\Omega)$. Therefore the limit u solves

$$\Delta p = \frac{u - v}{\tau} - (\lambda(f - u) + (\lambda_0 - \lambda)(v - u)). \quad (2.31)$$

If we additionally apply Poincare's inequality to Δp_k we conclude that

$$\|\nabla p_k - (\nabla p_k)_\Omega\|_{L^r(\Omega)} \leq C \|\nabla \cdot (\nabla p_k - (\nabla p_k)_\Omega)\|_{L^r(\Omega)},$$

where $(\nabla p_k)_\Omega = \frac{1}{|\Omega|} \int_\Omega \nabla p_k \, dx$. In addition, since $p_k \in \partial TV(u_k)$, it follows that $(p_k)_\Omega = 0$ and $\|p_k\|_{BV^*(\Omega)} \leq 1$. Thus $(\nabla p_k)_\Omega < \infty$ and p_k is uniformly bounded in $W^{1,r}(\Omega)$. Thus there exists a subsequence p_{k_l} such that $p_{k_l} \rightharpoonup p$ in $W^{1,r}(\Omega)$. In addition $L^{r'}(\Omega) \hookrightarrow BV^*(\Omega)$ for $2 < r' < \infty$ (this follows again from Theorem A.5.7 by a duality argument) and $W^{1,r}(\Omega) \hookrightarrow L^q(\Omega)$ for $1 \leq q < \frac{2r}{2-r}$ (Rellich-Kondrachov Compactness Theorem, cf. Theorem A.3.1 in Appendix A.3). By choosing $2 < q < \frac{2r}{2-r}$ we therefore have $W^{1,r}(\Omega) \hookrightarrow BV^*(\Omega)$. Thus $p_{k_l} \rightarrow p$ strongly in $BV^*(\Omega)$. Hence the element p in (2.31) is an element in $\partial TV(u)$.

Because the minimizer of (2.30) is unique, $u = \mathcal{A}(v)$, and therefore \mathcal{A} is continuous in $L^r(\Omega)$. The existence of a stationary solution follows from Schauder's fixed point theorem. \square

2.2.3 Characterization of Solutions

Finally we want to compute elements $p \in \partial TV(u)$. In particular we shall prove Theorem 2.2.6. Like in [BRH07] the model for the regularizing functional is the sum of a standard regularizer plus the indicator function of the L^∞ constraint. In particular, we have $TV(u) = |Du|(\Omega) + \chi_1(u)$, where $|Du|(\Omega)$ is the total variation of Du and

$$\chi_1(u) = \begin{cases} 0 & \text{if } |u| \leq 1 \text{ a.e. in } \Omega \\ +\infty & \text{otherwise.} \end{cases} \quad (2.32)$$

We want to compute the subgradients of TV by assuming $\partial TV(u) = \partial |Du|(\Omega) + \partial \chi_1(u)$. This means that we can separately compute the subgradients of χ_1 . To guarantee that the splitting above is allowed we have to consider a regularized functional of

the total variation, like $\int_{\Omega} \sqrt{|\nabla u|^2 + \delta} dx$. This is sufficient because both $|D.|(\Omega)$ and χ_1 are convex and $|D.|(\Omega)$ is continuous (compare [ET76, Proposition 5.6., pp. 26]).

The subgradient $\partial|Du|(\Omega)$ is already well described, as, for instance, in [AK06, Ve01]. We will just briefly recall its characterization. Thereby we do not insist on the details of the rigorous derivation of these conditions, and we limit ourself to mentioning the main facts.

It is well known [Ve01, Proposition 4.1] that $p \in \partial|Du|(\Omega)$ implies

$$\begin{cases} p = -\nabla \cdot \left(\frac{\nabla u}{|\nabla u|} \right) & \text{in } \Omega \\ \frac{\nabla u}{|\nabla u|} \cdot \nu = 0 & \text{on } \partial\Omega. \end{cases}$$

The previous conditions do not fully characterize $p \in \partial|Du|(\Omega)$, additional conditions would be required [AK06, Ve01], but the latter are, unfortunately, hardly numerically implementable. Since we anyway consider a regularized version of $|Du|(\Omega)$, the subdifferential becomes a gradient which reads

$$\begin{cases} p = -\nabla \cdot \left(\frac{\nabla u}{\sqrt{|\nabla u|^2 + \delta}} \right) & \text{in } \Omega \\ \frac{\nabla u}{\sqrt{|\nabla u|^2 + \delta}} \cdot \nu = 0 & \text{on } \partial\Omega. \end{cases}$$

The subgradient of χ_1 is computed like in the following Lemma.

Lemma 2.2.12. *Let $\chi_1 : L^r(\Omega) \rightarrow \mathbb{R} \cup \{\infty\}$ be defined by (2.32), and let $1 \leq r \leq \infty$. Then $p \in L^{r^*}(\Omega)$, for $r^* = \frac{r}{r-1}$, is a subgradient $p \in \partial\chi_1(u)$ for $u \in L^r(\Omega)$ with $\chi_1(u) = 0$, if and only if*

$$\begin{aligned} p &= 0 && \text{a.e. on } \text{supp}(\{|u| < 1\}) \\ p &\leq 0 && \text{a.e. on } \text{supp}(\{u = -1\}) \\ p &\geq 0 && \text{a.e. on } \text{supp}(\{u = 1\}). \end{aligned}$$

Proof. Let $p \in \partial\chi_1(u)$. Then we can choose $v = u + \epsilon w$ for w being any bounded function supported in $\{|u| < 1 - \alpha\}$ for arbitrary $0 < \alpha < 1$. If ϵ is sufficiently small we have $|v| \leq 1$. Hence

$$0 \geq \langle v - u, p \rangle_2 = \epsilon \int_{\{|u| < 1 - \alpha\}} wp \, dx.$$

Since we can choose ϵ either positive or negative, we obtain

$$\int_{\{|u|<1-\alpha\}} wp \, dx = 0.$$

Because $0 < \alpha < 1$ and w are arbitrary we conclude that $p = 0$ on the support of $\{|u| < 1\}$. If we choose $v = u + w$ with w an arbitrary bounded function with

$$\begin{cases} 0 \leq w \leq 1 & \text{on } \text{supp}(\{-1 \leq u \leq 0\}) \\ w = 0 & \text{on } \text{supp}(\{0 < u \leq 1\}), \end{cases}$$

then v is still between -1 and 1 and

$$0 \geq \langle v - u, p \rangle_2 = \int_{\{u=-1\}} wp \, dx + \int_{\{u=1\}} wp \, dx = \int_{\{u=-1\}} wp \, dx.$$

Because w is arbitrary and positive on $\{u = -1\}$ it follows that $p \leq 0$ a.e. on $\{u = -1\}$. If we choose now $v = u + w$ with w is an arbitrary bounded function with

$$\begin{cases} w = 0 & \text{on } \text{supp}(\{-1 \leq u \leq 0\}) \\ -1 \leq w \leq 0 & \text{on } \text{supp}(\{0 < u \leq 1\}), \end{cases}$$

then v is still between -1 and 1 and

$$0 \geq \langle v - u, p \rangle_2 = \int_{\{u=-1\}} wp \, dx + \int_{\{u=1\}} wp \, dx = \int_{\{u=1\}} wp \, dx.$$

Analogously to before, since w is arbitrary and negative on $\{u = 1\}$ it follows that $p \geq 0$ a.e. on $\{u = 1\}$.

On the other hand assume that

$$\begin{aligned} p &= 0 && \text{a.e. on } \text{supp}(\{|u| < 1\}) \\ p &\leq 0 && \text{a.e. on } \text{supp}(\{u = -1\}) \\ p &\geq 0 && \text{a.e. on } \text{supp}(\{u = 1\}). \end{aligned}$$

We need to verify the subgradient property

$$\langle v - u, p \rangle_2 \leq \chi_1(v) - \chi_1(u) = \chi_1(v) \quad \text{for all } v \in L^r(\Omega)$$

only for $\chi_1(v) = 0$, since it is trivial for $\chi_1(v) = \infty$. So let $v \in L^r(\Omega)$ be a function between -1 and 1 almost everywhere on Ω . Then with p as above we obtain

$$\begin{aligned} \langle v - u, p \rangle_2 &= \int_{\{u=-1\}} p(v - u) \, dx + \int_{\{u=1\}} p(v - u) \, dx \\ &= \int_{\{u=-1\}} p(v + 1) \, dx + \int_{\{u=1\}} p(v - 1) \, dx. \end{aligned}$$

Since $-1 \leq v \leq 1$ the first and the second term are always ≤ 0 since $p \leq 0$ for $\{u = -1\}$ and $p \geq 0$ for $\{u = 1\}$ respectively. Therefore $\langle v - u, p \rangle_2 \leq 0$ and we are done. \square

2.2.4 Error Estimation and Stability Analysis With the Bregman Distance

In the following analysis we want to present estimates for both the error we actually make in inpainting an image with our TV-H⁻¹approach (2.27) (see (2.40)) and for the stability of solutions for this problem (see (2.41)) in terms of the Bregman distance. This section is motivated by the error analysis for variational models in image restoration with Bregman iterations in [BRH07], and the error estimates for inpainting models developed in [CK06]. In [BRH07] the authors consider among other things the general optimality condition

$$p + \lambda_0 A^*(Au - f_{dam}) = 0, \quad (2.33)$$

where $p \in \partial R(u)$ for a regularizing term R , A is a bounded linear operator and A^* its adjoint. Now the error that is to be estimated depends on the form of smoothing of the image contained in (2.33). Considering this equation one realizes that smoothing consists of two steps. The first is created by the operator A which depends on the image restoration task at hand, and actually smooths the subgradient p . The second smoothing step is the one which is directly implied by the regularizing term, i.e., its subgradient p , and depends on the relationship between the primal variable u and the dual variable p . A condition that represents this dual smoothing property of functions, i.e., subgradients, is the so-called source condition. Letting f_{true} be the original image, the source condition for f_{true} reads

$$\text{There exists } \xi \in \partial R(f_{true}) \text{ such that } \xi = A^*q \text{ for a source element } q \in D(A^*), \quad (2.34)$$

where $D(A^*)$ is the domain of the operator A^* . It can be shown (cf. [BO05]) that this is equivalent to requiring from f_{true} to be a minimizer of

$$R(u) + \frac{\lambda_0}{2} \|Au - f_{dam}\|_2^2$$

for arbitrary $f_{dam} \in D(A^*)$ and $\lambda_0 \in \mathbb{R}$. Now, the source condition has a direct consequence for the Bregman distance, which gives rise to its use for subsequent error analysis. To be more precise, the Bregman distance is defined as

$$D_R^p(v, u) = R(v) - R(u) - \langle v - u, p \rangle_2, \quad p \in \partial R(u).$$

Then, if f_{true} fulfills the source condition with a particular subgradient ξ , we obtain

$$D_R^\xi(u, f_{true}) = R(u) - R(f_{true}) - \langle u - f_{true}, \xi \rangle_2 = R(u) - R(f_{true}) - \langle q, Au - Af_{true} \rangle_2,$$

and thus the Bregman distance can be related to both the error in the regularization functional ($R(u) - R(f_{true})$) and the output error ($Au - Af_{true}$). For the sake of symmetry properties in the sequel we shall consider the symmetric Bregman distance, which is defined as

$$D_R^{symm}(u_1, u_2) = D_R^{p_1}(u_2, u_1) + D_R^{p_2}(u_1, u_2) = \langle u_1 - u_2, p_1 - p_2 \rangle_2, \quad p_i \in \partial R(u_i).$$

Additionally to this error analysis we shall get a control on the inpainting error $|u - f_{true}|$ inside the inpainting domain D by means of estimates from [CK06]. Therein the authors analyzed the inpainting process by understanding how the regularizer continues level lines into the missing domain. The inpainting error was then determined by means of the definition of an error region, smoothness bounds on the level lines, and quantities taking into the account the shape of the inpainting domain. In the following we are going to implement both strategies, i.e., [BRH07, CK06], in order to prove Theorem 2.2.7.

Proof of Theorem 2.2.7. Let $f_{dam} \in L^2(\Omega)$ be the given damaged image with inpainting domain $D \subset \Omega$ and f_{true} the original image. We consider the stationary equation to (2.27), i.e.,

$$-\Delta p + \lambda(u - f_{dam}) = 0, \quad p \in \partial TV(u), \quad (2.35)$$

where $TV(u)$ is defined as in (2.28). More precisely $TV(u)$ is interpreted as a functional over $L^2(\Omega)$,

$$TV(u) = \begin{cases} |Du|(\Omega) & \text{if } u \in BV(\Omega), \|u\|_{L^\infty} \leq 1 \\ +\infty & \text{otherwise.} \end{cases}$$

In the subsequent we want to characterize the error we make by solving (2.35) for u , i.e., how large do we expect the distance between the restored image u and the original image f_{true} to be.

Now, let Δ^{-1} be the inverse operator to $-\Delta$ with zero Dirichlet boundary conditions as before. In our case the operator A in (2.33) is the embedding operator from $H_0^1(\Omega)$ into $H^{-1}(\Omega)$ and stands in front of the whole term $A(u - f_{dam})$, cf. (2.35). The adjoint operator is $A^* = \Delta^{-1}$ which maps $H^{-1}(\Omega)$ into $H_0^1(\Omega)$. We assume that the given image f_{dam} coincides with f_{true} outside of the inpainting domain, i.e.,

$$\begin{aligned} f_{dam} &= f_{true} && \text{in } \Omega \setminus D \\ f_{dam} &= 0 && \text{in } D. \end{aligned} \quad (2.36)$$

Further we assume that f_{true} satisfies the source condition (2.34), i.e.,

$$\text{There exists } \xi \in \partial TV(f_{true}) \text{ such that } \xi = \Delta^{-1}q \text{ for a source element } q \in H^{-1}(\Omega). \quad (2.37)$$

For the following analysis we first rewrite (2.35). For \hat{u} , a solution of (2.35), we get

$$\hat{p} + \lambda_0 \Delta^{-1}(\hat{u} - f_{true}) = \Delta^{-1} [(\lambda_0 - \lambda)(\hat{u} - f_{true})], \quad \hat{p} \in \partial TV(\hat{u}).$$

Here we replaced f_{dam} by f_{true} using assumption (2.36). By adding a $\xi \in \partial TV(f_{true})$ from (2.37) to the above equation we obtain

$$\hat{p} - \xi + \lambda_0 \Delta^{-1}(\hat{u} - f_{true}) = -\xi + \lambda_0 \Delta^{-1} \left[\left(1 - \frac{\lambda}{\lambda_0}\right) (\hat{u} - f_{true}) \right]$$

Taking the duality product with $\hat{u} - f_{true}$ (which is just the inner product in $L^2(\Omega)$ in our case) we get

$$\begin{aligned} D_{TV}^{symm}(\hat{u}, f_{true}) + \lambda_0 \|\hat{u} - f_{true}\|_{-1}^2 &= \langle \nabla \xi, \nabla \Delta^{-1}(\hat{u} - f_{true}) \rangle_2 \\ &\quad + \lambda_0 \left\langle \left(1 - \frac{\lambda}{\lambda_0}\right) (\hat{u} - f_{true}), \hat{u} - f_{true} \right\rangle_{-1}, \end{aligned}$$

where

$$D_{TV}^{symm}(\hat{u}, f_{true}) = \langle \hat{u} - f_{true}, \hat{p} - \xi \rangle_2, \quad \hat{p} \in \partial TV(\hat{u}), \quad \xi \in \partial TV(f_{true}).$$

An application of Young's inequality yields

$$D_{TV}^{symm}(\hat{u}, f_{true}) + \frac{\lambda_0}{2} \|\hat{u} - f_{true}\|_{-1}^2 \leq \frac{1}{\lambda_0} \|\xi\|_1^2 + \lambda_0 \left\| \left(1 - \frac{\lambda}{\lambda_0}\right) (\hat{u} - f_{true}) \right\|_{-1}^2 \quad (2.38)$$

For the last term we obtain

$$\begin{aligned} \left\| \left(1 - \frac{\lambda}{\lambda_0}\right) v \right\|_{-1} &= \sup_{\phi, \|\phi\|_{-1}=1} \left\langle \phi, \left(1 - \frac{\lambda}{\lambda_0}\right) v \right\rangle_{-1} \\ &= \sup_{\phi, \|\phi\|_{-1}=1} - \left\langle \Delta^{-1} \phi, \left(1 - \frac{\lambda}{\lambda_0}\right) v \right\rangle_2 \\ &= \sup_{\phi, \|\phi\|_{-1}=1} - \left\langle \left(1 - \frac{\lambda}{\lambda_0}\right) \Delta^{-1} \phi, v \right\rangle_2 \\ &\leq \text{H\"older} \|\phi\|_2 \cdot \sup_{\phi, \|\phi\|_{-1}=1} \left\| \left(1 - \frac{\lambda}{\lambda_0}\right) \Delta^{-1} \phi \right\|_2. \end{aligned}$$

With $\Delta^{-1} : H^{-1} \rightarrow H^1 \hookrightarrow L^r$, $2 < r < \infty$ we get

$$\begin{aligned} \int_{\Omega} \left(\left(1 - \frac{\lambda}{\lambda_0} \right) \Delta^{-1} \phi \right)^2 dx &= \int_D (\Delta^{-1} \phi)^2 dx \leq_{\text{Hölder}} |D|^{\frac{1}{q'}} \cdot \left(\int_{\Omega} (\Delta^{-1} \phi)^{2q} \right)^{\frac{1}{q}} \\ &= \text{choose } q = \frac{r}{2} \quad |D|^{\frac{r-2}{r}} \cdot \|\Delta^{-1} \phi\|_r^2 \leq_{H^1 \hookrightarrow L^r} C |D|^{\frac{r-2}{r}} \|\phi\|_{-1}^2 = C |D|^{\frac{r-2}{r}}, \end{aligned}$$

i.e.

$$\left\| \left(1 - \frac{\lambda}{\lambda_0} \right) v \right\|_{-1}^2 \leq C |D|^{\frac{r-2}{r}} \|v\|_2^2. \quad (2.39)$$

Applying (2.39) to (2.38) we see that

$$D_{TV}^{symm}(\hat{u}, f_{true}) + \frac{\lambda_0}{2} \|\hat{u} - f_{true}\|_{-1}^2 \leq \frac{1}{\lambda_0} \|\xi\|_1^2 + C \lambda_0 |D|^{(r-2)/r} \|\hat{u} - f_{true}\|_2^2.$$

To estimate the last term we use some error estimates for TV inpainting computed in [CK06]. First we have

$$\|\hat{u} - f_{true}\|_2^2 = \int_{\Omega \setminus D} (\hat{u} - f_{true})^2 dx + \int_D (\hat{u} - f_{true})^2 dx.$$

Since $\hat{u} - f_{true}$ is uniformly bounded in Ω (this follows from the L^∞ bound in the definition of $TV(u)$) we estimate the first term by a positive constant K_1 and the second term by the L^1 norm over D . We obtain

$$\|\hat{u} - f_{true}\|_2^2 \leq K_1 + K_2 \int_D |\hat{u} - f_{true}| dx.$$

Now let $\hat{u} \in BV(\Omega)$ be given by $\hat{u} = u^s + u^d$, where u^s is a smooth function and u^d is a piecewise constant function. Following the error analysis in [CK06, Theorem 8.] for functions $\hat{u} \in BV(\Omega)$ we have

$$\begin{aligned} \|\hat{u} - f_{true}\|_2^2 &\leq K_1 + K_2 \text{err}(D) \\ &\leq K_1 + K_2 \left(|D| C(M(u^s), \beta) + 2 |R(u^d)| \right), \end{aligned}$$

where $M(u^s)$ is the smoothness bound for u^s , β is determined from the shape of D , and the error region $R(u^d)$ is defined from the level lines of u^d . Note that in general the error region from higher-order inpainting models including the TV seminorm is smaller than that from TV-L²inpainting (cf. [CK06, Section 3.2.]).

Finally we end up with

$$D_{TV}^{symm}(\hat{u}, f_{true}) + \frac{\lambda_0}{2} \|\hat{u} - f_{true}\|_{-1}^2 \leq \frac{1}{\lambda_0} \|\xi\|_1^2 + C \lambda_0 |D|^{(r-2)/r} \text{err}_{\text{inpaint}}, \quad (2.40)$$

with

$$\text{err}_{\text{inpaint}} := K_1 + K_2 \left(|D| C(M(u^s), \beta) + 2 |R(u^d)| \right).$$

The first term in (2.40) depends on the regularizer TV , and the second term on the size of the inpainting domain D . \square

Remark 2.2.13. *From inequality (2.40) we derive an optimal scaling for λ_0 , i.e., a scaling which minimizes the inpainting error. It reads*

$$\lambda_0^2 |D|^{\frac{r-2}{r}} \sim 1$$

and therefore

$$\lambda_0 \sim |D|^{-\frac{r-2}{2r}}.$$

In two space dimensions r can be chosen arbitrarily big, which gives $\lambda_0 \sim 1/\sqrt{|D|}$ as the optimal order for λ_0 .

Stability estimates for (2.35) can also be derived with an analogous technique. For u_i being the solution of (2.35) with $f_{dam} = f_i$ (again assuming that $f_i = f_{true}$ in $\Omega \setminus D$), the estimate

$$D_{\mathcal{J}}^{symm}(u_1, u_2) + \frac{\lambda_0}{2} \|u_1 - u_2\|_{-1}^2 \leq \frac{\lambda_0}{2} \int_D (f_1 - f_2)^2 dx \quad (2.41)$$

holds.

2.2.5 Numerical Results

In this section numerical results for the TV-H⁻¹inpainting approach (2.27) are presented. The numerical scheme used is discussed in detail in Section 4.1, and in particular in Section 4.1.3 (see also [SB09, BHS08]).

In Figures 2.3–2.6 examples for the application of TV-H⁻¹inpainting to grayvalue images are shown. In all examples the total variation $|\nabla u|$ is approximated by its regularized version $\sqrt{|\nabla u|^2 + \delta}$ with $\delta = 0.01$ and the time stepsize τ is chosen to be equal to 1. In Figure 2.4 a comparison of the TV-H⁻¹inpainting result with the result obtained by the second-order TV-L²inpainting model for a crop of the image in Figure 2.3 is presented. The superiority of the fourth-order TV-H⁻¹inpainting model to the second-order model with respect to the desired continuation of edges into the missing domain is clearly visible. Other examples which support this claim are presented in Figures 2.5 and 2.6 where the line is connected by the TV-H⁻¹inpainting

model but clearly split by the second-order TV-L²model. It would be interesting to strengthen this numerical observation with a rigorous result as it was done in [BEG07b] for Cahn-Hilliard inpainting, cf. (2.2). The author considers this as another important contribution of future research.

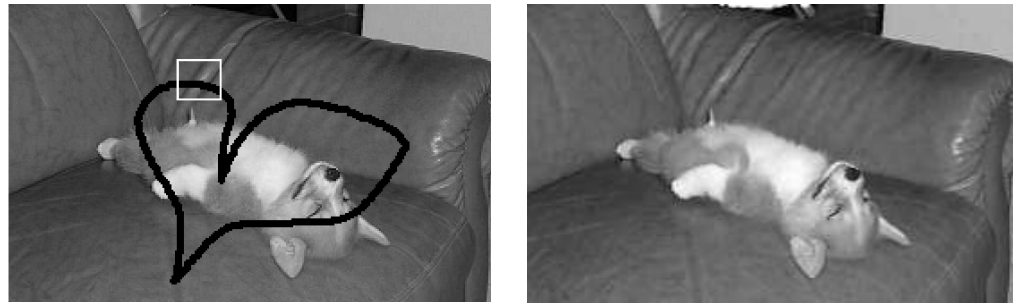


Figure 2.3: TV-H⁻¹inpainting: $u(1000)$ with $\lambda_0 = 10^3$

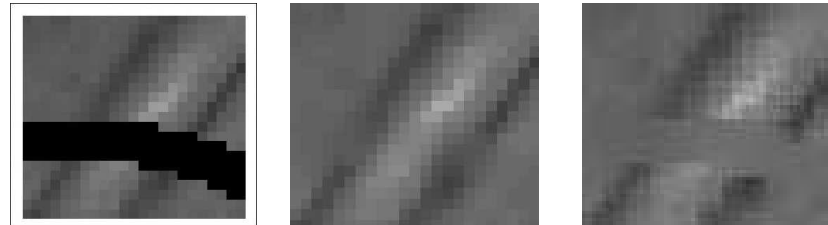


Figure 2.4: (l.) $u(1000)$ with TV-H⁻¹inpainting, (r.) $u(5000)$ with TV-L²inpainting

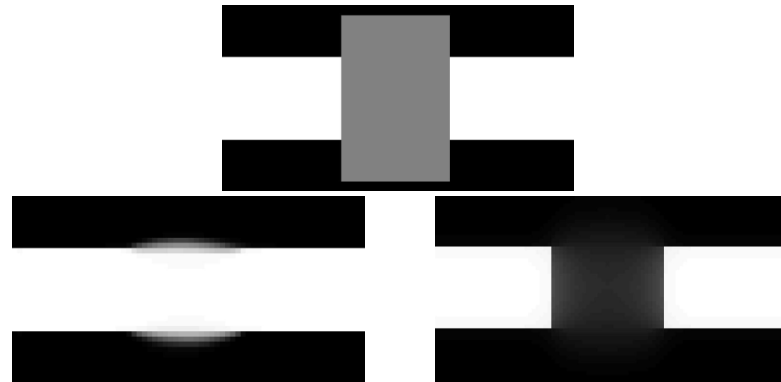


Figure 2.5: TV-H⁻¹inpainting compared to TV-L²inpainting: $u(5000)$ with $\lambda_0 = 10$

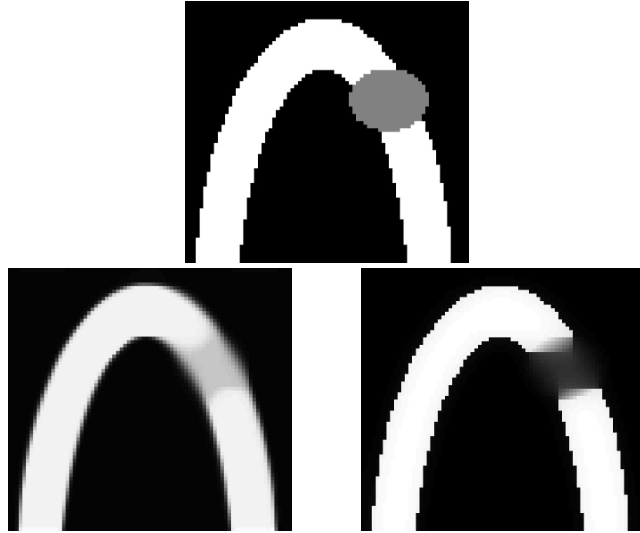


Figure 2.6: TV-H⁻¹inpainting compared to TV-L²inpainting: u(5000) with $\lambda_0 = 10$

2.3 Inpainting with LCIS

Another higher-order inpainting model proposed in [SB09] is inpainting with LCIS (low curvature image simplifiers). This approach is motivated by two famous second-order nonlinear PDEs in image processing, the work of Rudin, Osher and Fatemi [ROF92] and Perona & Malik [PM90]. These methods are based on a nonlinear version of the heat equation

$$u_t = \nabla \cdot (g(|\nabla u|)\nabla u),$$

in which g is small in regions of sharp gradients. LCIS represent a fourth-order relative of these nonlinear second-order approaches. They have been proposed in [TT99] and later used by Bertozzi and Greer in [BG04] for the denoising of piecewise linear signals. Related fourth-order equations, combining diffusion and convection, have been studied by the latter authors in [GB04a, GB04b]. In [SB09] we consider LCIS for image inpainting. With $f \in L^2(\Omega)$ our inpainted image u evolves in time as

$$u_t = -\nabla \cdot (g(\Delta u)\nabla\Delta u) + \lambda(f - u),$$

with thresholding function $g(s) = \frac{1}{1+s^2}$ and λ is defined as the indicator function of $\Omega \setminus D$ multiplied by a constant $\lambda_0 \gg 1$, as in the previous two sections. Note that with

$g(\Delta u) \nabla \Delta u = \nabla(\arctan(\Delta u))$ the above equation can be rewritten as

$$u_t = -\Delta(\arctan(\Delta u)) + \lambda(f - u). \quad (2.42)$$

Using the second derivative of the arctangent as a regularizing term, spikes in the initial signal are preserved versus step functions are diffused (cf. [BG04]). This means that solutions of this equation are piecewise linear functions and not piecewise constant functions as the ones produced by the TV model [ROF92]. Introducing a regularizing parameter $0 < \delta \leq 1$ in $G'(y) = \arctan(y/\delta)$ we are able to control the smoothing effect. Namely, the smaller δ the less diffusive the equation will be.

In [BG04] the authors prove regularity of solutions of (2.42) for the case $\lambda(x) \equiv \lambda_0$ in all of Ω . Namely they show that for smooth initial data $u(., t=0) = u_0$ and smooth data f a unique smooth solution exists, globally in time in one space dimension and locally in time in two dimensions. For numerical purposes it is sufficient to have well-posedness and certain regularity properties of (2.42) on a finite time interval. Although the difference between the equation in [BG04] and our inpainting equation (2.42) is that the fidelity term is discontinuous, the results in [BG04] suggest its validity also in this case. Nevertheless a rigorous analysis of the LCIS inpainting equation is still open for future research.

2.3.1 Numerical Results

In this section numerical results for the LCIS inpainting approach (2.42) are presented. The numerical scheme used is discussed in detail in Section 4.1, and in particular in Section 4.1.4 (cf. also [SB09]).

For the comparison with TV-H⁻¹inpainting we apply (2.42) to the same image as in Section 2.2.5. This example is presented in Figure 2.7. In Figure 2.8 the LCIS inpainting result is compared with TV-H⁻¹- and TV-L²inpainting, for a small part in the given image. Again the result of this comparison indicates the continuation of the gradient of the image function into the inpainting domain. A rigorous proof of this observation is a matter of future research.

2.4 The Inpainting Mechanisms of Transport and Diffusion - A Comparison

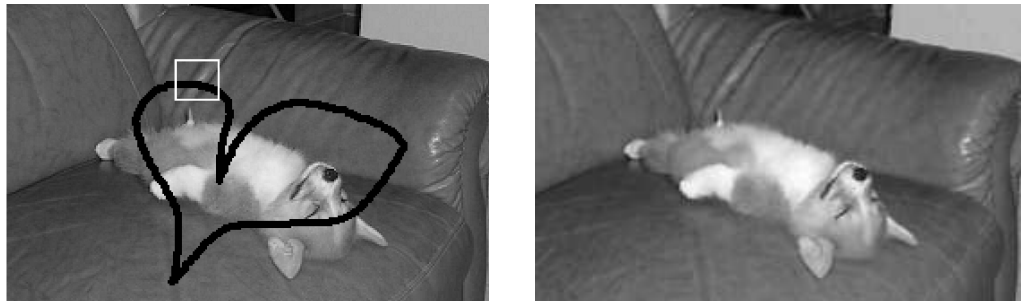


Figure 2.7: LCIS inpainting $u(500)$ with $\delta = 0.1$ and $\lambda_0 = 10^2$.

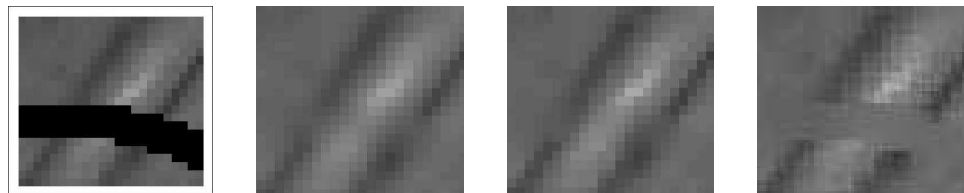


Figure 2.8: (l.) $u(1000)$ with LCIS inpainting, (m.) $u(1000)$ with $TV-H^{-1}$ inpainting, (r.) $u(5000)$ with $TV-L^2$ inpainting

2.4 The Inpainting Mechanisms of Transport and Diffusion - A Comparison

In [CKS02] the authors gave an interpretation of Euler's elastica inpainting in terms of the mechanisms of transport and diffusion. More precisely, they derived the optimality condition for elastica minimizing curves, and compared it with the transport equation of Bertalmio et al. [BSCB00] and the CDD inpainting approach of Chan and Shen [CS01c]. Thereby the optimality condition for elastica minimizing curves, or preferably the corresponding flux field, shows a natural decomposition into its normal and tangent field, cf. Theorem 2.4.1.

In this section we want to make a similar analysis for $TV-H^{-1}$ inpainting and inpainting with LCIS, presented in Section 2.2 and Section 2.3 respectively. To do so, let us briefly recall the results from [CKS02].

2.4 The Inpainting Mechanisms of Transport and Diffusion - A Comparison

Euler's Elastica Inpainting

For the following statement we assume that the image u is smooth enough and that the curvature κ is well defined as

$$\kappa = \nabla \cdot \left(\frac{\nabla u}{|\nabla u|} \right).$$

Then the authors of [CKS02] proved the following theorem.

Theorem 2.4.1. [CKS02, Theorem 5.1.] *Let $\phi \in C^1(\mathbb{R}, (0, \infty))$ be given and*

$$R(u) = \int_{\Omega} \phi(\kappa) |\nabla u| dx.$$

Then the gradient descent time marching is given by

$$\frac{\partial u(x, t)}{\partial t} = \nabla \cdot \vec{V}(x, t), \quad x \in \Omega, t > 0,$$

with the boundary conditions along $\partial\Omega$

$$\frac{\partial u}{\partial \nu} = 0, \quad \frac{\partial(\phi'(\kappa) |\nabla u|)}{\partial \nu} = 0,$$

where ν denotes the outward pointing normal on $\partial\Omega$. The flux field \vec{V} is given by

$$\vec{V} = \phi(\kappa) \vec{n} - \frac{\vec{t}}{|\nabla u|} \frac{\partial(\phi'(\kappa) |\nabla u|)}{\partial \vec{t}}.$$

Here \vec{n} is the ascending normal field $\nabla u / |\nabla u|$, and \vec{t} is the tangent field (whose exact orientation does not matter due to the parity of \vec{t} in the expression).

In particular, for the elastica inpainting model with

$$R(u) = \int_{\Omega} (a + b\kappa^2) |\nabla u| dx$$

Theorem 2.4.1 gives the following.

Corollary 2.4.2. [CKS02, Corollary 5.3.] *For the elastica inpainting model, the gradient descent is given by*

$$\frac{\partial u(x, t)}{\partial t} = \nabla \cdot \vec{V}(x, t) - \lambda(u(x) - u_0(x)), \quad x \in \Omega, t > 0,$$

with the boundary conditions as in Theorem 2.4.1 and

$$\vec{V} = (a + b\kappa^2) \vec{n} - \frac{2b}{|\nabla u|} \frac{\partial(\kappa |\nabla u|)}{\partial \vec{t}} \vec{t}.$$

2.4 The Inpainting Mechanisms of Transport and Diffusion - A Comparison

To see the connection to the inpainting models of Bertalmio et al. [BSCB00] and Chan and Shen [CS01c], let us recall them briefly. These two inpainting models have been already presented in the introduction of this work, i.e., in Section 1.3.1. Bertalmio's approach is based on solving the following transport equation inside of the inpainting domain D ,

$$\frac{\partial u}{\partial t} = \nabla^\perp u \cdot \nabla L(u),$$

where $\nabla^\perp = (-u_y, u_x) = |\nabla u| \vec{t}$, and $L(u)$ can be any smoothness measure of the image u . For their numerical experiments the authors in [BSCB00] chose $L(u) = \Delta u$, the Laplacian of u . For the equilibrium state the equation reads

$$\vec{t} \cdot \nabla L(u) = 0, \quad \text{i.e., } \frac{\partial L(u)}{\partial \vec{t}} = 0,$$

which means that the smoothness measure remains constant along any completed level line. In other words, assuming available boundary data, boundary smoothness gets transported along the level lines into the missing domain.

Orthogonal to this idea of smoothness transport along level lines, Chan and Shen proposed the CDD inpainting model in [CS01c], i.e.,

$$\frac{\partial u}{\partial t} = \nabla \cdot \left(\frac{g(\kappa)}{|\nabla u|} \nabla u \right),$$

where $g : B \rightarrow [0, +\infty)$ is a continuous function with $g(0) = 0$ and $g(\pm\infty) = +\infty$, and B equals, e.g., $C^2(\Omega)$. The function g penalizes large curvatures, and encourages diffusion when the curvature is small. This model diffuses the image contents across the level lines (since $\nabla u / |\nabla u|$ is the normal vector to the level lines!), which is completely orthogonal to the behavior of the Bertalmio et al. approach.

Now, in [CKS02] the authors showed that the Euler elastica inpainting model unifies these two mechanisms. Theorem 2.4.1 says that the flux \vec{V} for the inpainting energy consists of two components, the normal part

$$\vec{V}_n^{Euler} = \phi(\kappa) \cdot \vec{n},$$

and the tangential part

$$\vec{V}_t^{Euler} = -\frac{1}{|\nabla u|} \frac{\partial(\phi'(\kappa)|\nabla u|)}{\partial \vec{t}} \cdot \vec{t}.$$

We immediately see that the normal flux corresponds to the flux of the CDD inpainting equation with $g(\kappa) = \phi(\kappa)$. By rewriting the tangential component, we see that this

2.4 The Inpainting Mechanisms of Transport and Diffusion - A Comparison

corresponds to the Bertalmio flux with a special smoothness measure. In fact it turns out that the tangential component of the Euler's elastica flux corresponds to the scheme of Bertalmio with smoothness measure

$$L_{\phi}^{Euler} = \frac{-1}{|\nabla u|^2} \frac{\partial(\phi'(\kappa)|\nabla u|)}{\partial \vec{t}}.$$

This measure can be further rewritten in a way which makes its connection to the Laplacian visible. In the case $\phi(s) = |s|$ we get

$$L_{\phi}^{Euler} = \frac{\pm 1}{|\nabla u|^2} [\nabla \times \nabla u](\vec{n}, \vec{t}),$$

which closely resembles Bertalmio's choice of the Laplacian, which can be written as

$$L^{Bertalmio}(u) = \Delta u = \text{tr}(\nabla \times \nabla u) = [\nabla \times \nabla u](\vec{n}, \vec{n}) + [\nabla \times \nabla u](\vec{t}, \vec{t}).$$

TV-H⁻¹Inpainting

Now we want to do a similar analysis for TV-H⁻¹inpainting. The gradient descent of the TV-H⁻¹inpainting regularizer is given by

$$\frac{\partial u(x, t)}{\partial t} = -\Delta \left(\nabla \cdot \left(\frac{\nabla u}{|\nabla u|} \right) \right) = \nabla \cdot \left[-\nabla \left(\nabla \cdot \left(\frac{\nabla u}{|\nabla u|} \right) \right) \right],$$

with flux field

$$\vec{V}^{TV-H^{-1}} = -\nabla \left(\nabla \cdot \left(\frac{\nabla u}{|\nabla u|} \right) \right).$$

Now to write this flux as the sum of its normal and tangential component we project it both onto the normal and the tangential direction and use the fact that the sum of these projections gives the identity, i.e.,

$$\vec{n} \otimes \vec{n} + \vec{t} \otimes \vec{t} = Id,$$

where \otimes denotes the tensor product. With this the steepest descent for TV-H⁻¹inpainting reads

$$\begin{aligned} \frac{\partial u(x, t)}{\partial t} &= \nabla \cdot (-\nabla \kappa) \\ &= \nabla \cdot (-\nabla \kappa (\vec{t} \otimes \vec{t} + \vec{n} \otimes \vec{n})) \\ &= \nabla \cdot \left(-\left(\frac{\partial \kappa}{\partial \vec{t}} \vec{t} + \frac{\partial \kappa}{\partial \vec{n}} \vec{n} \right) \right). \end{aligned}$$

2.4 The Inpainting Mechanisms of Transport and Diffusion - A Comparison

Now we want to compare the normal and the tangential component with the components of the Euler's elastica inpainting approach and with the approaches of CDD and Bertalmio et al respectively. Let us start with the normal part of the TV-H⁻¹flow, which reads

$$\nabla \cdot \vec{V}_n^{TV-H^{-1}} = \nabla \cdot \left(-\frac{\partial \kappa}{\partial \vec{n}} \vec{n} \right).$$

At the same time the normal part in Euler's elastica is

$$\nabla \cdot \vec{V}_n^{Euler} = \nabla \cdot (\phi(\kappa) \vec{n}),$$

or more specifically

$$\nabla \cdot \vec{V}_n^{Euler} = \nabla \cdot ((a + b\kappa^2) \vec{n}),$$

and the CDD flux reads

$$\nabla \cdot \vec{V}^{CDD} = \nabla \cdot (g(\kappa) \vec{n}).$$

Note that the strength of the diffusion in all three approaches depends on the size of the diffusivity constant. This is, in the case of TV-H⁻¹inpainting $D = \frac{-\partial \kappa / \partial \vec{n}}{|\nabla u|}$, the diffusion depends on the change of the curvature across the level lines. The larger the curvature changes across the level lines, the more diffusive this approach is. Thereby the sign of the diffusion depends on the sign of the covariant derivative (forward or backward diffusion!). In particular this means that there is no diffusion in areas of the image with homogeneous grayvalue and strong diffusion of edge information into the missing domain.

Next we do the same for the tangential component in \vec{V} . For TV-H⁻¹inpainting this reads

$$\begin{aligned} \nabla \cdot \vec{V}_t^{TV-H^{-1}} &= \nabla \cdot \left(-\frac{\partial \kappa}{\partial \vec{t}} \vec{t} \right) \\ &= \nabla \cdot \left(\frac{\partial \kappa}{\partial \vec{t}} \frac{-1}{|\nabla u|} \cdot \nabla^\perp u \right) \\ &= \nabla^\perp u \cdot \nabla \left(\frac{-1}{|\nabla u|} \frac{\partial \kappa}{\partial \vec{t}} \right), \end{aligned}$$

since $\nabla^\perp u$ is divergence-free. This corresponds to the scheme of Bertalmio with smoothness measure

$$L^{TV-H^{-1}}(u) = \frac{-1}{|\nabla u|} \frac{\partial \kappa}{\partial \vec{t}},$$

whereas Euler's elastica tangent component has the smoothness measure

$$L^{Euler}(u) = \frac{-2b}{|\nabla u|^2} \frac{\partial(\kappa |\nabla u|)}{\partial \vec{t}}.$$

2.4 The Inpainting Mechanisms of Transport and Diffusion - A Comparison

LCIS Inpainting

The steepest descent for the LCIS regularizer reads

$$\frac{\partial u(x, t)}{\partial t} = \nabla \cdot \vec{V}^{LCIS} = \nabla \cdot (-g(\Delta u) \nabla \Delta u).$$

Taking $g(s) = 1/(1 + s^2)$, the divergence of the flux changes to

$$\nabla \cdot \vec{V}^{LCIS} = \nabla \cdot (\nabla(\arctan(\Delta u))).$$

Similarly as for Euler's elastica inpainting and the TV-H⁻¹ approach, we split the flux of LCIS into its normal and tangential component and compare it with CDD and Bertalmio et al.'s approach respectively. For the normal component we get

$$\nabla \cdot \vec{V}_n^{LCIS} = \nabla \cdot \left(-\frac{\partial \arctan(\Delta u)}{\partial \vec{n}} \vec{n} \right),$$

i.e., the normal flux diffuses the grayvalues with diffusivity constant

$$D = -\frac{\partial \arctan(\Delta u)}{\partial \vec{n}} \frac{1}{|\nabla u|}.$$

Next we compare the tangential component of LCIS with Bertalmio's approach. The divergence of the tangential flux of LCIS reads

$$\begin{aligned} \nabla \cdot \vec{V}_t^{LCIS} &= \nabla \cdot \left(-\frac{\partial \arctan(\Delta u)}{\partial \vec{t}} \vec{t} \right) \\ &= \nabla \cdot \left(-\frac{\partial \arctan(\Delta u)}{\partial \vec{t}} \frac{1}{|\nabla u|} \nabla^\perp u \right) \\ &= \nabla^\perp u \cdot \nabla \left(-\frac{\partial \arctan(\Delta u)}{\partial \vec{t}} \frac{1}{|\nabla u|} \right). \end{aligned}$$

This reassembles Bertalmio's smoothness transport along the level lines with smoothness measure

$$\begin{aligned} L^{LCIS}(u) &= -\frac{\partial \arctan(\Delta u)}{\partial \vec{t}} \frac{1}{|\nabla u|} \\ &= -\frac{1}{|\nabla u|} \frac{1}{1 + (\Delta u)^2} \frac{\partial(\Delta u)}{\partial \vec{t}} \end{aligned}$$

2.4 The Inpainting Mechanisms of Transport and Diffusion - A Comparison

	$\nabla \cdot \vec{V}_n$	$L(u)$
Bertalmio et al.'s transport	0	Δu
Cahn and Shen's CDD	$\nabla \cdot (g(\kappa)\vec{n})$	0
Euler's elastica	$\nabla \cdot ((a + b\kappa^2)\vec{n})$	$\frac{-2b}{ \nabla u ^2} \frac{\partial(\kappa \nabla u)}{\partial \vec{t}}$
TV-H ⁻¹	$\nabla \cdot (-\frac{\partial \kappa}{\partial \vec{n}}\vec{n})$	$\frac{-1}{ \nabla u } \frac{\partial \kappa}{\partial \vec{t}}$
LCIS	$\nabla \cdot (-\frac{\partial \text{arctan}(\Delta u)}{\partial \vec{n}}\vec{n})$	$-\frac{1}{ \nabla u } \frac{1}{1+(\Delta u)^2} \frac{\partial(\Delta u)}{\partial \vec{t}}$.

Table 2.1: A comparison of the normal flux field \vec{V}_n (which represents the diffusive part of the flux), and the smoothness measure $L(u)$, which is transported along the tangential flux, for all discussed inpainting approaches

Summary and Numerical Results

In Tabular 2.1 we summarize the comparison of the flux field of the discussed inpainting approaches.

For a better understanding of the derived geometric properties of TV-H⁻¹ inpainting and inpainting with LCIS we present a comparison of those with Euler's elastica inpainting for the inpainting of a straight line in Figure 2.9. For all three inpainting approaches several intermediate steps of the iteration (evolution) are shown. The processes seem quite similar. First the inpainting domain is filled in where homogeneous boundary condition are given, i.e., the intensity values are transported into the inpainting domain very fast. At the edges (black/white boundary) the evolution takes a longer time until the edge is continued. Note that at the edge the change of the curvature in normal direction is equal to 0. It becomes nonzero when approaching the boundary of the inpainting domain in between the two edges.

2.4 The Inpainting Mechanisms of Transport and Diffusion - A Comparison

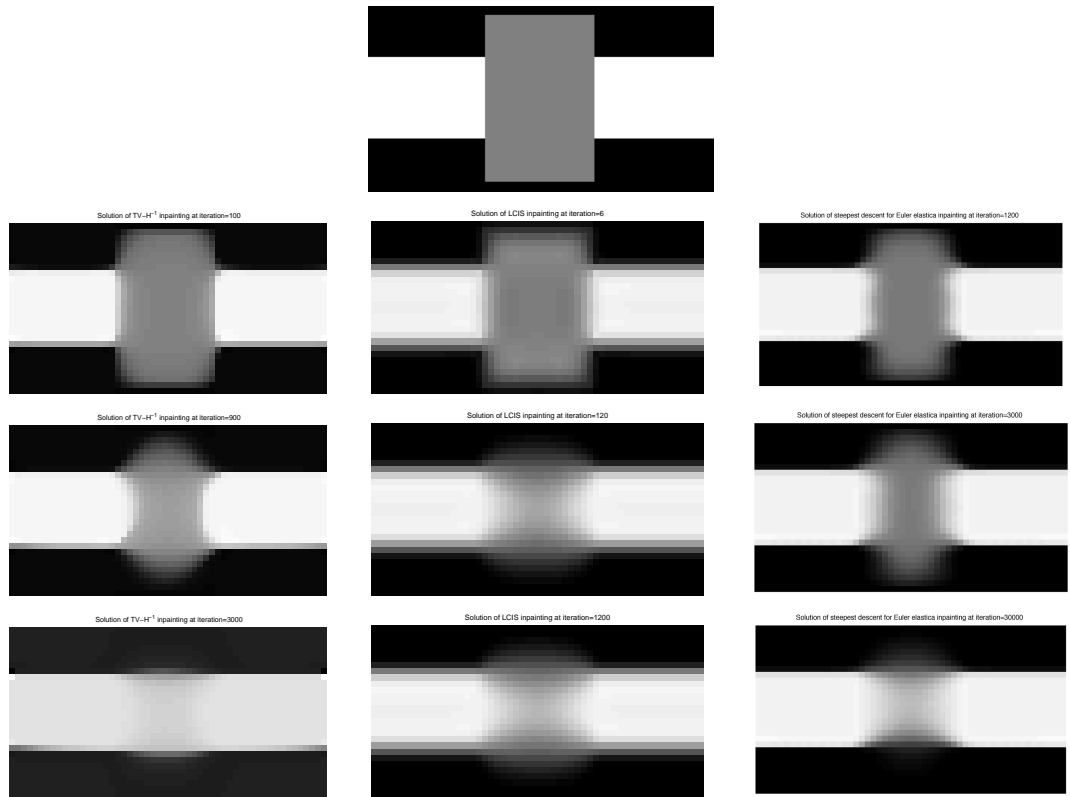


Figure 2.9: A comparison of the evolution of $TV-H^{-1}$ inpainting, inpainting with LCIS, and Euler's elastica inpainting at three different time steps: (l.) the evolution of $TV-H^{-1}$ inpainting at time steps $t = 100, 900$, and 3000 ; (m.) the evolution of LCIS inpainting at time steps $t = 6, 120$, and 1200 ; (r.) the evolution of Euler's elastica inpainting at time steps $t = 1200, 3000$, and 30000 .

Chapter 3

Analysis of Higher-Order Equations

The study of higher-order PDEs is still very young and therefore their theoretical analysis poses challenging problems. In this chapter we are especially interested in analytic properties of higher-order flows, i.e., PDEs of fourth differential order, that arise in image inpainting. In Section 3.1 we study the Cahn-Hilliard equation, which we already have discussed in the context of its inpainting application in Section 2.1. In particular we study instabilities of the Cahn-Hilliard equation and their connection to the Willmore functional. This work has been developed in collaboration with Martin Burger, Shun-Yin Chu, and Peter Markowich, and has been published in [BCMS08]. Section 3.2 is dedicated to the analysis of higher-order nonlocal evolution equations. This is based on joint work with Julio Rossi, cf. [RS09]. Nonlocal flows have been recently proposed for inpainting of texture images in [GO07] and are therefore within the scope of the present work.

3.1 Instabilities of the Cahn-Hilliard Equation and the Willmore Functional

In this section we are interested in the finite-time stability of transition solutions of the Cahn-Hilliard equation and its connection to the Willmore functional. We shall present the results from [BCMS08]. Therein we show that the Willmore functional locally decreases or increases in time in the linearly stable or unstable case respectively.

3.1 Instabilities in the Cahn-Hilliard Equation

This linear analysis explains the behavior near stationary solutions of the Cahn-Hilliard equation. We perform numerical examples in one and two dimensions and show that in the neighborhood of transition solutions local instabilities occur in finite time. Beside that we show convergence of solutions of the Cahn-Hilliard equation for arbitrary dimension to a stationary state by proving asymptotic decay of the Willmore functional in time.

We consider the Neumann problem for the Cahn-Hilliard equation,

$$\begin{cases} u_t = \Delta(-\epsilon^2 \Delta u + F'(u)) & x \in \Omega, \\ \frac{\partial u}{\partial n} = \frac{\partial}{\partial n}(-\epsilon^2 \Delta u + F'(u)) = 0, & x \in \partial\Omega, \end{cases} \quad (3.1)$$

with $\Omega \subseteq \mathbb{R}^d$ a bounded domain and $d \geq 1$, though we shall focus primarily on the cases $d = 1$ and 2 . F is a double-well potential with $F'(u) = \frac{1}{2}(u^3 - u)$ and $0 < \epsilon \ll 1$ is a small parameter. Note that the function F' is of bistable type. Considering only constant solutions $u = c$ of (3.1), these are classified in the following way. If $F''(u) < 0$ then u corresponds to the so-called spinodal interval ($|u| < \frac{1}{\sqrt{3}}$) and it is an unstable stationary state. Otherwise u corresponds to the metastable intervals (i.e. $u \in (-1, -\frac{1}{\sqrt{3}})$ or $u \in (\frac{1}{\sqrt{3}}, 1)$) and is asymptotically stable, see [Fi00] for a detailed description.

The Cahn-Hilliard equation

The Cahn-Hilliard equation is a classic model for phase separation and subsequent phase coarsening of binary alloys. There the solution $u(x, t)$ represents the concentration of one of the two metallic components of the alloy. For further information about the physical background of the Cahn-Hilliard equation we refer, for instance, to [CH58, Pe89, PF90, Gu88]. Numerical studies about the behavior of solutions of (3.1) can be found, e.g., in [EF87, FP05, MF05].

Solutions of (3.1) have a time-conserved mean value

$$\int_{\Omega} u(x, t) dx = \int_{\Omega} u(x, t=0) dx, \text{ for all } t > 0. \quad (3.2)$$

A way of deriving equation (3.1) has been suggested by Fife in [Fi00]. One takes the Ginzburg-Landau free energy

$$E[u](t) = \int_{\Omega} \left(\frac{\epsilon^2}{2} |\nabla u(x, t)|^2 + F(u(x, t)) \right) dx \quad (3.3)$$

3.1 Instabilities in the Cahn-Hilliard Equation

and looks for constrained (mass-conserving) gradient flows of this functional. The Cahn-Hilliard equation (3.1) is obtained by taking the gradient flow of (3.3) in the sense of the $H^{-1}(\Omega)$ inner product, cf. Section 2.1.3. The mass constraint is a consequence of the natural boundary conditions for (3.1).

Using the ideas of [Ha88] it is not hard to see that the Cahn-Hilliard equation possesses a global attractor. Zheng proved in [Zh86] convergence to equilibria for solutions of (3.1) in two and three dimensions. In [RH99] the authors proved that solutions of the Cahn-Hilliard equation converge to equilibria in dimensions $d = 1, 2$ and 3. In one space dimension the equilibria are isolated [NST89] and the global attractor is finite-dimensional. Further Grinfeld and Novick-Cohen give a full description of the stationary solutions of the viscous Cahn-Hilliard equation in one space dimension, compare [GN95, GN99]. So far equilibria have been determined and their properties studied only in the one dimensional case. It is a major problem characterizing the equilibria in more than one dimension. The reason is that the limit set of the solutions can be large. However, some papers as [WW98a, WW98b, WW98c, FKMW97, CK96] still provide certain special types of equilibrium solutions.

A special type of stationary solutions of (3.1) are so-called transition solutions, which continuously connect the two stable equilibria -1 and 1. In one dimension the so-called kink solution $u_0 = \tanh \frac{x}{2\epsilon}$ is such a stationary solution of the Cahn-Hilliard equation. The radially-symmetric analogue in two dimensions are the so-called bubble solutions. In [BK90] asymptotic stability was shown for the kink solution for fixed $\epsilon = 1$, i.e. small perturbations of u_0 in some suitable norm will decay to zero in time. Further studies for the one-dimensional case describe the motion of transition layers, compare [ABF91, BH92, BX94, Gr95]. In [AF94] Alikakos and Fusco proved spectral estimates of the linearized fourth-order Cahn-Hilliard operator in two dimensions near bubble solutions. Some of their results are discussed later in Section 3.1.2.

In this section we investigate the stability of transition solutions of the Cahn-Hilliard equation in finite time and its connection to the Willmore functional.

The backward second-order diffusion (for $|u| < \frac{1}{\sqrt{3}}$) in the equation gradually effects the solution, which can result in phenomena like local instabilities or oscillating patterns, controlled by the fourth-order term on scales of order ϵ . We are going to show that in the neighborhood of transition solutions small instabilities occur in finite time.

3.1 Instabilities in the Cahn-Hilliard Equation

In general it is natural to study stationary solutions of the Cahn-Hilliard equation by analyzing the energy functional (3.3). The energy functional decreases in time since

$$\frac{d}{dt} E[u](t) + \int_{\Omega} |\nabla(-\epsilon^2 \Delta u(x, t) + F'(u(x, t)))|^2 dx = 0. \quad (3.4)$$

Because of this monotonicity the energy functional is not suitable for the study of local (in space and time) behavior of the Cahn-Hilliard equation. Instead we present analytical and numerical evidence that the numerically observed instabilities are connected with the evolution of the Willmore functional.

The Willmore functional

The Willmore functional of the Cahn-Hilliard equation (3.1) is given by

$$W[u](t) = \frac{1}{4\epsilon} \int_{\Omega} (\epsilon \Delta u(x, t) - \frac{1}{\epsilon} F'(u(x, t)))^2 dx, \quad (3.5)$$

and is used to describe the geometric boundary of two different stable states and the movement of curves under anisotropic flows. It has its origin in differential geometry, where it appears as a phase field approximation for solutions of the so-called Willmore problem [Wi93]. The Willmore problem is to find a surface Γ in an admissible class embedded in \mathbb{R}^3 which minimizes the mean curvature energy $\int_{\Gamma} H^2 dS$ under certain constraints on the surface, where $H = (\kappa_1 + \kappa_2)/2$ is the mean curvature and κ_1, κ_2 are the principal curvatures of Γ . For the analytical and computational modeling of a minimizing surface of the Willmore problem the phase field method is considered among other approaches. In [DLRW05] the authors consider solutions of a constrained minimization problem for (3.5) of the form $u_{\epsilon}(x) = \tanh \frac{d(x)}{\sqrt{2\epsilon}} + \epsilon h$ with fixed mass and fixed energy (3.3) where d is the signed distance function to the zero level set of u_{ϵ} and h is an arbitrary function in $C^2(\Omega)$ independent of ϵ . They show that the level sets $\{u_{\epsilon} = 0\}$ converge uniformly to a critical point of the Willmore problem as $\epsilon \rightarrow 0$. Furthermore, the authors of [RS06] considered a modified De Giorgi conjecture, i.e., they considered functionals $F_{\epsilon} : L^1(\Omega) \rightarrow \mathbb{R}$ for domains $\Omega \in \mathbb{R}^2$ and \mathbb{R}^3 with

$$F_{\epsilon}[u](t) = E[u](t) + 4W[u](t)$$

if $u \in L^1(\Omega) \cap W^{2,2}(\Omega)$ and $F_{\epsilon}[u](t) = \infty$ if $u \in L^1(\Omega) \setminus W^{2,2}(\Omega)$. They showed that this sequence of functionals applied to characteristic functions $\chi = 2\chi_E - 1$ with $E \subset \Omega$

3.1 Instabilities in the Cahn-Hilliard Equation

$\Gamma-$ converges in $L^1(\Omega)$ as $\epsilon \rightarrow 0$ to a functional $F[\chi]$ given by

$$F[\chi](t) = \sigma \mathcal{H}^{n-1}(\partial E \cap \Omega) + \sigma \int_{\partial E \cap \Omega} |\mathbf{H}_{\partial E}|^2 d\mathcal{H}^{n-1}.$$

Here $\sigma = \int_{-1}^1 \sqrt{2F}$ (where F is the double well potential), $\mathbf{H}_{\partial E}$ denotes the mean curvature vector of ∂E and \mathcal{H}^{n-1} is the $n-1$ dimensional Hausdorff measure. This result indicates that possible instabilities of (3.1) disappear for the limit $\epsilon \rightarrow 0$. We will encounter this observation again in our numerical examples for small values of ϵ . For additional considerations of $\Gamma-$ limits of this type see [RT07], and especially [Ch96].

In [BCMS08] we use the Willmore functional to detect local instabilities in finite time of transition solutions of (3.1) for small values of $\epsilon \ll 1$. As said above, in one space dimension they are given by the kink solutions of the form $\tanh \frac{d(x)}{\sqrt{2}\epsilon}$. In two dimensions we consider their radially-symmetric analogues called bubble solutions.

To get an insight into the behavior of the Willmore functional for solutions of (3.1) we study the asymptotic limit of solutions of the Cahn-Hilliard equation for arbitrary space dimension $d \geq 1$ by showing asymptotic decay of the Willmore functional in time.

Asymptotic behavior

In Section 3.1.1 we study the asymptotic limit of solutions of the Cahn-Hilliard equation for arbitrary space dimension $d \geq 1$ by showing asymptotic decay of the Willmore functional in time. The main challenge of our proof of convergence is that we avoid the use of the Lojasiewicz inequality as say, in [RH99]. It was shown in [Lo93] that gradient flows in \mathbb{R}^d (and even in L^2 , compare [Si83]) fulfill the Lojasiewicz inequality which implies convergence to equilibrium of solutions of the gradient system. For the application to the Cahn-Hilliard equation it takes a serious effort to prove validity of the Lojasiewicz inequality for gradient flows in H^{-1} , as proved in [RH99]. We circumvent this difficulty and prove the following Theorem.

Theorem 3.1.1. *Let u be the solution of the Cahn-Hilliard equation with initial data $u^0 = u^0(x)$, posed either as a Cauchy problem in $\Omega = \mathbb{R}^d$, $d \geq 1$, or in a bounded domain Ω with Neumann boundary conditions. We assume that*

$$\int_{\Omega} F'(u) dx = 0 \text{ for all } t > 0. \quad (3.6)$$

3.1 Instabilities in the Cahn-Hilliard Equation

For $\Omega = \mathbb{R}^n$ further suppose that

$$\begin{cases} \epsilon^2 \Delta u^0 - F'(u^0) \text{ and } \nabla(\epsilon^2 \Delta u^0 - F'(u^0)) \text{ are} \\ \text{spatially exponentially decaying as } |x| \rightarrow \infty. \end{cases} \quad (3.7)$$

Then it follows that

$$\lim_{t \rightarrow \infty} W[u](t) = 0.$$

Remark 3.1.2. • Note that the assumption (3.6) in Theorem 3.1.1 is no restriction on F . Since $\int_{\Omega} F'(u) dx$ is a constant, we can rewrite the equation as

$$\begin{aligned} u_t &= \Delta(-\epsilon^2 \Delta u + F'(u) - \frac{1}{|\Omega|} \int_{\Omega} F'(u) dx) \\ &= \Delta(-\epsilon^2 \Delta u + \tilde{f}(u)), \end{aligned}$$

with $\int_{\Omega} \tilde{f}(u) dx = 0$ where $\tilde{f}(u)$ is equal to $F'(u)$ shifted by the constant $\frac{1}{|\Omega|} \int_{\Omega} F'(u) dx$. In the case of Neumann boundary conditions it further follows from (3.1) that

$$\frac{\partial u}{\partial n} = \frac{\partial(-\epsilon^2 \Delta u + \tilde{f}(u))}{\partial n} = 0.$$

Thus shifting $F'(u)$ by a constant does not change the equation and the assumption (3.6) is reasonable.

- Note further that condition (3.7) extends the exponential decay of the quantities therein to solutions $u(., t)$ for arbitrary times $t > 0$ due to the mass conservation (3.2) of solutions of (3.1).

The challenge of proving convergence of the Willmore functional is that it is generally not monotone in time. To overcome this we construct a nonnegative functional balancing the Willmore functional with the energy functional so that the strong decay property of the energy plays the main role in controlling increasing parts appearing in the Willmore functional.

Finite-time behavior

The next step is to analyze the behavior of the Willmore functional and its connection to the behavior of solutions of (3.1) in finite time. For this sake we consider the linearized Cahn-Hilliard equation. In fact the behavior of solutions of the nonlinear equation is similar in the neighborhood of stationary solutions to that of the linear equation. Sander and Wanner discussed in [SW00] that solutions of (3.1) which start

3.1 Instabilities in the Cahn-Hilliard Equation

near a homogeneous equilibrium and within the spinodal interval remain close to the corresponding solution of the linearized equation with high probability (depending on how likely it is to find an appropriate initial condition) for an unexpectedly long time.

In particular we are interested in instabilities that appear locally in both time and space. To motivate this better let us consider the Cahn-Hilliard equation near a constant equilibrium state \tilde{u} on the whole space $\Omega = \mathbb{R}^d$. Set $u = \tilde{u} + \delta v$, $\delta \in \mathbb{R}$ small, then the perturbation v fulfills in first approximation

$$\begin{aligned} v_t &= -\epsilon^2 \Delta^2 v + a \Delta v && \text{in } \mathbb{R}^d, t > 0 \\ v(t=0) &= v_0(x) && \text{in } \mathbb{R}^d, \end{aligned}$$

with $a = F''(\tilde{u}) = \frac{1}{2}(3\tilde{u}^2 - 1)$. The above equation reads after a Fourier transform

$$\begin{aligned} \hat{v}_t(\xi, t) &= (-\epsilon^2 |\xi|^4 - a |\xi|^2) \hat{v}, && \xi \in \mathbb{R}^d, t > 0 \\ \hat{v}(t=0) &= \hat{v}_0(\xi), && \xi \in \mathbb{R}^d. \end{aligned}$$

This equation can be explicitly solved:

$$\hat{v}(\xi, t) = \exp(-|\xi|^2 (\epsilon^2 |\xi|^2 + a)t) \hat{v}_0(\xi).$$

If $a = F''(\tilde{u}) < 0$ (this means that \tilde{u} lies in the spinodal interval $(-1/\sqrt{3}, 1/\sqrt{3})$) then $\hat{v}(\xi, t) \rightarrow \infty$ for $\xi \in \{|\xi| < \sqrt{|a|}/\epsilon\} \cap \text{supp } \hat{v}_0$, i.e. frequencies $< \sqrt{|a|}/\epsilon$ become amplified if they are present in the initial data. In our case we consider solutions in the neighborhood of transition solutions, i.e. transition solutions perturbed where they assume values from the spinodal interval. Referring again to [SW00] the linear instability explained above is also valid for the nonlinear Cahn-Hilliard equation for a finite time until the effect of the nonlinearity becomes strong enough to stabilize the solution again. This results in instabilities local in space and time.

In Section 3.1.2 spectral estimates for transition solutions tracing back to Alikakos, Bates and Fusco [ABF91, AF94] are presented for one and two dimensions. Further, the important role of the Willmore functional for finite-time stability/instability analysis for the Cahn-Hilliard equation is motivated. For ϵ fixed we linearize the Willmore functional at a stationary solution of the Cahn-Hilliard equation (3.1) perturbed by an eigenvector of the linearized Cahn-Hilliard operator. We show that the Willmore

3.1 Instabilities in the Cahn-Hilliard Equation

functional decreases in time for eigenvectors corresponding to a negative eigenvalue and increases in the case of a positive eigenvalue. In other words

$$\begin{aligned}\frac{d}{dt}W[v](t) \leq 0 &\iff \lambda < 0 \iff \text{linearly stable} \\ \frac{d}{dt}W[v](t) \geq 0 &\iff \lambda > 0 \iff \text{linearly unstable},\end{aligned}$$

where $v = \tilde{u} + \delta v_0$, with \tilde{u} a stationary solution of (3.1) and v_0 the eigenvector to the eigenvalue λ of the linearized equation. Roughly speaking this means that linear instabilities – which correspond to positive eigenvalues of the Cahn-Hilliard equation – can be detected by considering the evolution of the Willmore functional.

In Section 3.1.3 we perform numerical computations for (3.1) near transition solutions in one and two dimensions. We remark that in the past 20 years numerical approximations of the solutions of the Cahn-Hilliard equation – for purposes different from ours – have been studied by many authors, see [FP04, FP05] for further references. We use a semi-implicit approximation in time and finite elements for the space discretization. We start the computation at $t = 0$ with a transition solution perturbed within its transition area with values from the spinodal interval of the equation. Motivated by the linear stability analysis of subsection 3.1.2, we discuss stability in terms of the Willmore functional. We say a function $u(x, t)$ shows an unstable behavior at time $0 < t_0 < \infty$ if

$$\frac{d}{dt}W[u](t_0) > 0.$$

Conversely, we say the function $u(x, t)$ is stable for all times $0 < t < t_0$ if

$$\frac{d}{dt}W[u](t) \leq 0.$$

3.1.1 Asymptotic Behavior

In this section we present the proof of Theorem 3.1.1 which will be split into several lemmas and propositions.

In the following the long-time asymptotic behavior of solutions of the Cahn-Hilliard equation is studied by exploring the Willmore functional. We consider the d -dimensional case of the Cahn-Hilliard equation. All following arguments hold true both for the Neumann boundary problem and the Cauchy problem in \mathbb{R}^d with certain conditions on the spatial decay of the solutions. We start by introducing some useful properties of the functionals in our setting of the stationary profile.

3.1 Instabilities in the Cahn-Hilliard Equation

Lemma 3.1.3. *Let u be the solution of the Cahn-Hilliard equation as posed in Theorem 3.1.1. Then for any test function $\phi = \phi(x, t) \in C_0^\infty(\Omega \times (0, \infty))$ we have*

$$\begin{aligned} \frac{d}{dt} \int_{\Omega} \phi \left(\frac{\epsilon^2}{2} |\nabla u|^2 + F(u) \right) dx + \int_{\Omega} \phi |\nabla(\epsilon^2 \Delta u - F'(u))|^2 dx \\ = \int_{\Omega} \phi_t \left(\frac{\epsilon^2}{2} |\nabla u|^2 + F(u) \right) dx + \frac{1}{2} \int_{\Omega} \Delta \phi (F'(u) - \epsilon^2 \Delta u)^2 dx \\ - \epsilon^2 \int_{\Omega} \nabla(\nabla \phi \cdot \nabla u) \cdot \nabla(\epsilon^2 \Delta u - F'(u)) dx. \end{aligned}$$

Lemma 3.1.4. *Let u be the solution of the Cahn-Hilliard equation as posed in Theorem 3.1.1 then we have*

$$\begin{aligned} \frac{d}{dt} \int_{\Omega} (\epsilon \Delta u - \frac{1}{\epsilon} F'(u))^2 dx + 2\epsilon^2 \int_{\Omega} |\Delta(\epsilon \Delta u - \frac{1}{\epsilon} F'(u))|^2 dx \\ = 2 \int_{\Omega} F''(u) (\epsilon \Delta u - \frac{1}{\epsilon} F'(u)) \Delta(\epsilon \Delta u - \frac{1}{\epsilon} F'(u)) dx, \end{aligned}$$

and

$$\begin{aligned} \frac{d}{dt} \int_{\Omega} (\Delta(\epsilon \Delta u - \frac{1}{\epsilon} F'(u)))^2 dx + 2\epsilon^2 \int_{\Omega} (\Delta^2(\epsilon \Delta u - \frac{1}{\epsilon} F'(u)))^2 dx \\ = 2 \int_{\Omega} F''(u) \Delta(\epsilon \Delta u - \frac{1}{\epsilon} F'(u)) \Delta^2(\epsilon \Delta u - \frac{1}{\epsilon} F'(u)) dx. \end{aligned}$$

The proofs of Lemma 3.1.3 and 3.1.4 are straightforward. Note that both lemmas hold when Ω is a bounded domain as well as when Ω is unbounded, provided that condition (3.7) from Theorem 3.1.1 holds.

Proposition 3.1.5. *Let $f, g \in C^1([0, \infty))$ be nonnegative functions with $g'(t) \leq 0$ everywhere, $\text{supp } f \subset \text{supp } g$, $\sup_{t \in \text{supp } g} \frac{f}{g}$ and $\sup_{t \in \text{supp } g} \frac{(f')^+}{g}$ bounded, where $(f')^+(t) = \max\{f'(t), 0\}$. Under the same assumptions as in Theorem 3.1.1 and for a sufficiently large constant C we have*

$$\frac{d}{dt} \left[\int_{\Omega} f(t) (\epsilon \Delta u - \frac{1}{\epsilon} F'(u))^2 dx + \frac{C}{\epsilon^2} \int_{\Omega} g(t) \left(\frac{\epsilon^2}{2} |\nabla u|^2 + F(u) \right) dx \right] \leq 0.$$

In particular, $\epsilon^3 W[u](t) + CE[u](t) \leq \epsilon^3 W[u^0] + CE[u^0]$.

Proof. Consider the functional

$$U[u](t) = \int_{\Omega} f(t) (\epsilon \Delta u - \frac{1}{\epsilon} F'(u))^2 dx + \frac{C}{\epsilon^2} \int_{\Omega} g(t) \left(\frac{\epsilon^2}{2} |\nabla u|^2 + F(u) \right) dx.$$

3.1 Instabilities in the Cahn-Hilliard Equation

In the following we use the short form $\int := \int_{\Omega}$. By using the identity in Lemma 3.1.4 for the first term in $U[u](t)$ and 3.1.3 for the second term we derive

$$\begin{aligned} \frac{d}{dt} U[u](t) &= f'(t) \int (\epsilon \Delta u - \frac{1}{\epsilon} F'(u))^2 dx + \frac{C}{\epsilon^2} g'(t) \int \frac{\epsilon^2}{2} |\nabla u|^2 + F(u) dx \\ &\quad + f(t) \left[2 \int F''(u) (\epsilon \Delta u - \frac{1}{\epsilon} F'(u)) \Delta (\epsilon \Delta u - \frac{1}{\epsilon} F'(u)) dx \right. \\ &\quad \left. - 2\epsilon^2 \int |\Delta(\epsilon \Delta u - \frac{1}{\epsilon} F'(u))|^2 dx \right] - \frac{C}{\epsilon^2} g(t) \int |\nabla(-\epsilon^2 \Delta u + F'(u))|^2 dx. \end{aligned} \quad (3.1)$$

For the case $\Omega = \mathbb{R}^d$ we need the following Lemma to deal with the last term in (3.1).

Lemma 3.1.6 (modified Poincare inequality on \mathbb{R}^d). *Let $a > 0, C_1 > 0, C_2 > 0$ be fixed constants. Then there exists a positive constant $C_0 = C_0(a, C_1, C_2)$ such that for any functions f in*

$$V_{a,C_1,C_2} = \{f \in H^1(\mathbb{R}^d) : \int_{\mathbb{R}^d} f dx = 0, |f(x)| \leq C_1 e^{-a|x|} |f|_{L^2}, |f'(x)| \leq C_2 e^{-a|x|} |f|_{L^2} \text{ for } x \in \mathbb{R}^d\},$$

we have

$$|f|_{L^2(\mathbb{R}^d)} \leq C_0 |\nabla f|_{L^2(\mathbb{R}^d)}.$$

Taking into account condition (3.7) for the spatial decay of the involved quantities and by using Lemma 3.1.6 for $\Omega = \mathbb{R}^d$, the right side of (3.1) can be bounded by

$$\begin{aligned} &\left((f'(t))^+ - \frac{Cg(t)}{C_0} \right) \int (\epsilon \Delta u - \frac{1}{\epsilon} F'(u))^2 dx \\ &\quad + 2f(t) \sup_{|u| \leq 2} |F''(u)| \int |\epsilon \Delta u - \frac{1}{\epsilon} F'(u)| \cdot |\Delta(\epsilon \Delta u - \frac{1}{\epsilon} F'(u))| dx \\ &\quad - 2f(t)\epsilon^2 \int |\Delta(\epsilon \Delta u - \frac{1}{\epsilon} F'(u))|^2 dx + \frac{C}{\epsilon^2} g'(t) E[u](t). \end{aligned}$$

This term is non-positive when C is chosen to be large enough such that

$$f(t)^2 \sup_{|u| \leq 2} |F''(u)|^2 - \left((f'(t))^+ - \frac{Cg(t)}{C_0} \right) (-2f(t)\epsilon^2) \leq 0,$$

that is, choosing $C > \frac{C_0 f(t) (\sup_{|u| \leq 2} |F''(u)|)^2}{2\epsilon^2 g(t)} + \frac{C_0 (f'(t))^+}{g(t)}$ for $t \in \text{supp } g$. \square

Remark 3.1.7. Note that the Poincare inequality on \mathbb{R}^d is not valid in general. Consider for example the function $h_a(x) = a^{\frac{n+2}{2b}} x e^{-a|x|^b}$ with $a > 0$ and some fixed $b > 0$. Then $\int h_a^2 dx = O(1)$ and $\int h_a'^2 dx = O(a^{\frac{2}{b}})$ as $a \rightarrow 0+$. Therefore

$$\frac{|h_a'|_{L^2}}{|h_a|_{L^2}} = O(a^{\frac{1}{b}}) \rightarrow 0$$

3.1 Instabilities in the Cahn-Hilliard Equation

as a tends to zero, which contradicts the Poincare inequality.

Finally we arrive at the proof of the main result of this section, Theorem 3.1.1.

Proof of Theorem 3.1.1. Step 1: Let

$$f(t) = \begin{cases} \frac{1+t}{2}, & 0 \leq t \leq 1, \\ 2-t, & 1 \leq t \leq 2, \\ 0, & t \geq 2 \end{cases}$$

and

$$g(t) = \begin{cases} 1, & t \leq 2, \\ 0, & t \geq 3 \end{cases}.$$

Let C be a fixed constant chosen as in Proposition 3.1.5. The functional

$$U[u](t) \equiv 4\epsilon f(t)W[u](t) + \frac{C}{\epsilon^2}g(t)E[u](t)$$

is decreasing in time and $U[u](t=1) \leq U[u](t=0)$. That is,

$$W[u](t=1) + \frac{C}{4\epsilon^3}E[u](t=1) \leq \frac{1}{2}W[u](t=0) + \frac{C}{4\epsilon^3}E[u](t=0).$$

Step 2: For each $n \in \mathbb{N}$, setting $f(t-n+1)$ and $g(t-n+1)$ as in Proposition 3.1.5, we can write down the same inequality as in the previous step but for $n-1 \leq t \leq n$ and obtain

$$W[u](t=n) + \frac{C}{4\epsilon^3}E[u](t=n) \leq \frac{1}{2}W[u](t=n-1) + \frac{C}{4\epsilon^3}E[u](t=n-1). \quad (3.2)$$

Set $\alpha_n = W[u](t=n)$. Then (3.2) can be rewritten as

$$\alpha_n \leq \frac{1}{2}\alpha_{n-1} + \frac{C}{4\epsilon^3} \int_{n-1}^n \int_{\Omega} |\nabla(-\epsilon^2 \Delta u + F'(u))|^2 dx dt$$

where we used the decay property (3.4) of the energy functional.

Step 3: We want to show that α_n tends to zero as n tends to infinity. By an iterative argument we get

$$\begin{aligned} \alpha_n &\leq \left(\frac{1}{2}\right)^n \alpha_0 \\ &\quad + \frac{C}{4\epsilon^3} \left(\left(\frac{1}{2}\right)^{n-1} \int_0^1 \int_{\Omega} |\nabla(-\epsilon^2 \Delta u + F'(u))|^2 dx dt + \right. \\ &\quad \left(\frac{1}{2}\right)^{n-2} \int_1^2 \int_{\Omega} |\nabla(-\epsilon^2 \Delta u + F'(u))|^2 dx dt \right. \\ &\quad \left. + \cdots + \frac{1}{2} \int_{n-2}^{n-1} \int_{\Omega} |\nabla(-\epsilon^2 \Delta u + F'(u))|^2 dx dt \right. \\ &\quad \left. + \int_{n-1}^n \int_{\Omega} |\nabla(-\epsilon^2 \Delta u + F'(u))|^2 dx dt \right). \end{aligned}$$

3.1 Instabilities in the Cahn-Hilliard Equation

Using a standard fact from calculus formulated in the following Lemma 3.1.8, it follows that α_n converges to 0 for $n \rightarrow \infty$.

Lemma 3.1.8. *Let $(a_n), (b_n)$ are two nonnegative sequences such that their sums $\sum_n a_n$ and $\sum_n b_n$ are convergent. Then*

$$\lim_{n \rightarrow \infty} \sum_{i=0}^n a_i b_{n-i} = 0.$$

We conclude our proof in step 4.

Step 4: It remains to prove that for any sequence (t_n) tending to infinity, $W[u](t_n)$ converges to zero. To do so it suffices to prove that for any fixed integer $q > 0$, $(W[u](t = \frac{n}{q}))_n$ converges to zero. Repeating the computations of Step 3 for the inequality (3.2) for all rational values of t in between $n - 1$ and n the proof is similar and we omit the details here. \square

Remark 3.1.9. *Note that the proof of Theorem 3.1.1 also provides trivially for a decay of u_t in H^{-2} , namely*

$$\begin{aligned} \|u_t\|_{H^{-2}} &= \|\Delta(-\epsilon^2 \Delta u + F'(u))\|_{H^{-2}} \\ &\leq C \|\epsilon^2 \Delta u + F'(u)\|_{L^2} \\ &\rightarrow 0 \text{ as } t \rightarrow \infty. \end{aligned}$$

So we have shown that the Willmore functional asymptotically decreases to zero under the assumptions of Theorem 3.1.1. This additionally proves that $u_t \rightarrow 0$ for $t \rightarrow \infty$ in $H^{-2}(\Omega)$ for every $\epsilon > 0$ and arbitrary dimension d.

3.1.2 Linear Stability / Instability

In this section we consider the short-time behavior of solutions of the Cahn-Hilliard equation. We relate local-in-time instabilities of solutions with the Willmore functional by comparing the eigenvalues of the linearized operator of the equation with the evolution of the Willmore functional. We begin with a short discussion of spectral estimates and conclude with presenting the new result.

For the one dimensional case Alikakos, Bates and Fusco showed in [ABF91] that there is exactly one unstable eigenvalue of the linearized Cahn-Hilliard eigenvalue problem. For simplicity let $D = [0, 1]$. They consider the problem linearized at an invariant

3.1 Instabilities in the Cahn-Hilliard Equation

manifold \mathcal{M} formed by the translation of a self-similar solution $u_\epsilon^\xi(x) = u_\epsilon(x - \xi) \in \mathcal{M}$ with parameter ξ :

$$\begin{cases} -\epsilon^2 H''' + (F''(u_\epsilon^\xi)H')' = \lambda(\epsilon)H, & 0 < x < 1, \\ H = H'' = 0 & x = 0, 1. \end{cases} \quad (3.1)$$

The first eigenvalue is simple and exponentially small for small $\epsilon > 0$

$$0 < \lambda_1^\xi(\epsilon) = O\left(\frac{(u_{xx}^\xi(0))^2}{\epsilon^3}\right) = O\left(\frac{e^{-\frac{2\nu\delta_\xi}{\epsilon}}}{\epsilon^7}\right), \quad (3.2)$$

where δ_ξ is a small positive constant given in the proof of (3.2) in [ABF91] and ν is a generic constant, see [CGS84]. The remaining spectrum is bounded from above by

$$\lambda_i^\xi(\epsilon) \leq -C < 0, i = 2, 3, \dots$$

with C is positive and independent of ϵ, ξ . Both results are contained in [ABF91].

In two dimensions Alikakos and Fusco [AF94] proved that there is a two-dimensional invariant manifold with exponentially small eigenvalues where the solutions asymptotically develop droplets on the boundary with a speed which is exponentially small. These superslow solutions are called bubble solutions and correspond to an approximate spherical interface drifting slowly towards the boundary, without changing its shape. Solutions like that are typical in the final stages of evolution of (3.1) for general initial conditions. Further they showed that the dimension of eigenspaces of superslow eigenvalues of the linearized Cahn-Hilliard equation on $D \subseteq \mathbb{R}^d$ is at most d for $d \geq 2$. For simplicity of explanation we consider the eigenvalue problem of the linearized fourth-order Cahn-Hilliard operator in $D \subseteq \mathbb{R}^2$. The results in higher dimensions are analogous to this case. Let $U(\eta)$ be the unique increasing bounded solution of $U'' - F(U) = 0$ on \mathbb{R} , and $V(\eta)$ a bounded function that satisfies the orthogonality condition

$$\int_{-\infty}^{\infty} f''(U(\eta))\dot{U}^2(\eta)V(\eta)d\eta = 0,$$

where $f(u) = F'(u)$. We consider a one-parameter family of functions $u_\epsilon^\xi(x)$ represented by

$$u_\epsilon^\xi(x) = \begin{cases} U\left(\frac{x-\rho}{\epsilon}\right) + \epsilon V\left(\frac{x-\rho}{\epsilon}\right) + O(\epsilon^2), & |y - \rho| \leq \lambda, \\ q_\epsilon(x), & |y - \rho| > \lambda \end{cases}$$

where $y = |x - \xi|, \rho > 0$ and $q_\epsilon(x)$ is an arbitrary function with $f'(q_\epsilon(x)) \geq c > 0$. The function $u_\epsilon^\xi(x)$ represents a bubble with center $\xi \in D$ and radius ρ .

3.1 Instabilities in the Cahn-Hilliard Equation

The eigenvalue problem for the Cahn-Hilliard operator linearized in $u_\epsilon^\xi(x)$, i.e., $L^\xi = \Delta(-\epsilon^2 \Delta + F''(u_\epsilon^\xi))$, is given by

$$L^\xi(\phi) = \lambda\phi, \quad x \in D \subseteq \mathbb{R}^2 \quad (3.3)$$

with Neumann boundary conditions

$$\frac{\partial \phi}{\partial n} = \frac{\partial}{\partial n}(-\epsilon^2 \Delta \phi + F''(u_\epsilon^\xi)\phi) = 0, \quad x \in \partial D.$$

In [AF94] Alikakos and Fusco stated the following result.

Theorem 3.1.10. *Let $\lambda_1^\epsilon \geq \lambda_2^\epsilon \geq \lambda_3^\epsilon \geq \dots$ be the eigenvalues of (3.3). Let $\rho > 0, \delta > 0$ be fixed. Then there exists an $\epsilon_0 > 0$ and constants $c, C, C' > 0$, independent of ϵ , such that for $0 < \epsilon < \epsilon_0$ and $\xi \in D$ with $d(\xi, \partial D) > \delta$, the following estimates hold true:*

$$\begin{aligned} Ce^{-\frac{\epsilon}{\epsilon}} &\geq \lambda_1^\epsilon \geq \lambda_2^\epsilon \geq -Ce^{-\frac{\epsilon}{\epsilon}}, \\ \lambda_3^\epsilon &\leq -C'\epsilon. \end{aligned}$$

The first two eigenvalues $\lambda_1^\epsilon, \lambda_2^\epsilon$ are superslow and the others are negative.

Now we present the connection between linear stability properties of the Cahn-Hilliard equation and the Willmore functional. In the following we provide a linear stability analysis around an equilibrium state u_0 satisfying

$$-\epsilon^2 \Delta u_0 + F'(u_0) = 0.$$

More precisely, we look for a solution of the form

$$u(x, t) = u_0(x) + \delta v(x, t) + \mathcal{O}(\delta^2)$$

for sufficiently small $0 < \delta \ll 1$ and some perturbation $v(x, t)$. Due to mass conservation we assume that v has mean zero for all times

$$\int_{\Omega} v(x, t) dx = 0 \quad \forall t > 0.$$

We obtain the first-order evolution with respect to δ via the linearized equation

$$v_t = \Delta(-\epsilon^2 \Delta v + F''(u_0)v) := \Delta L_0 v. \quad (3.4)$$

We now compute the asymptotic expansion of the Willmore functional as $\delta \rightarrow 0$. It can be expanded as

$$W[u] = W[u_0] + \delta W'[u_0]v + \frac{\delta^2}{2} W''[u_0](v, v) + \mathcal{O}(\delta^3), \quad (3.5)$$

3.1 Instabilities in the Cahn-Hilliard Equation

where the first and second-order derivatives are taken as variations

$$W'[u_0]v = \int (-\epsilon^2 \Delta u_0 + F'(u_0))(-\epsilon^2 \Delta v + F''(u_0)v)dx$$

and

$$W''[u_0](v, w) = \int (L_0 v)(L_0 w)dx + \int (-\epsilon^2 \Delta u_0 + F'(u_0))F'''(u_0)vw dx.$$

Since u_0 is a stationary solution, we have

$$W'[u_0]v = 0 \quad \text{and} \quad W''[u_0](v, v) = \int (L_0 v)^2 dx.$$

Now let v_0 be an eigenfunction of the linearized fourth-order Cahn-Hilliard operator, i.e. there is $\lambda \neq 0$ such that

$$\Delta(L_0 v_0) = \lambda v_0,$$

with Neumann boundary condition $\frac{\partial v_0}{\partial n}|_{\partial\Omega} = 0$ and $\int_{\Omega} v_0 = 0$. Note that λ is real, since v_0 solves a symmetric eigenvalue problem in the scalar product of H^{-1} , defined here as the dual of $H^1(\Omega) \cap \{u : \int_{\Omega} u dx = 0\}$, cf. also Section 2.1.3.

The standard linear stability analysis yields that the perturbation of u_0 by δv_0 is linearly stable for $\lambda < 0$ and unstable for $\lambda > 0$. These two cases can be translated directly into the local-in-time behavior of the Willmore functional, whose time derivative at time $t = 0$ is given by

$$\begin{aligned} \frac{d}{dt}W[u(t)]|_{t=0} &= \delta W'[u_0]v_t|_{t=0} + \delta^2 W''[u_0](v, v_t)|_{t=0} + \mathcal{O}(\delta^3) \\ &= \delta^2 \int (L_0 v_0)(L_0 v_t)dx + \mathcal{O}(\delta^3) \\ &= \delta^2 \int (L_0 v_0)(L_0 \Delta L_0 v_0)dx + \mathcal{O}(\delta^3) \\ &= \delta^2 \int (L_0 v_0)(L_0(\lambda v_0))dx + \mathcal{O}(\delta^3) \\ &= \lambda \delta^2 \int (L_0 v_0)^2 dx + \mathcal{O}(\delta^3). \end{aligned}$$

This means that to leading order, the time derivative of $W[u]$ has the same sign as λ , i.e., the Willmore functional is locally increasing in time in the unstable case, and locally decreasing in the stable case.

3.1.3 Nonlinear Stability / Instability

We expect the behavior of solutions of the nonlinear equation (3.1) to be dominated by that of the linear equation in the neighborhood of stationary solutions. Therefore numerical examples may very well give us a good idea about the behavior of solutions and their connection to the Willmore functional even for the nonlinear case. In the following a semi-implicit finite element discretization for the Cahn-Hilliard equation is briefly described and numerical examples are discussed.

Numerical Discretization

To discretize a fourth-order equation with boundary conditions as above it is often convenient to write it as a system of two differential algebraic equations of second order. In our case of the Cahn-Hilliard equation this results in the following system

$$\begin{aligned} u_t &= \Delta v \\ v &= -\epsilon^2 \Delta u + F'(u), \end{aligned}$$

with Neumann boundary conditions

$$\frac{\partial u}{\partial n} = \frac{\partial v}{\partial n} = 0, \quad x \in \partial\Omega.$$

The following issues have to be taken into consideration.

- Explicit schemes for fourth-order equations restrict time steps to be of order $O((\Delta x)^4)$, where Δx is the spatial grid size.
- Fully implicit schemes can be unconditionally stable. The disadvantage is the high computational effort for solving nonlinear equations.
- Semi-implicit schemes are a compromise between explicit and implicit discretization. Briefly, semi-implicit means that the equation is split into a convex and a concave part and discretized implicitly and explicitly respectively, see ([BE92, Ey98]). Therefore the restriction on the step sizes is less severe and we do not have to solve nonlinear equations.

3.1 Instabilities in the Cahn-Hilliard Equation

For these reasons we use the following semi-implicit approximation

$$\begin{aligned}\frac{u(t, x) - u(t - \Delta t, x)}{\Delta t} &= \Delta v(t, x) \\ v(t, x) &= -\epsilon^2 \Delta u(t, x) + F'(u(t - \Delta t, x)) + F''(u(t - \Delta t, x)) \cdot (u(t, x) - u(t - \Delta t, x)).\end{aligned}$$

Note that F' is Taylor-expanded at the solution of the previous time step $u(t - \Delta t)$. For the space discretization we use linear finite elements on an equidistant grid in one dimension and on a rectangular grid in two dimensions.

Numerical Examples

In the following examples we consider the solution of the Cahn-Hilliard equation in one and two dimensions for different initial states in a neighborhood of a transition solution. In the one dimensional case the so-called kink solution is given by $u_0(x) = \tanh(\frac{x}{2\epsilon})$. As a first approach in the one dimensional analysis we take as initial value $u(x, t = 0) = u_0(x) + p(x)$. The function p denotes a particular kind of zero-mean perturbation, namely

$$p(x) = \begin{cases} a \cdot \sin(f\pi \frac{x}{C\epsilon}) & x \in (-C\epsilon, C\epsilon) \\ 0 & \text{otherwise,} \end{cases}$$

with amplitude $a > 0$, frequency $f > 0$ and support $(-C\epsilon, C\epsilon)$ with $C > 0$. The amplitude a is chosen so that the values of u within the support of the perturbation lie in the spinodal interval of the equation (which is the back diffusion interval).

Varying the parameter ϵ and the support, the amplitude and the frequency of p , we want to observe how the solutions evolve in time. The behavior of the solutions is further compared with the evolution of the corresponding energy functional and the Willmore functional.

We begin with a fixed $\epsilon = 0.1$. For the first two examples in Figure 3.1 and 3.2 a fixed step size in space and time discretization was used. As spatial step size we took $\Delta x = 0.05 \cdot \epsilon$ and for the time steps $\Delta t = 10^3 \cdot \epsilon$. The amplitude and the frequency of the perturbation are also fixed to 1. The difference between the two examples is the support of the perturbation and dependent on this is the convergence process.

In the first example an unstable state occurs. This means that over a certain time interval the perturbation locally grows. The second example is stable in the numerical computations.

3.1 Instabilities in the Cahn-Hilliard Equation

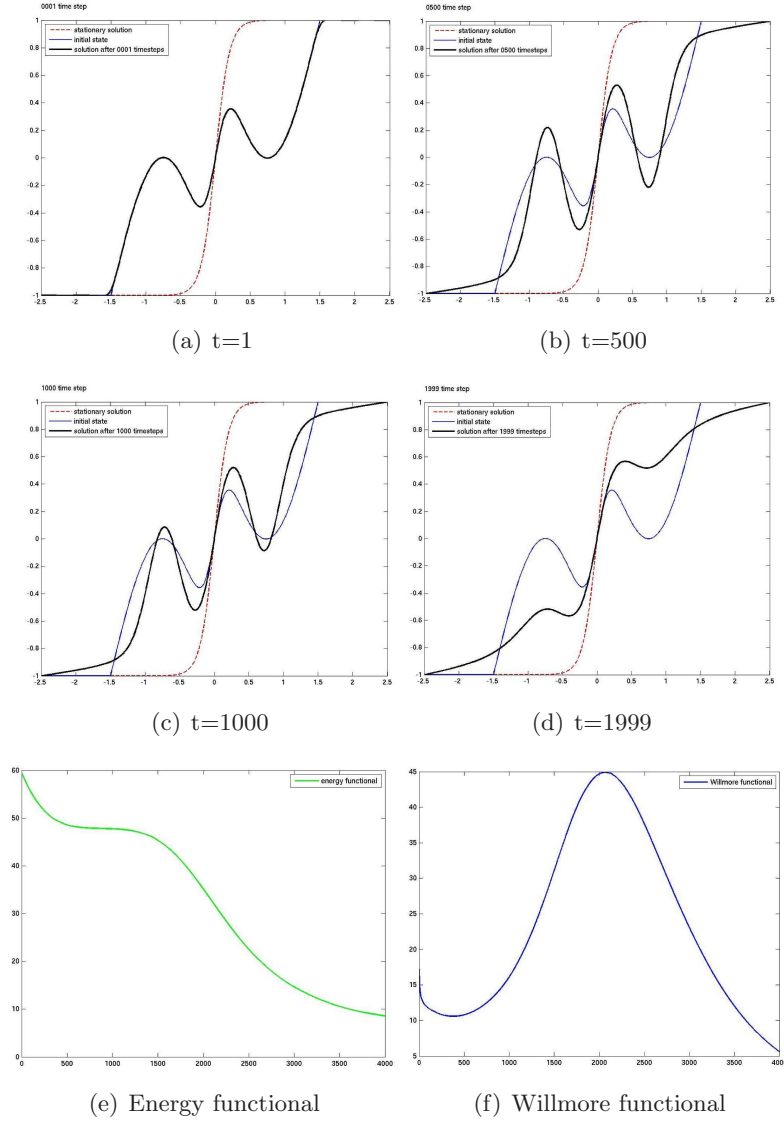


Figure 3.1: (a)-(d): Evolution of the solution in time for $\epsilon = 0.1$ and a zero-mean perturbation supported on $(-15\epsilon, 15\epsilon)$ with $a = 1$, $f = 1$ and with corresponding energy functional (e) and Willmore functional (f)

In the first case the supporting interval for the perturbation is $(-15\epsilon, 15\epsilon)$ (Figure 3.1) and we begin with an initial state having two peaks on both sides of zero. When time proceeds the peaks grow in the beginning, resulting in an unstable transient state. After this unstable state the solution converges to the kink solution. In the case of the

3.1 Instabilities in the Cahn-Hilliard Equation

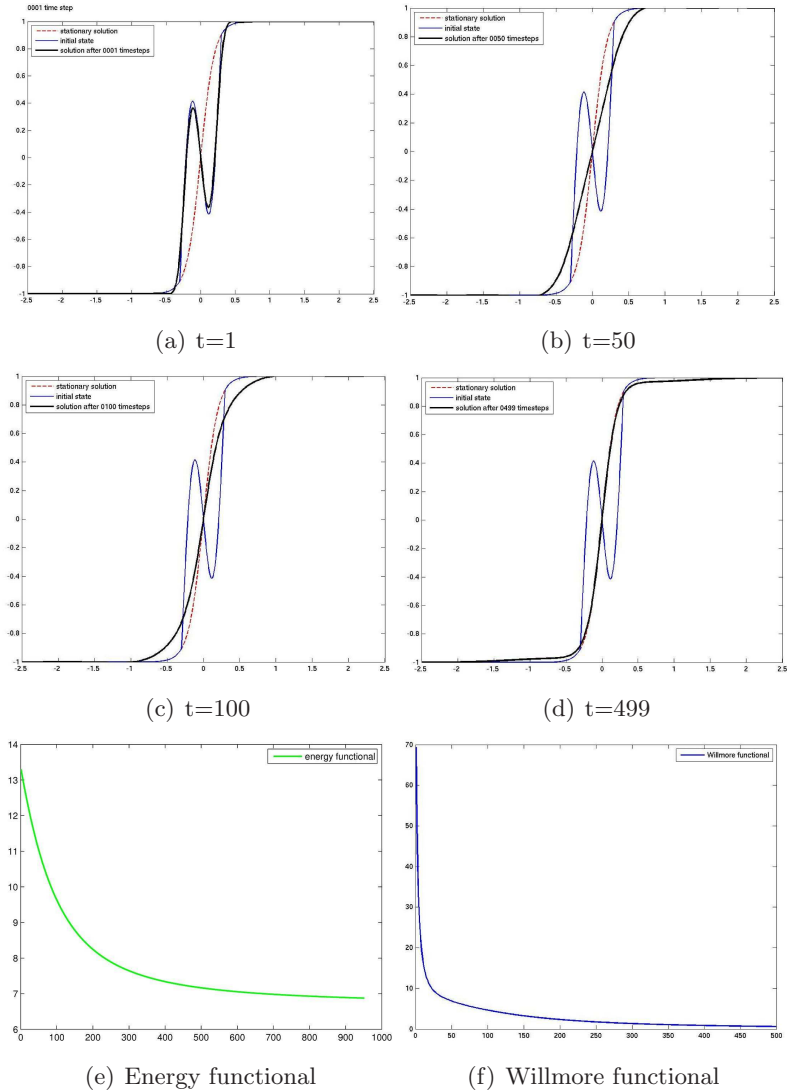


Figure 3.2: (a)-(d): Evolution of the solution in time for $\epsilon = 0.1$ and a zero-mean perturbation supported on $(-3\epsilon, 3\epsilon)$ with $a = 1$, $f = 1$ and with corresponding energy functional (e) and Willmore functional (f)

supporting interval $(-3\epsilon, 3\epsilon)$ in Figure 3.2 the solution converges uniformly to the kink solution without transitional state.

Comparing the time evolution of our first two examples with the corresponding energy functionals and Willmore functionals, we can easily see differences in the graphs of functionals. We can see that in the unstable case the energy functional almost has

3.1 Instabilities in the Cahn-Hilliard Equation

a saddle point, in the stable case it is rapidly decreasing. Also instabilities seem to correspond to peaks in the graph of the Willmore functional over time. The Willmore functional increases over a finite time interval in contrast to the stable case where it decreases for all times t .

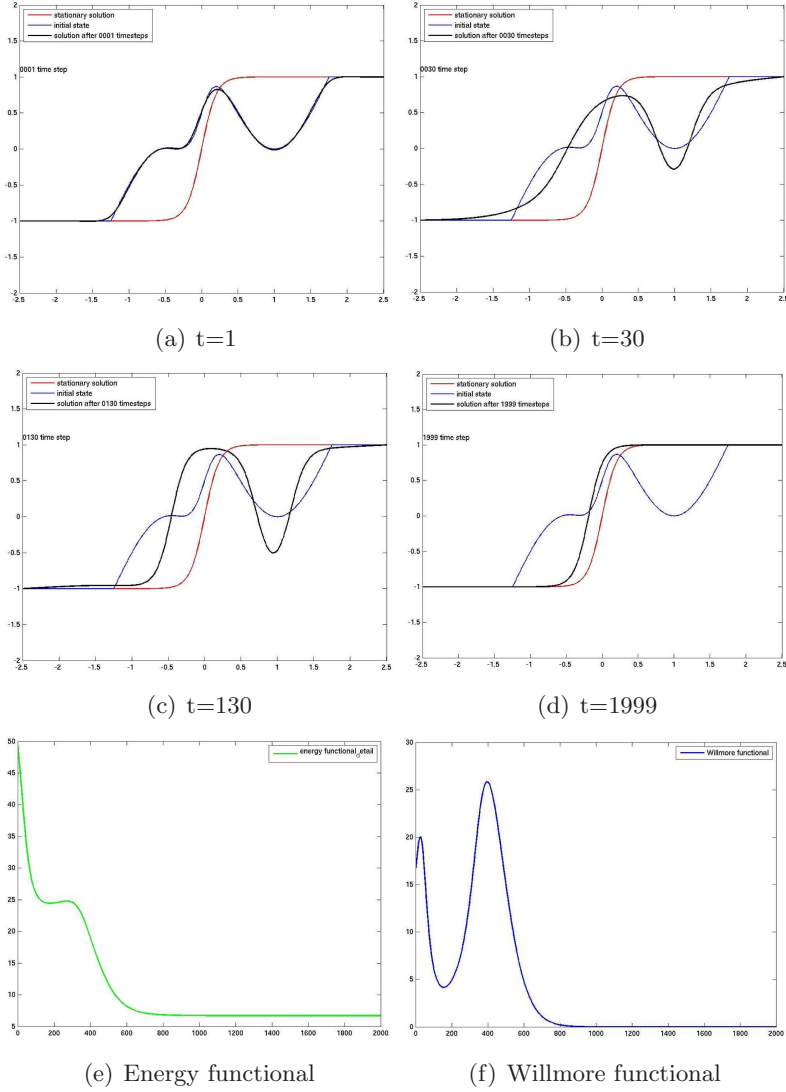


Figure 3.3: (a)-(d): Evolution of the shifted solution in time for $\epsilon = 0.1$ and a zero-mean perturbation supported on $(-15\epsilon, 15\epsilon)$ with $a = 1$, $f = 1$ and with corresponding energy functional (e) and Willmore functional (f)

Another interesting phenomenon can be seen by starting with modified versions of

3.1 Instabilities in the Cahn-Hilliard Equation

the perturbation p . For example we could shift the sinusoidal perturbation to the left or to the right of zero to start with an asymmetric initial state. The example in Figure 3.3 is a result of a shift of the perturbation used in the example of Figure 3.1. The shift of the perturbation leads to a shift of the kink solution asymptotically in time as a consequence of conservation of mass. Considering again the Willmore functional, an increase in time, visibly caused by a transitional instability, occurs.

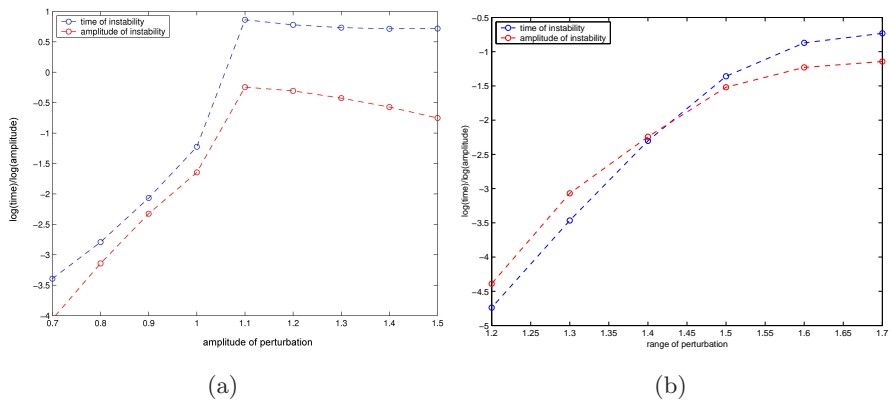


Figure 3.4: Length of time interval and maximal amplitude of the instability for different amplitudes of the perturbation (a) and different supporting intervals of the perturbation (b). $\epsilon = 0.1$ fixed.

Considering the behavior of the perturbed solution in several numerical tests we can further make claims on how the perturbation has to look like so that an unstable state occurs. For a fixed $\epsilon \ll 1$ we can see that the length of the supporting interval is most relevant. Extending the supporting interval of the perturbation brings with it an extension of the time interval and the size of the instability as a consequence, compare Figure 3.4 right diagram. If the supporting interval is too small, no unstable state can be seen, compare Figure 3.2. Also the amplitude and the frequency of the perturbation have an influence on the occurrence and size of the instability. With growing amplitude of the perturbation, the time interval and the size of the instability change, compare Figure 3.4, left diagram. If the amplitude exceeds a certain threshold the solution will not converge to the kink solution anymore. Furthermore the higher the frequency of the perturbation, the faster the solution converges to the kink solution. Therefore the higher the frequency of the perturbation, the smaller the time interval

3.1 Instabilities in the Cahn-Hilliard Equation

of the instability. Because of the important role of the support of the perturbation, it seems that perturbations with high frequency bring no additional information for the study of the time-local instability.

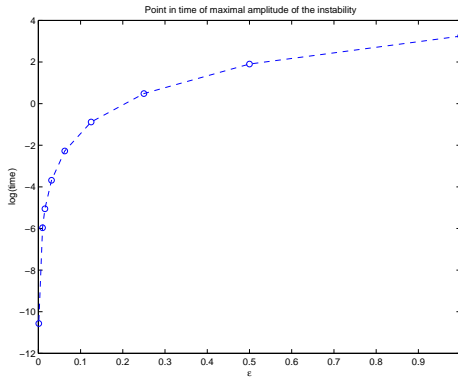


Figure 3.5: Length of the time interval of the instability for different values of ϵ for a perturbation supported on $(-15\epsilon, 15\epsilon)$ with $a = 1$, $f = 1$.

By changing the parameter ϵ one can see that with decreasing ϵ the time interval of the instability decreases. In Figure 3.5 the point in time of the maximal amplitude of the instability is shown for different ϵ . The maximal amplitude of the instability stays approximately the same.

In the two-dimensional case the analogue of the kink solutions are the so-called bubble solutions. In Figure 3.6 the evolution of a solution of the two dimensional Cahn-Hilliard equation near a bubble solution over a finite time interval is shown. In this example we used equidistant space and time discretization $\Delta x = \Delta y = \epsilon$ and $\Delta t = \epsilon^4$. Here the time stepsize is chosen rather small in order not to miss the instability which appears for a very short time period only. As initial value we take a radial-symmetric bubble solution perturbed by a sine wave in x_1 -direction. For a better comparison with the one-dimensional case a vertical cut in $x_2 = 0.5$ of the solution is shown. Again the solution exhibits a local growth of amplitude before converging uniformly to the stationary solution. Especially near $x_1 = 0.5$ the solution initially tends away from the bubble solution. As predicted, this phenomenon causes an increase of the Willmore functional in a short time interval before it decays to 0.

3.1 Instabilities in the Cahn-Hilliard Equation

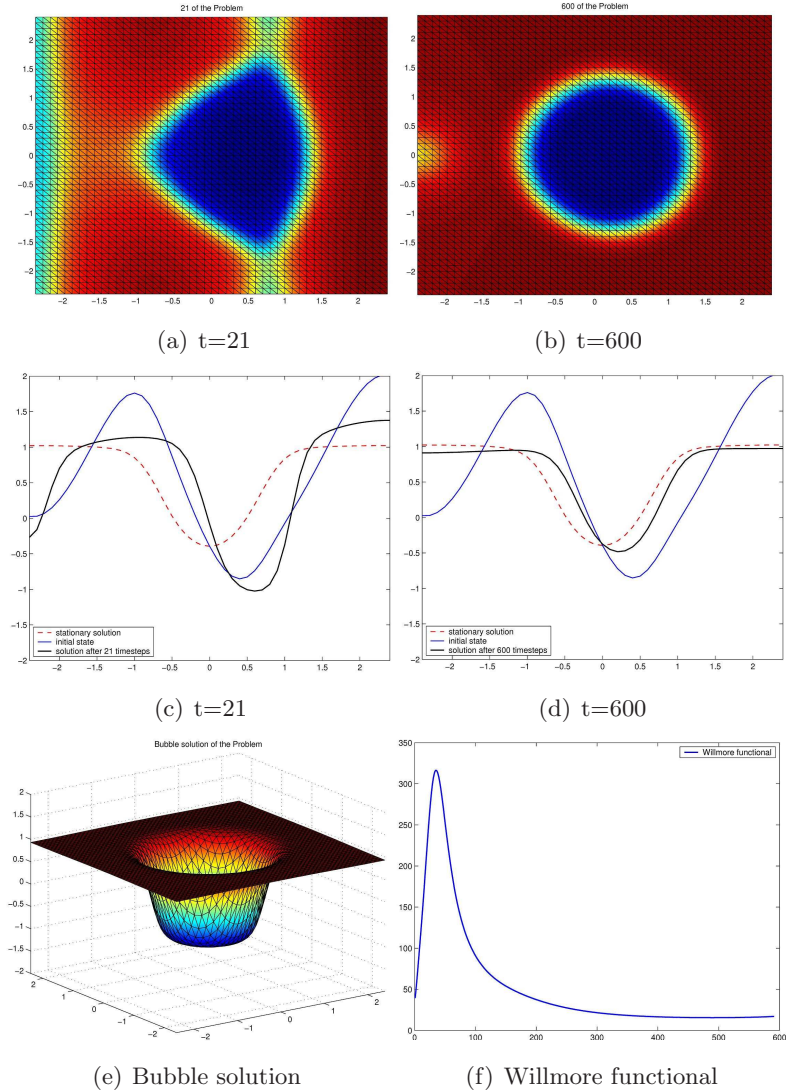


Figure 3.6: Surface plot (a)-(b) and vertical cut (c)-(d) of the solution for $\epsilon = 0.1$ perturbed with a sinusoidal wave in x -direction. (e) shows the bubble solution and (f) the Willmore functional

3.1.4 Consequences

We considered local instability and asymptotic behavior of the Cahn-Hilliard equation in the neighborhood of certain transition solutions. We found that studying instabilities of the Cahn-Hilliard equation in finite time is closely connected to studying the monotonicity behavior of the Willmore functional. We found that the Willmore

functional is a good monitoring quantity to study structures of instability patterns of the solutions. We found the Willmore functional to be monotonically decreasing if the solution converges to the equilibrium state without transitional instability and having maxima when local-time instabilities occur.

Therefore the Willmore functional could be used for the mathematical and numerical analysis of the Cahn-Hilliard equation, e.g., by providing a more efficient tool for determining stability/instability of solutions. Further it can be useful in applications of the Cahn-Hilliard equation as in its inpainting application presented in Section 2.1. The Willmore functional could thereby serve as an indicator reporting how far away from the steady state the solution is.

3.2 Nonlocal Higher-Order Evolution Equations

In this section we study the asymptotic behavior of solutions to the nonlocal operator $u_t(x, t) = (-1)^{n-1} (J * Id - 1)^n (u(x, t))$, $x \in \mathbb{R}^d$ which is the nonlocal analogue to the higher-order local evolution equation $v_t = (-1)^{n-1}(\Delta)^n v$. We prove that the solutions of the nonlocal problem converge to the solution of the higher-order problem with right hand side given by powers of the Laplacian when the kernel J is rescaled in an appropriate way. Moreover, we prove that solutions to both equations have the same asymptotic decay rate as t goes to infinity. This section traces the contents of [RS09].

Our main concern in the present section is the asymptotic behavior of solutions of a nonlocal diffusion operator of higher order in the whole \mathbb{R}^d , $d \geq 1$.

We consider the following nonlocal evolution problem:

$$\begin{cases} u_t(x, t) = (-1)^{n-1} (J * Id - 1)^n (u(x, t)) \\ \quad = (-1)^{n-1} \left(\sum_{k=0}^n \binom{n}{k} (-1)^{n-k} (J*)^k (u) \right) (x, t), \\ u(x, 0) = u_0(x), \end{cases} \quad (3.1)$$

for $x \in \mathbb{R}^d$, $t > 0$ and arbitrary $n \geq 1$. Here $(J * u)(x, t) = \int_{\mathbb{R}^d} J(x - y)u(y, t) dy$ is the usual convolution of J and u and $(J*)^k(u)$ denotes the convolution with J iterated k times. Further, let $J \in C(\mathbb{R}^d, \mathbb{R})$ be a nonnegative, radially invariant function with $\int_{\mathbb{R}^d} J(x) dx = 1$ and $u_0 \in L^1(\mathbb{R}^d)$ denote the initial condition for (3.1).

3.2 Nonlocal Higher-Order Evolution Equations

Nonlocal problems like (3.1) have been recently widely used to model diffusion processes, see [Fi03]. The solution $u(x, t)$ of (3.1) is thereby interpreted as the density of a single population at the point x at time t and $J(x - y)$ is the probability of “jumping” from location y to location x . The convolution $(J * u)(x)$ is then the rate at which individuals arrive to position x from all other positions, while $-u(x, t) = -\int_{\mathbb{R}^d} J(y - x)u(x, t) dy$ is the rate at which they leave position x to reach any other position. Their evolution is described by (3.1) for the case $n = 1$. For more references concerning the use of nonlocal evolution problems and their stationary counterparts for modeling diffusion processes we quote for instance [BCC05, BFRW97, Co06, Co07, CDM08, CD05, CD07, Zh04], devoted to traveling front type solutions.

Further nonlocal equations like (3.1) also found applications in image processing. The main advantage of nonlocal operators in image processing is the ability to process structures like edges (local image features), but also textures (nonlocal image features), within the same framework. In [BCM05] a nonlocal filter, referred to as nonlocal means, was suggested for image denoising. A variational understanding of this filter was first presented in [KOJ05] as a nonconvex functional and later in [GO07] as a convex quadratic functional. In the latter reference the authors investigated the functional

$$E(u) = \frac{1}{2} \int_{\Omega \times \Omega} |u(x) - u(y)|^2 w(x, y) dx dy,$$

where the weight function $w(x, y) \in \Omega \times \Omega$, $\Omega \subset \mathbb{R}^2$ open and bounded, is positive and symmetric, i.e. $w(x, y) = w(y, x)$. The proposed flow for minimizing the energy $E(u)$ was then defined as

$$\begin{cases} u_t(x) = \int_{\Omega} (u(y) - u(x)) w(x, y) dy, & x \in \Omega, \\ u(x, 0) = u_0(x), \end{cases} \quad (3.2)$$

taking the given (noisy) image u_0 as the initial condition. With $w(x, y) = J(x - y)$ equation (3.2) has the same structure as the nonlocal equation (3.1) for $n = 1$.

We call equation (3.1) a nonlocal diffusion equation of order n . Thereby the diffusion of the density u at a point x and time t does not only depend on u and its derivatives at the point (x, t) (local behavior), but on all the values of u in a fixed neighborhood of x through the convolution term $J * u$ (nonlocal behavior). In our problem (3.1) the application of the nonlocal operator $J * Id - 1$ on the density u is iterated n times.

3.2 Nonlocal Higher-Order Evolution Equations

This can be seen as a nonlocal generalization of higher-order equations of the form

$$v_t(x, t) = -A^n(-\Delta)^{\frac{\alpha n}{2}} v(x, t), \quad (3.3)$$

with A and α are positive constants specified later in this section. Note that when $\alpha = 2$ (3.3) is just $v_t(x, t) = -A^n(-\Delta)^n v(x, t)$. Higher-order diffusions of this type appear in various applications. The Cahn-Hilliard equation, for instance, is a fourth-order reaction diffusion equation which models phase separation and coarsening of binary alloys, see [Fi00] for more details and references. A modified Cahn-Hilliard equation was further proposed in [BEG07a, BEG07b] for inpainting, i.e., image interpolation of binary images. Another fourth-order example is the Kuramoto-Sivashinsky equation (cf. e.g. [Mi86]), used in the study of spatiotemporal chaos (cf. [CH93]). In both equations a linear fourth-order diffusion as in (3.3) for $n = \alpha = 2$ is involved. Nonlocal higher-order problems have been, for instance, proposed as models for periodic phase separation. Here the nonlocal character of the problem is associated with long-range interactions of “particles” in the system. An example is the nonlocal Cahn-Hilliard equation (cf. e.g. [Ha04, NO95, OK86]).

Problem (3.1) was studied in great detail for the case $n = 1$ only. In fact the Cauchy problem is considered in [CCR06, IR08], while the “Neumann” boundary condition for the same problem is treated in [AMRT08, CERW07, CERW08]. See also [IR07] for the appearance of convective terms and [CCEM07, CER05] for other interesting features in related nonlocal problems.

In this section we consider (3.1) as a model for higher-order nonlocal evolution for arbitrary $n \geq 1$ and extend the existing analysis for the Cauchy problem within this general setting. For this model, we first prove existence and uniqueness of a solution, but our main aim is to study the asymptotic behavior as $t \rightarrow \infty$ of solutions to (3.1). Moreover, we prove that solutions to (3.1) converge to the solution to (3.3) when the problem is rescaled in an appropriate way.

Now, let us proceed with the precise description of our main results.

Statement of the results. For a function f we denote by \hat{f} the Fourier transform of f and by \check{f} the inverse Fourier transform of f . Our hypotheses on the convolution kernel J that we will assume throughout the paper are:

3.2 Nonlocal Higher-Order Evolution Equations

The kernel $J \in C(\mathbb{R}^d, \mathbb{R})$ is a nonnegative, radial function with total mass equalling one, $\int_{\mathbb{R}^d} J(x) dx = 1$. This means that J is a radial density probability, which implies that its Fourier transform satisfies $|\hat{J}(\xi)| \leq 1$ with $\hat{J}(0) = 1$. Moreover, we assume that

$$\hat{J}(\xi) = 1 - A |\xi|^\alpha + o(|\xi|^\alpha) \quad \text{for } \xi \rightarrow 0, \quad (3.4)$$

for some $A > 0$ and $\alpha > 0$.

Remark 3.2.1. Note that assumption (3.4) on the behaviour of \hat{J} near the origin plays a central role in the following analysis of the nonlocal problem. In fact, the decay rate as t goes to infinity of solutions of this nonlocal problem is determined by (3.4).

Under these conditions on J we have the following results. First, we show existence and uniqueness of a solution

Theorem 3.2.2. Let $u_0 \in L^1(\mathbb{R}^d)$ such that $\hat{u}_0 \in L^1(\mathbb{R}^d)$. There exists a unique solution $u \in C^0([0, \infty); L^1(\mathbb{R}^d))$ of (3.1) that, in Fourier variables, is given by the explicit formula, $\hat{u}(\xi, t) = e^{(-1)^{n-1}(\hat{J}(\xi)-1)^n t} \hat{u}_0(\xi)$.

Next, we deal with the asymptotic behavior as $t \rightarrow \infty$.

Theorem 3.2.3. Let u be a solution of (3.1) with $u_0, \hat{u}_0 \in L^1(\mathbb{R}^d)$. Then the asymptotic behavior of $u(x, t)$ is given by

$$\lim_{t \rightarrow +\infty} t^{\frac{d}{\alpha n}} \max_x |u(x, t) - v(x, t)| = 0,$$

where v is the solution of $v_t(x, t) = -A^n (-\Delta)^{\frac{\alpha n}{2}} v(x, t)$ with the initial condition $v(x, 0) = u_0(x)$ and A and α as in (3.4). Moreover, we have that there exists a constant $C > 0$ such that

$$\|u(., t)\|_{L^\infty(\mathbb{R}^d)} \leq C t^{-\frac{d}{\alpha n}}$$

and the asymptotic profile is given by

$$\lim_{t \rightarrow +\infty} \max_y \left| t^{\frac{d}{\alpha n}} u(yt^{\frac{1}{\alpha n}}, t) - \|u_0\|_{L^1(\mathbb{R}^d)} G_A(y) \right| = 0,$$

where $G_A(y)$ satisfies $\hat{G}_A(\xi) = e^{-A^n |\xi|^{\alpha n}}$.

To prove this result we use ideas from [CCR06] using Fourier variables, but with a nontrivial extra refinement that is due to the fact that we are dealing with higher-order problems. In fact, we have to take extra care and distinguish between even and odd n .

Next, we show that solutions to nonlocal problems like (3.1), rescaled in an appropriate way, converge to a solution to the problem (3.3) as the scaling parameter tends to zero.

Theorem 3.2.4. *Let u_ε be the unique solution to*

$$\begin{cases} (u_\varepsilon)_t(x, t) = (-1)^{n-1} \frac{(J_\varepsilon * Id - 1))^n}{\varepsilon^{\alpha n}} (u_\varepsilon(x, t)), \\ u(x, 0) = u_0(x), \end{cases} \quad (3.5)$$

where $J_\varepsilon(s) = \varepsilon^{-d} J(\frac{s}{\varepsilon})$. Then, for every $T > 0$, we have

$$\lim_{\varepsilon \rightarrow 0} \|u_\varepsilon - v\|_{L^\infty(\mathbb{R}^d \times (0, T))} = 0,$$

where v is the solution to the local problem $v_t(x, t) = -A^n(-\Delta)^{\frac{\alpha n}{2}} v(x, t)$ with the same initial condition $v(x, 0) = u_0(x)$.

The previous proofs of convergence of nonlocal problems to their local counterparts were performed in physical space with subtle arguments, see [CERW08, IR07]. For our proof of this result, we just look at Fourier variables, simplifying the previous analysis. Note that this approach is valid only when linear problems in the whole space are considered.

The verification of our results is organized as follows: in Section 3.2.1 we prove existence and uniqueness of a solution; in Section 3.2.2 we deal with the asymptotic behavior and, finally, in Section 3.2.3 we approximate the local higher-order problem by nonlocal ones.

3.2.1 Existence and Uniqueness

To prove existence and uniqueness of solutions we make use of the Fourier transform.

Proof of Theorem 3.2.2. We have

$$u_t(x, t) = (-1)^{n-1} \left(\sum_{k=0}^n \binom{n}{k} (-1)^{n-k} (J*)^k (u) \right) (x, t).$$

Applying the Fourier transform to this equation we obtain

$$\begin{aligned} \hat{u}_t(\xi, t) &= (-1)^{n-1} \sum_{k=0}^n \binom{n}{k} (-1)^{n-k} (\hat{J}(\xi))^k \hat{u}(\xi, t) \\ &= (-1)^{n-1} (\hat{J}(\xi) - 1)^n \hat{u}(\xi, t). \end{aligned}$$

Hence

$$\hat{u}(\xi, t) = e^{(-1)^{n-1} (\hat{J}(\xi) - 1)^n t} \hat{u}_0(\xi).$$

Since $\hat{u}_0(\xi) \in L^1(\mathbb{R}^d)$ and $e^{(-1)^{n-1} (\hat{J}(\xi) - 1)^n t}$ is continuous and bounded, $\hat{u}(\cdot, t) \in L^1(\mathbb{R}^d)$ and the result follows by taking the inverse Fourier transform. \square

3.2 Nonlocal Higher-Order Evolution Equations

Now we prove a lemma concerning the fundamental solution of (3.1).

Lemma 3.2.5. *The fundamental solution w of (3.1), that is the solution of the equation with initial condition $u_0 = \delta_0$, can be decomposed as*

$$w(x, t) = e^{-t} \delta_0(x) + v(x, t), \quad (3.6)$$

with $v(x, t)$ smooth. Moreover, if u is a solution of (3.1) it can be written as

$$u(x, t) = (w * u_0)(x, t) = \int_{\mathbb{R}^d} w(x - z, t) u_0(z) dz.$$

Proof. By the previous result we have

$$\hat{w}_t(\xi, t) = (-1)^{n-1} (\hat{J}(\xi) - 1)^n \hat{w}(\xi, t).$$

Hence, as the initial data verifies $\hat{w}_0 = \hat{\delta}_0 = 1$, we get

$$\hat{w}(\xi, t) = e^{(-1)^{n-1} (\hat{J}(\xi) - 1)^n t} = e^{-t} + e^{-t} \left(e^{[(-1)^{n-1} (\hat{J}(\xi) - 1)^n + 1]t} - 1 \right).$$

The first part of the lemma follows applying the inverse Fourier transform.

To finish the proof we just observe that $w * u_0$ is a solution of (3.1) with $(w * u_0)(x, 0) = u_0(x)$. \square

3.2.2 Asymptotic Behavior

Next we prove the first part of Theorem 3.2.3.

Theorem 3.2.6. *Let u be a solution of (3.1) with $u_0, \hat{u}_0 \in L^1(\mathbb{R}^d)$. Then, the asymptotic behavior of $u(x, t)$ is given by*

$$\lim_{t \rightarrow +\infty} t^{\frac{d}{\alpha n}} \max_x |u(x, t) - v(x, t)| = 0,$$

where v is the solution of $v_t(x, t) = -A^n (-\Delta)^{\frac{\alpha n}{2}} v(x, t)$, with initial condition $v(x, 0) = u_0(x)$.

Proof. As in the previous section, we have, using Fourier variables,

$$\hat{u}_t(\xi, t) = (-1)^{n-1} (\hat{J}(\xi) - 1)^n \hat{u}(\xi, t).$$

Hence

$$\hat{u}(\xi, t) = e^{(-1)^{n-1} (\hat{J}(\xi) - 1)^n t} \hat{u}_0(\xi).$$

3.2 Nonlocal Higher-Order Evolution Equations

On the other hand, let $v(x, t)$ be a solution of $v_t(x, t) = -A^n(-\Delta)^{\frac{\alpha n}{2}} v(x, t)$, with the same initial data $v(x, 0) = u_0(x)$. Solutions of this equation are understood in the sense that

$$\hat{v}(\xi, t) = e^{-A^n|\xi|^{\alpha n}t} \hat{u}_0(\xi).$$

Hence in Fourier variables

$$\begin{aligned} \int_{\mathbb{R}^d} |\hat{u} - \hat{v}|(\xi, t) d\xi &= \int_{\mathbb{R}^d} \left| (e^{(-1)^{n-1}(\hat{J}(\xi)-1)^n t} - e^{-A^n|\xi|^{\alpha n}t}) \hat{u}_0(\xi) \right| d\xi \\ &\leq \int_{|\xi| \geq r(t)} \left| (e^{(-1)^{n-1}(\hat{J}(\xi)-1)^n t} - e^{-A^n|\xi|^{\alpha n}t}) \hat{u}_0(\xi) \right| d\xi \\ &\quad + \int_{|\xi| < r(t)} \left| (e^{(-1)^{n-1}(\hat{J}(\xi)-1)^n t} - e^{-A^n|\xi|^{\alpha n}t}) \hat{u}_0(\xi) \right| d\xi \\ &= I + II, \end{aligned}$$

where I and II denote the first and the second integral respectively, and $r(t)$ a non-negative function in t . To get a bound for I we decompose it in two parts,

$$\begin{aligned} I &\leq \int_{|\xi| \geq r(t)} \left| e^{-A^n|\xi|^{\alpha n}t} \hat{u}_0(\xi) \right| d\xi + \int_{|\xi| \geq r(t)} \left| e^{(-1)^{n-1}(\hat{J}(\xi)-1)^n t} \hat{u}_0(\xi) \right| d\xi \\ &= I_1 + I_2. \end{aligned}$$

First we consider I_1 . Setting $\eta = \xi t^{1/(\alpha n)}$ and writing I_1 in the new variable η we get,

$$I_1 \leq \|\hat{u}_0\|_{L^\infty(\mathbb{R}^d)} \int_{|\eta| \geq r(t)t^{\frac{1}{\alpha n}}} e^{-A^n|\eta|^{\alpha n}} t^{-\frac{d}{\alpha n}} d\eta,$$

and hence

$$t^{\frac{d}{\alpha n}} I_1 \leq \|\hat{u}_0\|_{L^\infty(\mathbb{R}^d)} \int_{|\eta| \geq r(t)t^{\frac{1}{\alpha n}}} e^{-A^n|\eta|^{\alpha n}} d\eta \xrightarrow{t \rightarrow \infty} 0$$

provided that we impose

$$r(t)t^{\frac{1}{\alpha n}} \xrightarrow{t \rightarrow \infty} \infty. \tag{3.7}$$

To deal with I_2 we have to use different arguments for n even and n odd. Let us begin with the easier case of an even n .

- *n even* - Using our hypotheses on J we get

$$I_2 \leq C e^{-t},$$

with $r(t) \xrightarrow{t \rightarrow \infty} 0$ and therefore

$$t^{\frac{d}{\alpha n}} I_2 \leq C e^{-t} t^{\frac{d}{\alpha n}} \xrightarrow{t \rightarrow \infty} 0.$$

3.2 Nonlocal Higher-Order Evolution Equations

Now consider the case when n is odd.

- n odd - From our hypotheses on J we have that \hat{J} satisfies

$$\hat{J}(\xi) \leq 1 - A|\xi|^\alpha + |\xi|^\alpha h(\xi),$$

where h is bounded and $h(\xi) \rightarrow 0$ as $\xi \rightarrow 0$. Hence there exists $D > 0$ and a constant a such that

$$\hat{J}(\xi) \leq 1 - D|\xi|^\alpha, \quad \text{for } |\xi| \leq a.$$

Moreover, because $|\hat{J}(\xi)| \leq 1$ and J is a radial function, there exists a $\delta > 0$ such that

$$\hat{J}(\xi) \leq 1 - \delta, \quad \text{for } |\xi| \geq a.$$

Therefore I_2 can be bounded by

$$\begin{aligned} I_2 &\leq \int_{a \geq |\xi| \geq r(t)} \left| e^{(-1)^{n-1}(\hat{J}(\xi)-1)^n t} \hat{u}_0(\xi) \right| d\xi + \int_{|\xi| \geq a} \left| e^{(-1)^{n-1}(\hat{J}(\xi)-1)^n t} \hat{u}_0(\xi) \right| d\xi \\ &\leq \|\hat{u}_0\|_{L^\infty(\mathbb{R}^d)} \int_{a \geq |\xi| \geq r(t)} e^{-D^n |\xi|^{\alpha n} t} d\xi + C e^{-\delta^n t}. \end{aligned}$$

Changing variables as before, $\eta = \xi t^{1/(\alpha n)}$, we get

$$\begin{aligned} t^{\frac{d}{\alpha n}} I_2 &\leq \|\hat{u}_0\|_{L^\infty(\mathbb{R}^d)} \int_{at^{\frac{1}{\alpha n}} \geq |\eta| \geq r(t)t^{\frac{1}{\alpha n}}} e^{-D^n |\eta|^{\alpha n}} d\eta + C t^{\frac{d}{\alpha n}} e^{-\delta^n t} \\ &\leq \|\hat{u}_0\|_{L^\infty(\mathbb{R}^d)} \int_{|\eta| \geq r(t)t^{\frac{1}{\alpha n}}} e^{-D^n |\eta|^{\alpha n}} d\eta + C t^{\frac{d}{\alpha n}} e^{-\delta^n t} \rightarrow 0, \end{aligned}$$

as $t \rightarrow \infty$ if (3.7) holds.

It remains only to estimate II. We proceed as follows

$$II = \int_{|\xi| < r(t)} e^{-A^n |\xi|^{\alpha n} t} \left| e^{t[(-1)^{n-1}(\hat{J}(\xi)-1)^n + A^n |\xi|^{\alpha n}]} - 1 \right| |\hat{u}_0(\xi)| d\xi.$$

Applying the binomial formula and taking into account the two different cases when n is even and odd we can conclude that

$$t^{\frac{d}{\alpha n}} II \leq C t^{\frac{d}{\alpha n}} \int_{|\xi| < r(t)} e^{-A^n |\xi|^{\alpha n} t} t(|\xi|^{\alpha n} h(\xi) + K(|\xi|^{\alpha k} h(\xi)^k)) d\xi,$$

where $K(|\xi|^{\alpha k} h(\xi)^k)$ is a polynomial in $|\xi|^\alpha$ and $h(\xi)$ with $0 < k \leq n$ and provided that we impose

$$t(r(t))^{\alpha n} h(r(t)) \rightarrow 0 \quad \text{as } t \rightarrow \infty. \tag{3.8}$$

3.2 Nonlocal Higher-Order Evolution Equations

In this case we have

$$\begin{aligned} t^{\frac{d}{\alpha n}} II &\leq C \int_{|\eta| < r(t)t^{\frac{1}{\alpha n}}} e^{-A^n |\eta|^{\alpha n}} (|\eta|^{\alpha n} h(\eta/t^{1/(\alpha n)})) \\ &\quad + K(|\eta|^{\alpha k} h(\eta/t^{1/(\alpha n)})^k) \frac{1}{t^{(\alpha k)/(\alpha n)}} d\eta. \end{aligned}$$

To show the convergence of II to zero we use dominated convergence. Because of our assumption on h we know that $h(\eta/t^{1/(\alpha n)}) \rightarrow 0$ as $t \rightarrow \infty$ (note that clearly also $h(\eta/t^{1/(\alpha n)})^k$ converges to zero for every $k > 0$). Further the integrand is dominated by $\|h\|_{L^\infty(\mathbb{R}^d)} e^{-A^n |\eta|^{\alpha n}} |\eta|^{\alpha n}$, which belongs to $L^1(\mathbb{R}^d)$.

Combining this with our previous results we have that

$$t^{\frac{d}{\alpha n}} \int_{\mathbb{R}^d} |\hat{u} - \hat{v}|(\xi, t) d\xi \leq t^{\frac{d}{\alpha n}} (I + II) \rightarrow 0 \quad \text{as } t \rightarrow \infty, \quad (3.9)$$

provided we can find a $r(t) \rightarrow 0$ as $t \rightarrow \infty$ which fulfills both conditions (3.7) and (3.8). This is done in Lemma 3.2.7, which is postponed to just after the present proof. To conclude we only have to observe that the convergence of $u - v$ in L^∞ follows from the convergence of the Fourier transforms $\hat{u}(\cdot, t) - \hat{v}(\cdot, t) \rightarrow 0$ in L^1 . Indeed, from (3.9) we obtain

$$t^{\frac{d}{\alpha n}} \max_x |u(x, t) - v(x, t)| \leq t^{\frac{d}{\alpha n}} \int_{\mathbb{R}^d} |\hat{u} - \hat{v}|(\xi, t) d\xi \rightarrow 0, \quad t \rightarrow \infty,$$

which completes the proof of the theorem. \square

The following Lemma shows that there exists a function $r(t)$ satisfying (3.7) and (3.8), as required in the proof of the previous theorem.

Lemma 3.2.7. *Given a real valued function $h \in C(\mathbb{R})$ such that $h(\rho) \rightarrow 0$ as $\rho \rightarrow 0$ with $h(\rho) > 0$ for small ρ , there exists a function r with $r(t) \rightarrow 0$ as $t \rightarrow \infty$ which for $\alpha > 0$ satisfies*

$$\lim_{t \rightarrow \infty} r(t)t^{\frac{1}{\alpha n}} = \infty$$

and

$$\lim_{t \rightarrow \infty} t(r(t))^{\alpha n} h(r(t)) = 0.$$

Proof. For fixed t large enough, we choose $r(t)$ as a solution of

$$r(h(r))^{\frac{1}{2\alpha n}} = t^{-\frac{1}{\alpha n}}. \quad (3.10)$$

This equation defines a function $r = r(t)$ which, by continuity arguments goes to zero as t tends to infinity, satisfying also the additional asymptotic conditions in the lemma. Indeed, if there exists $t_n \rightarrow \infty$ with no solution of (3.10) for $r \in (0, \delta)$ then $h(r) \equiv 0$ in $(0, \delta)$, which is a contradiction to our assumption that $h(r) > 0$ for r small. \square

3.2 Nonlocal Higher-Order Evolution Equations

As a consequence of Theorem 3.2.6, we obtain the following corollary which completes the results gathered in Theorem 3.2.3.

Corollary 3.2.8. *The asymptotic behavior of solutions of (3.1) is given by*

$$\|u(., t)\|_{L^\infty(\mathbb{R}^d)} \leq \frac{C}{t^{\frac{d}{\alpha n}}}.$$

Moreover, the asymptotic profile is given by

$$\lim_{t \rightarrow +\infty} \max_y \left| t^{\frac{d}{\alpha n}} u(yt^{\frac{1}{\alpha n}}, t) - \|u_0\|_{L^1(\mathbb{R}^d)} G_A(y) \right| = 0,$$

where $G_A(y)$ satisfies $\hat{G}_A(\xi) = e^{-A^n |\xi|^{\alpha n}}$.

Proof. From Theorem 3.2.6 we obtain that the asymptotic behavior is the same as the one for solutions of the evolution given by a power n of the fractional Laplacian. It is easy to check that the asymptotic behavior is in fact the one described in the statement of the corollary. In Fourier variables we have

$$\begin{aligned} \lim_{t \rightarrow \infty} \hat{v}(\eta t^{-\frac{1}{\alpha n}}, t) &= \lim_{t \rightarrow \infty} e^{-A^n |\eta|^{\alpha n}} \hat{u}_0(\eta t^{-\frac{1}{\alpha n}}) \\ &= e^{-A^n |\eta|^{\alpha n}} \hat{u}_0(0) \\ &= e^{-A^n |\eta|^{\alpha n}} \|u_0\|_{L^1(\mathbb{R}^d)}. \end{aligned}$$

Therefore

$$\lim_{t \rightarrow +\infty} \max_y \left| t^{\frac{d}{\alpha n}} v(yt^{\frac{1}{\alpha n}}, t) - \|u_0\|_{L^1(\mathbb{R}^d)} G_A(y) \right| = 0,$$

where $G_A(y)$ satisfies $\hat{G}_A(\xi) = e^{-A^n |\xi|^{\alpha n}}$. \square

With similar arguments as in the proof of Theorem 3.2.6 one can prove that also the asymptotic behavior of the derivatives of solutions u of (3.1) is the same as the one for derivatives of solutions v of the evolution of a power n of the fractional Laplacian, assuming sufficient regularity of the solutions u of (3.1).

Theorem 3.2.9. *Let u be a solution of (3.1) with $u_0 \in W^{k,1}(\mathbb{R}^d)$, $k \leq \alpha n$ and $\hat{u}_0 \in L^1(\mathbb{R}^d)$. Then, the asymptotic behavior of $D^k u(x, t)$ is given by*

$$\lim_{t \rightarrow +\infty} t^{\frac{d+k}{\alpha n}} \max_x \left| D^k u(x, t) - D^k v(x, t) \right| = 0,$$

where v is the solution of $v_t(x, t) = -A^n (-\Delta)^{\frac{\alpha n}{2}} v(x, t)$ with initial condition $v(x, 0) = u_0(x)$.

3.2 Nonlocal Higher-Order Evolution Equations

Proof. We begin again by transforming our problem for u and v into a problem for the corresponding Fourier transforms \hat{u} and \hat{v} . For this we consider

$$\begin{aligned} \max_x |D^k u(x, t) - D^k v(x, t)| &= \max_{\xi} \left| (\widehat{D^k u}(\xi, t))^{\vee} - (\widehat{D^k v}(\xi, t))^{\vee} \right| \\ &\leq \int_{\mathbb{R}^d} \left| \widehat{D^k u}(\xi, t) - \widehat{D^k v}(\xi, t) \right| d\xi = \int_{\mathbb{R}^d} |\xi|^k |\hat{u}(\xi, t) - \hat{v}(\xi, t)| d\xi. \end{aligned}$$

Showing $\int_{\mathbb{R}^d} |\xi|^k |\hat{u}(\xi, t) - \hat{v}(\xi, t)| d\xi \rightarrow 0$ as $t \rightarrow \infty$ works analogue to the proof of Theorem 3.2.6. The additional term $|\xi|^k$ is always dominated by the exponential terms. \square

3.2.3 Scaling the Kernel

In this section we show that the problem $v_t(x, t) = -A^n(-\Delta)^{\frac{\alpha n}{2}} v(x, t)$ can be approximated by nonlocal problems like (3.1) when rescaled in an appropriate way.

Proof of Theorem 3.2.4. The proof uses once more the explicit formula for the solutions in Fourier variables. We have, arguing exactly as before,

$$\hat{u}_\varepsilon(\xi, t) = e^{(-1)^{n-1} \frac{(\widehat{J_\varepsilon}(\xi)-1)^n}{\varepsilon^{\alpha n}} t} \hat{u}_0(\xi).$$

and

$$\hat{v}(\xi, t) = e^{-A^n |\xi|^{\alpha n} t} \hat{u}_0(\xi).$$

Now, we just observe that $\widehat{J_\varepsilon}(\xi) = \widehat{J}(\varepsilon \xi)$ and therefore we obtain

$$\begin{aligned} \int_{\mathbb{R}^d} |\hat{u}_\varepsilon - \hat{v}|(\xi, t) d\xi &= \int_{\mathbb{R}^d} \left| (e^{(-1)^{n-1} \frac{(\widehat{J}(\varepsilon \xi)-1)^n}{\varepsilon^{\alpha n}} t} - e^{-A^n |\xi|^{\alpha n} t}) \hat{u}_0(\xi) \right| d\xi \\ &\leq \|\hat{u}_0\|_{L^\infty(\mathbb{R}^d)} \left(\int_{|\xi| \geq r(\varepsilon)} \left| e^{(-1)^{n-1} \frac{(\widehat{J}(\varepsilon \xi)-1)^n}{\varepsilon^{\alpha n}} t} - e^{-A^n |\xi|^{\alpha n} t} \right| d\xi \right. \\ &\quad \left. + \int_{|\xi| < r(\varepsilon)} \left| e^{(-1)^{n-1} \frac{(\widehat{J}(\varepsilon \xi)-1)^n}{\varepsilon^{\alpha n}} t} - e^{-A^n |\xi|^{\alpha n} t} \right| d\xi \right). \end{aligned}$$

For $t \in [0, T]$ we can proceed as in the proof of Theorem 3.2.3 (Section 3.2.2) to obtain that

$$\max_x |u_\varepsilon(x, t) - v(x, t)| \leq \int_{\mathbb{R}^d} |\hat{u}_\varepsilon - \hat{v}|(\xi, t) d\xi \rightarrow 0, \quad \varepsilon \rightarrow 0.$$

I leave the details to the reader. \square

Chapter 4

Numerical Solution of Higher-Order Inpainting Approaches

One main challenge in inpainting with higher-order flows is their effective numerical implementation. For example the straightforward discretization of a fourth-order evolution equation may result in a strong restriction on the time step Δt , i.e., $\Delta t \leq O(\Delta x)^4$ where Δx denotes the mesh size. Therefore high-order equations and possible non-convex flows require elaborate discretization schemes to guarantee stability and a fast convergence of the algorithm. For an overview of numerical methods for higher-order inpainting approaches see Section 1.3.3.

In this chapter we present numerical algorithms that approximate solutions of the three inpainting approaches presented in Sections 2.1-2.3. Our first approach are semi-implicit solvers, presented in Section 4.1. This section mainly follows the lines of [SB09] and is joint work with Andrea Bertozzi. We show the application of these schemes to Cahn-Hilliard inpainting (2.1), TV- H^{-1} inpainting (2.27), and inpainting with LCIS (2.42), and present rigorous estimates verifying, e.g., their unconditional stability in the sense that the numerical solution is uniformly bounded on a finite time interval. In Section 4.2 we present an alternative method to solve TV- H^{-1} inpainting. This method is based on a dual solver for TV minimization, introduced by Chambolle in [Ch04] for an L^2 constraint, and generalized by the author in [Sc09] for an H^{-1} constraint. Section 4.2 is based on ideas of [Sc09] with emphasis on the inpainting application. In the last

section we present a domain decomposition approach for TV minimization. This work is mainly based on results obtained in joint work with Massimo Fornasier in [FS07]. Domain decomposition methods are able to decrease the computational complexity of a numerical scheme by means of parallel computation. In particular for the higher-order TV-H⁻¹ inpainting approach, the potential consequences with respect to computation time are of major interest. Numerical results for both TV-L²- and TV-H⁻¹ minimization are presented.

4.1 Unconditionally Stable Solvers

In this section we discuss an efficient semi-implicit approach presented in Eyre [Eyre98] (also cf.

citeVLR) called *convexity splitting* for its application to higher-order inpainting approaches. We consider the following problem: Let $\mathcal{J} \in C^2(\mathbb{R}^N, \mathbb{R})$ be a smooth functional from \mathbb{R}^N into \mathbb{R} , where N is the dimension of the data space. Let Ω be the spatial domain of the data space. Find $u \in \mathbb{R}^N$ such that

$$\begin{cases} u_t = -\nabla \mathcal{J}(u) & \text{in } \Omega, \\ u(., t=0) = u_0 & \text{in } \Omega, \end{cases} \quad (4.1)$$

with initial condition $u_0 \in \mathbb{R}^N$. The basic idea of convexity splitting is to split the functional \mathcal{J} into a convex and a concave part. In the semi implicit scheme the convex part is treated implicitly and the concave one explicitly in time. Under additional assumptions on (4.1) this discretization approach is unconditionally stable, of order 2 in time, and relatively easy to apply to a large range of variational problems. Moreover we shall see that the idea of convexity splitting can be applied to more general evolution equations, and in particular to those that do not follow a variational principle. The main focus of this section is to illustrate the application of the convexity splitting idea to the three fourth-order inpainting approaches (2.1), (2.27) and (2.42) presented in Sections 2.1-2.3. We show that this idea results in an unconditionally stable finite difference scheme and allows us to (approximately) compute strong solutions of the continuous problem. Moreover, we prove consistency of these schemes, and convergence to the exact solution under possible additional restrictions on the latter. For Cahn-Hilliard inpainting and TV-H⁻¹ inpainting the developed convexity splitting schemes can be

proven to be of order 1 in time. For inpainting with LCIS the numerical scheme is of order 2 in time.

Notation

In this section we discuss the numerical solution of evolutionary differential equations. Therefore we have to distinguish between the exact solution u of the continuous equation and the approximate solution U of the corresponding time-discrete numerical scheme. We write capital U_k for the solution of the time-discrete equation at time $k\Delta t$ and small $u_k = u(k\Delta t)$ for a solution of the continuous inpainting equation at time $k\Delta t$ with time step size Δt . Let e_k denote the discretization error given by $e_k = u_k - U_k$. In Subsection 4.1.1 u and U_k are vectors in \mathbb{R}^N , where N denotes the dimension of the data. In all other parts of this section u and U_k are assumed to be elements in $L^2(\Omega)$. Let $\mathcal{J} \in C^2(\mathcal{H}, \mathbb{R})$ denote a functional from a suitable Hilbert space \mathcal{H} to \mathbb{R} , and $\nabla\mathcal{J}(u)$ its first variation with respect to u . In the discrete setting $\mathcal{H} = \mathbb{R}^N$. Finally, in the discrete setting, $\langle \cdot, \cdot \rangle$ denotes the inner product on \mathbb{R} with corresponding norm $\|u\|^2 = \langle u, u \rangle$. In the continuous setting we stick to the notation specified in the prefix of the thesis.

4.1.1 The Convexity Splitting Idea

Convexity splitting was originally proposed to solve energy minimizing equations. Nevertheless we will see that it can also be applied to more general PDEs, such as (2.1) and (2.27), which do not fulfill a variational principle. Convexity splitting methods, although known under different names, have a long tradition in several parts of numerical analysis. For example Barrett, Blowley, and Garcke used the idea of convexity splitting in [BB97, Equation (3.42)] to approximate the solution of a phase separation model with finite elements. In [ES02, Equation (5.4)] a finite difference scheme for second-order parabolic equations is presented which also uses the convexity splitting idea. A discussion on convexity splitting in the context of more general optimization problems can be found in [YR03, Chapter 2.].

First we would like to introduce the notion of gradient flows and the application of convexity splitting methods in this context. To do so we follow the work of Eyre

[Eyre98]. We consider equation (4.1). If \mathcal{J} satisfies

$$(i) \quad \mathcal{J}(u) \geq 0, \quad \forall u \in \mathbb{R}^N \quad (4.2)$$

$$(ii) \quad \mathcal{J}(u) \rightarrow \infty \text{ as } \|u\| \rightarrow \infty \quad (4.3)$$

$$(iii) \quad \langle J(\nabla \mathcal{J})(u)u, u \rangle \geq \lambda \in \mathbb{R}, \quad \forall u \in \mathbb{R}^N \quad (4.4)$$

then we refer to (4.1) as a *gradient system* and to its solutions as *gradient flows*. Here $J(\nabla \mathcal{J})(u)$ denotes the Jacobian of $\nabla \mathcal{J}$ in u . All gradient systems fulfill the dissipation property, i.e.,

$$\frac{d\mathcal{J}(u)}{dt} = -\|\nabla \mathcal{J}(u)\|^2$$

and therefore $\mathcal{J}(u(t)) \leq \mathcal{J}(u_0)$ for all $t \geq 0$.

If $\mathcal{J}(u)$ is convex, i.e., $\lambda > 0$ in (4.2), then the system has a single equilibrium. In this case unconditionally stable and uniquely solvable numerical schemes exist (cf. [SH94]). If $\mathcal{J}(u)$ is not convex, i.e., $\lambda < 0$, multiple minimizers may exist and the gradient flow can possibly expand in $u(t)$. The stability of an explicit gradient descent algorithm, i.e., $U_{k+1} = U_k - \Delta t \nabla \mathcal{J}(U_k)$, in this case may require extremely small time steps, depending of course on the functional \mathcal{J} . Therefore the development of stable and efficient discretizations for non-convex functionals \mathcal{J} is highly desirable.

The basic idea of convexity splitting is to write the functional \mathcal{J} as

$$\mathcal{J}(u) = \mathcal{J}_c(u) - \mathcal{J}_e(u), \quad (4.5)$$

where

$$\mathcal{J}_o \in C^2(\mathbb{R}^N, \mathbb{R}) \text{ and } \mathcal{J}_o(u) \text{ is strictly convex for all } u \in \mathbb{R}^N, \quad o \in \{c, e\}. \quad (4.6)$$

The semi-implicit discretization of (4.1) is then given by

$$U_{k+1} - U_k = -\Delta t (\nabla \mathcal{J}_c(U_{k+1}) - \nabla \mathcal{J}_e(U_k)), \quad (4.7)$$

where $U_0 = u_0$.

Remark 4.1.1. *We want to anticipate that the setting of Eyre, and hence the subsequent presentation of convexity splitting, is a purely discrete one. Nevertheless it actually holds in a more general framework, i.e., for more general gradient flows. In the case of an L^2 gradient flow for example, the Jacobian J of the discrete functional \mathcal{J} just has to be replaced by the second variation of the continuous functional \mathcal{J} in $L^2(\Omega)$.*

In the following we will show that convexity splitting can be applied to the inpainting approaches (2.1), (2.27), and (2.42) and produces unconditionally gradient stable or unconditionally stable numerical schemes. Let us first define what unconditionally gradient stable and unconditionally stable schemes are.

Definition 4.1.2. [Eyre 1998] A one-step numerical integration scheme is **unconditionally gradient stable** if there exists a function $\mathcal{J}(\cdot) : \mathbb{R}^N \rightarrow \mathbb{R}$ such that, for all $\Delta t > 0$ and for all initial data:

- (i) $\mathcal{J}(U) \geq 0$ for all $U \in \mathbb{R}^N$
- (ii) $\mathcal{J}(U) \rightarrow \infty$ as $\|U\| \rightarrow \infty$
- (iii) $\mathcal{J}(U_{k+1}) \leq \mathcal{J}(U_k)$ for all $U_k \in \mathbb{R}^N$
- (iv) If $\mathcal{J}(U_k) = \mathcal{J}(U_0)$ for all $k \geq 0$ then U_0 is a zero of $\nabla \mathcal{J}$ for (4.1) and (4.2).

Now, Cahn-Hilliard inpainting (2.1) and TV-H⁻¹inpainting (2.27), are not given by gradient flows. Hence, in the context of these inpainting models the meaning of unconditional stability has to be redefined. Namely, in the case of an evolution equation which does not follow a gradient flow, a corresponding discrete time stepping scheme is said to be unconditionally stable if solutions of the difference equation are bounded within a finite time interval, independently from the step size Δt .

Definition 4.1.3. Let u be an element of a suitable function space defined on $\Omega \times [0, T]$, with $\Omega \subset \mathbb{R}^2$ open and bounded, and $T > 0$. Let further F be a real valued function and $u_t = F(u, D^\alpha u)$ be a partial differential equation with space derivatives $D^\alpha u$, $\alpha = 1, \dots, 4$. A corresponding discrete time stepping method

$$U_{k+1} = U_k + \Delta t F_k, \quad (4.8)$$

where F_k is a suitable approximation of F in U_k and U_{k+1} , is **unconditionally stable**, if all solutions of (4.8) are bounded for all $\Delta t > 0$ and all k such that $k\Delta t \leq T$.

We start with a theorem proved by Eyre in [Eyre 1998].

Theorem 4.1.4. [Eyre 1998, Theorem 1] Let \mathcal{J} satisfy (4.2), and \mathcal{J}_c and \mathcal{J}_e satisfy (4.5)-(4.6). If $\mathcal{J}_e(u)$ additionally satisfies

$$\langle J(\nabla \mathcal{J}_e)(u)u, u \rangle \geq -\lambda \quad (4.9)$$

when $\lambda < 0$ in (4.2)(iii), then for any initial condition, the numerical scheme (4.7) is consistent with (4.1), gradient stable for all $\Delta t > 0$, and possesses a unique solution for each time step. The local truncation error for each step is

$$\tau_k = \frac{(\Delta t)^2}{2} (J(\nabla \mathcal{J}_c(\hat{u})) + J(\nabla \mathcal{J}_e(\hat{u}))) \nabla \mathcal{J}(u(\xi)),$$

for some $\xi \in (k\Delta t, (k+1)\Delta t)$ and for some \hat{u} in the parallelopiped with opposite vertices at U_k and U_{k+1} .

Remark 4.1.5. Condition (4.9) in Theorem 4.1.4 is equivalent to the requirement that all the eigenvalues of $J(\nabla \mathcal{J}_e)$ dominate the largest eigenvalue $-\lambda$ of $-J(\nabla \mathcal{J})$, i.e.,

$$\langle J(\nabla \mathcal{J}_e)(u), u \rangle \stackrel{(4.9)}{\geq} -\lambda \stackrel{(4.2)}{\geq} \langle -J(\nabla \mathcal{J})(u), u \rangle$$

for all $u \in \mathbb{R}^N$, i.e.,

$$\hat{\lambda} \geq |\lambda|, \quad \text{for all eigenvalues } \hat{\lambda} > 0 \text{ of } \mathcal{J}_e. \quad (4.10)$$

In the following we apply the idea of convexity splitting to our three inpainting models (2.1), (2.27), and (2.42). For this we change from the discrete setting to the continuous setting, i.e., considering functions u in a suitable Hilbert space instead of vectors u in \mathbb{R}^N . Although the first two of these inpainting approaches, i.e., Cahn-Hilliard inpainting and TV-H⁻¹inpainting, are not given by gradient flows, we shall see that the resulting numerical schemes are still unconditionally stable (in the sense of Definition 4.1.3) and therefore suitable to solve them accurately and reasonably fast. For inpainting with LCIS (2.42) the results of Eyre can be directly applied, even in the continuous setting, cf. Remark 4.1.1. Nevertheless, also for this case, we additionally present a rigorous analysis, similar to the one done for Cahn-Hilliard- and TV-H⁻¹inpainting.

4.1.2 Cahn-Hilliard Inpainting

In this section we show that the application of convexity splitting to Cahn-Hilliard inpainting (2.1) yields a consistent, unconditionally stable and convergent numerical scheme. Recall that the inpainted version $u(x)$ of $f(x)$ is constructed by following the evolution equation

$$u_t = \Delta \left(-\epsilon \Delta u + \frac{1}{\epsilon} F'(u) \right) + \lambda(f - u).$$

The application of convexity splitting to Cahn-Hilliard inpainting (2.1) was originally introduced in [BEG07a]. The numerical results presented there already suggested the usefulness of this scheme. Although the authors did not analyze the scheme rigorously, they concluded that based on their numerical results, the scheme is unconditionally stable. In the following we will present this numerical scheme and derive some additional properties based on its rigorous analysis.

The original Cahn-Hilliard equation is a gradient flow in H^{-1} for the energy

$$\mathcal{J}_1(u) = \int_{\Omega} \left(\frac{\epsilon}{2} |\nabla u|^2 + \frac{1}{\epsilon} F(u) \right) dx,$$

while the fitting term in (2.1) can be derived from a gradient flow in L^2 for the energy

$$\mathcal{J}_2(u) = \frac{1}{2} \int_{\Omega} \lambda(f - u)^2 dx.$$

Note that equation (2.1) as a whole does not result in a gradient system anymore. Hence, we apply the convexity splitting discussed in Section 4.1.1 to both functionals \mathcal{J}_1 and \mathcal{J}_2 separately. Namely we split \mathcal{J}_1 in $\mathcal{J}_1 = \mathcal{J}_{1c} - \mathcal{J}_{1e}$ with

$$\mathcal{J}_{1c}(u) = \int_{\Omega} \frac{\epsilon}{2} |\nabla u|^2 + \frac{C_1}{2} |u|^2 dx, \quad \mathcal{J}_{1e}(u) = \int_{\Omega} -\frac{1}{\epsilon} F(u) + \frac{C_1}{2} |u|^2 dx.$$

A possible splitting for \mathcal{J}_2 is $\mathcal{J}_2 = \mathcal{J}_{2c} - \mathcal{J}_{2e}$ with

$$\mathcal{J}_{2c}(u) = \frac{1}{2} \int_{\Omega} \frac{C_2}{2} |u|^2 dx, \quad \mathcal{J}_{2e}(u) = \frac{1}{2} \int_{\Omega} -\lambda(f - u)^2 + \frac{C_2}{2} |u|^2 dx.$$

To make sure that $\mathcal{J}_{1c}, \mathcal{J}_{1e}$ and $\mathcal{J}_{2c}, \mathcal{J}_{2e}$ are strictly convex the constants C_1 and C_2 have to be chosen such that $C_1 > \frac{1}{\epsilon}$, $C_2 > \lambda_0$, compare [BEG07b].

Then the resulting discrete time-stepping scheme for an initial condition $U_0 = u_0$ is given by

$$\frac{U_{k+1} - U_k}{\Delta t} = -\nabla_{H^{-1}}(\mathcal{J}_{1c}(U_{k+1}) - \mathcal{J}_{1e}(U_k)) - \nabla_{L^2}(\mathcal{J}_{2c}(U_{k+1}) - \mathcal{J}_{2e}(U_k)),$$

where $\nabla_{H^{-1}}$ and ∇_{L^2} represent gradient descent with respect to the H^{-1} and the L^2 inner product respectively. This translates to a numerical scheme of the form

$$\begin{aligned} \frac{U_{k+1} - U_k}{\Delta t} + \epsilon \Delta \Delta U_{k+1} - C_1 \Delta U_{k+1} + C_2 U_{k+1} &= \frac{1}{\epsilon} \Delta F'(U_k) - C_1 \Delta U_k \\ &\quad + \lambda(f - U_k) + C_2 U_k, \quad \text{in } \Omega. \end{aligned} \quad (4.11)$$

We imply Neumann boundary conditions on $\partial\Omega$, i.e.,

$$\frac{\partial U_{k+1}}{\partial \nu} = \frac{\partial \Delta U_{k+1}}{\partial \nu} = 0, \quad \text{on } \partial\Omega,$$

and intend to compute U_{k+1} in (4.11) in the spectral domain using the discrete cosine transform (DCT).

Note that in order to derive Neumann boundary conditions for (4.11) the standard space H^{-1} as defined in Appendix A.4 has to be replaced by H_∂^{-1} as defined in Section 2.1.3.

Spectral methods, like the DCT, are a classical tool for the discretization of Laplacian operators. In the case of a Laplacian operator, their main advantage is that the resulting matrix is of diagonal type, which allows fast computations. In addition, fast numerical methods for the Fourier transform exist. Let \hat{U} be the DCT of U and λ_i the eigenvalues of the discrete Laplacian with Neumann boundary conditions. Then equation (4.11) in \hat{U} reads

$$\begin{aligned} \hat{U}_{k+1}(i, j) &= \frac{(1 - C_1 \Delta t (\frac{1}{\Delta x^2} \lambda_i + \frac{1}{\Delta y^2} \lambda_j) + C_2 \Delta t) \hat{U}_k(i, j)}{c_{i,j}} \\ &\quad + \frac{\frac{\Delta t}{\epsilon} \widehat{\Delta F'(U_k)}(i, j) + \Delta t \lambda_i \widehat{(f - U_k)}}{c_{i,j}}, \end{aligned}$$

where $c_{i,j}$ is defined as

$$c_{i,j} = 1 + C_2 \Delta t + \epsilon \Delta t \left(\frac{1}{\Delta x^2} \lambda_i + \frac{1}{\Delta y^2} \lambda_j \right)^2 - C_1 \Delta t \left(\frac{1}{\Delta x^2} \lambda_i + \frac{1}{\Delta y^2} \lambda_j \right).$$

Rigorous Estimates for the Scheme

From Theorem 4.1.4 we know that (at least in the spatially discrete framework) the convexity splitting scheme (4.5)-(4.7) is unconditionally stable, i.e., separate numerical schemes for the gradient flows of the energies $\mathcal{J}_1(u)$ and $\mathcal{J}_2(u)$ are not increasing for all $\Delta t > 0$. But this does not guarantee that our numerical scheme (4.11) is unconditionally stable, since it combines the flows of two energies. In this section we shall analyze the scheme in more detail and derive some rigorous estimates for its solutions. In particular we will show that the scheme (4.11) is unconditionally stable in the sense of Definition 4.1.3. Our results are summarized in the following theorem.

Theorem 4.1.6. Let u be the exact solution of (2.1) and $u_k = u(k\Delta t)$ the exact solution at time $k\Delta t$, for a time step $\Delta t > 0$ and $k \in \mathbb{N}$. Let further U_k be the k th iterate of (4.11) with constants $C_1 > 1/\epsilon$, $C_2 > \lambda_0$. Then the following statements are true:

- (i) Under the assumption that $\|u_{tt}\|_{-1}$, $\|\nabla \Delta u_t\|_2$ and $\|u_t\|_2$ are bounded, the numerical scheme (4.11) is consistent with the continuous equation (2.1) and of order 1 in time.

Under the additional assumption that

$$F''(U_{k-1}) \leq K \quad (4.12)$$

for a nonnegative constant K , we further have

- (ii) The solution sequence U_k is bounded on a finite time interval $[0, T]$, for all $\Delta t > 0$.
- (iii) The discretization error e_k , given by $e_k = u_k - U_k$, converges to zero as $\Delta t \rightarrow 0$.

Remark 4.1.7. Note that our assumptions for the consistency of the numerical scheme, only hold if the time derivative of the solution of the continuous equation (2.1) is uniformly bounded. This is true, for smooth and bounded solutions of the equation.

Further, since we are interested in bounded solutions U_k of the discrete equation (4.11), it is natural to assume (4.12), i.e., that the nonlinearity F'' in the previous time step $\Delta(k-1)$ is bounded.

The proof of Theorem 4.1.6 is organized in the following three Propositions 4.1.8–4.1.10.

Proposition 4.1.8. (Consistency (i)) Under the same assumptions as in Theorem 4.1.6 and in particular under the assumption that $\|u_{tt}\|_{-1}$, $\|\nabla \Delta u_t\|_2$ and $\|u_t\|_2$ are bounded, the numerical scheme (4.11) is consistent with the continuous equation (2.1) with local truncation error $\|\tau_k\|_{-1} = O(\Delta t)$.

Proof. Let $F_k(U) = 0$ represent the difference equation approximating the PDE at time $k\Delta t$. If the discrete solution U is replaced by the exact solution u of (2.1), the value $\tau_k = F_k(u)$ is the local truncation error defined over a time step. Then

$$\tau_k = \tau_k^1 + \tau_k^2,$$

with

$$\begin{aligned}\tau_k^1 &= \frac{u_{k+1} - u_k}{\Delta t} - u_t(k\Delta t) \\ \tau_k^2 &= \epsilon \Delta \Delta (u_{k+1} - u_k) - C_1 \Delta (u_{k+1} - u_k) + C_2 (u_{k+1} - u_k) \\ &= \epsilon \Delta t \Delta^2 \frac{u_{k+1} - u_k}{\Delta t} - C_1 \Delta t \Delta^2 \frac{u_{k+1} - u_k}{\Delta t} + C_2 \Delta t \frac{u_{k+1} - u_k}{\Delta t},\end{aligned}$$

i.e.,

$$\tau_k = \frac{u_{k+1} - u_k}{\Delta t} + \epsilon \Delta^2 u_{k+1} - \frac{1}{\epsilon} \Delta F'(u_k) - \lambda(f - u_k) - C_1 \Delta (u_{k+1} - u_k) + C_2 (u_{k+1} - u_k). \quad (4.13)$$

Using standard Taylor series arguments and assuming that $\|u_{tt}\|_{-1}$, $\|\nabla \Delta u_t\|_2$ and $\|u_t\|_2$ are bounded we deduce that

$$\|\tau_k\|_{-1} = O(\Delta t). \quad (4.14)$$

□

Proposition 4.1.9. (Unconditional stability (ii)) *Under the same assumptions as in Theorem 4.1.6 and in particular assuming that (4.12) holds, the solution sequence U_k with $k\Delta t \leq T$ for $T > 0$ fixed, fulfills for every $\Delta t > 0$*

$$\|\nabla U_k\|_2^2 + \Delta t K_1 \|\Delta U_k\|_2^2 \leq e^{K_2 T} \left(\|\nabla U_0\|_2^2 + \Delta t C_1 \|\Delta U_0\|_2^2 + \Delta t T C(\Omega, D, \lambda_0, f) \right), \quad (4.15)$$

for suitable constants K_1 and K_2 , and constant C depending on Ω, D, λ_0, f only. This gives boundedness of the solution sequence on $[0, T]$.

Proof. We consider our discrete model

$$\frac{U_{k+1} - U_k}{\Delta t} + \epsilon \Delta \Delta U_{k+1} - C_1 \Delta U_{k+1} + C_2 U_{k+1} = \frac{1}{\epsilon} \Delta F'(U_k) - C_1 \Delta U_k + \lambda(f - U_k) + C_2 U_k,$$

multiply the equation with $-\Delta U_{k+1}$ and integrate over Ω . We obtain

$$\begin{aligned}\frac{1}{\Delta t} \left(\|\nabla U_{k+1}\|_2^2 - \langle \nabla U_k, \nabla U_{k+1} \rangle_2 \right) + \epsilon \|\nabla \Delta U_{k+1}\|_2^2 + C_1 \|\Delta U_{k+1}\|_2^2 + C_2 \|\nabla U_{k+1}\|_2^2 \\ = \frac{1}{\epsilon} \langle F''(U_k) \nabla U_k, \nabla \Delta U_{k+1} \rangle_2 + C_1 \langle \Delta U_k, \Delta U_{k+1} \rangle_2 \\ + \langle \nabla \lambda(f - U_k), \nabla U_{k+1} \rangle_2 + C_2 \langle \nabla U_k, \nabla U_{k+1} \rangle_2.\end{aligned}$$

Using Cauchy's inequality we obtain

$$\begin{aligned}\frac{1}{2\Delta t} \left(\|\nabla U_{k+1}\|_2^2 - \|\nabla U_k\|_2^2 \right) + \epsilon \|\nabla \Delta U_{k+1}\|_2^2 + C_1 \|\Delta U_{k+1}\|_2^2 + C_2 \|\nabla U_{k+1}\|_2^2 \\ \leq \frac{1}{2\epsilon\delta} \|F''(U_k) \nabla U_k\|_2^2 + \frac{\delta}{2\epsilon} \|\nabla \Delta U_{k+1}\|_2^2 + \frac{C_1}{2} \|\Delta U_k\|_2^2 + \frac{C_1}{2} \|\Delta U_{k+1}\|_2^2 \\ + \frac{C_2}{2} \|\nabla U_k\|_2^2 + \frac{C_2}{2} \|\nabla U_{k+1}\|_2^2 + \frac{1}{2} \|\nabla \lambda(f - U_k)\|_2^2 + \frac{1}{2} \|\nabla U_{k+1}\|_2^2.\end{aligned}$$

Using the estimate

$$\|\nabla \lambda(f - U_k)\|_2^2 \leq 2\lambda_0^2 \|\nabla U_k\|_2^2 + C(\Omega, D, \lambda_0, f)$$

and reordering the terms we obtain

$$\begin{aligned} & \left(\frac{1}{2\Delta t} + \frac{C_2}{2} - \frac{1}{2} \right) \|\nabla U_{k+1}\|_2^2 + \frac{C_1}{2} \|\Delta U_{k+1}\|_2^2 + \left(\epsilon - \frac{\delta}{2\epsilon} \right) \|\nabla \Delta U_{k+1}\|_2^2 \\ & \leq \left(\frac{1}{2\Delta t} + \frac{C_2}{2} + \lambda_0^2 \right) \|\nabla U_k\|_2^2 + \frac{1}{2\epsilon\delta} \|F''(U_k) \nabla U_k\|_2^2 + \frac{C_1}{2} \|\Delta U_k\|_2^2 + C(\Omega, D, \lambda_0, f). \end{aligned}$$

By choosing $\delta = 2\epsilon^2$, the third term on the left side of the inequality is zero. Because of assumption (4.12) we obtain the following bound on the right side of the inequality

$$\|F''(U_k) \nabla U_k\|_2^2 \leq K^2 \|\nabla U_k\|_2^2$$

and we have

$$\begin{aligned} & \left(\frac{1}{2\Delta t} + \frac{C_2}{2} - \frac{1}{2} \right) \|\nabla U_{k+1}\|_2^2 + \frac{C_1}{2} \|\Delta U_{k+1}\|_2^2 \\ & \leq \left(\frac{1}{2\Delta t} + \frac{C_2}{2} + \lambda_0^2 + \frac{K^2}{4\epsilon^3} \right) \|\nabla U_k\|_2^2 + \frac{C_1}{2} \|\Delta U_k\|_2^2 + C(\Omega, D, \lambda_0, f). \end{aligned}$$

Now we multiply the above inequality by $2\Delta t$ and define

$$\begin{aligned} \tilde{C} &= 1 + \Delta t(C_2 - 1), \\ \tilde{\tilde{C}} &= 1 + \Delta t(C_2 + 2\lambda_0^2 + \frac{K^2}{2\epsilon^3}). \end{aligned}$$

Since C_2 is chosen greater than $\lambda_0 > 1$, the first coefficient \tilde{C} is positive and we can divide the inequality by it. We obtain

$$\|\nabla U_{k+1}\|_2^2 + \Delta t \frac{C_1}{\tilde{C}} \|\Delta U_{k+1}\|_2^2 \leq \frac{\tilde{\tilde{C}}}{\tilde{C}} \|\nabla U_k\|_2^2 + \Delta t \frac{C_1}{\tilde{C}} \|\Delta U_k\|_2^2 + \Delta t C(\Omega, D, \lambda_0, f),$$

where we updated the constant $C(\Omega, D, \lambda_0, f)$ by $C(\Omega, D, \lambda_0, f)/\tilde{C}$.

Since $\frac{\tilde{\tilde{C}}}{\tilde{C}} \geq 1$, we can multiply the second term on the right side of the inequality by this quotient to obtain

$$\|\nabla U_{k+1}\|_2^2 + \Delta t \frac{C_1}{\tilde{C}} \|\Delta U_{k+1}\|_2^2 \leq \frac{\tilde{\tilde{C}}}{\tilde{C}} \left(\|\nabla U_k\|_2^2 + \Delta t \frac{C_1}{\tilde{C}} \|\Delta U_k\|_2^2 \right) + \Delta t C(\Omega, D, \lambda_0, f).$$

We deduce by induction that

$$\begin{aligned}
 \|\nabla U_k\|_2^2 + \Delta t \frac{C_1}{\tilde{C}} \|\Delta U_k\|_2^2 &\leq \left(\frac{\tilde{C}}{\tilde{C}} \right)^k \left(\|\nabla U_0\|_2^2 + \Delta t \frac{C_1}{\tilde{C}} \|\Delta U_0\|_2^2 \right) \\
 &\quad + \Delta t \sum_{i=0}^{k-1} \left(\frac{\tilde{C}}{\tilde{C}} \right)^i C(\Omega, D, \lambda_0, f) \\
 &= \frac{(1+K_2\Delta t)^k}{(1+K_1\Delta t)^k} \left(\|\nabla U_0\|_2^2 + \Delta t \frac{C_1}{\tilde{C}} \|\Delta U_0\|_2^2 \right) \\
 &\quad + \Delta t \sum_{i=0}^{k-1} \frac{(1+K_2\Delta t)^i}{(1+K_1\Delta t)^i} C(\Omega, D, \lambda_0, f).
 \end{aligned}$$

For $k\Delta t \leq T$ we have

$$\begin{aligned}
 \|\nabla U_k\|_2^2 + \Delta t \frac{C_1}{\tilde{C}} \|\Delta U_k\|_2^2 &\leq e^{(K_2-K_1)T} \left(\|\nabla U_0\|_2^2 + \Delta t \frac{C_1}{\tilde{C}} \|\Delta U_0\|_2^2 \right) \\
 &\quad + \Delta t T e^{(K_2-K_1)T} C(\Omega, D, \lambda_0, f) \\
 &= e^{(K_2-K_1)T} \left(\|\nabla U_0\|_2^2 + \Delta t \frac{C_1}{\tilde{C}} \|\Delta U_0\|_2^2 \right. \\
 &\quad \left. + \Delta t T C(\Omega, D, \lambda_0, f) \right),
 \end{aligned}$$

which gives boundedness of the solution sequence on $[0, T]$ for any $T > 0$ assuming that (4.12) holds. \square

The convergence of the discrete solution to the continuous one as the time step $\Delta t \rightarrow 0$ is verified in the following proposition.

Proposition 4.1.10. (Convergence (iii)) *Under the same assumptions as in Theorem 4.1.6 and in particular under assumption (4.12) the discretization error e_k fulfills, for suitable constants C, C_1, K_1, K_2 ,*

$$\|\nabla e_k\|_2^2 + \Delta t \frac{C_1}{\tilde{C}} \|\Delta e_k\|_2^2 \leq T \Delta t e^{4(K_1+K_2)T} \cdot C, \tag{4.16}$$

for $k\Delta t \leq T$ and a fixed $T > 0$.

Proof. Let us follow the lines of the consistency proof in (4.13). Then the discretization

4.1 Unconditionally Stable Solvers

error e_k satisfies

$$\begin{aligned}
& \frac{e_{k+1} - e_k}{\Delta t} + \epsilon \Delta^2 e_{k+1} - C_1 \Delta e_{k+1} + C_2 e_{k+1} \\
= & \frac{1}{\Delta t} (u_{k+1} - u_k) - \frac{1}{\Delta t} (U_{k+1} - U_k) + \epsilon \Delta^2 u_{k+1} - \epsilon \Delta^2 U_{k+1} \\
& - C_1 \Delta u_{k+1} + C_1 \Delta U_{k+1} + C_2 u_{k+1} - C_2 U_{k+1} \\
= & - \left(\frac{1}{\epsilon} \Delta F'(U_k) - C_1 \Delta U_k + \lambda(f - U_k) + C_2 U_k \right) \\
& + \left(\frac{1}{\epsilon} \Delta F'(u_k) + \lambda(f - u_k) - C_1 \Delta u_k + C_2 u_k \right) + \tau_k \\
= & - \left(\frac{1}{\epsilon} \Delta(F'(U_k) - F'(u_k)) - C_1 \Delta(U_k - u_k) + C_2(U_k - u_k) - \lambda(U_k - u_k) \right) + \tau_k.
\end{aligned}$$

Multiplication with $-\Delta e_{k+1}$ leads to

$$\begin{aligned}
& \frac{1}{\Delta t} \langle \nabla(e_{k+1} - e_k), \nabla e_{k+1} \rangle_2 + \epsilon \|\nabla \Delta e_{k+1}\|_2^2 + C_1 \|\Delta e_{k+1}\|_2^2 + C_2 \|\nabla e_{k+1}\|_2^2 \\
= & \frac{1}{\epsilon} \langle \Delta(F'(U_k) - F'(u_k)), \Delta e_{k+1} \rangle_2 - C_1 \langle \Delta(U_k - u_k), \Delta e_{k+1} \rangle_2 \\
& + \langle \nabla \lambda(U_k - u_k), \nabla e_{k+1} \rangle_2 - C_2 \langle \nabla(U_k - u_k), \nabla e_{k+1} \rangle_2 + \langle \nabla \Delta^{-1} \tau_k, \nabla \Delta e_{k+1} \rangle_2.
\end{aligned}$$

Further, because

$$\frac{1}{\Delta t} \left(\|\nabla e_{k+1}\|_2^2 - \langle \nabla e_k, \nabla e_{k+1} \rangle_2 \right) \geq \frac{1}{2\Delta t} (\|\nabla e_{k+1}\|_2^2 - \|\nabla e_k\|_2^2),$$

we obtain

$$\begin{aligned}
& \frac{1}{2\Delta t} (\|\nabla e_{k+1}\|_2^2 - \|\nabla e_k\|_2^2) + \epsilon \|\nabla \Delta e_{k+1}\|_2^2 + C_1 \|\Delta e_{k+1}\|_2^2 + C_2 \|\nabla e_{k+1}\|_2^2 \\
\leq & \frac{1}{\epsilon} \langle \Delta(F'(U_k) - F'(u_k)), \Delta e_{k+1} \rangle_2 + C_1 \langle \Delta e_k, \Delta e_{k+1} \rangle_2 - \langle \nabla \lambda e_k, \nabla e_{k+1} \rangle_2 \\
& + C_2 \langle \nabla e_k, \nabla e_{k+1} \rangle_2 + \langle \nabla \Delta^{-1} \tau_k, \nabla \Delta e_{k+1} \rangle_2.
\end{aligned}$$

Applying Cauchy's inequality leads to

$$\begin{aligned}
& \frac{1}{2\Delta t} (\|\nabla e_{k+1}\|_2^2 - \|\nabla e_k\|_2^2) + \epsilon \|\nabla \Delta e_{k+1}\|_2^2 + C_1 \|\Delta e_{k+1}\|_2^2 + C_2 \|\nabla e_{k+1}\|_2^2 \\
\leq & -\frac{1}{\epsilon} \langle (F''(U_k) \nabla U_k - F''(u_k) \nabla u_k), \nabla \Delta e_{k+1} \rangle_2 + \frac{C_1}{\delta_1} \|\Delta e_k\|_2^2 + C_1 \delta_1 \|\Delta e_{k+1}\|_2^2 \\
& + \frac{\lambda_0^2}{\delta_3} \|\nabla e_k\|_2^2 + \delta_3 \|\nabla e_{k+1}\|_2^2 + \frac{C_2}{\delta_2} \|\nabla e_k\|_2^2 + C_2 \delta_2 \|\nabla e_{k+1}\|_2^2 \\
& + \frac{1}{\delta_4} \|\tau_k\|_{-1}^2 + \delta_4 \|\nabla \Delta e_{k+1}\|_2^2.
\end{aligned}$$

Since (4.12) holds, we obtain

$$\begin{aligned} & -\frac{1}{\epsilon} \langle (F''(U_k) \nabla U_k - F''(u_k) \nabla u_k), \nabla \Delta e_{k+1} \rangle_2 \\ & \leq \frac{1}{2\epsilon\delta_5} \|F''(U_k) \nabla U_k - F''(u_k) \nabla u_k\|_2^2 + \frac{\delta_5}{2\epsilon} \|\nabla \Delta e_{k+1}\|_2^2 \\ & \leq \frac{K}{\epsilon\delta_5} \|\nabla U_k\|_2^2 + \frac{K}{\epsilon\delta_5} \|\nabla u_k\|_2^2 + \frac{\delta_5}{2\epsilon} \|\nabla \Delta e_{k+1}\|_2^2, \end{aligned}$$

and therefore

$$\begin{aligned} & \left(\frac{1}{2\Delta t} + C_2(1 - \delta_2) - \delta_3 \right) \|\nabla e_{k+1}\|_2^2 + C_1(1 - \delta_1) \|\Delta e_{k+1}\|_2^2 \\ & \quad + \left(\epsilon - \delta_4 - \frac{\delta_5}{2\epsilon} \right) \|\nabla \Delta e_{k+1}\|_2^2 \\ & \leq \left(\frac{1}{2\Delta t} + \frac{\lambda_0^2}{\delta_3} + \frac{C_2}{\delta_2} \right) \|\nabla e_k\|_2^2 + \frac{C_1}{\delta_1} \|\Delta e_k\|_2^2 + \frac{1}{\delta_4} \|\tau_k\|_{-1}^2 + \frac{K}{\epsilon\delta_5} (\|\nabla U_k\|_2^2 + \|\nabla u_k\|_2^2). \end{aligned}$$

Next we choose $\delta_1 = 1/2$ and multiply the inequality with $2\Delta t$

$$\begin{aligned} & (1 + 2\Delta t(C_2(1 - \delta_2) - \delta_3)) \|\nabla e_{k+1}\|_2^2 + \Delta t C_1 \|\Delta e_{k+1}\|_2^2 \\ & \quad + 2\Delta t \left(\epsilon - \delta_4 - \frac{\delta_5}{\epsilon} \right) \|\nabla \Delta e_{k+1}\|_2^2 \\ & \leq \left(1 + 2\Delta t \left(\frac{\lambda_0^2}{\delta_3} + \frac{C_2}{\delta_2} \right) \right) \|\nabla e_k\|_2^2 + 4\Delta t C_1 \|\Delta e_k\|_2^2 + \frac{2\Delta t}{\delta_4} \|\tau_k\|_{-1}^2 \\ & \quad + \Delta t \frac{2K}{\epsilon} (\|\nabla U_k\|_2^2 + \|\nabla u_k\|_2^2). \end{aligned}$$

Now choosing all δ s such that the coefficients of all terms in the inequality are nonnegative and estimating the last term on the left side from below by zero we get

$$\begin{aligned} \|\nabla e_{k+1}\|_2^2 + \Delta t \frac{C_1}{\tilde{C}} \|\Delta e_{k+1}\|_2^2 & \leq \frac{\tilde{C}}{\tilde{C}} \|\nabla e_k\|_2^2 + 4\Delta t \frac{C_1}{\tilde{C}} \|\Delta e_k\|_2^2 + \frac{2\Delta t}{\delta_4 \tilde{C}} \|\tau_k\|_{-1}^2 \\ & \quad + \Delta t \frac{2K}{\epsilon \tilde{C}} (\|\nabla U_k\|_2^2 + \|\nabla u_k\|_2^2), \end{aligned}$$

where

$$\tilde{C} = 1 + 2\Delta t(C_2(1 - \delta_2) - \delta_3), \quad \tilde{C} = 1 + 2\Delta t \left(\frac{\lambda_0^2}{\delta_3} + \frac{C_2}{\delta_2} \right).$$

Further,

$$\begin{aligned} \|\nabla e_{k+1}\|_2^2 + \Delta t \frac{C_1}{\tilde{C}} \|\Delta e_{k+1}\|_2^2 & \leq 4 \frac{\tilde{C}}{\tilde{C}} \left(\|\nabla e_k\|_2^2 + \Delta t \frac{C_1}{\tilde{C}} \|\Delta e_k\|_2^2 \right) \\ & \quad + \Delta t \left(\frac{2}{\delta_4 \tilde{C}} \|\tau_k\|_{-1}^2 + \frac{2K}{\epsilon \tilde{C}} (\|\nabla U_k\|_2^2 + \|\nabla u_k\|_2^2) \right). \end{aligned}$$

In addition we apply the consistency result (4.14) and the uniform bound (4.15) to the above inequality and obtain

$$\begin{aligned} \|\nabla e_{k+1}\|_2^2 + \Delta t \frac{C_1}{\tilde{C}} \|\Delta e_{k+1}\|_2^2 &\leq 4 \frac{\tilde{C}}{\tilde{C}} \left(\|\nabla e_k\|_2^2 + \Delta t \frac{C_1}{\tilde{C}} \|\Delta e_k\|_2^2 \right) \\ &\quad + \Delta t \left(\frac{2}{\delta_4 \tilde{C}} (\Delta t)^2 + \frac{2K}{\epsilon \tilde{C}} (C_2 + \|\nabla u_k\|_2^2) \right). \end{aligned}$$

To proceed we assume for now that the exact solution is uniformly bounded in $H^1(\Omega)$, i.e.,

$$\exists C_3 > 0 \text{ such that } \|\nabla u_k\|_2 \leq C_3 \text{ for all } k\Delta t < T. \quad (4.17)$$

This assumption will be proven in Lemma 4.1.11 just after the end of this proof. Now, implementing (4.17) in our computation we have

$$\begin{aligned} \|\nabla e_{k+1}\|_2^2 + \Delta t \frac{C_1}{\tilde{C}} \|\Delta e_{k+1}\|_2^2 &\leq 4 \frac{\tilde{C}}{\tilde{C}} \left(\|\nabla e_k\|_2^2 + \Delta t \frac{C_1}{\tilde{C}} \|\Delta e_k\|_2^2 \right) \\ &\quad + \Delta t \left(\frac{2}{\delta_4 \tilde{C}} (\Delta t)^2 + \frac{2K}{\epsilon \tilde{C}} (C_2 + C_3) \right). \end{aligned}$$

By induction we deduce that

$$\begin{aligned} \|\nabla e_k\|_2^2 + \Delta t \frac{C_1}{\tilde{C}} \|\Delta e_k\|_2^2 &\leq \left(4 \frac{\tilde{C}}{\tilde{C}} \right)^k \left(\|\nabla e_0\|_2^2 + \Delta t \frac{C_1}{\tilde{C}} \|\Delta e_0\|_2^2 \right) \\ &\quad + \Delta t \sum_{i=0}^{k-1} \left(4 \frac{\tilde{C}}{\tilde{C}} \right)^i \left(\frac{2}{\delta_4 \tilde{C}} (\Delta t)^2 + \frac{2K}{\epsilon \tilde{C}} (C_2 + C_3) \right). \quad (4.18) \end{aligned}$$

Since $e_0 = U_0 - u_0 = 0$, the first term on the right-hand side of the above inequality vanishes. For $k\Delta t \leq T$ we finally have

$$\|\nabla e_k\|_2^2 + \Delta t \frac{C_1}{\tilde{C}} \|\Delta e_k\|_2^2 \leq T \Delta t e^{4(K_1 + K_2)T} \cdot C. \quad \square$$

From [BEG07a, BEG07b] we know that the solution u_k to the continuous equation globally exists and is uniformly bounded in $L^2(\Omega)$. Next we show that assumption (4.17) holds.

Lemma 4.1.11. *Let u_k be the exact solution of (2.1) at time $t = k\Delta t$ and let $T > 0$. Then there exists a constant $C > 0$ such that $\|\nabla u_k\|_2 \leq C$ for all $k\Delta t < T$.*

Proof. Let $K(u) = -\epsilon \Delta u + \frac{1}{\epsilon} F'(u)$. We multiply the continuous evolution equation (2.1) with $K(u)$ and obtain

$$\langle u_t, K(u) \rangle_2 = \langle \Delta K(u), K(u) \rangle_2 + \langle \lambda(f - u), K(u) \rangle_2.$$

Let us further define

$$\mathcal{J}(u) := \frac{\epsilon}{2} \int_{\Omega} |\nabla u|^2 dx + \frac{1}{\epsilon} \int_{\Omega} F(u) dx.$$

Then we have

$$\begin{aligned} \langle u_t, K(u) \rangle_2 &= \left\langle u_t, -\epsilon \Delta u + \frac{1}{\epsilon} F'(u) \right\rangle_2 \\ &= \langle \nabla u_t, \epsilon \nabla u \rangle_2 + \left\langle u_t, \frac{1}{\epsilon} F'(u) \right\rangle_2 \\ &= \frac{d}{dt} \mathcal{J}(u), \end{aligned}$$

since u satisfies Neumann boundary conditions. Therefore we get

$$\frac{d}{dt} \mathcal{J}(u) = - \int_{\Omega} |\nabla K(u)|^2 dx + \langle \lambda(f - u), -\epsilon \Delta u \rangle_2 + \left\langle \lambda(f - u), \frac{1}{\epsilon} F'(u) \right\rangle_2. \quad (4.19)$$

Since $F(u)$ is bounded from below, we only have to show that $\mathcal{J}(u)$ is uniformly bounded on $[0, T]$, and we automatically have that $|\nabla u|$ is uniformly bounded on $[0, T]$. We start with the last term, and recall the following bounds on $F'(u)$ (cf. [Te88]): There exist positive constants C_1, C_2 such that

$$F'(s)s \geq C_1 s^2 - C_2, \quad \forall s \in \mathbb{R}$$

and, for every $\delta > 0$, there exists a constant C_3 such that

$$|F'(s)| \leq \delta C_1 s^2 + C_3(\delta), \quad \forall s \in \mathbb{R}.$$

Use the last two estimates to obtain the following

$$\begin{aligned} \left\langle \lambda(f - u), \frac{1}{\epsilon} F'(u) \right\rangle_2 &= \frac{\lambda_0}{\epsilon} \int_{\Omega \setminus D} F'(u) f dx - \frac{\lambda_0}{\epsilon} \int_{\Omega \setminus D} F'(u) u dx \\ &\leq \frac{\lambda_0}{\epsilon} \int_{\Omega \setminus D} |F'(u)| dx \cdot \|f\|_{L^\infty(\Omega)} - \frac{\lambda_0 C_1}{\epsilon} \int_{\Omega \setminus D} u^2 dx + \frac{\lambda_0 C_2 |\Omega \setminus D|}{\epsilon} \\ &\leq \lambda_0 C(f, \Omega) \left(\delta \frac{C_1}{\epsilon} \int_{\Omega \setminus D} u^2 dx + \frac{C_3(\delta) |\Omega \setminus D|}{\epsilon} \right) - \frac{\lambda_0 C_1}{\epsilon} \int_{\Omega \setminus D} u^2 dx \\ &\quad + \frac{\lambda_0 C_2 |\Omega \setminus D|}{\epsilon} \\ &\leq -\frac{\lambda_0 C_1}{\epsilon} (1 - \delta C(f, \Omega)) \int_{\Omega \setminus D} u^2 dx + C(\lambda_0, \epsilon, \delta, \Omega, D, f), \end{aligned}$$

where we choose $\delta < 1/C(f, \Omega)$. Therefore integrating (4.19) over the time interval $[0, T]$ results in

$$\begin{aligned} \int_0^T \frac{d}{dt} \mathcal{J}(u(t)) dt &\leq \int_0^T - \int_{\Omega} |\nabla K(u)|^2 dx dt + \int_0^T \langle \lambda(f - u), -\epsilon \Delta u \rangle_2 dt \\ &\quad - \frac{\lambda_0 C_1}{\epsilon} (1 - \delta C(f, \Omega)) \int_0^T \int_{\Omega \setminus D} u^2 dx dt + T \cdot C(\lambda_0, \epsilon, \delta, \Omega, D, f). \end{aligned}$$

Next we consider the second term on the right side of the last inequality. From Theorem 4.1 in [BEG07a] we know that a solution u of (2.1) is an element in $L^2(0, T; H^2(\Omega))$ for all $T > 0$. Hence $\Delta u \in L^2(0, T; L^2(\Omega))$ and the second term is bounded by a constant depending on T . Consequently for each $0 \leq t \leq T$ we get,

$$\begin{aligned} \mathcal{J}(u(t)) &\leq \mathcal{J}(u(0)) + C(T) + T \cdot C(\lambda_0, \epsilon, \delta, \Omega, D, f) \\ &\quad - \int_0^T \left[\int_{\Omega} |\nabla K(u)|^2 dx + \frac{\lambda_0 C_1}{\epsilon} (1 - \delta C(f, \Omega)) \int_{\Omega \setminus D} u^2 dx \right] dt, \end{aligned}$$

and with this, for a fixed $T > 0$, that $|\nabla u|$ is uniformly bounded in $[0, T]$. \square

4.1.3 TV-H⁻¹Inpainting

In this section we discuss convexity splitting for TV-H⁻¹inpainting (2.27). To avoid numerical difficulties we approximate an element p in the subdifferential of the total variation functional $TV(u)$ by a smoothed version of $\nabla \cdot (\frac{\nabla u}{|\nabla u|})$, the square root regularization for instance. With the latter regularization the smoothed version of (2.27) reads

$$u_t = -\Delta \nabla \cdot \left(\frac{\nabla u}{\sqrt{|\nabla u|^2 + \delta^2}} \right) + \lambda(f - u), \quad (4.20)$$

with $0 < \delta \ll 1$. In contrast to its second-order analogue, the well-posedness of (2.27) strongly depends on the smoothing used for $\nabla \cdot (\frac{\nabla u}{|\nabla u|})$. In fact there are smoothing functions for which (2.27) produces singularities in finite time. This is caused by the lack of maximum principles which in the second-order case guarantee the well-posedness for all smooth monotone regularizations. In [BGOV05] the authors considered (2.27) with $\lambda = \lambda_0$ in all of Ω , i.e., the fourth-order analogue to TV-L²denoising, which was originally introduced in [OSV03]. They proved well-posedness in one space dimension for a set of smooth monotone regularizations which include the square root smoothing

$$\left(\frac{u_x}{\sqrt{|u_x|^2 + \delta^2}} \right)_x \quad (4.21)$$

and, the arctan regularization

$$\left(\frac{2}{\pi} \arctan(u_x/\delta) \right)_x, \quad (4.22)$$

for $0 < \delta \ll 1$. The behavior of the fourth-order PDE in one dimension is also relevant for two-dimensional images since a lot of structure involves edges which are one-dimensional objects. In two dimensions similar results are much more difficult to obtain, since energy estimates and the Sobolev lemma involved in its proof might not hold in higher dimensions anymore.

In the following we will present the convexity splitting method applied to (2.27) for both the square root and the arctan regularization. Similarly to the convexity splitting for Cahn-Hilliard inpainting, we propose the following splitting for the TV- H^{-1} inpainting equation. The regularizing term in (2.27) can be modeled by a gradient flow in H^{-1} of the energy

$$\mathcal{J}_1(u) = \int_{\Omega} |\nabla u| dx,$$

where $|\nabla u|$ is replaced by its regularized version, e.g., $\sqrt{|\nabla u|^2 + \delta^2}$, $\delta > 0$. We split \mathcal{J}_1 in $\mathcal{J}_{1c} - \mathcal{J}_{1e}$ with

$$\mathcal{J}_{1c}(u) = \int_{\Omega} \frac{C_1}{2} |\nabla u|^2 dx, \text{ and } \mathcal{J}_{1e}(u) = \int_{\Omega} -|\nabla u| + \frac{C_1}{2} |\nabla u|^2 dx.$$

The fitting term is split into $\mathcal{J}_2 = \mathcal{J}_{2c} - \mathcal{J}_{2e}$ analogous to the Cahn-Hilliard inpainting. The resulting time-stepping scheme is given by

$$\frac{U_{k+1} - U_k}{\Delta t} + C_1 \Delta \Delta U_{k+1} + C_2 U_{k+1} = C_1 \Delta \Delta U_k - \Delta \left(\nabla \cdot \left(\frac{\nabla U_k}{|\nabla U_k|} \right) \right) + C_2 U_k + \lambda(f - U_k). \quad (4.23)$$

We assume that U_{k+1} satisfies zero Neumann boundary conditions and use the DCT to solve (4.23). Note again that in the case of Neumann boundary conditions the standard space H^{-1} as defined in Appendix A.4 has to be replaced by H_{∂}^{-1} as defined in Section 2.1.3.

The constants C_1 and C_2 have to be chosen such that $\mathcal{J}_{1c}, \mathcal{J}_{1e}, \mathcal{J}_{2c}, \mathcal{J}_{2e}$ are all strictly convex. In the following we will demonstrate how to compute the appropriate constants. Let us consider C_1 first. The functional \mathcal{J}_{1c} is strictly convex for all $C_1 > 0$. The choice of C_1 for the convexity of \mathcal{J}_{1e} depends on the regularization of the total variation we are using. We use the square regularization (4.21), i.e., instead of $|\nabla u|$ we have

$$\int G(|\nabla u|) dx, \text{ with } G(s) = \sqrt{s^2 + \delta^2}.$$

4.1 Unconditionally Stable Solvers

Setting $y = |\nabla u|$ we have to choose C_1 such that $\frac{C_1}{2}y^2 - G(y)$ is convex. The convexity condition for the second derivative gives us that

$$C_1 > G''(y) \iff C_1 > \frac{\delta^2}{(\delta^2 + y^2)^{3/2}} \iff C_1 > \frac{1}{\delta},$$

is sufficient as $\frac{\delta^2}{(\delta^2 + y^2)^{3/2}}$ has its maximum value at $y = 0$. Next we would like to compare this with the arctan regularization (4.22), i.e., replacing $\frac{\nabla u}{|\nabla u|}$ by $\frac{2}{\pi}\arctan(\frac{\nabla u}{\delta})$, as proposed in [BGOV05]. Here the convexity condition for the second derivative reads

$$C_1 \pm \frac{d}{ds} \left(\frac{2}{\pi} \arctan\left(\frac{s}{\delta}\right) \right) > 0.$$

The \pm sign results from the absent absolute value in the regularization definition. We obtain

$$C_1 \pm \frac{2}{\pi} \frac{1}{\delta(1 + s^2/\delta^2)} > 0.$$

The inequality with a plus sign instead of \pm is true for all constants $C_1 > 0$. In the other case we obtain

$$C_1 > \frac{2}{\pi} \frac{\delta}{\delta^2 + s^2},$$

which is fulfilled for all $s \in \mathbb{R}$ if $C_1 > \frac{2}{\delta\pi}$. Note that this condition is almost the same as in the case of the square regularization.

Now we consider $\mathcal{J}_2 = \mathcal{J}_{2c} - \mathcal{J}_{2e}$. The functional \mathcal{J}_{2c} is strictly convex if $C_2 > 0$. For the convexity of \mathcal{J}_{2e} we rewrite

$$\begin{aligned} \mathcal{J}_{2e}(u) &= \frac{1}{2} \int_{\Omega} -\lambda(f - u)^2 + C_2|u|^2 \, dx \\ &= \int_D \frac{C_2}{2}|u|^2 \, dx + \int_{\Omega \setminus D} -\frac{\lambda_0}{2}(f - u)^2 + \frac{C_2}{2}|u|^2 \, dx \\ &= \int_D \frac{C_2}{2}|u|^2 \, dx + \int_{\Omega \setminus D} \left(\frac{C_2}{2} - \frac{\lambda_0}{2} \right)|u|^2 + \lambda_0 f u - \frac{\lambda_0}{2}|f|^2. \end{aligned}$$

This is convex for $C_2 > \lambda_0$, e.g., with $C_2 = \lambda_0 + 1$ we can write

$$\mathcal{J}_{2e}(u) = \int_D \frac{C_2}{2}|u|^2 \, dx + \int_{\Omega \setminus D} \left(\frac{1}{2}u + \lambda_0 f \right)^2 - \left(\lambda_0^2 + \frac{\lambda_0}{2} \right)|f|^2 \, dx.$$

Rigorous Estimates for the Scheme

As in Section 4.1.2 for Cahn-Hilliard inpainting, we proceed with a more detailed analysis of (4.23). Throughout this section we consider the square-root regularization of the total variation both in our numerical scheme and in the continuous evolution equation (2.27). Note that similar results are true for other monotone regularizers such as the arctan smoothing. Our results are summarized in the following theorem.

Theorem 4.1.12. *Let u be the exact solution of (4.20) and $u_k = u(k\Delta t)$ be the exact solution at time $k\Delta t$ for a time step $\Delta t > 0$ and $k \in \mathbb{N}$. Let further U_k be the k th iterate of (4.23) with constants $C_1 > 1/\delta$, $C_2 > \lambda_0$. Then the following statements are true:*

- (i) *Under the assumption that $\|u_{tt}\|_{-1}$, $\|\nabla \Delta u_t\|_2$ and $\|u_t\|_2$ are bounded, the numerical scheme (4.23) is consistent with the continuous equation (2.27) and of order 1 in time.*
- (ii) *The solution sequence U_k is bounded on a finite time interval $[0, T]$, for all $\Delta t > 0$.*
- (iii) *Let further $e_k = u_k - U_k$. If*

$$\|\nabla u_k\|_2^2 + \|\nabla \Delta u_k\|_2^2 \leq K \text{ for a constant } K > 0, \text{ and for all } k\Delta t < T, \quad (4.24)$$

then the error e_k converges to zero as $\Delta t \rightarrow 0$.

Remark 4.1.13. *Note that assumption (4.24) in Theorem 4.1.12 (iii) does not hold in general. Given the results in [BGOV05] for the one dimensional equation with $\lambda(x) = \lambda_0$ on all of Ω , which guarantee the existence of a unique smooth solution for both the square root and the arctan regularization, this assumption nevertheless seem to be reasonable in an heuristic sense. Heuristically speaking, this assumption holds for one dimensional structures, like edges, in the two dimensional image. Rigorously, the well-posedness and regularity of solutions in the two dimensional case with non constant λ is still a matter for further research.*

The proof of Theorem 4.1.12 is split into three separate Propositions 4.1.14-4.1.16.

Proposition 4.1.14. (Consistency (i)) *Under the same assumptions as in Theorem 4.1.12 and in particular under the assumption that $\|u_{tt}\|_{-1}$, $\|\nabla \Delta u_t\|_2$ and $\|u_t\|_2$ are bounded, the numerical scheme (4.23) is consistent with the continuous equation (4.20) with local truncation error $\|\tau_k\|_{-1} = O(\Delta t)$.*

4.1 Unconditionally Stable Solvers

Proof. The local truncation error is defined over a time step as satisfying

$$\tau_k = \tau_k^1 + \tau_k^2,$$

where

$$\tau_k^1 = \frac{u_{k+1} - u_k}{\Delta t} - u_t(k\Delta t), \quad \tau_k^2 = C_1 \Delta^2 (u_{k+1} - u_k) + C_2 (u_{k+1} - u_k),$$

i.e.,

$$\begin{aligned} \tau_k = \frac{u_{k+1} - u_k}{\Delta t} + \Delta \left(\nabla \cdot \left(\frac{\nabla u_k}{\sqrt{|\nabla u_k|^2 + \delta^2}} \right) \right) - \lambda(f - u_k) \\ + C_1 \Delta^2 (u_{k+1} - u_k) + C_2 (u_{k+1} - u_k). \end{aligned} \quad (4.25)$$

Using standard Taylor series arguments and assuming that $\|u_{tt}\|_{-1}$, $\|\nabla \Delta u_t\|_2$ and $\|u_t\|_2$ are bounded we deduce that

$$\|\tau_k\|_{-1} = O(\Delta t). \quad (4.26)$$

□

Proposition 4.1.15. (Unconditional stability (ii)) *Under the same assumptions as in Theorem 4.1.12 the solution sequence U_k with $k\Delta t \leq T$ for $T > 0$ fixed, fulfills for every $\Delta t > 0$*

$$\|\nabla U_k\|_2^2 + \Delta t K_1 \|\nabla \Delta U_k\|_2^2 \leq e^{K_2 T} \left(\|\nabla U_0\|_2^2 + \Delta t K_1 \|\nabla \Delta U_0\|_2^2 + \Delta t T C(\Omega, D, \lambda_0, f) \right), \quad (4.27)$$

for suitable constants K_1 , K_2 , and a constant C , which depends on Ω, D, λ_0, f only. This gives boundedness of the solution sequence on $[0, T]$.

Proof. If we multiply (4.23) with $-\Delta U_{k+1}$ and integrate over Ω we obtain

$$\begin{aligned} \frac{1}{\Delta t} \left(\|\nabla U_{k+1}\|_2^2 - \langle \nabla U_k, \nabla U_{k+1} \rangle_2 \right) + C_2 \|\nabla U_{k+1}\|_2^2 + C_1 \|\nabla \Delta U_{k+1}\|_2^2 \\ = \left\langle \Delta \nabla \cdot \left(\frac{\nabla U_k}{\sqrt{|\nabla U_k|^2 + \delta^2}} \right), \Delta U_{k+1} \right\rangle_2 + C_1 \langle \nabla \Delta U_k, \nabla \Delta U_{k+1} \rangle_2 \\ + \langle \nabla (\lambda(f - U_k)), \nabla U_{k+1} \rangle_2 + C_2 \langle \nabla U_k, \nabla U_{k+1} \rangle_2. \end{aligned}$$

Applying Cauchy's inequality to the inner products on the right and estimating

$$\|\nabla \lambda(f - U_k)\|_2^2 \leq 2\lambda_0^2 \|\nabla U_k\|_2^2 + C(\Omega, D, \lambda_0, f)$$

results in

$$\begin{aligned} & \frac{1}{2\Delta t} \left(\|\nabla U_{k+1}\|_2^2 - \|\nabla U_k\|_2^2 \right) + C_2 \|\nabla U_{k+1}\|_2^2 + C_1 \|\nabla \Delta U_{k+1}\|_2^2 \\ & \leq \left\langle \Delta \nabla \cdot \left(\frac{\nabla U_k}{\sqrt{|\nabla U_k|^2 + \delta^2}} \right), \Delta U_{k+1} \right\rangle_2 + \frac{C_1}{\delta_1} \|\nabla \Delta U_k\|_2^2 + C_1 \delta_1 \|\nabla \Delta U_{k+1}\|_2^2 \\ & \quad + \frac{2\lambda_0^2}{\delta_2} \|\nabla U_k\|_2^2 + \delta_2 \|\nabla U_{k+1}\|_2^2 + \frac{C_2}{\delta_3} \|\nabla U_k\|_2^2 + C_2 \delta_3 \|\nabla U_{k+1}\|_2^2 + C(\Omega, D, \lambda_0, f). \end{aligned}$$

Now, the first term on the right side of the inequality can be estimated as follows

$$\begin{aligned} & \left\langle \Delta \nabla \cdot \left(\frac{\nabla U_k}{\sqrt{|\nabla U_k|^2 + \delta^2}} \right), \Delta U_{k+1} \right\rangle_2 = - \left\langle \nabla \nabla \cdot \left(\frac{\nabla U_k}{\sqrt{|\nabla U_k|^2 + \delta^2}} \right), \nabla \Delta U_{k+1} \right\rangle_2 \\ & \leq \frac{1}{\delta_4} \left\| \nabla \nabla \cdot \left(\frac{\nabla U_k}{\sqrt{|\nabla U_k|^2 + \delta^2}} \right) \right\|_2^2 + \delta_4 \|\nabla \Delta U_{k+1}\|_2^2. \end{aligned}$$

Applying Poincaré's and Cauchy's inequality to the first term leads to

$$\left\| \nabla \nabla \cdot \left(\frac{\nabla U_k}{\sqrt{|\nabla U_k|^2 + \delta^2}} \right) \right\|_2^2 \leq O(1/\delta)(\|\nabla U_k\|_2^2 + \|\Delta U_k\|_2^2 + \|\nabla \Delta U_k\|_2^2).$$

Interpolating the L^2 norm of Δu by the L^2 norms of ∇u and $\nabla \Delta u$, we obtain

$$\begin{aligned} & \left(\frac{1}{2\Delta t} + C_2(1 - \delta_3) - \delta_2 \right) \|\nabla U_{k+1}\|_2^2 + (C_1(1 - \delta_1) - \delta_4) \|\nabla \Delta U_{k+1}\|_2^2 \\ & \leq \left(\frac{1}{2\Delta t} + \frac{2\lambda_0^2}{\delta_2} + \frac{C_2}{\delta_3} + \frac{C(1/\delta, \Omega)}{\delta_4} \right) \|\nabla U_k\|_2^2 + \left(\frac{C_1}{\delta_1} + \frac{C(1/\delta, \Omega)}{\delta_4} \right) \|\nabla \Delta U_k\|_2^2 \\ & \quad + C(\Omega, D, \lambda_0, f). \end{aligned}$$

For $\delta_i = 1/2$, $i = 1, \dots, 4$ we obtain

$$\begin{aligned} & \left(\frac{1}{2\Delta t} + \frac{C_2 - 1}{2} \right) \|\nabla U_{k+1}\|_2^2 + \frac{C_1 - 1}{2} \|\nabla \Delta U_{k+1}\|_2^2 \\ & \leq \left(\frac{1}{2\Delta t} + 4\lambda_0^2 + 2(C_2 + C) \right) \|\nabla U_k\|_2^2 + 2(C_1 + C) \|\nabla \Delta U_k\|_2^2 + C(\Omega, D, \lambda_0, f). \end{aligned}$$

Since C_1 and C_2 are chosen such that $C_1 > 1/\delta > 1$ and $C_2 > \lambda_0 > 1$, the coefficients in the inequality above are positive. The rest of the proof is similar to the proof of Proposition 4.1.9. We multiply the inequality by $2\Delta t$ and set

$$C_a = 1 + \Delta t(C_2 - 1), \quad C_b = C_1 - 1, \quad C_c = 1 + 2\Delta t(4\lambda_0^2 + 2(C_2 + C)), \quad C_d = 4(C_1 + C).$$

We obtain

$$\begin{aligned} C_a \|\nabla U_{k+1}\|_2^2 + \Delta t C_b \|\nabla \Delta U_{k+1}\|_2^2 &\leq C_c \|\nabla U_k\|_2^2 + \Delta t C_d \|\nabla \Delta U_k\|_2^2 \\ &\quad + 2\Delta t C(\Omega, D, \lambda_0, f). \end{aligned}$$

Dividing by C_a and multiplying the first and the second term on the right side of the inequality by C_d and $C_c C_b$ respectively we have

$$\begin{aligned} \|\nabla U_{k+1}\|_2^2 + \Delta t \frac{C_b}{C_a} \|\nabla \Delta U_{k+1}\|_2^2 &\leq \frac{C_c C_d}{C_a} \left(\|\nabla U_k\|_2^2 + \Delta t \frac{C_b}{C_a} \|\nabla \Delta U_k\|_2^2 \right) \\ &\quad + \frac{2}{C_a} \Delta t C(\Omega, D, \lambda_0, f). \end{aligned}$$

By induction it follows that

$$\begin{aligned} \|\nabla U_{k+1}\|_2^2 + \Delta t \frac{C_b}{C_a} \|\nabla \Delta U_{k+1}\|_2^2 &\leq \left(\frac{C_c C_d}{C_a} \right)^k \left(\|\nabla U_0\|_2^2 + \Delta t \frac{C_b}{C_a} \|\nabla \Delta U_0\|_2^2 \right) \\ &\quad + \Delta t \sum_{i=0}^{k-1} \left(\frac{C_c C_d}{C_a} \right)^i \frac{2}{C_a} C(\Omega, D, \lambda_0, f). \end{aligned}$$

Therefore we obtain for $k\Delta t \leq T$

$$\begin{aligned} \|\nabla U_k\|_2^2 + \Delta t \frac{C_b}{C_a} \|\nabla \Delta U_k\|_2^2 &\leq e^{KT} \left(\|\nabla U_0\|_2^2 + \Delta t \frac{C_b}{C_a} \|\nabla \Delta U_0\|_2^2 \right. \\ &\quad \left. + \Delta t T \frac{2}{C_a} C(\Omega, D, \lambda_0, f) \right). \quad \square \end{aligned}$$

Finally we show that the discrete solution converges to the continuous one as Δt tends to zero.

Proposition 4.1.16. (Convergence (iii)) *Under the same assumptions as in Theorem 4.1.12 and in particular under assumption (4.24) the error e_k fulfills, for suitable nonnegative constants M_1, M_2 and M_3 ,*

$$\|\nabla e_k\|_2^2 + \Delta t M_1 \|\nabla \Delta e_k\|_2^2 \leq T \Delta t e^{M_2 T} \cdot M_3, \quad (4.28)$$

for $k\Delta t \leq T$ and a fixed $T > 0$.

Proof. By our discrete approximation (4.23) and the consistency computation (4.25),

we have for $e_k = u_k - U_k$

$$\begin{aligned}
 & \frac{e_{k+1} - e_k}{\Delta t} + C_1 \Delta^2 e_{k+1} + C_2 e_{k+1} \\
 = & \frac{1}{\Delta t} (u_{k+1} - u_k) - \frac{1}{\Delta t} (U_{k+1} - U_k) + C_1 \Delta^2 u_{k+1} - C_1 \Delta^2 U_{k+1} + C_2 u_{k+1} - C_2 U_{k+1} \\
 = & - \left(C_1 \Delta^2 U_k - \Delta \left(\nabla \cdot \left(\frac{\nabla U_k}{\sqrt{|\nabla U_k|^2 + \delta^2}} \right) \right) + \lambda(f - U_k) + C_2 U_k \right) \\
 & - \left(\Delta \left(\nabla \cdot \left(\frac{\nabla u_k}{\sqrt{|\nabla u_k|^2 + \delta^2}} \right) \right) - \lambda(f - u_k) - C_1 \Delta^2 u_k - C_2 u_k \right) + \tau_k \\
 = & -[-\Delta \left(\nabla \cdot \left(\frac{\nabla U_k}{\sqrt{|\nabla U_k|^2 + \delta^2}} \right) - \nabla \cdot \left(\frac{\nabla u_k}{\sqrt{|\nabla u_k|^2 + \delta^2}} \right) \right) \\
 & + C_1 \Delta^2 (U_k - u_k) + C_2 (U_k - u_k) - \lambda(U_k - u_k)] + \tau_k.
 \end{aligned}$$

Taking the inner product with $-\Delta e_{k+1}$, we have

$$\begin{aligned}
 & \frac{1}{\Delta t} \langle \nabla(e_{k+1} - e_k), \nabla e_{k+1} \rangle_2 + C_1 \|\nabla \Delta e_{k+1}\|_2^2 + C_2 \|\nabla e_{k+1}\|_2^2 \\
 = & \left\langle -\Delta \left(\nabla \cdot \left(\frac{\nabla U_k}{\sqrt{|\nabla U_k|^2 + \delta^2}} \right) - \nabla \cdot \left(\frac{\nabla u_k}{\sqrt{|\nabla u_k|^2 + \delta^2}} \right) \right), \Delta e_{k+1} \right\rangle_2 \\
 & + C_1 \langle \Delta^2 (U_k - u_k), \Delta e_{k+1} \rangle_2 + \langle \nabla \lambda(U_k - u_k), \nabla e_{k+1} \rangle_2 \\
 & - C_2 \langle \nabla(U_k - u_k), \nabla e_{k+1} \rangle_2 + \langle \nabla \Delta^{-1} \tau_k, \nabla \Delta e_{k+1} \rangle_2
 \end{aligned}$$

Using the same arguments as in the proof of Proposition 4.1.10 we obtain

$$\begin{aligned}
 & \frac{1}{2\Delta t} (\|\nabla e_{k+1}\|_2^2 - \|\nabla e_k\|_2^2) + C_1 \|\nabla \Delta e_{k+1}\|_2^2 + C_2 \|\nabla e_{k+1}\|_2^2 \\
 \leq & \left\langle -\Delta \left(\nabla \cdot \left(\frac{\nabla U_k}{\sqrt{|\nabla U_k|^2 + \delta^2}} \right) - \nabla \cdot \left(\frac{\nabla u_k}{\sqrt{|\nabla u_k|^2 + \delta^2}} \right) \right), \Delta e_{k+1} \right\rangle_2 \\
 & + \frac{C_1}{\delta_1} \|\nabla \Delta e_k\|_2^2 + C_1 \delta_1 \|\nabla \Delta e_{k+1}\|_2^2 + \frac{\lambda_0^2}{\delta_3} \|\nabla e_k\|_2^2 + \delta_3 \|\nabla e_{k+1}\|_2^2 \\
 & + \frac{C_2}{\delta_2} \|\nabla e_k\|_2^2 + C_2 \delta_2 \|\nabla e_{k+1}\|_2^2 + \frac{1}{\delta_4} \|\tau_k\|_{-1}^2 + \delta_4 \|\nabla \Delta e_{k+1}\|_2^2.
 \end{aligned}$$

We consider the first term on the right side of the above inequality in detail,

$$\begin{aligned}
 & \left\langle -\Delta \left(\nabla \cdot \left(\frac{\nabla U_k}{\sqrt{|\nabla U_k|^2 + \delta^2}} \right) - \nabla \cdot \left(\frac{\nabla u_k}{\sqrt{|\nabla u_k|^2 + \delta^2}} \right) \right), \Delta e_{k+1} \right\rangle_2 \\
 &= \left\langle \nabla \left(\nabla \cdot \left(\frac{\nabla U_k}{\sqrt{|\nabla U_k|^2 + \delta^2}} \right) - \nabla \cdot \left(\frac{\nabla u_k}{\sqrt{|\nabla u_k|^2 + \delta^2}} \right) \right), \nabla \Delta e_{k+1} \right\rangle_2 \\
 &\leq \frac{1}{2} \left\| \nabla \left(\nabla \cdot \left(\frac{\nabla U_k}{\sqrt{|\nabla U_k|^2 + \delta^2}} \right) - \nabla \cdot \left(\frac{\nabla u_k}{\sqrt{|\nabla u_k|^2 + \delta^2}} \right) \right) \right\|_2^2 + \frac{1}{2} \|\nabla \Delta e_{k+1}\|_2^2 \\
 &\leq \left\| \nabla \left(\nabla \cdot \left(\frac{\nabla U_k}{\sqrt{|\nabla U_k|^2 + \delta^2}} \right) \right) \right\|_2^2 + \left\| \nabla \left(\nabla \cdot \left(\frac{\nabla u_k}{\sqrt{|\nabla u_k|^2 + \delta^2}} \right) \right) \right\|_2^2 \\
 &\quad + \frac{1}{2} \|\nabla \Delta e_{k+1}\|_2^2 \\
 &\leq C(1/\delta, \Omega) \left(\|\nabla U_k\|_2^2 + \|\nabla \Delta U_k\|_2^2 + \|\nabla u_k\|_2^2 + \|\nabla \Delta u_k\|_2^2 \right) \\
 &\quad + \frac{1}{2} \|\nabla \Delta e_{k+1}\|_2^2,
 \end{aligned}$$

for a constant $C > 0$ (cf. the estimate for the regularizer in the proof of Proposition 4.1.15). Therefore we obtain

$$\begin{aligned}
 & \left(\frac{1}{2\Delta t} + C_2(1 - \delta_2) - \delta_3 \right) \|\nabla e_{k+1}\|_2^2 + \left(C_1(1 - \delta_1) - \delta_4 - \frac{1}{2} \right) \|\nabla \Delta e_{k+1}\|_2^2 \\
 &\leq \left(\frac{1}{2\Delta t} + \frac{C_2}{\delta_2} + \frac{\lambda_0^2}{\delta_3} \right) \|\nabla e_k\|_2^2 + \frac{C_1}{\delta_1} \|\nabla \Delta e_k\|_2^2 + \frac{1}{\delta_4} \|\tau_k\|_{-1}^2 \\
 &\quad + C(1/\delta, \Omega) \left(\|\nabla U_k\|_2^2 + \|\nabla \Delta U_k\|_2^2 + \|\nabla u_k\|_2^2 + \|\nabla \Delta u_k\|_2^2 \right).
 \end{aligned}$$

Proposition 4.1.15 guarantees that U_k is bounded by a constant, and assumption (4.24) that the exact solution u_k is bounded. Therefore by following the lines of the proof of Proposition 4.1.10 we finally have for $k\Delta t \leq T$

$$\|\nabla e_k\|_2^2 + \Delta t M_1 \|\nabla \Delta e_k\|_2^2 \leq T \Delta t e^{M_2 T} \cdot M_3,$$

for suitable positive constants M_1, M_2 and M_3 . □

4.1.4 LCIS Inpainting

Our last example for the applicability of the convexity splitting method to higher-order inpainting approaches is inpainting with LCIS (2.42). With $f \in L^2(\Omega)$ our inpainted

image u evolves in time as

$$u_t = -\Delta(\arctan(\Delta u)) + \lambda(f - u).$$

In contrast to the other two inpainting methods that we discussed, this inpainting equation is a gradient flow in L^2 for the energy

$$\mathcal{J}(u) = \int_{\Omega} G(\Delta u) dx + \frac{1}{2} \int_{\Omega} \lambda(f - u)^2,$$

with $G'(y) = \arctan(y)$. Therefore Eyre's result in Theorem 4.1.4 can be applied directly. The functional $\mathcal{J}(u)$ is split into $\mathcal{J}_1 - \mathcal{J}_2$ with

$$\begin{aligned} \mathcal{J}_1(u) &= \int_{\Omega} \frac{C_1}{2} (\Delta u)^2 dx + \frac{1}{2} \int_{\Omega} \frac{C_2}{2} |u|^2 dx, \\ \mathcal{J}_2(u) &= \int_{\Omega} -G(\Delta u) + \frac{C_1}{2} (\Delta u)^2 dx + \frac{1}{2} \int_{\Omega} -\lambda(f - u)^2 + \frac{C_2}{2} |u|^2 dx. \end{aligned}$$

The resulting time-stepping scheme is

$$\frac{U_{k+1} - U_k}{\Delta t} + C_1 \Delta^2 U_{k+1} + C_2 U_{k+1} = -\Delta(\arctan(\Delta U_k)) + C_1 \Delta^2 U_k + \lambda(f - U_k) + C_2 U_k. \quad (4.29)$$

Again we impose homogeneous Neumann boundary conditions, use DCT to solve (4.29) and we choose the constants C_1 and C_2 such that \mathcal{J}_1 and \mathcal{J}_2 are all strictly convex and condition (4.9) is satisfied. The functional \mathcal{J}_1 is convex for all $C_1, C_2 > 0$. The first term in \mathcal{J}_2 is convex if $C_1 > 1$. This follows from its second variation, namely

$$\begin{aligned} \nabla^2 \mathcal{J}_{1e}(u)(v, w) &= \left(\frac{d}{ds} \int (C_1 \Delta(u + sw) - \arctan(\Delta(u + sw))) \Delta v dx \right)_{s=0} \\ &= \int \left(C_1 - \frac{1}{1 + (\Delta u)^2} \right) \Delta v \Delta w dx. \end{aligned}$$

For \mathcal{J}_{1e} being convex $\nabla^2 \mathcal{J}_{1e}(u)(v, w)$ has to be > 0 for all $v, w \in C^\infty$ and therefore

$$C_1 - \frac{1}{1 + (\Delta u)^2} > 0.$$

Substituting $s = \Delta u$ we obtain

$$C_1 > \frac{1}{1 + s^2} \quad \forall s \in \mathbb{R}.$$

This inequality is fulfilled for all $s \in \mathbb{R}$ if $C_1 > 1$. We obtain the same condition on C_1 for $G'(s) = \arctan(\frac{s}{\delta})$. For the convexity of the second term of \mathcal{J}_2 , the second constant has to fulfill $C_2 > \lambda_0$, cf. the computation for the fitting term in Section 4.1.3. With these choices of C_1 and C_2 also condition (4.9) of Theorem 4.1.4 is automatically satisfied.

Rigorous Estimates for the Scheme

Finally we present rigorous results for (4.29). In contrast to the inpainting equations (2.1) and (2.27), inpainting with LCIS follows a variational principle. Hence, by choosing the constants C_1 and C_2 appropriately, i.e., $C_1 > 1$, $C_2 > \lambda_0$ (cf. the computations above), Theorem 4.1.4 ensures that the iterative scheme (4.29) is unconditionally gradient stable. Additionally to this property, we present similar results as before for Cahn-Hilliard- and TV-H⁻¹inpainting.

Theorem 4.1.17. *Let u be the exact solution of (2.42) and $u_k = u(k\Delta t)$ the exact solution at time $k\Delta t$, for a time step $\Delta t > 0$ and $k \in \mathbb{N}$. Let further U_k be the k th iterate of (4.29) with constants $C_1 > 1$, $C_2 > \lambda_0$. Then the following statements are true:*

- (i) *Under the assumption that $\|u_{tt}\|_{-1}$, $\|\nabla \Delta u_t\|_2$ and $\|u_t\|_2$ are bounded, the numerical scheme (4.29) is consistent with the continuous equation (2.42) and of order 1 in time.*
- (ii) *The solution sequence U_k is bounded on a finite time interval $[0, T]$, for all $\Delta t > 0$.*
- (iii) *Let further $e_k = u_k - U_k$. If*

$$\|\nabla \Delta u_k\|_2^2 \leq K, \text{ for a constant } K > 0, \text{ and for all } k\Delta t < T, \quad (4.30)$$

then the error e_k converges to zero as $\Delta t \rightarrow 0$.

Remark 4.1.18. *Note that the consistency result of Theorem 4.1.17 is weaker than than the one following from Theorem 4.1.4. In fact Eyre's theorem shows that the scheme is of order 2, which is a stronger result than Theorem 4.1.17 (i).*

Note that assumption (4.30) does not hold in general. Given the results of [BG04] for the denoising case $\lambda(x) = \lambda_0$ in all of Ω and for smooth initial data and smooth f , this assumption nevertheless seems to be reasonable in an heuristic sense. Rigorously, the well-posedness and regularity of solutions in the two-dimensional case with non constant λ is a matter for future research.

The proof of Theorem 4.1.17 is organized in the following three Propositions 4.1.19-4.1.21. Since the proof of consistency follows the lines of Proposition 4.1.8 and Proposition 4.1.14, we just state the result.

Proposition 4.1.19. (Consistency (i)) *Under the same assumptions as in Theorem 4.1.17 and in particular assuming that $\|u_{tt}\|_{-1}$, $\|\nabla \Delta u_t\|_2$ and $\|u_t\|_2$ are bounded, we have*

$$\|\tau_k\|_{-1} = O(\Delta t).$$

Next we would like to show the boundedness of a solution of (4.29) in the following proposition.

Proposition 4.1.20. (Unconditional stability (ii)) *Under the same assumptions as in Theorem 4.1.17 the solution sequence U_k fulfills, for $k\Delta t < T$*

$$\begin{aligned} \|\nabla U_k\|_2^2 + \Delta t K_1 \|\nabla \Delta U_k\|_2^2 &\leq e^{K_2 T} \left(\|\nabla U_0\|_2^2 + \Delta t K_1 \|\nabla \Delta U_0\|_2^2 \right. \\ &\quad \left. + \Delta t T C(\Omega, D, \lambda_0, f) \right) \end{aligned}$$

for suitable constants K_1 , K_2 , and constant C depending on Ω, D, λ_0, f only.

Proof. If we multiply (4.29) with $-\Delta U_{k+1}$ and integrate over Ω we obtain

$$\begin{aligned} \frac{1}{\Delta t} \left(\|\nabla U_{k+1}\|_2^2 - \langle \nabla U_k, \nabla U_{k+1} \rangle_2 \right) + C_2 \|\nabla U_{k+1}\|_2^2 + C_1 \|\nabla \Delta U_{k+1}\|_2^2 \\ = \langle \Delta \arctan(\Delta U_k), \Delta U_{k+1} \rangle_2 + C_1 \langle \nabla \Delta U_k, \nabla \Delta U_{k+1} \rangle_2 \\ + \langle \nabla (\lambda(f - U_k)), \nabla U_{k+1} \rangle_2 + C_2 \langle \nabla U_k, \nabla U_{k+1} \rangle_2. \end{aligned}$$

Using the same arguments as in the proofs of Proposition 4.1.9 and 4.1.15 we obtain

$$\begin{aligned} \frac{1}{2\Delta t} \left(\|\nabla U_{k+1}\|_2^2 - \|\nabla U_k\|_2^2 \right) + C_2 \|\nabla U_{k+1}\|_2^2 + C_1 \|\nabla \Delta U_{k+1}\|_2^2 \\ \leq \langle \Delta \arctan(\Delta U_k), \Delta U_{k+1} \rangle_2 + \frac{C_1}{\delta_1} \|\nabla \Delta U_k\|_2^2 + C_1 \delta_1 \|\nabla \Delta U_{k+1}\|_2^2 + \frac{\lambda_0^2}{2\delta_2} \|\nabla U_k\|_2^2 \\ + \delta_2 \|\nabla U_{k+1}\|_2^2 + \frac{C_2}{\delta_3} \|\nabla U_k\|_2^2 + C_2 \delta_3 \|\nabla U_{k+1}\|_2^2 + C(\Omega, D, \lambda_0, f). \end{aligned}$$

Now, the first term on the right side of the inequality can be estimated as follows

$$\begin{aligned} \langle \Delta \arctan(\Delta U_k), \Delta U_{k+1} \rangle_2 &= -\langle \nabla \arctan(\Delta U_k), \nabla \Delta U_{k+1} \rangle_2 \\ &= -\left\langle \frac{1}{1 + (\Delta U_k)^2} \nabla \Delta U_k, \nabla \Delta U_{k+1} \right\rangle_2 \\ &\leq \frac{1}{\delta_4} \left\| \frac{1}{1 + (\Delta U_k)^2} \nabla \Delta U_k \right\|_2^2 + \delta_4 \|\nabla \Delta U_{k+1}\|_2^2 \\ &\leq \frac{1}{\delta_4} \|\nabla \Delta U_k\|_2^2 + \delta_4 \|\nabla \Delta U_{k+1}\|_2^2. \end{aligned} \tag{4.31}$$

From this we get

$$\begin{aligned} & \left(\frac{1}{2\Delta t} + C_2(1 - \delta_3) - \delta_2 \right) \|\nabla U_{k+1}\|_2^2 + (C_1(1 - \delta_1) - \delta_4) \|\nabla \Delta U_{k+1}\|_2^2 \\ & \leq \left(\frac{1}{2\Delta t} + \frac{\lambda_0^2}{2\delta_2} + \frac{C_2}{\delta_3} \right) \|\nabla U_k\|_2^2 + \left(\frac{C_1}{\delta_1} + \frac{1}{\delta_4} \right) \|\nabla \Delta U_k\|_2^2 + C(\Omega, D, \lambda_0, f). \end{aligned}$$

Analogously to Section 4.1.3, with

$$C_a = 1 + \Delta t(C_2 - 1), \quad C_b = C_1 - 1, \quad C_c = 1 + 2\Delta t(\lambda_0^2 + 2C_2), \quad C_d = 4(C_1 + 1),$$

we obtain

$$\begin{aligned} \|\nabla U_k\|_2^2 + \Delta t \frac{C_b}{C_a} \|\nabla \Delta U_k\|_2^2 & \leq e^{KT} \left(\|\nabla U_0\|_2^2 + \Delta t \frac{C_b}{C_a} \|\nabla \Delta U_0\|_2^2 \right. \\ & \quad \left. + \Delta t T \frac{2}{C_a} C(\Omega, D, \lambda_0, f) \right), \end{aligned}$$

which gives boundedness of the solution sequence on $[0, T]$ for any $T > 0$ and any $\Delta t > 0$. \square

The convergence of the discrete solution to the continuous one as $\Delta t \rightarrow 0$ is verified in the following proposition.

Proposition 4.1.21. (Convergence (iii)) *Under the same assumptions as in Theorem 4.1.17 and in particular under assumption (4.30), the error e_k fulfills, for suitable nonnegative constants M_1, M_2 and M_3 ,*

$$\|\nabla e_k\|_2^2 + \Delta t M_1 \|\nabla \Delta e_k\|_2^2 \leq T \Delta t e^{M_2 T} \cdot M_3, \quad (4.32)$$

for $k\Delta t \leq T$ and a fixed $T > 0$.

Proof. Since all the computations in the convergence proof for (4.29) are the same as in Section 4.1.3 for (4.23) except of the estimate for the regularizer $\Delta(\arctan(\Delta u))$, we only give the details for the latter and leave the rest to the reader. Thus for the inner product involving the regularizer of (4.29) within the convergence proof we apply the arguments from (4.31) and obtain

$$\begin{aligned} & \langle -\Delta(\arctan(\Delta U_k) - \arctan(\Delta u_k)), \Delta e_{k+1} \rangle_2 \\ & = \langle \nabla(\arctan(\Delta U_k) - \arctan(\Delta u_k)), \nabla \Delta e_{k+1} \rangle_2 \\ & \leq \|\nabla \Delta U_k\|_2^2 + \|\nabla \Delta u_k\|_2^2 + \frac{1}{2} \|\nabla \Delta e_{k+1}\|_2^2. \end{aligned}$$

By assumption (4.30) and by following the same steps as in the proof of Proposition 4.1.16 we finally have for $k\Delta t \leq T$

$$\|\nabla e_k\|_2^2 + \Delta t M_1 \|\nabla \Delta e_k\|_2^2 \leq T \Delta t e^{M_2 T} \cdot M_3,$$

for suitable positive constants M_1, M_2 and M_3 . \square

4.1.5 Numerical Discussion

Numerical results for all three inpainting schemes have already been presented in Sections 2.1.2, 2.2.5, and 2.3.1. In Figures 4.1, 4.2, and 4.3 one additional numerical result for each approach is presented.

In all three inpainting schemes, for the discretization in space we used finite differences and spectral methods, i.e., the discrete cosine transform or the fast Fourier transform, to simplify the inversion of the Laplacian Δ for the computation of U_{k+1} . Note that in the case of Cahn-Hilliard inpainting (2.1) special attention has to be paid to the correct choice of the mesh size Δx , which has to be of the order ϵ , also cf. the numerical examples in Section 3.1.3 and [GI03, VR03]. Further, recall that Cahn-Hilliard inpainting is applied in a two-step procedure with changing ϵ value, cf. Section 3.1.3 for details. For Cahn-Hilliard- and TV-H⁻¹inpainting the optimal time step size Δt turned out to be $\Delta t = 1$ or 10 (depending also on the size of ϵ and λ_0). For the numerical computation of inpainting with LCIS the time step size Δt was chosen to be equal to 0.01 .



Figure 4.1: Destroyed binary image and the solution of Cahn-Hilliard inpainting with $\lambda_0 = 10^9$ and switching ϵ value: $u(200)$ with $\epsilon = 0.8$, $u(500)$ with $\epsilon = 0.01$

Although the proposed discrete schemes in this paper are unconditionally stable, their numerical performance is still far of being in real-time. The reason is the damping



Figure 4.2: $\text{TV}-\text{H}^{-1}$ inpainting: $u(1000)$ with a regularization parameter $\epsilon = 0.01$ and $\lambda_0 = 10^2$



Figure 4.3: LCIS inpainting result $u(1000)$ with $\delta = 0.1$ and $\lambda_0 = 10^3$.

introduced by the conditions on the constants C_1 , and C_2 in all three schemes (4.11), (4.23), and (4.29). In Figure 4.2 for instance, we need around 1000 iterations to receive the restored image. If now additionally the data dimension is large, e.g., when we have to process 2D images of high resolution, of sizes 3000×3000 pixels for instance, or even 3D image data, each iteration step itself is computationally expensive and we are far from real-time computations. As already discussed in Section 1.3.3 in more detail, the field of research on fast numerical solvers for higher-order inpainting models is still in its infancy. The construction of such solvers is very favorable though, in particular for the use of these inpainting models in practice. TV approaches for example already turned out to be an effective tool for the reconstruction of medical images as the

ones gained from PET (Positron Emission Tomography) measurements (cf. [JHC98], for instance). These imaging approaches need to deal with 3D or even 4D image date (including time dependence) in a fast and robust way. Motivated by this we are thinking about alternative ways to reduce the dimensionality of the data and hence speed up the reconstruction process. This will be the interest of Section 4.3 where we present a domain decomposition approach to be applied, among others, to TV inpainting models.

4.2 A Dual Solver for TV-H⁻¹Minimization

In this section we are concerned with the numerical minimization of total variation functionals with an H^{-1} constraint. We present an algorithm for its solution, which is based on the dual formulation of total variation and show its application in several areas of image processing, among them also TV-H⁻¹inpainting. In fact a major motivation for this algorithm is the creation of a fast numerical method to solve TV-H⁻¹inpainting. Namely, we shall see in Section 4.3 that this dual solver enables us to apply a domain decomposition algorithm to TV-H⁻¹inpainting.

4.2.1 Introduction and Motivation

Let $\Omega \subset \mathbb{R}^2$ be a bounded and open domain with Lipschitz boundary. For a given function $f \in L^2(\Omega)$ we are interested in the numerical realization of the following minimization problem

$$\min_{u \in BV(\Omega)} \mathcal{J}(u), \text{ where } \mathcal{J}(u) = \|Tu - f\|_{-1}^2 + 2\alpha |Du|(\Omega), \quad (4.33)$$

where $T \in \mathcal{L}(L^2(\Omega))$ is a bounded linear operator and $\alpha > 0$ is a tuning parameter. The function $|Du|(\Omega)$ is the total variation of u and $\|\cdot\|_{-1}$ is the norm in $H^{-1}(\Omega)$, the dual of $H_0^1(\Omega)$. Please compare the Appendix for the definition of these terms.

Problem (4.33) is a model for minimizing the total variation of a function u which obeys an H^{-1} constraint, i.e., $\|Tu - f\|_{-1}$ is small, for a given function $f \in L^2(\Omega)$. In the terminology of inverse problems this means that from an observed datum f one wants to determine the original function u , from which a priori we know that $Tu = f$ and u has some regularity properties modeled by the total variation and the H^{-1} norm.

Minimization problems like this have important applications in a wide range of image processing tasks. We give their overview in the following subsections.

The main interest of this section is the numerical solution of (4.33). In [Ch04] Chambolle proposes an algorithm to solve total variation minimization with an L^2 constraint and $T = Id$. This approach was extended to more general operators T in a subsequent work [BBAC04]. In the following we shall introduce a generalization of Chambolle's algorithm for the case of an H^{-1} norm in the problem. Moreover, we present strategies to extend the use of this algorithm from problems with $T = Id$ to problems (4.33) with an arbitrary linear operator T . Additional to the theory of this algorithm we present its applications in image processing, in particular for image denoising, image decomposition and inpainting. Finally we show how to speed up numerical computations by considering a domain decomposition approach for our problem.

Note that the existence and uniqueness of minimizers for (4.33) is guaranteed. In fact the existence of a unique solution of (4.33) follows as a special case from the following theorem.

Theorem 4.2.1. [LV08, Theorem 3.1] *Given $\Omega \subset \mathbb{R}^2$, open, bounded and connected, with Lipschitz boundary, $f \in H^{-s}(\mathbb{R}^2)$ ($s > 0$), $f = 0$ outside of $\bar{\Omega}$, $\alpha > 0$, and $T \in \mathcal{L}(L^2(\Omega))$ an injective continuous linear operator such that $T\mathbf{1}_\Omega \neq 0$, then the minimization problem*

$$\min_{u \in BV(\Omega)} \|Tu - f\|_{-s}^2 + 2\alpha |Du|(\Omega), \quad s > 0,$$

where $\|\cdot\|_{-s}$ denotes the norm in $H^{-s}(\mathbb{R}^2)$, has a unique solution in $BV(\Omega)$.

Proof. The proof is a standard application of methods from variational calculus and can be found, e.g., in [LV08]. The main ingredients in the proof, in order to guarantee compactness, are the Poincaré-Wirtinger inequality (cf. [AV94] for instance) which bounds the L^2 - and the L^1 - norm by the total variation, and the fact that $L^2(\Omega)$ can be embedded in $H^{-1}(\Omega)$. \square

In the subsequent two subsections we shall present two main applications of TV-H⁻¹minimization (4.33) for image denoising / decomposition, and image inpainting.

TV-H⁻¹Minimization for Image Denoising and Image Decomposition

In taking $T = Id$ in (4.33), we encounter two interesting areas in image processing, namely image denoising and image decomposition. In many image denoising models a given noisy image f is decomposed into its piecewise smooth part u and its oscillatory, noisy part v , i.e., $f = u + v$. Similarly, in image decomposition the piecewise smooth part u represents the structure/cartoon part of the image, and the oscillatory part v the texture part of the image. We call the latter task also cartoon-texture decomposition. The most famous model within this range is the TV-L²denoising model proposed by Rudin, Osher and Fatemi [ROF92]

$$\mathcal{J}(u) = \|u - f\|_2^2 + 2\alpha |Du|(\Omega) \rightarrow \min_{u \in BV(\Omega)}. \quad (4.34)$$

This model produces very good results for removing noise and preserving edges in structured images, meaning images without texture-like components, i.e., high oscillatory edges. Unfortunately it fails in the presence of the latter. Namely it cannot separate pure noise from high oscillatory edges but removes both equally.

To overcome this situation, Y. Meyer [Me01] suggested to replace the L^2 -fidelity term by a weaker norm. Namely he proposes the following model:

$$\mathcal{J}(u) = \|u - f\|_* + 2\alpha |Du|(\Omega) \rightarrow \min_{u \in BV(\Omega)},$$

where the $\|\cdot\|_*$ is defined as follows.

Definition 4.2.2. Let G denote the Banach space consisting of all generalized functions $f(x, y)$ which can be written as

$$f(x, y) = \nabla \cdot (\vec{g}(x, y)), \quad \vec{g} = (g_1, g_2), \quad g_1, g_2 \in L^\infty(\Omega), \quad \vec{g} \cdot \vec{n} = 0 \text{ on } \partial\Omega,$$

where \vec{n} is the unit normal on $\partial\Omega$. Then $\|f\|_*$ is the induced norm of G defined as

$$\|f\|_* = \inf_{f=\nabla \cdot \vec{g}} \left\| \sqrt{g_1(x, y)^2 + g_2(x, y)^2} \right\|_{L^\infty(\Omega)}.$$

In fact, the space G is the dual space of $W_0^{1,1}(\Omega)$. In [Me01] Meyer further introduces two other spaces with similar properties to G but we are not going into detail here. We only mention that these spaces are intrinsically appropriate for modeling textured or oscillatory patterns and in fact they provide for them norms which are smaller than the L^2 norm.

The drawback of Y. Meyer's model is that it can not be solved directly with respect to the minimizer u and therefore has to be approximated, cf. [VO04]. Thereby the \ast -norm is replaced by

$$\frac{1}{2\mu} \|(u + \nabla \cdot \vec{g}) - f\|_2^2 + \left\| \sqrt{g_1^2 + g_2^2} \right\|_{L_p(\Omega)},$$

with $\mu > 0$ and $p \geq 1$. In the case $p = 2$ the second term in the above expression is equivalent to the H^{-1} norm. In particular $v = \nabla \cdot \vec{g}$ corresponds to $v \in H^{-1}(\Omega)$. Indeed, for $v \in H^{-1}(\Omega)$, there is a unique $v^* \in H_0^1(\Omega)$ such that

$$\|v\|_{-1}^2 = \|\nabla v^*\|_2^2 = \|\nabla \Delta^{-1} v\|_2^2 = \left\| \sqrt{g_1^2 + g_2^2} \right\|_2^2.$$

Limiting to the case $p = 2$ and the limit $\mu \rightarrow 0$ the TV-H⁻¹denoising model was created, cf. [OSV03, MG01, LV08], i.e.,

$$\|u - f\|_{-1}^2 + 2\alpha |\nabla u|(\Omega) \rightarrow \min_{u \in BV(\Omega)}. \quad (4.35)$$

Numerical experiments showed that (4.35) gives much better results than (4.34) under the presence of oscillatory data, cf. [OSV03, LV08]. In Section 4.2.3 we will present some numerical results that support this claim.

TV-H⁻¹Inpainting

The second application we are interested in is TV-H⁻¹inpainting (2.27). This inpainting approach was already discussed in Section 2.2 in great detail. Let us recall the basic setup of this inpainting approach: the inpainted image u of $f \in L^2(\Omega)$, shall evolve via (2.27), i.e.,

$$u_t = \Delta p + \lambda(f - u), \quad p \in \partial |\nabla u|(\Omega),$$

where $\partial |\nabla u|(\Omega)$ denotes the subdifferential of the total variation, cf. Appendix A.5, and λ is the indicator function of the domain outside of the missing domain D multiplied by a constant $\lambda_0 \gg 1$. As Cahn-Hilliard inpainting in Section 2.1, also TV-H⁻¹inpainting does not follow a variational principle. In fact the most natural formulation of (4.33) in terms of inpainting would be in the setting $T = \mathbf{1}_{\Omega \setminus D}$ and $\alpha = 1/\lambda_0$. Similarly to the Cahn-Hilliard case, cf. (2.4), this only results in an optimality condition which describes a second-order anisotropic diffusion inside of the inpainting domain D , i.e., $p = 0$ in

D . Hence it is not immediately clear how a numerical method for the minimization problem (4.33) is applicable to solve the inpainting equation (2.27). How this is possible though, will be explained in the following sections, cf. especially (4.47) and (4.48).

Numerical Solution for TV-H⁻¹Minimization

The numerical solution of TV-H⁻¹minimization depends on the specific problem at hand. In [LV08] Lieu and Vese proposed a numerical method to solve TV-H⁻¹denoising / decomposition (4.35) by using the Fourier representation of the H^{-1} norm on the whole \mathbb{R}^d , $d \geq 1$. Therein the space $H^{-1}(\mathbb{R}^d)$ is defined to be the Hilbert space equipped with the inner product

$$\langle f, g \rangle_{-1} = \int \left(1 + |\xi|^2\right)^{-1} \hat{f} \bar{\hat{g}} \, d\xi$$

and associated norm $\|f\|_{-1} = \sqrt{\langle f, f \rangle_{-1}}$, cf. also [DL88]. Here \hat{g} denotes the Fourier transform of g in $L^2(\mathbb{R}^d)$, i.e.,

$$\hat{g}(\xi) := \frac{1}{(2\pi)^{2d}} \int_{\mathbb{R}^d} e^{-ix\xi} g(x) \, dx, \quad \xi \in \mathbb{R}^d, \quad (4.36)$$

and \bar{g} the complex conjugate of g . Equivalently to this definition $H^{-1}(\mathbb{R}^d)$ is the dual space of $H^1(\mathbb{R}^d)$. Note that we consider functions g defined in \mathbb{R}^d rather than on a bounded domain which can be done by considering zero extensions of the image function. With this definition of the H^{-1} norm the corresponding optimality condition for total variation denoising/decomposition (4.35) reads

$$\begin{cases} \alpha p + \left[2 \operatorname{Re} \left\{ \widetilde{\frac{\hat{f} - \bar{u}}{(1 + |\xi|^2)^{-1}}} \right\} \right] = 0 & \text{in } \Omega \\ \frac{\nabla u}{|\nabla u|} \cdot \vec{n} = 0 & \text{on } \partial\Omega \\ u = 0 & \text{outside } \bar{\Omega}, \end{cases} \quad (4.37)$$

where $\widetilde{\{f\}}$ denotes the inverse Fourier transform of f , defined in analogy to (4.36), Re denotes the real part of a complex number, and \vec{n} is the outward-pointing unit normal vector on $\partial\Omega$. For the numerical computation of a solution of (4.37), we approximate an element p of the subdifferential of $|Du|(\Omega)$, by its relaxed version

$$p \approx \nabla \cdot (\nabla u / |\nabla u|_\epsilon), \quad (4.38)$$

where $|\nabla u|_\epsilon = \sqrt{|\nabla u|^2 + \epsilon}$.

Equation (4.37) leads to solve a second-order PDE rather than a fourth-order PDE, resulting in a better CFL condition for the numerical scheme, cf. [LV08].

In the case of TV-H⁻¹inpainting (2.27) the situation is completely different since (2.27) does not fulfill a variational principle, cf. Section 4.2.1. In Section 4.1.3 we proposed the semi-implicit scheme (4.23) for the solution of (2.27). Let U_k denote the approximate solution to the exact solution $u(k\tau)$ (where τ denotes the time step). Then this scheme reads

$$\begin{aligned} \frac{U_{k+1} - U_k}{\tau} + C_1 \Delta^2 U_{k+1} + C_2 U_{k+1} &= C_1 \Delta^2 U_k - \Delta(\nabla \cdot (\frac{\nabla U_k}{|\nabla U_k|_\epsilon})) \\ &\quad + C_2 U_k + \lambda(f - U_k), \end{aligned}$$

where $\Delta^2 = \Delta \Delta$ and with constants $C_1 > \frac{1}{\epsilon}$ and $C_2 > \lambda_0$. Since usually in inpainting tasks λ_0 is chosen comparatively large, e.g., $\lambda_0 = 10^3$, the condition on C_2 makes the numerical scheme, although unconditionally stable, quite slow. To our knowledge this is the only existing numerical method proposed for TV-H⁻¹inpainting, except for the one presented in this section.

In the following we are going to present a method introduced by Chambolle [Ch04] for TV-L²minimization (4.34) and its generalization for the TV-H⁻¹case (4.33). This algorithm will give us the opportunity to address TV-H⁻¹minimization in a general way.

4.2.2 The Algorithm

Preliminaries

Throughout this section $\|\cdot\|$ denotes the norm in $X = L^2(\Omega)$ in the continuous setting and the Euclidean norm in $X = \mathbb{R}^{N \times M}$ in the discrete setting. In the discrete setting the continuous image domain $\Omega = [a, b] \times [c, d] \subset \mathbb{R}^2$ is approximated by a finite grid $\{a = x_1 < \dots < x_N = b\} \times \{c = y_1 < \dots < y_M = d\}$ with equidistant step-size $h = x_{i+1} - x_i = \frac{b-a}{N} = \frac{d-c}{M} = y_{j+1} - y_j$ equal to 1 (one pixel). The digital image u is an element in X . We denote $u(x_i, y_j) = u_{i,j}$ for $i = 1, \dots, N$ and $j = 1, \dots, M$.

Further we define $Y = X \times X$ with Euclidean norm $\|\cdot\|_Y$ and inner product $\langle \cdot, \cdot \rangle_Y$. Moreover the operators gradient ∇ , divergence $\nabla \cdot$ and Laplacian Δ in the discrete setting are defined as follows:

4.2 A Dual Solver for $\mathbf{TV-H}^{-1}$ Minimization

The gradient ∇u is a vector in Y given by forward differences

$$(\nabla u)_{i,j} = ((\nabla_x u)_{i,j}, (\nabla_y u)_{i,j}),$$

with

$$(\nabla_x u)_{i,j} = \begin{cases} u_{i+1,j} - u_{i,j} & \text{if } i < N \\ 0 & \text{if } i = N, \end{cases} \quad (\nabla_y u)_{i,j} = \begin{cases} u_{i,j+1} - u_{i,j} & \text{if } j < M \\ 0 & \text{if } j = M, \end{cases}$$

for $i = 1, \dots, N$, $j = 1, \dots, M$.

We further introduce a discrete divergence $\nabla \cdot : Y \rightarrow X$ defined, by analogy with the continuous setting, by $\nabla \cdot = -\nabla^*$ (∇^* is the adjoint of the gradient ∇). That is, the discrete divergence operator is given by backward differences like

$$(\nabla \cdot p)_{ij} = \begin{cases} p_{i,j}^x - p_{i-1,j}^x & \text{if } 1 < i < N \\ p_{i,j}^x & \text{if } i = 1 \\ -p_{i-1,j}^x & \text{if } i = N \end{cases} + \begin{cases} p_{i,j}^y - p_{i,j-1}^y & \text{if } 1 < j < M \\ p_{i,j}^y & \text{if } j = 1 \\ -p_{i,j-1}^y & \text{if } j = M, \end{cases}$$

for every $p = (p^x, p^y) \in Y$.

Finally we define the discrete Laplacian as $\Delta = \nabla \cdot \nabla$, i.e.,

$$(\Delta u)_{i,j} = \begin{cases} u_{i+1,j} - 2u_{i,j} + u_{i-1,j} & \text{if } 1 < i < N \\ u_{i+1,j} - u_{i,j} & \text{if } i = 1 \\ u_{i-1,j} - u_{i,j} & \text{if } i = N \end{cases} + \begin{cases} u_{i,j+1} - 2u_{i,j} + u_{i,j-1} & \text{if } 1 < j < M \\ u_{i,j+1} - u_{i,j} & \text{if } j = 1 \\ u_{i,j-1} - u_{i,j} & \text{if } j = M, \end{cases}$$

and its inverse operator Δ^{-1} , as in the continuous setting (cf. Appendix A.4), i.e., $u = \Delta^{-1}f$ is the unique solution of

$$\begin{cases} -(\Delta u)_{i,j} = f_{i,j} & 1 < i < N, 1 < j < M \\ u_{i,j} = 0 & i = 1, N; j = 1, M. \end{cases}$$

Moreover, without always indicating it, when in the discrete setting, instead of minimizing

$$\mathcal{J}(u) = \|Tu - f\|_{-1}^2 + 2\alpha |Du|(\Omega),$$

we consider the discretized functional

$$\mathcal{J}^\delta(u) := \sum_{\substack{1 \leq i \leq N \\ 1 \leq j \leq M}} (\nabla \Delta^{-1}((Tu)_{i,j} - f_{i,j}))^2 + 2\alpha |(\nabla u)_{i,j}|,$$

with $|y| = \sqrt{y_1^2 + y_2^2}$ for every $y = (y_1, y_2) \in \mathbb{R}^2$. To give a meaning to $(Tu)_{i,j}$ we assume that T is applied to the piecewise interpolant \hat{u} of the matrix $(u_{i,j})$.

Chambolle's Algorithm for Total Variation Minimization

In [Ch04] Chambolle proposes an algorithm to compute numerically a minimizer of

$$\mathcal{J}(u) = \|u - f\|_2^2 + 2\alpha |Du|(\Omega).$$

His algorithm is based on considerations of the convex conjugate of the total variation and on exploiting the corresponding optimality condition. It amounts to computing the minimizer u of \mathcal{J} as

$$u = f - \mathbb{P}_{\alpha K}(f),$$

where \mathbb{P}_K denotes the orthogonal projection over $L^2(\Omega)$ on the convex set K which is the closure of the set

$$\{\nabla \cdot \xi : \xi \in C_c^1(\Omega; \mathbb{R}^2), |\xi(x)|_\infty \leq 1 \forall x \in \mathbb{R}^2\}.$$

To compute numerically the projection $\mathbb{P}_{\alpha K}(f)$ Chambolle uses a fixed point algorithm. More precisely, in two dimensions the following semi-implicit gradient descent algorithm is given to approximate $\mathbb{P}_{\alpha K}(f)$:

Choose $\tau > 0$, let $p^{(0)} = 0$ and, for any $n \geq 0$, iterate

$$p_{i,j}^{(n+1)} = p_{i,j}^{(n)} + \tau \left((\nabla(\nabla \cdot p^{(n)} - f/\alpha))_{i,j} - \left| (\nabla(\nabla \cdot p^{(n)} - f/\alpha))_{i,j} \right| p_{i,j}^{(n+1)} \right),$$

so that

$$p_{i,j}^{(n+1)} = \frac{p_{i,j}^{(n)} + \tau(\nabla(\nabla \cdot p^{(n)} - f/\alpha))_{i,j}}{1 + \tau \left| (\nabla(\nabla \cdot p^{(n)} - f/\alpha))_{i,j} \right|}. \quad (4.39)$$

For $\tau \leq 1/8$ the iteration $\alpha \nabla \cdot p^{(n)}$ converges to $\mathbb{P}_{\alpha K}(f)$ as $n \rightarrow \infty$ (compare [Ch04, Theorem 3.1]). All this will be explained in more detail in the context of TV-H⁻¹minimization in the following subsection.

A Generalization of Chambolle's Algorithm for TV-H⁻¹Minimization

The main contribution of this section is to generalize Chambolle's algorithm to the case of an H^{-1} constrained minimization of the total variation and to the case where T is an arbitrary linear and bounded operator. In short we shall see how to solve (4.33) using a similar strategy as in [Ch04]. We start with solving the simplified problem when $T = Id$ and as a second step present a method how to use this solution in order

4.2 A Dual Solver for $\mathbf{TV} \cdot \mathbf{H}^{-1}$ Minimization

to solve the general case (4.33). Hence for the time being we consider the minimization problem

$$\min_u \{\mathcal{J}(u) = \|u - f\|_{-1}^2 + 2\alpha |Du|(\Omega)\}. \quad (4.40)$$

We proceed by exploiting the optimality condition of (4.40), i.e.,

$$0 \in \partial |Du|(\Omega) + \Delta^{-1}(u - f) \frac{1}{\alpha}.$$

This can be rewritten as

$$\frac{\Delta^{-1}(f - u)}{\alpha} \in \partial |Du|(\Omega). \quad (4.41)$$

Since

$$s \in \partial f(x) \iff x \in \partial f^*(s),$$

where f^* is the convex conjugate (or Fenchel transform) of f , it follows that

$$u \in \partial |D \cdot|(\Omega)^* \left(\frac{\Delta^{-1}(f - u)}{\alpha} \right).$$

Here

$$|D \cdot|(\Omega)^*(v) = \chi_K(v) = \begin{cases} 0 & \text{if } v \in K \\ +\infty & \text{otherwise,} \end{cases} \quad (4.42)$$

where, as before, K is the closure of the set

$$\{\nabla \cdot \xi : \xi \in C_c^1(\Omega; \mathbb{R}^2), |\xi(x)|_\infty \leq 1 \forall x \in \mathbb{R}^2\}.$$

Rewriting the above inclusion again we have

$$\frac{f}{\alpha} \in \frac{f - u}{\alpha} + \frac{1}{\alpha} \partial |D \cdot|(\Omega)^* \left(\frac{\Delta^{-1}(f - u)}{\alpha} \right),$$

i.e., with $w = \Delta^{-1}(f - u)/\alpha$ it reads

$$\begin{cases} 0 \in (-\Delta w - f/\alpha) + \frac{1}{\alpha} \partial |D \cdot|(\Omega)^*(w) & \text{in } \Omega \\ w = 0 & \text{on } \partial\Omega. \end{cases}$$

In other words, w is a minimizer of

$$\frac{\|w - \Delta^{-1}f/\alpha\|_{H_0^1(\Omega)}^2}{2} + \frac{1}{\alpha} |D \cdot|(\Omega)^*(w),$$

where $H_0^1(\Omega) = \{v \in H^1(\Omega) : v = 0 \text{ on } \partial\Omega\}$ and $\|v\|_{H_0^1(\Omega)} = \|\nabla v\|$. Because of (4.42), for w to be a minimizer of the above functional it is necessary that $|D\cdot|(\Omega)^*(w) = 0$, i.e., $w \in K$. Hence a minimizer w fulfills

$$w = \mathbb{P}_K^1(\Delta^{-1}f/\alpha),$$

where \mathbb{P}_K^1 is the orthogonal projection on K over $H_0^1(\Omega)$, i.e.,

$$\mathbb{P}_K^1(u) = \operatorname{argmin}_{v \in K} \|u - v\|_{H_0^1(\Omega)}.$$

Hence the solution u of problem (4.40) is given by

$$u = f + \Delta(\mathbb{P}_{\alpha K}^1(\Delta^{-1}f)),$$

where $-\Delta$ denotes the Laplacian with zero Dirichlet boundary conditions as before.

Computing the nonlinear projection $\mathbb{P}_{\alpha K}^1(\Delta^{-1}f)$ in the discrete setting amounts to solving the following problem:

$$\min \left\{ \left\| (\nabla(\alpha \nabla \cdot p - \Delta^{-1}f))_{i,j} \right\|^2 : p \in Y, |p_{i,j}| \leq 1 \forall i = 1, \dots, N; j = 1, \dots, M \right\}. \quad (4.43)$$

Analogously to [Ch04] we use the Karush-Kuhn-Tucker conditions for the above constrained minimization. Then there exist $\beta_{i,j} \geq 0$ such that the corresponding Euler-Lagrange equation reads

$$[\nabla(\Delta(\alpha \nabla \cdot p - \Delta^{-1}f))]_{i,j} + \beta_{i,j} p_{i,j} = 0, \quad \forall i = 1, \dots, N; j = 1, \dots, M.$$

Since $\beta_{i,j}(|p_{i,j}|^2 - 1) = 0$, either $\beta_{i,j} > 0$ and $|p_{i,j}| = 1$ or $|p_{i,j}| < 1$ and $\beta_{i,j} = 0$. Now, following the arguments in [Ch04], in both cases this yields

$$\beta_{i,j} = \left| (\nabla \Delta(\nabla \cdot p^n - \Delta^{-1}f/\alpha))_{i,j} \right|, \quad \forall i = 1, \dots, N; j = 1, \dots, M.$$

Then the gradient descent algorithm for solving (4.43) reads: for an initial $p^0 = 0$, iterate for $n \geq 0$

$$p_{i,j}^{n+1} = \frac{p_{i,j}^n - \tau (\nabla \Delta(\nabla \cdot p^n - \Delta^{-1}f/\alpha))_{i,j}}{1 + \tau |(\nabla \Delta(\nabla \cdot p^n - \Delta^{-1}f/\alpha))_{i,j}|}. \quad (4.44)$$

Redoing the convergence proof in [Ch04] we end up with a similar result:

Theorem 4.2.3. *Let $\tau \leq 1/64$. Then, $\alpha \nabla \cdot p^n$ converges to $\mathbb{P}_{\alpha K}^1(\Delta^{-1}f)$ as $n \rightarrow \infty$.*

Proof. The proof proceeds similarly to the proof in [Ch04]. For the sake of completeness and clarity we still present the detailed proof here, keeping close to the notation in [Ch04]. By induction we easily see that for every $n \geq 0$, $|p_{i,j}^n| \leq 1$ for all i, j . Indeed, starting with p^n , with $|p_{i,j}^n| \leq 1$ for all $i = 1, \dots, N; j = 1, \dots, M$, we have

$$|p_{i,j}^{n+1}| \leq \frac{|p_{i,j}^n| + \tau |(\nabla(-\Delta)(\nabla \cdot p^n - \Delta^{-1}f/\alpha))_{i,j}|}{1 + \tau |(\nabla(-\Delta)(\nabla \cdot p^n - \Delta^{-1}f/\alpha))_{i,j}|} \leq 1.$$

Now, let us fix an $n \geq 0$ and consider $\|\nabla(\nabla \cdot p^{n+1} - \Delta^{-1}(f/\alpha))\|_Y$. We want to show that this norm is decreasing with n . In what follows we will abbreviate $\|\cdot\|_Y$ by $\|\cdot\|$. We have

$$\begin{aligned} \|\nabla(\nabla \cdot p^{n+1} - \Delta^{-1}(f/\alpha))\|^2 &= \|\nabla \nabla \cdot (p^{n+1} - p^n) + \nabla(\nabla \cdot p^n - \Delta^{-1}(f/\alpha))\|^2 \\ &= \|\nabla(\nabla \cdot p^n - \Delta^{-1}(f/\alpha))\|^2 \\ &\quad + 2 \langle \nabla \nabla \cdot (p^{n+1} - p^n), \nabla(\nabla \cdot p^n - \Delta^{-1}(f/\alpha)) \rangle_2 \\ &\quad + \|\nabla \nabla \cdot (p^{n+1} - p^n)\|^2. \end{aligned}$$

Inserting $\eta = (p^{n+1} - p^n)/\tau$ in the above equation and integrating by parts in the second term we get

$$\begin{aligned} \|\nabla(\nabla \cdot p^{n+1} - \Delta^{-1}(f/\alpha))\|^2 &= \|\nabla(\nabla \cdot p^n - \Delta^{-1}(f/\alpha))\|^2 \\ &\quad + 2\tau \langle \eta, \nabla \Delta(\nabla \cdot p^n - \Delta^{-1}(f/\alpha)) \rangle_2 + \tau^2 \|\nabla \nabla \cdot \eta\|^2. \end{aligned}$$

By further estimating $\|\nabla \nabla \cdot \eta\| \leq \kappa \|\eta\|$, where $\kappa = \|\nabla \nabla \cdot\| = \sup_{\|p\| \leq 1} \|\nabla \nabla \cdot p\|$ the norm of the operator $\nabla \nabla \cdot : Y \rightarrow Y$, we deduce

$$\begin{aligned} \|\nabla(\nabla \cdot p^{n+1} - \Delta^{-1}(f/\alpha))\|^2 &\leq \|\nabla(\nabla \cdot p^n - \Delta^{-1}(f/\alpha))\|^2 \\ &\quad + \tau \left[2 \langle \eta, \nabla \Delta(\nabla \cdot p^n - \Delta^{-1}(f/\alpha)) \rangle_2 + \kappa^2 \tau \|\eta\|^2 \right]. \end{aligned}$$

The operator norm κ will be bounded by the end of the proof. For now we are going to show that the term multiplied by τ is always negative as long as $p^{n+1} \neq p^n$ and $\tau \leq 1/\kappa^2$, and hence that $\|\nabla(\nabla \cdot p^n - \Delta^{-1}(f/\alpha))\|^2$ is decreasing. To do so we consider

$$\begin{aligned} 2 \langle \eta, \nabla \Delta(\nabla \cdot p^n - \Delta^{-1}(f/\alpha)) \rangle_2 + \kappa^2 \tau \|\eta\|^2 \\ = \sum_{\substack{1 \leq i \leq N \\ 1 \leq j \leq M}} 2\eta_{i,j} [\nabla \Delta(\nabla \cdot p^n - \Delta^{-1}(f/\alpha))]_{i,j} + \kappa^2 \tau |\eta_{i,j}|^2. \quad (4.45) \end{aligned}$$

Now, from the fixed point equation we have

$$\eta_{i,j} = - \left[(\nabla \Delta(\nabla \cdot p^n - \Delta^{-1}(f/\alpha)))_{i,j} + \left| (\nabla \Delta(\nabla \cdot p^n - \Delta^{-1}(f/\alpha)))_{i,j} \right| \cdot p_{i,j}^{n+1} \right].$$

Setting $\rho_{i,j} = \left|(\nabla\Delta(\nabla \cdot p^n - \Delta^{-1}(f/\alpha)))_{i,j}\right| \cdot p_{i,j}^{n+1}$ and inserting the above expression for $\eta_{i,j}$ into (4.45) we have for every i, j

$$\begin{aligned} 2\eta_{i,j} (\nabla\Delta(\nabla \cdot p^n - \Delta^{-1}(f/\alpha)))_{i,j} + \kappa^2\tau |\eta_{i,j}|^2 \\ = (\kappa^2\tau - 1) |\eta_{i,j}|^2 - \left|(\nabla\Delta(\nabla \cdot p^n - \Delta^{-1}(f/\alpha)))_{i,j}\right|^2 + |\rho_{i,j}|^2. \end{aligned}$$

Since $|p_{i,j}^{n+1}| \leq 1$ it follows that $|\rho_{i,j}| \leq \left|(\nabla\Delta(\nabla \cdot p^n - \Delta^{-1}(f/\alpha)))_{i,j}\right|$, and hence

$$2\eta_{i,j} (\nabla\Delta(\nabla \cdot p^n - \Delta^{-1}(f/\alpha)))_{i,j} + \kappa^2\tau |\eta_{i,j}|^2 \leq (\kappa^2\tau - 1) |\eta_{i,j}|^2.$$

The last term is negative or zero if and only if $\kappa^2\tau - 1 \leq 0$. Hence, if

$$\tau \leq 1/\kappa^2,$$

we see that $\|\nabla(\nabla \cdot p^n - \Delta^{-1}(f/\alpha))\|$ is nonincreasing with n . For $\tau < 1/\kappa^2$ it is immediately clear that the norm is even decreasing, unless $\eta = 0$, that is, $p^{n+1} = p^n$. The same holds for $\kappa^2\tau = 1$. Indeed, in this case, if $\|\nabla(\nabla \cdot p^{n+1} - \Delta^{-1}(f/\alpha))\|^2 = \|\nabla(\nabla \cdot p^n - \Delta^{-1}(f/\alpha))\|^2$ it follows that

$$\begin{aligned} 0 &= 2 \langle \eta, \nabla\Delta(\nabla \cdot p^n - \Delta^{-1}(f/\alpha)) \rangle_2 + \tau \|\nabla\nabla \cdot \eta\|^2 \\ &\leq 2 \langle \eta, \nabla\Delta(\nabla \cdot p^n - \Delta^{-1}(f/\alpha)) \rangle_2 + \kappa^2\tau \|\eta\|^2 \\ &= \sum_{\substack{1 \leq i \leq N \\ 1 \leq j \leq M}} - \left|(\nabla\Delta(\nabla \cdot p^n - \Delta^{-1}(f/\alpha)))_{i,j}\right|^2 + |\rho_{i,j}|^2, \end{aligned}$$

and therefore $\left|(\nabla\Delta(\nabla \cdot p^n - \Delta^{-1}(f/\alpha)))_{i,j}\right| \leq |\rho_{i,j}|$. Since in turn

$$|\rho_{i,j}| \leq \left|(\nabla\Delta(\nabla \cdot p^n - \Delta^{-1}(f/\alpha)))_{i,j}\right|$$

we deduce $|\rho_{i,j}| = \left|(\nabla\Delta(\nabla \cdot p^n - \Delta^{-1}(f/\alpha)))_{i,j}\right|$ for each i, j . But this can only be if either $\left|(\nabla\Delta(\nabla \cdot p^n - \Delta^{-1}(f/\alpha)))_{i,j}\right| = 0$ or $|p_{i,j}^{n+1}| = 1$. In both cases, the fixed point iteration (4.44) yields $p_{i,j}^{n+1} = p_{i,j}^n$ for all i, j .

Now, since $\|\nabla(\nabla \cdot p^n - \Delta^{-1}(f/\alpha))\|$ is decreasing with n , the norm is uniformly bounded and hence there exists an $m \geq 0$ such that

$$m = \lim_{n \rightarrow \infty} \|\nabla(\nabla \cdot p^n - \Delta^{-1}(f/\alpha))\|.$$

Moreover the sequence p^n has converging subsequences. Let \bar{p} be the limit of a subsequence (p^{n_k}) and \bar{p}' be the limit of (p^{n_k+1}) . Inserting p^{n_k+1} and p^{n_k} into the fixed

point equation (4.44) and passing to the limit we have

$$\bar{p}'_{i,j} = \frac{\bar{p}_{i,j} - \tau (\nabla \Delta (\nabla \cdot \bar{p} - \Delta^{-1} f / \alpha))_{i,j}}{1 + \tau |(\nabla \Delta (\nabla \cdot \bar{p} - \Delta^{-1} f / \alpha))_{i,j}|}.$$

Repeating the previous calculations we see that since

$$m = \|\nabla (\nabla \cdot \bar{p} - \Delta^{-1} (f / \alpha))\| = \|\nabla (\nabla \cdot \bar{p}' - \Delta^{-1} (f / \alpha))\|,$$

it is true that $\bar{\eta}_{i,j} = (\bar{p}'_{i,j} - \bar{p}_{i,j})/\tau = 0$ for every i, j , that is, $\bar{p} = \bar{p}'$. Hence \bar{p} is a fixed point of (4.44), i.e.,

$$(\nabla \Delta (\nabla \cdot \bar{p} - \Delta^{-1} f / \alpha))_{i,j} + |(\nabla \Delta (\nabla \cdot \bar{p} - \Delta^{-1} f / \alpha))_{i,j}| \bar{p}_{i,j} = 0, \quad \forall \begin{cases} i = 1, \dots, N \\ j = 1, \dots, M \end{cases}$$

which is the Euler equation for a solution of (4.43). One can deduce that \bar{p} solves (4.43) and that $\alpha \nabla \cdot \bar{p}$ is the projection $\mathbb{P}_K^1(\Delta^{-1} f)$. Since this projection is unique, we deduce that all the sequence $\alpha \nabla \cdot p^n$ converges to $\mathbb{P}_K^1(\Delta^{-1} f)$. The theorem is proved if we can show that $\kappa^2 \leq 64$. By definition

$$\kappa = \|\nabla \nabla \cdot p\| = \sup_{\|p\| \leq 1} \|\nabla \nabla \cdot p\|.$$

Then for every i, j , we have

$$\|\nabla \nabla \cdot p\|^2 = \sum_{\substack{1 \leq i \leq N \\ 1 \leq j \leq M}} |(\nabla \nabla \cdot p)_{i,j}|^2.$$

For more clarity let us set $u := \nabla \cdot p \in X$ for now. With the convention that $p_{0,j} = p_{N,j} = p_{i,0} = p_{i,M} = 0$ we get

$$\begin{aligned} \|\nabla \nabla \cdot p\|^2 &= \sum_{\substack{1 \leq i \leq N \\ 1 \leq j \leq M}} |(\nabla u)_{i,j}|^2 = \sum_{\substack{1 \leq i \leq N \\ 1 \leq j \leq M}} |(\nabla_x u)_{i,j}|^2 + |(\nabla_y u)_{i,j}|^2 \\ &= \sum_{\substack{1 \leq i < N \\ 1 \leq j \leq M}} (u_{i+1,j} - u_{i,j})^2 + \sum_{\substack{1 \leq i \leq N \\ 1 \leq j < M}} (u_{i,j+1} - u_{i,j})^2 \\ &= \sum_{\substack{1 \leq i < N \\ 1 \leq j \leq M}} ((\nabla \cdot p)_{i+1,j} - (\nabla \cdot p)_{i,j})^2 + \sum_{\substack{1 \leq i \leq N \\ 1 \leq j < M}} ((\nabla \cdot p)_{i,j+1} - (\nabla \cdot p)_{i,j})^2 \\ &= \sum_{\substack{1 \leq i < N \\ 1 \leq j \leq M}} \left[(p_{i+1,j}^x - p_{i,j}^x + p_{i+1,j}^y - p_{i+1,j-1}^y) - (p_{i,j}^x - p_{i-1,j}^x + p_{i,j}^y - p_{i,j-1}^y) \right]^2 \\ &\quad + \sum_{\substack{1 \leq i \leq N \\ 1 \leq j < M}} \left[(p_{i,j+1}^x - p_{i-1,j+1}^x + p_{i,j+1}^y - p_{i,j}^y) - (p_{i,j}^x - p_{i-1,j}^x + p_{i,j}^y - p_{i,j-1}^y) \right]^2, \end{aligned}$$

and further

$$\begin{aligned}
 \|\nabla \nabla \cdot p\|^2 &\leq 8 \cdot \sum_{\substack{1 \leq i \leq N \\ 1 \leq j \leq M}} |p_{i+1,j}^x|^2 + |p_{i,j}^x|^2 + |p_{i+1,j}^y|^2 + |p_{i+1,j-1}^y|^2 \\
 &\quad + |p_{i,j}^x|^2 + |p_{i-1,j}^x|^2 + |p_{i,j}^y|^2 + |p_{i,j-1}^y|^2 \\
 &\quad + 8 \cdot \sum_{\substack{1 \leq i \leq N \\ 1 \leq j < M}} |p_{i,j+1}^x|^2 + |p_{i-1,j+1}^x|^2 + |p_{i,j+1}^y|^2 + |p_{i,j}^y|^2 \\
 &\quad + |p_{i,j}^x|^2 + |p_{i-1,j}^x|^2 + |p_{i,j}^y|^2 + |p_{i,j-1}^y|^2 \\
 &\leq 64 \cdot \|p\|^2 \leq 64. \tag*{\square}
 \end{aligned}$$

Remark 4.2.4. In our numerical computations we stop the fixed point iteration (4.44) as soon as the distance between the iterates is small enough, i.e.,

$$\|p^{n+1} - p^n\| \leq e \cdot \|p^{n+1}\|, \tag{4.46}$$

where e is a chosen error bound.

Then, in summary, to minimize (4.40) we apply the following algorithm

Algorithm (P)

- For an initial $p^0 = 0$, iterate (4.44) until (4.46);
- Set $\mathbb{P}_{\alpha K}^1(\Delta^{-1}f) = \alpha \nabla \cdot p^{\hat{n}}$, where \hat{n} is the first iterate of (4.44) which fulfills (4.46);
- Compute a minimizer u of (4.40) by

$$u = f + \Delta(\mathbb{P}_{\alpha K}^1(\Delta^{-1}f)) = f + \Delta(\alpha \nabla \cdot p^{\hat{n}}).$$

The second step is to use the presented algorithm for (4.40) in order to solve (4.33), i.e.,

$$\min_u \{\mathcal{J}(u) = \|Tu - f\|_{-1}^2 + 2\alpha |Du|(\Omega)\},$$

for an arbitrary bounded linear operator T . To do so we first approximate a minimizer of (4.33) iteratively by a sequence of minimizers of “surrogate” functionals \mathcal{J}^s . This approach is inspired by similar methods used, e.g., in [BBAC04, DTV07].

Let $\tau > 0$ be a fixed stepsize. Starting with an initial condition $u^0 = f$, we solve for $k \geq 0$

$$u^{k+1} = \operatorname{argmin}_u \mathcal{J}^s(u, u^k), \tag{4.47}$$

where

$$\mathcal{J}^s(u, u^k) = \frac{1}{2\tau} \|u - u^k\|_{-1}^2 + \frac{1}{2\alpha} \left\| u - \left(f + (Id - T)u^k \right) \right\|_{-1}^2 + |Du|(\Omega).$$

Note that a fixed point of \mathcal{J}^s is a potential minimizer for \mathcal{J} . In the case of TV-H⁻¹inpainting (4.47) was actually used as a fixed point approach in the proof of a stationary solution of (2.27), cf. Section 2.2. A rigorous proof of convergence properties is still missing and is a matter for future investigation. Note however that in the case of image inpainting, i.e., $T = \mathbf{1}_{\Omega \setminus D}$ and f is replaced by $\mathbf{1}_{\Omega \setminus D}f$, the optimality condition of (4.47) indeed describes a fourth-order diffusion inside of the inpainting domain D . Hence, in this case, minimizing (4.47) rather describes the behavior of solutions of the inpainting approach (2.27) than directly minimizing (4.33), cf. also Subsection 4.2.1. Despite the missing theory, the numerical results obtained by using this scheme for inpainting issues indicate its correct asymptotic behavior, see Section 4.2.3.

Now, the corresponding optimality condition to (4.47) reads

$$0 \in \partial |Du|(\Omega) + \frac{1}{\tau} \Delta^{-1}(u - u^k) + \frac{1}{\alpha} \Delta^{-1} \left(u - \left(f + (Id - T)u^k \right) \right),$$

which can be rewritten as

$$\Delta^{-1} \left(\frac{f_1 - u}{\tau} + \frac{f_2 - u}{\alpha} \right) \in \partial |Du|(\Omega),$$

where $f_1 = u^k$, $f_2 = f + (Id - T)u^k$. Setting

$$\begin{aligned} f &= \frac{f_1\alpha + f_2\tau}{\alpha + \tau} \\ \mu &= \frac{\alpha\tau}{\alpha + \tau}, \end{aligned}$$

we end up with the same inclusion as (4.41), i.e.,

$$\frac{\Delta^{-1}(f - u)}{\mu} \in \partial |Du|(\Omega),$$

and **Algorithm (P)** for solving (4.40) can be directly applied.

Algorithm TV-H⁻¹:

- In the case $T = Id$ directly apply **Algorithm (P)** to compute a minimizer of (4.33).
- In the case $T \neq Id$ iterate (4.47) by solving **Algorithm (P)** in every iteration step until the two subsequent iterates u^k and u^{k+1} are sufficiently close.

4.2.3 Applications

In this section we present applications of our new algorithm for solving (4.33) for image denoising, decomposition and inpainting, and present numerical results. For comparison, we also present results for the TV-L²model in [ROF92] on the same images.

Now, in order to compute the minimizer u of (4.33), we have the following algorithm.

Note that in our numerical examples e in (4.46) is chosen to be 10^{-4} .

Image Denoising and Decomposition

In the case of image denoising and image decomposition the operator $T = Id$ and thus **Algorithm (P)** can be directly applied. For image denoising the signal to noise ratio (SNR) is computed as

$$SNR = 20 \log \left(\frac{\langle f \rangle_2}{\sigma} \right),$$

with $\langle f \rangle_2$ the average value of the pixels $f_{i,j}$ and σ the standard deviation of the noise. For our numerical results the parameter α in (4.33) was chosen so that the best residual-mean-squared-error (RMSE) is obtained. We define the RMSE as

$$RMSE = \frac{1}{NM} \sqrt{ \sum_{\substack{1 \leq i \leq N \\ 1 \leq j \leq M}} (u_{i,j} - \hat{u}_{i,j})^2 },$$

where \hat{u} is the original image without noise, cf. [LV08]. Numerical examples for image denoising with TV-H⁻¹minimization and their comparison with the results obtained by the TV-L²approach are presented in Figures 4.4-4.7. In both examples the superiority of the TV-H⁻¹minimization approach with respect to the separation of noise and edges is clearly visible.

We also apply (4.33) for texture removal in images, i.e., image decomposition, and compare the numerical results with those of the TV-L²approach, cf. Figure 4.8.

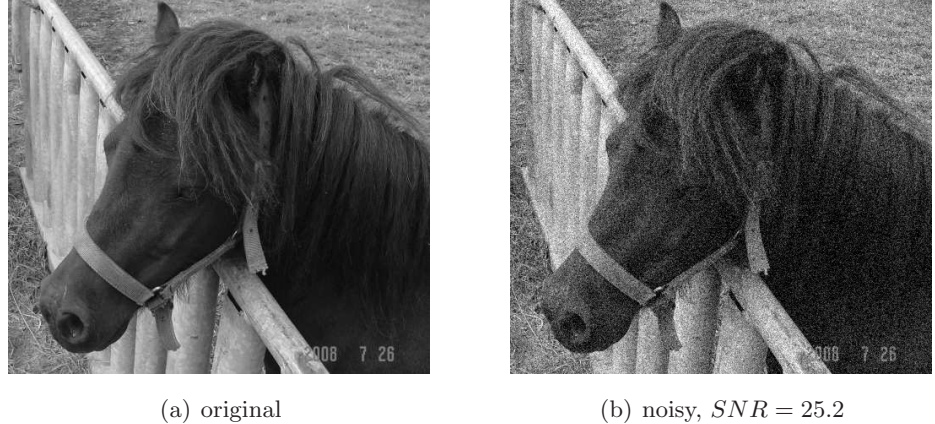


Figure 4.4: Image of a horse and its noisy version with additive white noise

The cartoon-texture decomposition in this example works better in the case of TV-H⁻¹minimization, since this approach differentiates between small oscillations and strong edges, better than the TV-L²approach.

Image Inpainting

In order to apply our algorithm to TV-H⁻¹inpainting we follow the method of surrogate functionals from Section 4.2.2. In fact it turns out that a fixed point of the corresponding optimality condition of (4.47) with $T = \mathbf{1}_{\Omega \setminus D}$ and f replaced by $\mathbf{1}_{\Omega \setminus D}f$ is indeed a stationary solution of (2.27). This approach is also motivated by the fixed point approach used in [BHS08] in order to prove existence of a stationary solution of (2.27). Hence a stationary solution to (2.27) can be computed iteratively by the following algorithm: Take $u^0 = f$, with any trivial (zero) expansion to the inpainting domain, and solve for $k \geq 0$

$$\min_{u \in BV(\Omega)} \left\{ |Du|(\Omega) + \frac{1}{2\tau} \|u - u^k\|_{-1}^2 + \frac{1}{2\alpha} \|u - \mathbf{1}_{\Omega \setminus D}f - (1 - \mathbf{1}_{\Omega \setminus D})u^k\|_{-1}^2 \right\} \rightarrow u^{k+1}, \quad (4.48)$$

for positive iterationsteps $\tau > 0$, and $\alpha = 1/\lambda_0$. Now, as before, let $f_1 = u^k$, $f_2 = \mathbf{1}_{\Omega \setminus D}f + (1 - \mathbf{1}_{\Omega \setminus D})u^k$ and

$$f = \frac{f_1\alpha + f_2\tau}{\alpha + \tau}$$

$$\mu = \frac{\alpha\tau}{\alpha + \tau},$$

4.2 A Dual Solver for $\text{TV}-\mathbf{H}^{-1}$ Minimization

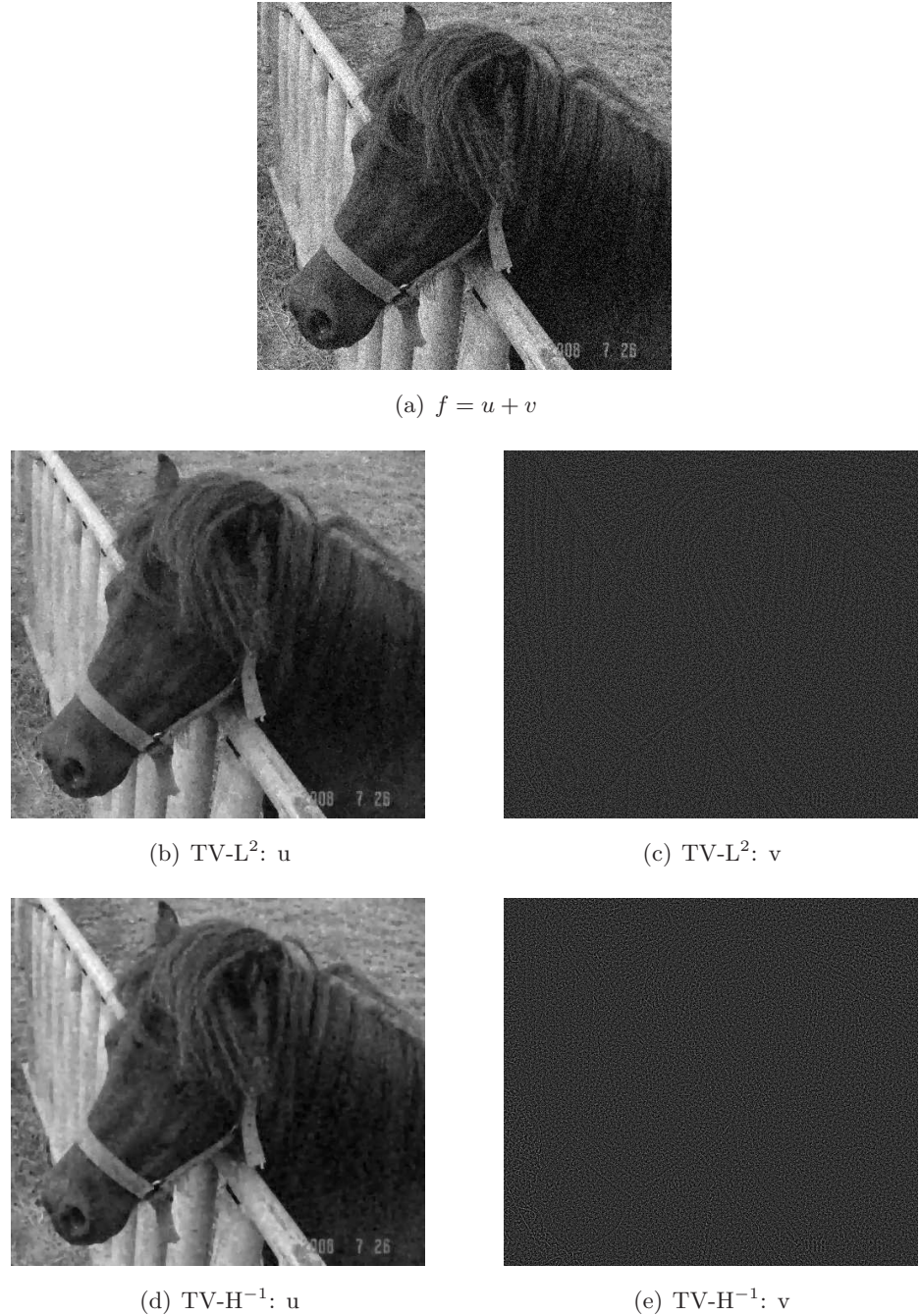


Figure 4.5: Denoising results for the image of a horse in Figure 4.4. Results from the $\text{TV}-\mathbf{L}^2$ denoising model compared with $\text{TV}-\mathbf{H}^{-1}$ denoising with $\alpha = 0.05$ for both.

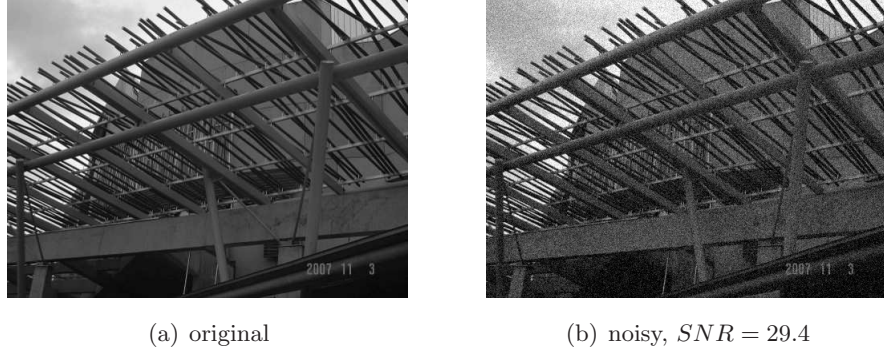


Figure 4.6: Image of the roof of a house in Scotland and its noisy version with additive white noise

then we end up with the same inclusion as (4.41), i.e.,

$$\frac{\Delta^{-1}(f - u)}{\mu} \in \partial |Du|(\Omega),$$

and **Algorithm (P)** can be directly applied. Compare Figure 4.9 for a numerical example.

In the following section we shall see how the dual algorithm of the present section can be used in order to formulate a domain decomposition approach for TV-H⁻¹ inpainting.

4.3 Domain Decomposition for TV Minimization

Domain decomposition methods are a special instance of subspace splitting methods and were introduced as techniques for solving partial differential equations based on a decomposition of the spatial domain of the problem into several subdomains [Li88, BPWX91, Xu92, CM94, QV99, XZ02, LXZ03, BDHP03, NS05]. The initial equation restricted to the subdomains defines a sequence of new local problems. The main goal is to solve the initial equation via the solution of the local problems. This procedure induces a dimension reduction which is the major aspect responsible for the success of such a method. Indeed, one of the principal motivations is the formulation of solvers which can be easily parallelized.

The current section is mainly based on a joint work with Massimo Fornasier developed in [FS07]. Therein we are concerned with the numerical minimization by means of

4.3 Domain Decomposition for TV Minimization

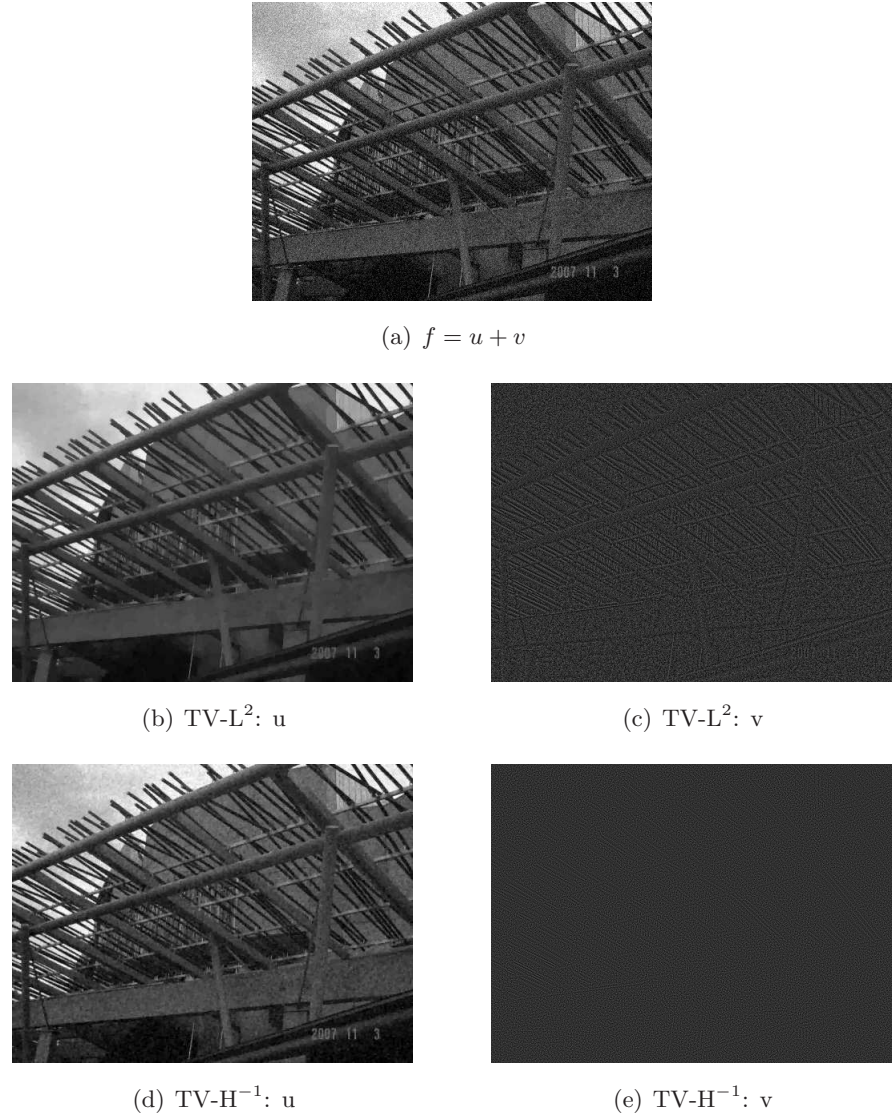
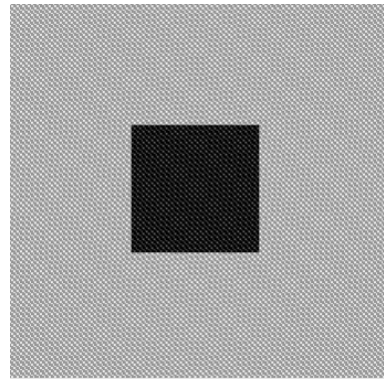


Figure 4.7: Denoising results for the image of the roof in Figure 4.6. Results from the TV-L^2 denoising model with $\alpha = 0.05$ compared with TV-H^{-1} denoising with $\alpha = 0.01$

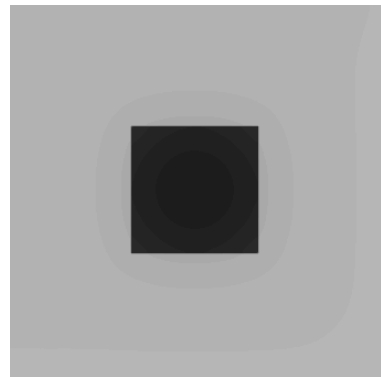
subspace splittings of energy functionals in Hilbert spaces involving convex constraints coinciding with a semi-norm for a subspace. In more detail: Let \mathcal{H} be a real separable Hilbert space. We are interested in the numerical minimization in \mathcal{H} of the general form of functionals

$$\mathcal{J}(u) := \|Tu - f\|_{\mathcal{H}}^2 + 2\alpha\psi(u), \quad (4.49)$$

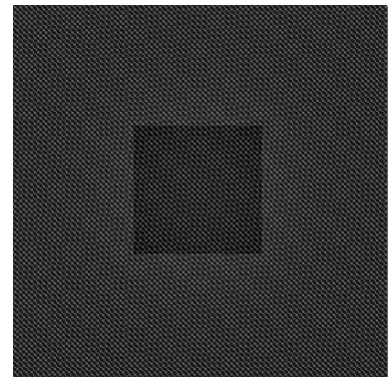
4.3 Domain Decomposition for TV Minimization



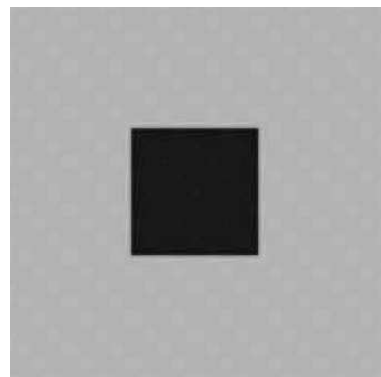
(a) $f = u + v$



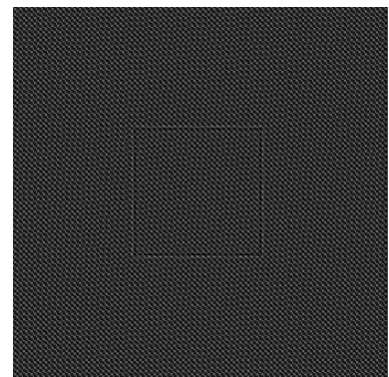
(b) $\text{TV-L}^2: u$



(c) $\text{TV-L}^2: v$



(d) $\text{TV-H}^{-1}: u$



(e) $\text{TV-H}^{-1}: v$

Figure 4.8: Decomposition into cartoon and texture of a synthetic image. Results from the TV-L^2 model with $\alpha = 1$ and TV-H^{-1} minimization with $\alpha = 0.1$.

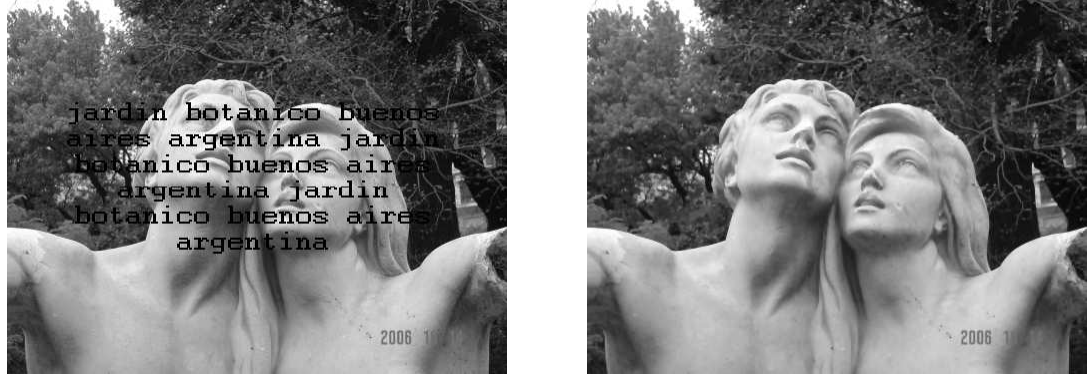


Figure 4.9: $\text{TV}-\mathbf{H}^{-1}$ inpainting result for the image of the two statues with $\alpha = 1/\lambda_0 = 0.005$.

where $T \in \mathcal{L}(\mathcal{H})$ is a bounded linear operator, $f \in \mathcal{H}$ is a datum, and $\alpha > 0$ is a fixed constant. The function $\psi : \mathcal{H} \rightarrow \mathbb{R}_+ \cup \{+\infty\}$ is a semi-norm for a suitable subspace \mathcal{H}^ψ of \mathcal{H} .

The optimization is realized by alternating minimizations of the functional on a sequence of orthogonal subspaces. In particular, we investigate splittings into arbitrary orthogonal subspaces $\mathcal{H} = V_1 \oplus V_2$ for which we may have

$$\psi(\pi_{V_1}(u) + \pi_{V_2}(v)) \neq \psi(\pi_{V_1}(u)) + \psi(\pi_{V_2}(v)), \quad u, v \in \mathcal{H}, \quad (4.50)$$

where π_{V_i} is the orthogonal projection onto V_i . With this splitting we want to minimize \mathcal{J} by suitable instances of the following alternating algorithm: Pick an initial $V_1 \oplus V_2 \ni u_1^{(0)} + u_2^{(0)} := u^{(0)} \in \mathcal{H}^\Psi$, for example $u^{(0)} = 0$, and iterate

$$\begin{cases} u_1^{(n+1)} \approx \operatorname{argmin}_{v_1 \in V_1} \mathcal{J}(v_1 + u_2^{(n)}) \\ u_2^{(n+1)} \approx \operatorname{argmin}_{v_2 \in V_2} \mathcal{J}(u_1^{(n+1)} + v_2) \\ u^{(n+1)} := u_1^{(n+1)} + u_2^{(n+1)}. \end{cases} \quad (4.51)$$

Different to situations already encountered in the literature we shall propose a domain decomposition algorithm for the minimization of functionals for which we neither can guarantee smoothness nor additivity with respect to its local problems. In [TT98, TX02], for instance, the authors consider the minimization of a convex function F which is assumed to be Gateaux differentiable in a real reflexive Banach space and prove convergence for an asynchronous space decomposition method applied to this

general problem. In contrast to this work our functional \mathcal{J} consists of a non-smooth part which is not Gateaux-differentiable and hence the analysis carried out in [TT98, TX02] is not directly applicable to our problem. Further domain decomposition methods have been proposed for the case when ψ is not a smooth function, but it is additive, i.e.,

$$\psi(\pi_{V_1}(u) + \pi_{V_2}(v)) = \psi(\pi_{V_1}(u)) + \psi(\pi_{V_2}(v)), \quad u, v \in \mathcal{H},$$

see [Ca97] for instance. The additivity of ψ is crucial for the proof of convergence of the algorithm and cannot be directly generalized for functions ψ without this property. To our knowledge no results and methods are presented in the literature related to the situation described by our fundamental assumptions, where ψ is not smooth (in particular is not differentiable) and is not additive (only subadditive), cf. (4.50).

In [FS07] we present a subspace minimization algorithm (4.51) for the general problem in (4.49) with (4.50). On each subspace an iterative proximity-map algorithm is implemented via *oblique thresholding* (cf. Section 4.3.3), which is the main new tool introduced in [FS07]. We provide convergence conditions for the algorithm in order to compute minimizers of the target energy. Analogous results are derived for a parallel variant of the algorithm.

In particular we apply the theory and the algorithms developed in [FS07] to adapt domain decompositions to the minimization of functionals with total variation constraints. Therefore interesting solutions may be discontinuous, e.g., along curves in 2D. These discontinuities may cross the interfaces of the domain decomposition patches. Hence, the crucial difficulty is the correct treatment of interfaces, with the preservation of crossing discontinuities and the correct matching where the solution is continuous instead. We consider the minimization of the functional \mathcal{J} in the following setting: Let $\Omega \subset \mathbb{R}^d$, for $d = 1, 2$, be a bounded open set with Lipschitz boundary. We are interested in the case when $\mathcal{H} = L^2(\Omega)$, $\mathcal{H}^\psi = BV(\Omega)$ and $\psi(u) = |Du|(\Omega)$, the variation of u . Then a domain decomposition $\Omega_1 \cup \Omega_2 \subset \Omega \subset \bar{\Omega}_1 \cup \bar{\Omega}_2$ induces the space splitting into $V_i := \{u \in L^2(\Omega) : \text{supp}(u) \subset \Omega_i\}$, $i = 1, 2$. This means we shall solve (2.26), i.e., we will minimize the functional

$$\mathcal{J}(u) := \|Tu - f\|_{L^2(\Omega)}^2 + 2\alpha|Du|(\Omega)$$

4.3 Domain Decomposition for TV Minimization

by means of the alternating subspace minimizations (4.51). Moreover, we shall see that also the TV-H⁻¹minimization problem (4.33) from Section 4.2, i.e.,

$$\mathcal{J}(u) := \|Tu - f\|_{H^{-1}(\Omega)}^2 + 2\alpha|Du|(\Omega),$$

can be treated within this framework, cf. Section 4.3.7. In contrast to [Ca97], in the case of total variation minimization (2.26) and (4.33) in general we have

$$|D(u_{\Omega_1} + u_{\Omega_2})|(\Omega) \neq |Du_{\Omega_1}|(\Omega_1) + |Du_{\Omega_2}|(\Omega_2),$$

compare (4.55) for a more detailed presentation. We limit ourself to mentioning that, to our knowledge, the work contained in this section is the first in presenting a successful domain decomposition approach to total variation minimization. The motivation is that several approaches are directed to the solution of the Euler-Lagrange equations associated to the functional \mathcal{J} , which determine a singular elliptic PDE involving the 1-Laplace operator. Due to the fact that $|Du|(\Omega)$ is not differentiable, one has to discretize its subdifferential, and its characterization is indeed hard to implement numerically in a correct way. The lack of a simple characterization of the subdifferential of the total variation especially raises significant difficulties in dealing with discontinuous interfaces between patches of a domain decomposition.

There is another and partially independent attempt of addressing domain decomposition methods for total variation minimization within the group of Martin Burger at the University of Münster (Germany)¹, in particular the diploma thesis of Jahn Müller [Mu08]², in cooperation with Sergej Gorlatch. Their approach differs from ours in the sense that their domain decomposition is based on computing a minimizer of the functional \mathcal{J} by a primal-dual Newton method for the function u and its dual variable p . There, the function u and its dual p are defined in alternating grid points, i.e., the degrees of freedom of the dual variable are placed in the center between the pixels of u . Their numerical results are very satisfactory, but their theory is still not conclusive.

Our current approach overcomes the difficulties, which may arise when attempting the direct solution of the Euler-Lagrange equations, by minimizing the functional via an iterative proximity map algorithm, as proposed, e.g., in [Ch04, CW05, DDD04,

¹http://wwwmath.uni-muenster.de/u/burger/index_en.html

²available online under http://wwwmath.uni-muenster.de/num/Arbeitsgruppen/ag_burger/organization/burger/pictures/DA%20Mueller.pdf

[DFL08](#), [DTV07](#), [Fo07](#)]. Using this algorithm for the solution of the subproblems has additionally the advantage that its numerical solution is already quite established in the literature, e.g., in [\[Ch04\]](#), and that is very simple to implement and very flexible with respect to acceleration for instance. Further this algorithm is perfectly designed to provide us with desirable convergence properties, as the monotonicity of the energy \mathcal{J} , which decreases at each iteration, cf. Sections [4.3.4](#) and [4.3.5](#) for details.

Note that another specific example for the minimization problem [\(4.49\)](#) is that of ℓ_1 minimization, which found growing interest in recent years in the context of sparse recovery and compressed sensing (cf. e.g., the review papers [\[Ba07, Ca06\]](#)). The application of the following domain decomposition method, i.e., subspace correction algorithm, to ℓ_1 minimization is presented in [\[FS07\]](#) as a second example for the use of such a method. We shall not present this part of our work here, since it is clearly beyond the scope of this thesis.

It is also worth mentioning that, due to the generality of our setting, our approach can be extended to more general subspace decompositions, not only those arising from a domain splitting. This can open room to more sophisticated multiscale algorithms where V_i are multilevel spaces, e.g., originating in a wavelet decomposition.

In what follows we trace the results developed in [\[FS07, Sc09\]](#).

4.3.1 Preliminary Assumptions

We begin this section with a short description of the generic notation used in this section.

In the following \mathcal{H} is a real separable Hilbert space endowed with the norm $\|\cdot\|_{\mathcal{H}}$, and $\Omega \subset \mathbb{R}^d$ denotes an open bounded set with Lipschitz boundary. For some countable index set Λ we denote by $\ell_p = \ell_p(\Lambda)$, $1 \leq p \leq \infty$, the space of real sequences $u = (u_\lambda)_{\lambda \in \Lambda}$ with norm

$$\|u\|_p = \|u\|_{\ell_p} := \left(\sum_{\lambda \in \Lambda} |u_\lambda|^p \right)^{1/p}, \quad 1 \leq p < \infty$$

and $\|u\|_\infty := \sup_{\lambda \in \Lambda} |u_\lambda|$ as usual. If (v_λ) is a sequence of positive weights then we define the weighted spaces $\ell_{p,v} = \ell_{p,v}(\Lambda) = \{u, (u_\lambda v_\lambda) \in \ell_p(\Lambda)\}$ with norm

$$\|u\|_{p,v} = \|u\|_{\ell_{p,v}} = \|(u_\lambda v_\lambda)\|_p = \left(\sum_{\lambda \in \Lambda} v_\lambda^p |u_\lambda|^p \right)^{1/p}$$

4.3 Domain Decomposition for TV Minimization

(with the standard modification for $p = \infty$).

Depending on the context, the symbol \simeq may define an equivalence of norms or an isomorphism of spaces or sets.

More specific notation will be defined, where they turn out to be useful. Remaining notation follows the prefix of the thesis.

The convex constraint function ψ

We are given a function $\psi : \mathcal{H} \rightarrow \mathbb{R}_+ \cup \{+\infty\}$ with the following properties:

($\Psi 1$) ψ is sublinear, i.e., $\psi(u + v) \leq \psi(u) + \psi(v)$ for all $u, v \in \mathcal{H}$;

($\Psi 2$) ψ is 1-homogeneous, i.e., $\psi(\lambda u) = |\lambda| \psi(u)$ for all $\lambda \in \mathbb{R}$.

($\Psi 3$) ψ is lower-semicontinuous in \mathcal{H} , i.e., for any converging sequence $u_n \rightarrow u$ in \mathcal{H}

$$\psi(u) \leq \liminf_{n \in \mathbb{N}} \psi(u_n).$$

Associated with ψ we assume that there exists a dense subspace $\mathcal{H}^\psi \subset \mathcal{H}$ for which $\psi|_{\mathcal{H}^\psi}$ is a seminorm and \mathcal{H}^ψ endowed with the norm

$$\|u\|_{\mathcal{H}^\psi} := \|u\|_{\mathcal{H}} + \psi(u),$$

is a Banach space. We do not assume instead that \mathcal{H}^ψ is reflexive in general; note that due to the dense embedding $\mathcal{H}^\psi \subset \mathcal{H}$ we have

$$\mathcal{H}^\psi \subset \mathcal{H} \simeq \mathcal{H}^* \subset (\mathcal{H}^\psi)^*,$$

and the duality $\langle \cdot, \cdot \rangle_{(\mathcal{H}^\psi)^* \times \mathcal{H}^\psi}$ extends the scalar product on \mathcal{H} . In particular, \mathcal{H} is weakly-*-dense in $(\mathcal{H}^\psi)^*$. In the following we require

- ($H1$) bounded subsets in \mathcal{H}^ψ are sequentially bounded in some other topology τ^ψ of \mathcal{H}^ψ ;
- ($H2$) ψ is lower-semicontinuous with respect to the topology τ^ψ , i.e., for any sequence u_n in \mathcal{H}^ψ which converges to $u \in \mathcal{H}^\psi$ with the τ^ψ -topology satisfies $\psi(u) \leq \liminf_{n \in \mathbb{N}} \psi(u_n)$;

In practice, we will always require also that

4.3 Domain Decomposition for TV Minimization

(H3) $\mathcal{H}^\psi = \{u \in \mathcal{H} : \psi(u) < \infty\}$.

We list in the following the specific examples we consider in this section.

Examples 4.3.1. 1. Let $\Omega \subset \mathbb{R}^d$, for $d = 1, 2$ be a bounded open set with Lipschitz boundary, and $\mathcal{H} = L^2(\Omega)$. Let $V(u, \Omega)$ be defined as in (2.25) and for $u \in BV(\Omega)$ let $|D(u)|(\Omega) = V(u, \Omega)$ total variation of the finite Radon measure Du , cf. Appendix A.5. We define $\psi(u) = V(u, \Omega)$ and it is immediate to see that \mathcal{H}^ψ must coincide with $BV(\Omega)$. Due to the embedding $L^2(\Omega) \subset L^1(\Omega)$ and the Sobolev embedding [AFP00, Theorem 3.47] we have

$$\|u\|_{\mathcal{H}^\psi} = \|u\|_2 + V(u, \Omega) \simeq \|u\|_1 + |Du|(\Omega) = \|u\|_{BV}.$$

Hence $(\mathcal{H}^\psi, \|\cdot\|_{\mathcal{H}^\psi})$ is indeed a Banach space. It is known that $V(\cdot, \Omega)$ is lower-semicontinuous with respect to $L^2(\Omega)$ [AFP00, Proposition 3.6]. We say that a sequence $(u_n)_n$ in $BV(\Omega)$ converges to $u \in BV(\Omega)$ with the weak-*-topology if $(u_n)_n$ converges to u in $L^1(\Omega)$ and Du_n converges to Du with the weak-*-topology in the sense of finite Radon measures. Bounded sets in $BV(\Omega)$ are sequentially weakly-*-compact [AFP00, Proposition 3.13], and $V(\cdot, \Omega)$ is lower-semicontinuous with respect to the weak-*-topology.

2. Let $\mathcal{H} = \mathbb{R}^N$ endowed with the Euclidean norm, and $Q : \mathbb{R}^N \rightarrow \mathbb{R}^n$, for $n \leq N$, is a fixed linear operator. We define $\psi(u) = \|Qu\|_{\ell_1^n}$. Clearly $\mathcal{H}^\psi = \mathbb{R}^N$ and all the requested properties are trivially fulfilled. One particular example of this finite dimensional situation is associated with the choice of $Q : \mathbb{R}^N \rightarrow \mathbb{R}^{N-1}$ given by $Q(u)_i := N(u_{i+1} - u_i)$, $i = 0, \dots, N-2$. In this case $\psi(u) = \|Qu\|_{\ell_1}$ is the discrete variation of the vector u and the model can be seen as an approximation to the situation encountered in the first example, by discrete sampling and finite differences, i.e., setting $u_i := u(\frac{i}{N})$ and $u \in BV(0, 1)$.

Bounded subspace decompositions

In the following we will consider orthogonal decompositions of \mathcal{H} into closed subspaces. We will also require that such a splitting is bounded in \mathcal{H}^ψ .

Assume that V_1, V_2 are two mutually orthogonal, and complementary subspaces of \mathcal{H} , i.e., $\mathcal{H} = V_1 \oplus V_2$, and π_{V_i} are the corresponding orthogonal projections, for $i = 1, 2$. Moreover we require the mapping property

$$\pi_{V_i}|_{\mathcal{H}^\psi} : \mathcal{H}^\psi \rightarrow V_i^\psi := \mathcal{H}^\psi \cap V_i, \quad i = 1, 2,$$

continuously in the norm of \mathcal{H}^ψ , and that $\text{Range}(\pi_{V_i}|_{\mathcal{H}^\psi}) = V_i^\psi$ is closed. This implies that \mathcal{H}^ψ splits into the direct sum $\mathcal{H}^\psi = V_1^\psi \oplus V_2^\psi$.

Example 4.3.2. Let $\Omega_1 \subset \Omega \subset \mathbb{R}^d$, for $d = 1, 2$, be two bounded open sets with Lipschitz boundaries, and $\Omega_2 = \Omega \setminus \Omega_1$. We define

$$V_i := \{u \in L^2(\Omega) : \text{supp}(u) \subset \Omega_i\}, \quad i = 1, 2.$$

Then $\pi_{V_i}(u) = u1_{\Omega_i}$. For $\psi(u) = V(u, \Omega)$, by [AFP00, Corollary 3.89], $V_i^\psi = BV(\Omega) \cap V_i$ is a closed subspace of $BV(\Omega)$ and $\pi_{V_i}(u) = u1_{\Omega_i} \in V_i^\psi$, $i = 1, 2$, for all $u \in BV(\Omega)$.

4.3.2 A Convex Variational Problem and Subspace Splitting

We are interested in the minimization in \mathcal{H} (actually in \mathcal{H}^ψ) of the functional

$$\mathcal{J}(u) := \|Tu - f\|_{\mathcal{H}}^2 + 2\alpha\psi(u),$$

where $T \in \mathcal{L}(\mathcal{H})$ is a bounded linear operator, $f \in \mathcal{H}$ is a datum, and $\alpha > 0$ is a fixed constant. In order to guarantee the existence of its minimizers we assume that:

- (C) \mathcal{J} is coercive in \mathcal{H} , i.e., $\{\mathcal{J} \leq C\} := \{u \in \mathcal{H} : \mathcal{J}(u) \leq C\}$ is bounded in \mathcal{H} for all constants $C > 0$.

Example 4.3.3. Assume $\Omega \subset \mathbb{R}^d$, for $d = 1, 2$ be a bounded open set with Lipschitz boundary, $\mathcal{H} = L^2(\Omega)$ and $\psi(u) = V(u, \Omega)$ (compare Examples 4.3.1.1). In this case we deal with total variation minimization. It is well-known that if $T1_\Omega \neq 0$ then condition (C) is indeed satisfied, see [Ve01, Proposition 3.1] and [CL97].

Lemma 4.3.4. Under the assumptions above, \mathcal{J} has minimizers in \mathcal{H}^ψ .

Proof. The proof is a standard application of the direct method of calculus of variations and can be found for example in [CW05].

Let $(u_n)_n \subset \mathcal{H}$, a minimizing sequence. By assumption (C) we have $\|u_n\|_{\mathcal{H}} + \psi(u_n) \leq C$ for all $n \in \mathbb{N}$. Therefore by (H1) we can extract a subsequence in \mathcal{H}^ψ converging in the topology τ^ψ . Possibly passing to a further subsequence we can assume that it also converges weakly in \mathcal{H} . By lower-semicontinuity of $\|Tu - f\|_{\mathcal{H}}^2$ with respect to the weak topology of \mathcal{H} and the lower-semicontinuity of ψ with respect to the topology τ^ψ , ensured by assumption (H2), we have the desired existence of minimizers. \square

4.3 Domain Decomposition for TV Minimization

The minimization of \mathcal{J} is a classical problem [ET76] which was recently reconsidered by several authors, [Ch04, CW05, DDD04, DTV07, SCD02, Ti96], with emphasis on the computability of minimizers in particular cases. They studied essentially the same algorithm for the minimization.

For ψ with properties $(\Psi 1 - \Psi 3)$, there exists a closed convex set $K_\psi \subset \mathcal{H}$ such that

$$\begin{aligned}\psi^*(u) &= \sup_{v \in \mathcal{H}} \{\langle v, u \rangle - \psi(v)\} \\ &= \chi_{K_\psi}(u) = \begin{cases} 0 & \text{if } u \in K_\psi \\ +\infty & \text{otherwise.} \end{cases}\end{aligned}$$

See also Examples 4.3.6.2 below. In the following we assume furthermore that $K_\psi = -K_\psi$. For any closed convex set $K \subset \mathcal{H}$ we denote $\mathbb{P}_K(u) = \operatorname{argmin}_{v \in K} \|u - v\|_{\mathcal{H}}$ the orthogonal projection onto K . For $\mathbb{S}_\alpha^\psi := I - \mathbb{P}_{\alpha K_\psi}$, called the *generalized thresholding map* in the signal processing literature, the iteration

$$u^{(n+1)} = \mathbb{S}_\alpha^\psi(u^{(n)} + T^*(f - Tu^{(n)})) \quad (4.52)$$

converges weakly to a minimizer $u \in \mathcal{H}^\psi$ of \mathcal{J} , for any initial choice $u^{(0)} \in \mathcal{H}^\psi$, provided that T and f are suitably rescaled so that $\|T\| < 1$. For particular situations, e.g., $\mathcal{H} = \ell_2(\Lambda)$ and $\psi(u) = \|u\|_{\ell_{1,w}}$, one can prove the convergence in norm [DDD04, DTV07].

As it is pointed out, for example in [DFL08, Fo07], this algorithm converges at a poor rate, unless T is non-singular or has additional special spectral properties. For this reason acceleration by means of projected steepest descent iterations [DFL08] and domain decomposition methods [Fo07] were proposed.

The particular situation considered in [Fo07] is $\mathcal{H} = \ell_2(\Lambda)$ and $\psi(u) = \|u\|_{\ell_1(\Lambda)}$. In this case one takes advantage of the fact that for a disjoint partition of the index set $\Lambda = \Lambda_1 \cup \Lambda_2$ we have the splitting $\psi(u_{\Lambda_1} + u_{\Lambda_2}) = \psi(u_{\Lambda_1}) + \psi(u_{\Lambda_2})$ for any vector u_{Λ_i} supported on Λ_i , $i = 1, 2$. Thus, a decomposition into column subspaces (i.e., componentwise) of the operator T (if identified with a suitable matrix) is realized, and alternating minimizations on these subspaces are performed by means of iterations of the type (4.52). This leads, e.g., to the following sequential algorithm: Pick an initial

4.3 Domain Decomposition for TV Minimization

$u_{\Lambda_1}^{(0,L)} + u_{\Lambda_2}^{(0,M)} := u^{(0)} \in \ell_1(\Lambda)$, for example $u^{(0)} = 0$, and iterate

$$\begin{cases} \begin{cases} u_{\Lambda_1}^{(n+1,0)} = u_{\Lambda_1}^{(n,L)} \\ u_{\Lambda_1}^{(n+1,\ell+1)} = \mathbb{S}_\alpha \left(u_{\Lambda_1}^{(n+1,\ell)} + T_{\Lambda_1}^* ((f - T_{\Lambda_2} u_{\Lambda_2}^{(n,M)}) - T_{\Lambda_1} u_{\Lambda_1}^{(n+1,\ell)}) \right) \end{cases} & \ell = 0, \dots, L-1 \\ \begin{cases} u_{\Lambda_2}^{(n+1,0)} = u_{\Lambda_2}^{(n,M)} \\ u_{\Lambda_2}^{(n+1,\ell+1)} = \mathbb{S}_\alpha \left(u_{\Lambda_2}^{(n+1,\ell)} + T_{\Lambda_2}^* ((f - T_{\Lambda_1} u_{\Lambda_1}^{(n+1,L)}) - T_{\Lambda_2} u_{\Lambda_2}^{(n+1,\ell)}) \right) \end{cases} & \ell = 0, \dots, M-1 \\ u^{(n+1)} := u_{\Lambda_1}^{(n+1,L)} + u_{\Lambda_2}^{(n+1,M)}. \end{cases} \quad (4.53)$$

Here the operator \mathbb{S}_α is the soft-thresholding operator which acts componentwise $\mathbb{S}_\alpha v = (S_\alpha v_\lambda)_{\lambda \in \Lambda}$ and defined by

$$S_\alpha(x) = \begin{cases} x - \text{sgn}(x)\alpha, & |x| > \alpha \\ 0, & \text{otherwise.} \end{cases} \quad (4.54)$$

The expected benefit from this approach is twofold:

1. Instead of solving one large problem with many iteration steps, we can solve approximatively several smaller subproblems, which might lead to an acceleration of convergence and a reduction of the overall computational effort, due to possible conditioning improvements;
2. The subproblems do not need more sophisticated algorithms, simply reproduce at smaller dimension the original problem, and they can be solved in parallel.

The nice splitting of ψ as a sum of evaluations on subspaces does not occur, for instance, when $\mathcal{H} = L^2(\Omega)$, $\psi(u) = V(u, \Omega) = |Du|(\Omega)$, and $\Omega_1 \cup \Omega_2 \subset \Omega \subset \bar{\Omega}_1 \cup \bar{\Omega}_2$ is a disjoint decomposition of Ω . Indeed, cf. [AFP00, Theorem 3.84], we have

$$|D(u_{\Omega_1} + u_{\Omega_2})|(\Omega) = |Du_{\Omega_1}|(\Omega_1) + |Du_{\Omega_2}|(\Omega_2) + \underbrace{\int_{\partial\Omega_1 \cap \partial\Omega_2} |u_{\Omega_1}^+(x) - u_{\Omega_2}^-(x)| d\mathcal{H}_1(x)}_{\text{additional interface term}}. \quad (4.55)$$

Here one should not confuse \mathcal{H}_d with any \mathcal{H}^ψ since the former indicates the Hausdorff measure of dimension d . The symbols v^+ and v^- denote the left and right approximated limits at jump points [AFP00, Proposition 3.69]. The presence of the additional boundary interface term $\int_{\partial\Omega_1 \cap \partial\Omega_2} |u_{\Omega_1}^+(x) - u_{\Omega_2}^-(x)| d\mathcal{H}_1(x)$ does not allow to use in a straightforward way iterations as in (4.52) to minimize the local problems on Ω_i .

Moreover, also in the sequence space setting mentioned above, the hope for a better conditioning by column subspace splitting as in [Fo07] might be ill-posed, no such splitting needs to be well conditioned in general (good cases are provided in [Tr08] instead).

Therefore, one may want to consider arbitrary subspace decompositions and, in order to deal with these more general situations, we investigate splittings into arbitrary orthogonal subspaces $\mathcal{H} = V_1 \oplus V_2$ for which we may have

$$\psi(\pi_{V_1}(u) + \pi_{V_2}(v)) \neq \psi(\pi_{V_1}(u)) + \psi(\pi_{V_2}(v)).$$

In principle, in this work we limit ourself to consider the detailed analysis for two subspaces V_1, V_2 . Nevertheless, the arguments can be easily generalized to multiple subspaces V_1, \dots, V_N , see, e.g., [Fo07], and in the numerical experiments we will also test this more general situation.

With this splitting we want to minimize \mathcal{J} by suitable instances of the following alternating algorithm: Pick an initial $V_1 \oplus V_2 \ni u_1^{(0)} + u_2^{(0)} := u^{(0)} \in \mathcal{H}^\Psi$, for example $u^{(0)} = 0$, and iterate

$$\begin{cases} u_1^{(n+1)} \approx \operatorname{argmin}_{v_1 \in V_1} \mathcal{J}(v_1 + u_2^{(n)}) \\ u_2^{(n+1)} \approx \operatorname{argmin}_{v_2 \in V_2} \mathcal{J}(u_1^{(n+1)} + v_2) \\ u^{(n+1)} := u_1^{(n+1)} + u_2^{(n+1)}. \end{cases} \quad (4.56)$$

We use “ \approx ” (the approximation symbol) because in practice we never perform the exact minimization, as in (4.53). In the following section we discuss how to realize the approximation to the individual subspace minimizations. As pointed out above, this cannot just reduce to a simple iteration of the type (4.52).

4.3.3 Local Minimization by Lagrange Multipliers

Let us consider, for example,

$$\operatorname{argmin}_{v_1 \in V_1} \mathcal{J}(v_1 + u_2) = \operatorname{argmin}_{v_1 \in V_1} \|Tv_1 - (f - Tu_2)\|_{\mathcal{H}}^2 + 2\alpha\psi(v_1 + u_2). \quad (4.57)$$

First of all, observe that $\{u \in \mathcal{H} : \pi_{V_2}u = u_2, \mathcal{J}(u) \leq C\} \subset \{\mathcal{J} \leq C\}$, hence the former set is also bounded by assumption (C). By the same argument as in Lemma 4.3.4, the minimization (4.57) has a solution. It is useful to introduce an auxiliary functional

4.3 Domain Decomposition for TV Minimization

\mathcal{J}_1^s , called the *surrogate functional* of \mathcal{J} (cf. also (4.47) in Section 4.2.2 for a similar approach): Assume $a, u_1 \in V_1$ and $u_2 \in V_2$ and define

$$\mathcal{J}_1^s(u_1 + u_2, a) := \mathcal{J}(u_1 + u_2) + \|u_1 - a\|_{\mathcal{H}}^2 - \|T(u_1 - a)\|_{\mathcal{H}}^2. \quad (4.58)$$

A straightforward computation shows that

$$\mathcal{J}_1^s(u_1 + u_2, a) = \|u_1 - (a + \pi_{V_1} T^*(f - Tu_2 - Ta))\|_{\mathcal{H}}^2 + 2\alpha\psi(u_1 + u_2) + \varphi(a, f, u_2),$$

where φ is a function of a, f, u_2 only. We want to realize an approximate solution to (4.57) by using the following algorithm: For $u_1^{(0)} \in V_1^\psi$,

$$u_1^{(\ell+1)} = \operatorname{argmin}_{u_1 \in V_1} \mathcal{J}_1^s(u_1 + u_2, u_1^{(\ell)}), \quad \ell \geq 0. \quad (4.59)$$

Before proving the convergence of this algorithm, we need to investigate first how to compute practically $u_1^{(n+1)}$ for given $u_1^{(n)}$. To this end we need to introduce further concepts and to recall some useful results.

Generalized Lagrange multipliers for nonsmooth objective functions

Let us begin this subsection with recalling the concept of a subdifferential, cf. also Appendix A.2.

Definition 4.3.5. *For a locally convex space V and for a convex function $F : V \rightarrow \mathbb{R} \cup \{-\infty, +\infty\}$, we define the subdifferential of F at $x \in V$, as $\partial F(x) = \emptyset$ if $F(x) = \infty$, otherwise*

$$\partial F(x) := \partial F_V(x) := \{x^* \in V^* : \langle x^*, y - x \rangle + F(x) \leq F(y) \quad \forall y \in V\},$$

where V^* denotes the dual space of V . It is obvious from this definition that $0 \in \partial F(x)$ if and only if x is a minimizer of F . Since we deal with several spaces, namely, $\mathcal{H}, \mathcal{H}^\psi, V_i, V_i^\psi$, it will turn out to be useful to distinguish sometimes in which space (and associated topology) the subdifferential is defined by imposing a subscript $\partial_V F$ for the subdifferential considered on the space V .

Examples 4.3.6. 1. Let $V = \ell_1(\Lambda)$ and let $F(x) := \|x\|_1$ be the ℓ_1 -norm. We have

$$\partial\|\cdot\|_1(x) = \{\xi \in \ell_\infty(\Lambda) : \xi_\lambda \in \partial|\cdot|(x_\lambda), \lambda \in \Lambda\} \quad (4.60)$$

where $\partial|\cdot|(z) = \{\operatorname{sgn}(z)\}$ if $z \neq 0$ and $\partial|\cdot|(0) = [-1, 1]$.

4.3 Domain Decomposition for TV Minimization

2. Assume, $V = \mathcal{H}$ and $\varphi \geq 0$ is a proper lower-semicontinuous convex function. For $F(u; z) = \|u - z\|_{\mathcal{H}}^2 + 2\varphi(u)$, we define the function

$$\text{prox}_\varphi(z) := \operatorname{argmin}_{u \in V} F(u; z),$$

which is called the proximity map in the convex analysis literature, e.g., [ET76, CW05], and generalized thresholding in the signal processing literature, e.g., [DDD04, DFL08, DTV07, Fo07]. Observe that by $\varphi \geq 0$ the function F is coercive in \mathcal{H} and by lower-semicontinuity and strict convexity of the term $\|u - z\|_{\mathcal{H}}^2$ this definition is well-posed. In particular, $\text{prox}_\varphi(z)$ is the unique solution of the following differential inclusion

$$0 \in (u - z) + \partial\varphi(u).$$

It is well known [ET76, RW98] that the proximity map is nonexpansive, i.e.,

$$\|\text{prox}_\varphi(z_1) - \text{prox}_\varphi(z_2)\|_{\mathcal{H}} \leq \|z_1 - z_2\|_{\mathcal{H}}.$$

In particular, if φ is a 1-homogeneous function then

$$\text{prox}_\varphi(z) = (I - \mathbb{P}_{K_\varphi})(z),$$

where K_φ is a suitable closed convex set associated to φ , see for instance [CW05].

Under the notations of Definition 4.3.5, we consider the following constrained minimization problem

$$\operatorname{argmin}_{x \in V} \{F(x) : G(x) = 0\}, \quad (4.61)$$

where $G : V \rightarrow \mathbb{R}$ is a bounded linear operator on V . We have the following useful result.

Theorem 4.3.7. (Generalized Lagrange multipliers for nonsmooth objective functions, Theorem 1.8, [BP96])

If F is continuous at a point of $\ker G$ and G^* has closed range in V then a point $x_0 \in \ker G$ is an optimal solution of (4.61) if and only if

$$\partial F(x_0) \cap \operatorname{Range} G^* \neq \emptyset.$$

Oblique thresholding

We want to exploit Theorem 4.3.7 in order to produce an algorithmic solution to each iteration step (4.59).

4.3 Domain Decomposition for TV Minimization

Theorem 4.3.8 (Oblique thresholding). *For $u_2 \in V_2^\psi$ and for $z \in V_1$ the following statements are equivalent:*

- (i) $u_1^* = \operatorname{argmin}_{u \in V_1} \|u - z\|_{\mathcal{H}}^2 + 2\alpha\psi(u + u_2)$;
- (ii) there exists $\eta \in \operatorname{Range}(\pi_{V_2}|_{\mathcal{H}^\psi})^* \simeq (V_2^\psi)^*$ such that $0 \in u_1^* - (z - \eta) + \alpha\partial_{\mathcal{H}^\psi}\psi(u_1^* + u_2)$.

Moreover, the following statements are equivalent and imply (i) and (ii).

- (iii) there exists $\eta \in V_2$ such that $u_1^* = (I - \mathbb{P}_{\alpha K_\psi})(z + u_2 - \eta) - u_2 = \mathbb{S}_\alpha^\psi(z + u_2 - \eta) - u_2 \in V_1$;
- (iv) there exists $\eta \in V_2$ such that $\eta = \pi_{V_2}\mathbb{P}_{\alpha K_\psi}(\eta - (z + u_2))$.

Proof. Let us show the equivalence between (i) and (ii). The problem in (i) can be reformulated as

$$u_1^* = \operatorname{argmin}_{u \in \mathcal{H}^\psi} \{F(u) := \|u - z\|_{\mathcal{H}}^2 + 2\alpha\psi(u + u_2), \pi_{V_2}(u) = 0\}.$$

The latter is a special instance of (4.61). Moreover, F is continuous in $V_1^\psi \subset V_1 = \ker \pi_{V_2}$ in the norm-topology of \mathcal{H}^ψ (while in general it is not in V_1 with the norm topology of \mathcal{H}). Recall now that $\pi_{V_2}|_{\mathcal{H}^\psi}$ is assumed to be a bounded and surjective map with closed range in the norm topology of \mathcal{H}^ψ (see Section 4.3.1). This means that $(\pi_{V_2}|_{\mathcal{H}^\psi})^*$ is injective and that $\operatorname{Range}(\pi_{V_2}|_{\mathcal{H}^\psi})^* \simeq (V_2^\psi)^*$ is closed. Therefore, by an application of Theorem 4.3.7, the optimality of u_1^* is equivalent to the existence of $\eta \in \operatorname{Range}(\pi_{V_2}|_{\mathcal{H}^\psi})^* \simeq (V_2^\psi)^*$ such that

$$-\eta \in \partial_{\mathcal{H}^\psi} F(u_1^*).$$

Due to the continuity of $\|u - z\|_{\mathcal{H}}$ in \mathcal{H}^ψ , we have, by [ET76, Proposition 5.6], that

$$\partial_{\mathcal{H}^\psi} F(u_1^*) = 2(u_1^* - z) + 2\alpha\partial_{\mathcal{H}^\psi}\psi(u_1^* + u_2).$$

Thus, the optimality of u_1^* is equivalent to

$$0 \in u_1^* - (z - \eta) + \alpha\partial_{\mathcal{H}^\psi}\psi(u_1^* + u_2).$$

This concludes the equivalence of (i) and (ii). Let us show now that (iii) implies (ii). The condition in (iii) can be rewritten as

$$\xi = (I - \mathbb{P}_{\alpha K_\psi})(z + u_2 - \eta), \quad \xi = u_1^* + u_2.$$

4.3 Domain Decomposition for TV Minimization

Since $\psi \geq 0$ is 1-homogeneous and lower-semicontinuous, by Examples 4.3.6.2, the latter is equivalent to

$$0 \in \xi - (z + u_2 - \eta) + \alpha \partial_{\mathcal{H}} \psi(\xi)$$

or, by (H3),

$$\begin{aligned} \xi &= \operatorname{argmin}_{u \in \mathcal{H}} \|u - (z + u_2 - \eta)\|_{\mathcal{H}}^2 + 2\alpha\psi(u) \\ &= \operatorname{argmin}_{u \in \mathcal{H}^\psi} \|u - (z + u_2 - \eta)\|_{\mathcal{H}}^2 + 2\alpha\psi(u). \end{aligned}$$

The latter optimal problem is equivalent to

$$0 \in \xi - (z + u_2 - \eta) + \alpha \partial_{\mathcal{H}^\psi} \psi(\xi) \text{ or } 0 \in u_1^* - (z - \eta) + \alpha \partial_{\mathcal{H}^\psi} \psi(u_1^* + u_2).$$

Since $V_2 \subset (V_2^\psi)^* \simeq \operatorname{Range}(\pi_{V_2}|_{\mathcal{H}^\psi})^*$ we deduce that (iii) implies (ii). We prove now the equivalence between (iii) and (iv). We have

$$\begin{aligned} u_1^* &= (I - \mathbb{P}_{\alpha K_\psi})(z + u_2 - \eta) - u_2 \in V_1 \\ &= z - \eta - \mathbb{P}_{\alpha K_\psi}(z + u_2 - \eta). \end{aligned}$$

By applying π_{V_2} to both sides of the latter equality we get

$$0 = -\eta - \pi_{V_2} \mathbb{P}_{\alpha K_\psi}(z + u_2 - \eta).$$

By recalling that $K_\psi = -K_\psi$, we obtain the fixed point equation

$$\eta = \pi_{V_2} \mathbb{P}_{\alpha K_\psi}(\eta - (z + u_2)). \quad (4.62)$$

Conversely, assume $\eta = \pi_{V_2} \mathbb{P}_{\alpha K_\psi}(\eta - (z + u_2))$ for some $\eta \in V_2$. Then

$$\begin{aligned} (I - \mathbb{P}_{\alpha K_\psi})(z + u_2 - \eta) - u_2 &= z - \eta - \mathbb{P}_{\alpha K_\psi}(z + u_2 - \eta) \\ &= z - \pi_{V_2} \mathbb{P}_{\alpha K_\psi}(\eta - (z + u_2)) - \mathbb{P}_{\alpha K_\psi}(z + u_2 - \eta) \\ &= z - (I - \pi_{V_2}) \mathbb{P}_{\alpha K_\psi}(z + u_2 - \eta) \\ &= z - \pi_{V_1} \mathbb{P}_{\alpha K_\psi}(z + u_2 - \eta) = u_1^* \in V_1. \end{aligned} \quad \square$$

Remark 4.3.9. 1. Unfortunately in general we have $V_2 \subsetneq (V_2^\psi)^*$ which excludes the complete equivalence of the previous conditions (i)-(iv). For example, in the case $\mathcal{H} = \ell_2(\Lambda)$ and $\psi(u) = \|u\|_{\ell_1}$, $\Lambda = \Lambda_1 \cup \Lambda_2$, $V_i = \ell_2^{\Lambda_i}(\Lambda) := \{u \in \ell_2(\Lambda) : \operatorname{supp}(u) \subset \Lambda_i\}$, $i = 1, 2$, we have $V_2^\psi = \ell_1^{\Lambda_2}(\Lambda) = \{u \in \ell_1(\Lambda) : \operatorname{supp}(u) \subset \Lambda_2\}$, hence, $V_2 \subsetneq (V_2^\psi)^* \simeq \ell_\infty^{\Lambda_2}(\Lambda) = \{u \in \ell_\infty(\Lambda) : \operatorname{supp}(u) \subset \Lambda_2\}$. It might well be that $\eta \in \ell_\infty^{\Lambda_2}(\Lambda) \setminus \ell_2^{\Lambda_2}(\Lambda)$. However, since $\psi(u_{\Lambda_1} + u_{\Lambda_2}) = \psi(u_{\Lambda_1}) + \psi(u_{\Lambda_2})$ in this case, we have $0 \in u_1^* - z + \alpha \partial \|\cdot\|_1(u_2)$. Following [Fo07], u_2 is assumed $\|_1(u_1^*)$ and therefore may choose any η in $\partial \|\cdot\|_1(u_2)$.

to be the result of soft-thresholding iterations, hence u_2 is a finitely supported vector. Therefore, by Examples 4.3.6.1, we can choose η to be also a finitely supported vector, hence $\eta \in \ell_2^{\Lambda_2}(\Lambda) = V_2$. This means that the existence of $\eta \in V_2$ as in (iii) or (iv) of the previous theorem may occur also in those cases for which $V_2 \subsetneq (V_2^\psi)^*$. In general, we can only observe that V_2 is weakly-*-dense in $(V_2^\psi)^*$.

2. For \mathcal{H} of finite dimension – which is the relevant case in numerical applications – all the spaces are independent of the particular attached norm and coincide with their duals, hence all the statements (i)-(iv) of the previous theorem are equivalent in this case.

A simple constructive test for the existence of $\eta \in V_2$ as in (iii) or (iv) of the previous theorem is provided by the following iterative algorithm:

$$\eta^{(0)} \in V_2, \quad \eta^{(m+1)} = \pi_{V_2} \mathbb{P}_{\alpha K_\psi}(\eta^{(m)} - (z + u_2)), \quad m \geq 0. \quad (4.63)$$

Proposition 4.3.10. *The following statements are equivalent:*

- (i) *there exists $\eta \in V_2$ such that $\eta = \pi_{V_2} \mathbb{P}_{\alpha K_\psi}(\eta - (z + u_2))$ (which is in turn the condition (iv) of Theorem 4.3.8)*
- (ii) *the iteration (4.63) converges weakly to any $\eta \in V_2$ that satisfies (4.62).*

In particular, there are no fixed points of (4.62) if and only if $\|\eta^{(m)}\|_{\mathcal{H}} \rightarrow \infty$, for $m \rightarrow \infty$.

For the proof of this Proposition we need to recall some classical concepts and results.

Definition 4.3.11. *A nonexpansive map $T : \mathcal{H} \rightarrow \mathcal{H}$ is strongly nonexpansive if for $(u_n - v_n)_n$ bounded and $\|T(u_n) - T(v_n)\|_{\mathcal{H}} - \|u_n - v_n\|_{\mathcal{H}} \rightarrow 0$ we have*

$$u_n - v_n - (T(u_n) - T(v_n)) \rightarrow 0, \quad n \rightarrow \infty.$$

Proposition 4.3.12. [BR77, Corollaries 1.3, 1.4, and 1.5] *Let $T : \mathcal{H} \rightarrow \mathcal{H}$ be a strongly nonexpansive map. Then $\text{fix } T = \{u \in \mathcal{H} : T(u) = u\} \neq \emptyset$ if and only if $(T^n u)_n$ converges weakly to a fixed point $u_0 \in \text{fix } T$ for any choice of $u \in \mathcal{H}$.*

Proof of Proposition 4.3.10. Orthogonal projections onto convex sets are strongly nonexpansive [BBL97, Corollary 4.2.3]. Moreover, composition of strongly nonexpansive maps are strongly nonexpansive [BR77, Lemma 2.1]. By an application of Proposition 4.3.12 we immediately have the result, since any map of the type $T(\xi) = Q(\xi) + \xi_0$

4.3 Domain Decomposition for TV Minimization

is strongly nonexpansive whenever Q is, (this is a simple observation from the definition of strongly nonexpansive map). Indeed, we are looking for fixed points of $\eta = \pi_{V_2} \mathbb{P}_{\alpha K_\psi}(\eta - (z + u_2))$ or, equivalently, of $\xi = \underbrace{\pi_{V_2} \mathbb{P}_{\alpha K_\psi}(\xi)}_{:=Q} - \underbrace{(z + u_2)}_{:=\xi_0}$. \square

In Examples 4.3.6, we have already observed that

$$u_1^* = \text{prox}_{\alpha\psi(\cdot+u_2)}(z).$$

For consistency with the terminology of generalized thresholding in signal processing, we call the map $\text{prox}_{\alpha\psi(\cdot+u_2)}$ an *oblique thresholding* and denote it by

$$\mathbb{S}_\alpha^{\psi, V_1, V_2}(z; u_2) := \text{prox}_{\alpha\psi(\cdot+u_2)}(z).$$

The attribute “*oblique*” emphasizes the presence of an additional subspace which contributes to the computation of the solution. By using results in [CW05, Subsection 2.3] (see also [ET76, II.2-3]) we can already infer that

$$\|S_\alpha^{\psi, V_1, V_2}(z_1; u_2) - S_\alpha^{\psi, V_1, V_2}(z_2; u_2)\|_{\mathcal{H}} \leq \|z_1 - z_2\|_{\mathcal{H}}, \quad \text{for all } z_1, z_2 \in V_1.$$

For a finite dimensional \mathcal{H} (and, more generally, for any situation where for any choice of $u_2 \in V_2^\psi$ and $z \in V_1$ there exists $\eta \in V_2$ which solves (4.62)) we can show the nonexpansiveness of $S_\alpha^{\psi, V_1, V_2}(\cdot; u_2)$ by a simple direct argument which exploits the orthogonality of V_1 and V_2 and the relationships revealed by Theorem 4.3.8. For the sake of completeness, we would like to report this short argument.

Lemma 4.3.13. *Assume that $\dim(\mathcal{H}) < \infty$. The oblique thresholding $S_\alpha^{\psi, V_1, V_2}(\cdot; u_2)$ is a nonexpansive map for any choice of $u_2 \in V_2$.*

Proof. Let us denote $\xi = z + u_2 - \eta$, where $\eta = \eta(z, u_2) = \pi_{V_2} \mathbb{P}_{\alpha K_\psi}(\eta - (z + u_2))$. We have $\xi = \pi_{V_2} \mathbb{P}_{\alpha K_\psi}(\xi) + (z + u_2)$, and, by using the latter equivalence,

$$\begin{aligned} S_\alpha^{\psi, V_1, V_2}(z; u_2) &= \xi - \mathbb{P}_{\alpha K_\psi}(\xi) - u_2 \\ &= \pi_{V_2} \mathbb{P}_{\alpha K_\psi}(\xi) - \mathbb{P}_{\alpha K_\psi}(\xi) + z \\ &= z - \pi_{V_1} \mathbb{P}_{\alpha K_\psi}(\xi). \end{aligned}$$

Then $S_\alpha^{\psi, V_1, V_2}(z; u_2) + u_2 - \eta = \xi - \pi_{V_1} \mathbb{P}_{\alpha K_\psi}(\xi) = (I - \pi_{V_1} \mathbb{P}_{\alpha K_\psi})(\xi)$. Let us denote $\xi_i = z_i + u_2 - \eta_i$, where $\eta_i = \eta(z_i, u_2) = \pi_{V_2} \mathbb{P}_{\alpha K_\psi}(\eta_i - (z_i + u_2))$. We have the equivalence

$$\underbrace{S_\alpha^{\psi, V_1, V_2}(z_1; u_2) - S_\alpha^{\psi, V_1, V_2}(z_2; u_2)}_{\in V_1} + \underbrace{\eta_2 - \eta_1}_{\in V_2} = (I - \pi_{V_1} \mathbb{P}_{\alpha K_\psi})(\xi_1) - (I - \pi_{V_1} \mathbb{P}_{\alpha K_\psi})(\xi_2)$$

4.3 Domain Decomposition for TV Minimization

which implies, by orthogonality of V_1 and V_2 ,

$$\|S_\alpha^{\psi, V_1, V_2}(z_1; u_2) - S_\alpha^{\psi, V_1, V_2}(z_2; u_2)\|_{\mathcal{H}}^2 + \|\eta_2 - \eta_1\|_{\mathcal{H}}^2 \leq \|z_1 - z_2\|_{\mathcal{H}}^2 + \|\eta_2 - \eta_1\|_{\mathcal{H}}^2.$$

In the latter inequality we also used the nonexpansiveness of $I - \pi_{V_1} \mathbb{P}_{\alpha K_\psi}$. This concludes the proof:

$$\|S_\alpha^{\psi, V_1, V_2}(z_1; u_2) - S_\alpha^{\psi, V_1, V_2}(z_2; u_2)\|_{\mathcal{H}} \leq \|z_1 - z_2\|_{\mathcal{H}}. \quad \square$$

Convergence of the subspace minimization

In light of the results of the previous subsection, the iterative algorithm (4.59) can be equivalently rewritten as

$$u_1^{(\ell+1)} = S_\alpha^{\psi, V_1, V_2}(u_1^{(\ell)} + \pi_{V_1} T^*(f - Tu_2 - Tu_1^{(\ell)}); u_2). \quad (4.64)$$

In certain cases, e.g., in finite dimensions, the iteration can be explicitly computed by

Oblique Thresholding:

$$u_1^{(\ell+1)} = S_\alpha^{\psi}(u_1^{(\ell)} + \pi_{V_1} T^*(f - Tu_2 - Tu_1^{(\ell)}) + u_2 - \eta^{(\ell)}) - u_2,$$

where $\eta^{(\ell)} \in V_2$ is any solution of the fixed point equation

$$\eta = \pi_{V_2} \mathbb{P}_{\alpha K_\psi}(\eta - (u_1^{(\ell)} + \pi_{V_1} T^*(f - Tu_2 - Tu_1^{(\ell)}) + u_2)).$$

The computation of $\eta^{(\ell)}$ can be (approximately) implemented by the algorithm (4.63).

Theorem 4.3.14. *Assume that $u_2 \in V_2^\psi$ and $\|T\| < 1$. Then the iteration (4.64) converges weakly to a solution $u_1^* \in V_1^\psi$ of (4.57) for any initial choice of $u_1^{(0)} \in V_1^\psi$.*

Proof. For the sake of completeness, we report the proof of this theorem, which follows the same strategy already proposed in [DDD04], compare also similar results in [CW05]. In particular we want to apply Opial's fixed point theorem:

Theorem 4.3.15. [Op67] *Let the mapping A from \mathcal{H} to \mathcal{H} satisfy the following conditions:*

- (i) *A is nonexpansive: for all $z, z' \in \mathcal{H}$, $\|Az - Az'\|_{\mathcal{H}} \leq \|z - z'\|_{\mathcal{H}}$;*
- (ii) *A is asymptotically regular: for all $z \in \mathcal{H}$, $\|A^{n+1}z - A^n z\|_{\mathcal{H}} \rightarrow 0$, for $n \rightarrow \infty$;*

4.3 Domain Decomposition for TV Minimization

(iii) the set $\mathcal{F} = \text{fix } A$ of fixed points of A in \mathcal{H} is not empty.

Then for all $z \in \mathcal{H}$, the sequence $(A^n z)_{n \in \mathbb{N}}$ converges weakly to a fixed point in \mathcal{F} .

A simple proof of this theorem can be found in the appendix of [DDD04].

We need to prove that $A(u_1) := S_\alpha^{\psi, V_1, V_2}(u_1 + \pi_{V_1} T^*(f - Tu_2 - Tu_1); u_2)$ fulfills the assumptions of the Opial's theorem on V_1 .

Step 1. As stated at the beginning of this section, there exist solutions $u_1^* \in V_1^\psi$ to (4.57). With similar argument to the one used to prove the equivalence of (i) and (ii) in Theorem 4.3.8, the optimality of u_1^* can be readily proved as equivalent to

$$0 \in -\pi_{V_1} T^*(f - Tu_2 - Tu_1^*) + \eta + \alpha \partial_{\mathcal{H}^\psi} \psi(u_1^* + u_2),$$

for some $\eta \in (V_2^\psi)^*$. By adding and subtracting u_1^* we obtain

$$0 \in u_1^* - \underbrace{((u_1^* + \pi_{V_1} T^*(f - Tu_2 - Tu_1^*)) - \eta)}_{:= z} + \alpha \partial_{\mathcal{H}^\psi} \psi(u_1^* + u_2),$$

Applying the equivalence of (i) and (ii) in Theorem 4.3.8, we deduce that u_1^* is a fixed point of the following equation

$$u_1^* = S_\alpha^{\psi, V_1, V_2}(u_1^* + \pi_{V_1} T^*(f - Tu_2 - Tu_1^*); u_2),$$

hence $\text{fix } A \neq \emptyset$.

Step 2. The algorithm produces iterations which are asymptotically regular, i.e., $\|u_1^{(\ell+1)} - u_1^{(\ell)}\|_{\mathcal{H}} \rightarrow 0$. Indeed, by using $\|T\| < 1$ and $C := 1 - \|T\|^2 > 0$, we have the following estimates

$$\begin{aligned} \mathcal{J}(u_1^{(\ell)} + u_2) &= \mathcal{J}_1^s(u_1^{(\ell)} + u_2, u_1^{(\ell)}) \\ &\geq \mathcal{J}_1^s(u_1^{(\ell+1)} + u_2, u_1^{(\ell)}) \\ &\geq \mathcal{J}_1^s(u_1^{(\ell+1)} + u_2, u_1^{(\ell+1)}) = \mathcal{J}(u_1^{(\ell+1)} + u_2), \end{aligned}$$

See also (4.67) and (4.68) below. Since $(\mathcal{J}(u_1^{(\ell)} + u_2))_\ell$ is monotonically decreasing and bounded from below by 0, it is necessarily a convergent sequence. Moreover,

$$\mathcal{J}(u_1^{(\ell)} + u_2) - \mathcal{J}(u_1^{(\ell+1)} + u_2) \geq C \|u_1^{(\ell+1)} - u_1^{(\ell)}\|_{\mathcal{H}}^2,$$

and the latter convergence implies $\|u_1^{(\ell+1)} - u_1^{(\ell)}\|_{\mathcal{H}} \rightarrow 0$.

Step 3. We are left with showing the nonexpansiveness of A . By nonexpansiveness of $S_\alpha^{\psi, V_1, V_2}(\cdot; u_2)$ we obtain

$$\begin{aligned} & \|S_\alpha^{\psi, V_1, V_2}(u_1^1 + \pi_{V_1} T^*(f - Tu_2 - Tu_1^1; u_2) \\ & - S_\alpha^{\psi, V_1, V_2}(u_1^2 + \pi_{V_1} T^*(f - Tu_2 - Tu_1^2; u_2)\|_{\mathcal{H}} \\ & \leq \|u_1^1 + \pi_{V_1} T^*(f - Tu_2 - Tu_1^1) - (u_1^2 + \pi_{V_1} T^*(f - Tu_2 - Tu_1^2)\|_{\mathcal{H}} \\ & = \|(I - \pi_{V_1} T^* T \pi_{V_1})(u_1^1 - u_1^2)\|_{\mathcal{H}} \\ & \leq \|u_1^1 - u_1^2\|_{\mathcal{H}} \end{aligned}$$

In the latter inequality we used once more the fact that $\|T\| < 1$. \square

We do not insist on conditions for strong convergence of the iteration (4.64), which is not a relevant issue, see, e.g., [CW05, DTV07] for a further discussion of this issue. Indeed, the practical realization of (4.56) will never solve completely the subspace minimizations.

Let us conclude this section mentioning that all the results presented here hold symmetrically for the minimization on V_2 , provided that the notation is suitably adjusted.

4.3.4 Convergence of the Sequential Alternating Subspace Minimization

We return to the algorithm (4.56). In the following we denote $u_i = \pi_{V_i} u$ for $i = 1, 2$. Let us express explicitly the algorithm as follows: Pick an initial $V_1 \oplus V_2 \ni u_1^{(0,L)} + u_2^{(0,M)} := u^{(0)} \in \mathcal{H}^\psi$, for example $u^{(0)} = 0$, and iterate

$$\left\{ \begin{array}{l} \left\{ \begin{array}{l} u_1^{(n+1,0)} = u_1^{(n,L)} \\ u_1^{(n+1,\ell+1)} = \operatorname{argmin}_{u_1 \in V_1} \mathcal{J}_1^s(u_1 + u_2^{(n,M)}, u_1^{(n+1,\ell)}) \quad \ell = 0, \dots, L-1 \\ u_2^{(n+1,0)} = u_2^{(n,M)} \\ u_2^{(n+1,m+1)} = \operatorname{argmin}_{u_2 \in V_2} \mathcal{J}_2^s(u_1^{(n+1,L)} + u_2, u_2^{(n+1,m)}) \quad m = 0, \dots, M-1 \\ u^{(n+1)} := u_1^{(n+1,L)} + u_2^{(n+1,M)} \end{array} \right. \end{array} \right. \quad (4.65)$$

Note that we do prescribe a finite number, L and M respectively, of inner iterations for each subspace. In this section we want to prove convergence of the algorithm for any choice of L and M .

Observe that, for $a \in V_i$ and $\|T\| < 1$,

$$\|u_i - a\|_{\mathcal{H}}^2 - \|Tu_i - Ta\|_{\mathcal{H}}^2 \geq C\|u_i - a\|_{\mathcal{H}}^2, \quad (4.66)$$

4.3 Domain Decomposition for TV Minimization

for $C = (1 - \|T\|^2) > 0$. Hence

$$\mathcal{J}(u) = \mathcal{J}_i^s(u, u_i) \leq \mathcal{J}_i^s(u, a), \quad (4.67)$$

and

$$\mathcal{J}_i^s(u, a) - \mathcal{J}_i^s(u, u_i) \geq C\|u_i - a\|_{\mathcal{H}}^2. \quad (4.68)$$

Theorem 4.3.16 (Convergence properties). *The algorithm in (4.65) produces a sequence $(u^{(n)})_{n \in \mathbb{N}}$ in \mathcal{H}^ψ with the following properties:*

- (i) $\mathcal{J}(u^{(n)}) > \mathcal{J}(u^{(n+1)})$ for all $n \in \mathbb{N}$ (unless $u^{(n)} = u^{(n+1)}$);
- (ii) $\lim_{n \rightarrow \infty} \|u^{(n+1)} - u^{(n)}\|_{\mathcal{H}} = 0$;
- (iii) the sequence $(u^{(n)})_{n \in \mathbb{N}}$ has subsequences which converge weakly in \mathcal{H} and in \mathcal{H}^ψ , both endowed with the topology τ^ψ ;
- (iv) if we additionally assume, for simplicity, that $\dim \mathcal{H} < \infty$, $(u^{(n_k)})_{k \in \mathbb{N}}$ is a strongly converging subsequence, and $u^{(\infty)}$ is its limit, then $u^{(\infty)}$ is a minimizer of \mathcal{J} whenever one of the following conditions holds
 - (a) $\psi(u_1^{(\infty)} + \eta_2) + \psi(u_2^{(\infty)} + \eta_1) - \psi(u_1^{(\infty)} + u_2^{(\infty)}) \leq \psi(\eta_1 + \eta_2)$ for all $\eta_i \in V_i$, $i = 1, 2$;
 - (b) ψ is differentiable at $u^{(\infty)}$ with respect to V_i for one $i \in \{1, 2\}$, i.e., there exists $\frac{\partial}{\partial V_i} \psi(u^{(\infty)}) := \zeta_i \in (V_i)^*$ such that
$$\langle \zeta_i, v_i \rangle = \lim_{t \rightarrow 0} \frac{\psi(u_1^{(\infty)} + u_2^{(\infty)} + tv_i) - \psi(u_1^{(\infty)} + u_2^{(\infty)})}{t}, \text{ for all } v_i \in V_i.$$

Proof. Let us first observe that

$$\mathcal{J}(u^{(n)}) = \mathcal{J}_1^s(u_1^{(n)} + u_2^{(n)}, u_1^{(n)}) = \mathcal{J}_1^s(u_1^{(n,L)} + u_2^{(n)}, u_1^{(n+1,0)}).$$

By definition of $u_1^{(n+1,1)}$ and the minimal properties of $u_1^{(n+1,1)}$ in (4.65) we have

$$\mathcal{J}_1^s(u_1^{(n,L)} + u_2^{(n)}, u_1^{(n+1,0)}) \geq \mathcal{J}_1^s(u_1^{(n+1,1)} + u_2^{(n)}, u_1^{(n+1,0)}).$$

From (4.67) we have

$$\mathcal{J}_1^s(u_1^{(n+1,1)} + u_2^{(n)}, u_1^{(n+1,0)}) \geq \mathcal{J}_1^s(u_1^{(n+1,1)} + u_2^{(n)}, u_1^{(n+1,1)}).$$

Putting together these inequalities we obtain

$$\mathcal{J}(u^{(n)}) \geq \mathcal{J}(u_1^{(n+1,1)} + u_2^{(n)})$$

4.3 Domain Decomposition for TV Minimization

In particular, from (4.68) we have

$$\mathcal{J}(u^{(n)}) - \mathcal{J}(u_1^{(n+1,1)} + u_2^{(n)}) \geq C \|u_1^{(n+1,1)} - u_1^{(n+1,0)}\|_{\mathcal{H}}^2.$$

After L steps we conclude with the estimate

$$\mathcal{J}(u^{(n)}) \geq \mathcal{J}(u_1^{(n+1,L)} + u_2^{(n)}),$$

and

$$\mathcal{J}(u^{(n)}) - \mathcal{J}(u_1^{(n+1,L)} + u_2^{(n)}) \geq C \sum_{\ell=0}^{L-1} \|u_1^{(n+1,\ell+1)} - u_1^{(n+1,\ell)}\|_{\mathcal{H}}^2.$$

By definition of $u_2^{(n+1,1)}$ and its minimal properties we have

$$\mathcal{J}(u_1^{(n+1,L)} + u_2^{(n)}) \geq \mathcal{J}_2^s(u_1^{(n+1,L)} + u_2^{(n+1,1)}, u_2^{(n+1,0)}).$$

By similar arguments as above we finally find the decreasing estimate

$$\mathcal{J}(u^{(n)}) \geq \mathcal{J}_2^s(u_1^{(n+1,L)} + u_2^{(n+1,M)}) = \mathcal{J}(u^{(n+1)}), \quad (4.69)$$

and

$$\begin{aligned} & \mathcal{J}(u^{(n)}) - \mathcal{J}(u^{(n+1)}) \\ & \geq C \left(\sum_{\ell=0}^{L-1} \|u_1^{(n+1,\ell+1)} - u_1^{(n+1,\ell)}\|_{\mathcal{H}}^2 + \sum_{m=0}^{M-1} \|u_2^{(n+1,m+1)} - u_2^{(n+1,m)}\|_{\mathcal{H}}^2 \right). \end{aligned} \quad (4.70)$$

From (4.69) we have $\mathcal{J}(u^{(0)}) \geq \mathcal{J}(u^{(n)})$. By the coerciveness condition (C) $(u^{(n)})_{n \in \mathbb{N}}$ is uniformly bounded in \mathcal{H}^ψ , hence there exists a \mathcal{H} -weakly- and τ^ψ -convergent subsequence $(u^{(n_j)})_{j \in \mathbb{N}}$. Let us denote by $u^{(\infty)}$ the weak limit of this subsequence. For simplicity, we rename such a subsequence as $(u^{(n)})_{n \in \mathbb{N}}$. Moreover, since the sequence $(\mathcal{J}(u^{(n)}))_{n \in \mathbb{N}}$ is monotonically decreasing and bounded from below by 0, it is also convergent. From (4.70) and the latter convergence we deduce that

$$\left(\sum_{\ell=0}^{L-1} \|u_1^{(n+1,\ell+1)} - u_1^{(n+1,\ell)}\|_{\mathcal{H}}^2 + \sum_{m=0}^{M-1} \|u_2^{(n+1,m+1)} - u_2^{(n+1,m)}\|_{\mathcal{H}}^2 \right) \rightarrow 0, \quad n \rightarrow \infty. \quad (4.71)$$

In particular, by the standard inequality $(a^2 + b^2) \geq \frac{1}{2}(a+b)^2$ for $a, b > 0$ and the triangle inequality, we have also

$$\|u^{(n)} - u^{(n+1)}\|_{\mathcal{H}} \rightarrow 0, \quad n \rightarrow \infty. \quad (4.72)$$

We would like now to show that the following outer lower semicontinuity holds,

$$0 \in \lim_{n \rightarrow \infty} \partial \mathcal{J}(u^{(n)}) \subset \partial \mathcal{J}(u^{(\infty)}).$$

4.3 Domain Decomposition for TV Minimization

For this we need to assume that \mathcal{H} -weakly-convergence and τ^ψ -convergence do imply strong convergence in \mathcal{H} . This is the case, e.g., when $\dim(\mathcal{H}) < \infty$. The optimality condition for $u_1^{(n+1,L)}$ is equivalent to

$$0 \in u_1^{(n+1,L)} - z_1^{(n+1)} + \alpha \partial_{V_1} \psi(\cdot + u_2^{(n,M)})(u_1^{(n+1,L)}), \quad (4.73)$$

where

$$z_1^{(n+1)} := u_1^{(n+1,L-1)} + \pi_{V_1} T^*(f - Tu_2^{(n,M)} - Tu_1^{(n+1,L-1)}).$$

Analogously we have

$$0 \in u_2^{(n+1,M)} - z_2^{(n+1)} + \alpha \partial_{V_2} \psi(\cdot + u_1^{(n+1,L)})(u_2^{(n+1,M)}), \quad (4.74)$$

where

$$z_2^{(n+1)} := u_2^{(n+1,M-1)} + \pi_{V_2} T^*(f - Tu_1^{(n+1,L)} - Tu_2^{(n+1,M-1)}).$$

Due to the strong convergence of the sequence $u^{(n)}$ and by (4.71) we have the following limits for $n \rightarrow \infty$

$$\begin{aligned} \xi_1^{(n+1)} &:= u_1^{(n+1,L)} - z_1^{(n+1)} \rightarrow \xi_1 := -\pi_{V_1} T^*(f - Tu_2^{(\infty)} - Tu_1^{(\infty)}) \in V_1, \\ \xi_2^{(n+1)} &:= u_2^{(n+1,M)} - z_2^{(n+1)} \rightarrow \xi_2 := -\pi_{V_2} T^*(f - Tu_2^{(\infty)} - Tu_1^{(\infty)}) \in V_2, \end{aligned}$$

and

$$\xi_1^{(n+1)} + \xi_2^{(n+1)} \rightarrow \xi := T^*(Tu^{(\infty)} - f).$$

Moreover, we have

$$-\frac{1}{\alpha} \xi_1^{(n+1)} \in \partial_{V_1} \psi(\cdot + u_2^{(n,M)})(u_1^{(n+1,L)}),$$

meaning that

$$\left\langle -\frac{1}{\alpha} \xi_1^{(n+1)}, \eta_1 - u_1^{(n+1,L)} \right\rangle + \psi(u_1^{(n+1,L)} + u_2^{(n,M)}) \leq \psi(\eta_1 + u_2^{(n,M)}), \quad \text{for all } \eta_1 \in V_1.$$

Analogously we have

$$\left\langle -\frac{1}{\alpha} \xi_2^{(n+1)}, \eta_2 - u_2^{(n+1,M)} \right\rangle + \psi(u_1^{(n+1,L)} + u_2^{(n+1,M)}) \leq \psi(\eta_2 + u_1^{(n+1,L)}), \quad \text{for all } \eta_2 \in V_2.$$

By taking the limits for $n \rightarrow \infty$ and by (4.71) we obtain

$$\left\langle -\frac{1}{\alpha} \xi_1, \eta_1 - u_1^{(\infty)} \right\rangle + \psi(u_1^{(\infty)}) \leq \psi(\eta_1 + u_2^{(\infty)}), \quad \text{for all } \eta_1 \in V_1. \quad (4.75)$$

$$\left\langle -\frac{1}{\alpha} \xi_2, \eta_2 - u_2^{(\infty)} \right\rangle + \psi(u_1^{(\infty)}) \leq \psi(\eta_2 + u_1^{(\infty)}), \quad \text{for all } \eta_2 \in V_2. \quad (4.76)$$

4.3 Domain Decomposition for TV Minimization

These latter conditions are rewritten in vector form as

$$0 \in \begin{pmatrix} \xi_1 \\ \xi_2 \end{pmatrix} + \alpha \left(\partial_{V_1} \psi(\cdot + u_2^{(\infty)}) (u_1^{(\infty)}) \times \partial_{V_2} \psi(\cdot + u_1^{(\infty)}) (u_2^{(\infty)}) \right). \quad (4.77)$$

Observe now that

$$2\xi + 2\alpha \partial_{\mathcal{H}} \psi(u^{(\infty)}) = 2T^*(Tu^{(\infty)} - f) + 2\alpha \partial_{\mathcal{H}} \psi(u^{(\infty)}) = \partial \mathcal{J}(u^{(\infty)}).$$

If $0 \in \xi + \alpha \partial_{\mathcal{H}} \psi(u^{(\infty)})$ then we would have the required minimality condition. While the inclusion

$$\partial_{\mathcal{H}} \psi(u^{(\infty)}) \subset \partial_{V_1} \psi(\cdot + u_2^{(\infty)}) (u_1^{(\infty)}) \times \partial_{V_2} \psi(\cdot + u_1^{(\infty)}) (u_2^{(\infty)}),$$

easily follows from the definition of a subdifferential, the converse inclusion, which would imply from (4.77) the desired minimality condition, does not hold in general. Thus, we show the converse inclusion under one of the following two conditions:

- (a) $\psi(u_1^{(\infty)} + \eta_2) + \psi(u_2^{(\infty)} + \eta_1) - \psi(u_1^{(\infty)} + u_2^{(\infty)}) \leq \psi(\eta_1 + \eta_2)$ for all $\eta_i \in V_i$, $i = 1, 2$;
- (b) ψ is differentiable at $u^{(\infty)}$ with respect to V_i for a single $i \in \{1, 2\}$, i.e., there exists $\frac{\partial}{\partial V_i} \psi(u^{(\infty)}) := \zeta_i \in (V_i)^*$ such that

$$\langle \zeta_i, v_i \rangle = \lim_{t \rightarrow 0} \frac{\psi(u_1^{(\infty)} + u_2^{(\infty)} + tv_i) - \psi(u_1^{(\infty)} + u_2^{(\infty)})}{t}, \text{ for all } v_i \in V_i.$$

Let us start with condition (a). We want to show that

$$\left\langle -\frac{1}{\alpha} \xi, \eta - u^{(\infty)} \right\rangle + \psi(u^{(\infty)}) \leq \psi(\eta), \quad \text{for all } \eta \in \mathcal{H},$$

or, equivalently, that

$$\left\langle -\frac{1}{\alpha} \xi_1, \eta_1 - u_1^{(\infty)} \right\rangle + \left\langle -\frac{1}{\alpha} \xi_2, \eta_2 - u_2^{(\infty)} \right\rangle + \psi(u_1^{(\infty)} + u_2^{(\infty)}) \leq \psi(\eta_1 + \eta_2), \quad \text{for all } \eta_i \in V_i,$$

By the differential inclusions (4.75) and (4.76) we have

$$\left\langle -\frac{1}{\alpha} \xi_1, \eta_1 - u_1^{(\infty)} \right\rangle + \left\langle -\frac{1}{\alpha} \xi_2, \eta_2 - u_2^{(\infty)} \right\rangle + 2\psi(u_1^{(\infty)} + u_2^{(\infty)}) \leq \psi(u_1^{(\infty)} + \eta_2) + \psi(u_2^{(\infty)} + \eta_1),$$

for all $\eta_i \in V_i$, hence

$$\begin{aligned} & \left\langle -\frac{1}{\alpha} \xi_1, \eta_1 - u_1^{(\infty)} \right\rangle + \left\langle -\frac{1}{\alpha} \xi_2, \eta_2 - u_2^{(\infty)} \right\rangle + \psi(u_1^{(\infty)} + u_2^{(\infty)}) \\ & \leq \psi(u_1^{(\infty)} + \eta_2) + \psi(u_2^{(\infty)} + \eta_1) - \psi(u_1^{(\infty)} + u_2^{(\infty)}), \quad \text{for all } \eta_i \in V_i. \end{aligned}$$

4.3 Domain Decomposition for TV Minimization

An application of condition (a) concludes the proof of the required differential inclusion.

Let us now show the inclusion under the assumption of condition (b). Without loss of generality, we assume that ψ is differentiable at $u^{(\infty)}$ with respect to V_2 . First of all we define $\tilde{\psi}(u_1, u_2) := \psi(u_1 + u_2)$. Since ψ is convex, by an application of [RW98, Corollary 10.11] we have

$$\begin{aligned}\partial_{V_1} \psi(\cdot + u_2)(u_1) &\simeq \partial_{u_1} \tilde{\psi}(u_1, u_2) \\ &= \{\zeta_1 \in V_1^* : \exists \zeta_2 \in V_2^* : (\zeta_1, \zeta_2)^T \in \partial \tilde{\psi}(u_1, u_2) \simeq \partial_{\mathcal{H}} \psi(u_1 + u_2)\}.\end{aligned}$$

Since ψ is differentiable at $u^{(\infty)}$ with respect to V_2 , for any $(\zeta_1, \zeta_2)^T \in \partial \tilde{\psi}(u_1, u_2) \simeq \partial_{\mathcal{H}} \psi(u_1 + u_2)$ we have necessarily $\zeta_2 = \frac{\partial}{\partial V_2} \psi(u^{(\infty)})$ as the unique member of $\partial_{V_2} \psi(\cdot + u_1^{(\infty)})(u_2^{(\infty)})$. Hence, the following inclusion must also hold

$$\begin{aligned}0 &\in \left(\begin{array}{c} \xi_1 \\ \xi_2 \end{array} \right) + \alpha \left(\partial_{V_1} \psi(\cdot + u_2^{(\infty)})(u_1^{(\infty)}) \times \partial_{V_2} \psi(\cdot + u_1^{(\infty)})(u_2^{(\infty)}) \right) \\ &\subset \left(\begin{array}{c} \xi_1 \\ \xi_2 \end{array} \right) + \alpha \partial_{V_1 \times V_2} \tilde{\psi}(u_1, u_2) \\ &\simeq \xi + \alpha \partial_{\mathcal{H}} \psi(u^{(\infty)}).\end{aligned}\quad \square$$

Remark 4.3.17. Observe that, by choosing $\eta_1 = \eta_2 = 0$, condition (a) and $(\Psi 2)$ for the case $\lambda = 0$ imply that

$$\psi(u_1^{(\infty)}) + \psi(u_2^{(\infty)}) \leq \psi(u_1^{(\infty)} + u_2^{(\infty)})$$

The sublinearity $(\Psi 1)$ finally implies the splitting

$$\psi(u_1^{(\infty)}) + \psi(u_2^{(\infty)}) = \psi(u_1^{(\infty)} + u_2^{(\infty)})$$

Conversely, if $\psi(v_1) + \psi(v_2) = \psi(v_1 + v_2)$ for all $v_i \in V_i$, $i = 1, 2$, then condition (a) easily follows. As previously discussed, this latter splitting condition holds only in special cases. Also condition (b) is not in practice always verified, cf. the numerical examples for ℓ_1 minimization in [FS07]. Hence, we can affirm that in general we cannot expect convergence of the algorithm to minimizers of \mathcal{J} , although it certainly converges to points for which \mathcal{J} is smaller than the starting choice $\mathcal{J}(u^{(0)})$. However, as we will show in the numerical experiments related to total variation minimization (Sections 4.3.6 and 4.3.7), the computed limit can be very close to the expected minimizer.

4.3.5 A Parallel Alternating Subspace Minimization and its Convergence

The most immediate modification to (4.65) is provided by substituting $u_1^{(n,L)}$ instead of $u_1^{(n+1,L)}$ in the second iteration, producing the following parallel algorithm:

$$\left\{ \begin{array}{l} \left\{ \begin{array}{l} u_1^{(n+1,0)} = u_1^{(n,L)} \\ u_1^{(n+1,\ell+1)} = \operatorname{argmin}_{u_1 \in V_1} \mathcal{J}_1^s(u_1 + u_2^{(n,M)}, u_1^{(n+1,\ell)}) \quad \ell = 0, \dots, L-1 \end{array} \right. \\ \left\{ \begin{array}{l} u_2^{(n+1,0)} = u_2^{(n,M)} \\ u_2^{(n+1,m+1)} = \operatorname{argmin}_{u_2 \in V_2} \mathcal{J}_2^s(u_1^{(n,L)} + u_2, u_2^{(n+1,m)}) \quad m = 0, \dots, M-1 \end{array} \right. \\ u^{(n+1)} := u_1^{(n+1,L)} + u_2^{(n+1,M)}. \end{array} \right. \quad (4.78)$$

Unfortunately, this modification violates the monotonicity property $\mathcal{J}(u^{(n)}) \geq \mathcal{J}(u^{(n+1)})$ and the overall algorithm does not converge in general. In order to preserve the monotonicity of the iteration with respect to \mathcal{J} a simple trick can be applied, i.e., modifying $u^{(n+1)} := u_1^{(n+1,L)} + u_2^{(n+1,M)}$ by the average of the current iteration and the previous one. This leads to the following parallel algorithm:

$$\left\{ \begin{array}{l} \left\{ \begin{array}{l} u_1^{(n+1,0)} = u_1^{(n,L)} \\ u_1^{(n+1,\ell+1)} = \operatorname{argmin}_{u_1 \in V_1} \mathcal{J}_1^s(u_1 + u_2^{(n,M)}, u_1^{(n+1,\ell)}) \quad \ell = 0, \dots, L-1 \end{array} \right. \\ \left\{ \begin{array}{l} u_2^{(n+1,0)} = u_2^{(n,M)} \\ u_2^{(n+1,m+1)} = \operatorname{argmin}_{u_2 \in V_2} \mathcal{J}_2^s(u_1^{(n,L)} + u_2, u_2^{(n+1,m)}) \quad m = 0, \dots, M-1 \end{array} \right. \\ u^{(n+1)} := \frac{u_1^{(n+1,L)} + u_2^{(n+1,M)} + u^{(n)}}{2}. \end{array} \right. \quad (4.79)$$

In this section we prove similar convergence properties of this algorithm to that of (4.65).

Theorem 4.3.18 (Convergence properties). *The algorithm in (4.79) produces a sequence $(u^{(n)})_{n \in \mathbb{N}}$ in \mathcal{H}^ψ with the following properties:*

- (i) $\mathcal{J}(u^{(n)}) > \mathcal{J}(u^{(n+1)})$ for all $n \in \mathbb{N}$ (unless $u^{(n)} = u^{(n+1)}$);
- (ii) $\lim_{n \rightarrow \infty} \|u^{(n+1)} - u^{(n)}\|_{\mathcal{H}} = 0$;
- (iii) the sequence $(u^{(n)})_{n \in \mathbb{N}}$ has subsequences which converge weakly in \mathcal{H} and in \mathcal{H}^ψ , both endowed with the topology τ^ψ ;
- (iv) if we additionally assume that $\dim \mathcal{H} < \infty$, $(u^{(n_k)})_{k \in \mathbb{N}}$ is a strongly converging subsequence, and $u^{(\infty)}$ is its limit, then $u^{(\infty)}$ is a minimizer of \mathcal{J} whenever one of the following conditions holds

4.3 Domain Decomposition for TV Minimization

(a) $\psi(u_1^{(\infty)} + \eta_2) + \psi(u_2^{(\infty)} + \eta_1) - \psi(u_1^{(\infty)} + u_2^{(\infty)}) \leq \psi(\eta_1 + \eta_2)$ for all $\eta_i \in V_i$,
 $i = 1, 2$;

(b) ψ is differentiable at $u^{(\infty)}$ with respect to V_i for one $i \in \{1, 2\}$, i.e., there exists $\frac{\partial}{\partial V_i} \psi(u^{(\infty)}) := \zeta_i \in (V_i)^*$ such that

$$\langle \zeta_i, v_i \rangle = \lim_{t \rightarrow 0} \frac{\psi(u_1^{(\infty)} + u_2^{(\infty)} + tv_i) - \psi(u_1^{(\infty)} + u_2^{(\infty)})}{t}, \text{ for all } v_i \in V_i.$$

Proof. With the same argument as in the proof of Theorem 4.3.16, we obtain

$$\mathcal{J}(u^{(n)}) - \mathcal{J}(u_1^{(n+1,L)} + u_2^{(n)}) \geq C \sum_{\ell=0}^{L-1} \|u_1^{(n+1,\ell+1)} - u_1^{(n+1,\ell)}\|_{\mathcal{H}}^2.$$

and

$$\mathcal{J}(u^{(n)}) - \mathcal{J}(u_1^{(n)} + u_2^{(n+1,M)}) \geq C \sum_{m=0}^{M-1} \|u_2^{(n+1,m+1)} - u_2^{(n+1,m)}\|_{\mathcal{H}}^2.$$

Hence, by summing and halving

$$\begin{aligned} & \mathcal{J}(u^{(n)}) - \frac{1}{2}(\mathcal{J}(u_1^{(n+1,L)} + u_2^{(n)}) + \mathcal{J}(u_1^{(n)} + u_2^{(n+1,M)})) \\ & \geq \frac{C}{2} \left(\sum_{\ell=0}^{L-1} \|u_1^{(n+1,\ell+1)} - u_1^{(n+1,\ell)}\|_{\mathcal{H}}^2 + \sum_{m=0}^{M-1} \|u_2^{(n+1,m+1)} - u_2^{(n+1,m)}\|_{\mathcal{H}}^2 \right). \end{aligned}$$

By convexity we have

$$\begin{aligned} \|Tu^{(n+1)} - f\|_{\mathcal{H}}^2 &= \left\| T \left(\frac{(u_1^{(n+1,L)} + u_2^{(n+1,M)}) + u^{(n)}}{2} \right) - f \right\|_{\mathcal{H}}^2 \\ &\leq \frac{1}{2} \|T(u_1^{(n+1,L)} + u_2^{(n)}) - f\|_{\mathcal{H}}^2 + \frac{1}{2} \|T(u_1^{(n)} + u_2^{(n+1,M)}) - f\|_{\mathcal{H}}^2. \end{aligned}$$

Moreover, by sublinearity ($\Psi 1$) and 1-homogeneity ($\Psi 2$) we have

$$\psi(u^{(n+1)}) \leq \frac{1}{2} (\psi(u_1^{(n+1,L)} + u_2^{(n)}) + \psi(u_1^{(n)} + u_2^{(n+1,M)}))$$

By the last two inequalities we immediately show that

$$\mathcal{J}(u^{(n+1)}) \leq \frac{1}{2} (\mathcal{J}(u_1^{(n+1,L)} + u_2^{(n)}) + \mathcal{J}(u_1^{(n)} + u_2^{(n+1,M)})),$$

hence

$$\begin{aligned} & \mathcal{J}(u^{(n)}) - \mathcal{J}(u^{(n+1)}) \\ & \geq \frac{C}{2} \left(\sum_{\ell=0}^{L-1} \|u_1^{(n+1,\ell+1)} - u_1^{(n+1,\ell)}\|_{\mathcal{H}}^2 + \sum_{\ell=0}^{M-1} \|u_2^{(n+1,\ell+1)} - u_2^{(n+1,\ell)}\|_{\mathcal{H}}^2 \right) \geq 0. \quad (4.80) \end{aligned}$$

4.3 Domain Decomposition for TV Minimization

Since the sequence $(\mathcal{J}(u^{(n)}))_{n \in \mathbb{N}}$ is monotonically decreasing and bounded from below by 0, it is also convergent. From (4.80) and the latter convergence we deduce

$$\left(\sum_{\ell=0}^{L-1} \|u_1^{(n+1,\ell+1)} - u_1^{(n+1,\ell)}\|_{\mathcal{H}}^2 + \sum_{m=0}^{M-1} \|u_2^{(n+1,m+1)} - u_2^{(n+1,m)}\|_{\mathcal{H}}^2 \right) \rightarrow 0, \quad n \rightarrow \infty. \quad (4.81)$$

In particular, by the standard inequality $(a^2 + b^2) \geq \frac{1}{2}(a+b)^2$ for $a, b > 0$ and the triangle inequality, we have also

$$\begin{aligned} \sum_{\ell=0}^{L-1} \|u_1^{(n+1,\ell+1)} - u_1^{(n+1,\ell)}\|_{\mathcal{H}}^2 &\geq C'' \left(\sum_{\ell=0}^{L-1} \|u_1^{(n+1,\ell+1)} - u_1^{(n+1,\ell)}\|_{\mathcal{H}} \right)^2 \\ &\geq C'' \|u_1^{(n+1,L)} - u_1^{(n)}\|_{\mathcal{H}}^2 \\ &= C'' \|u_1^{(n+1,L)} + u_1^{(n)} - 2u_1^{(n)}\|_{\mathcal{H}}^2. \end{aligned}$$

Analogously we have

$$\sum_{\ell=0}^{M-1} \|u_2^{(n+1,\ell+1)} - u_2^{(n+1,\ell)}\|_{\mathcal{H}}^2 \geq C'' \|u_2^{(n+1,M)} + u_2^{(n)} - 2u_2^{(n)}\|_{\mathcal{H}}^2.$$

By denoting $C'' = \frac{1}{2}C'''$ we obtain

$$\begin{aligned} &\frac{C}{2} \left(\sum_{\ell=0}^{L-1} \|u_1^{(n+1,\ell+1)} - u_1^{(n+1,\ell)}\|_{\mathcal{H}}^2 + \sum_{\ell=0}^{M-1} \|u_2^{(n+1,\ell+1)} - u_2^{(n+1,\ell)}\|_{\mathcal{H}}^2 \right) \\ &\geq \frac{CC'''}{4} \|u_1^{(n+1,L)} + u_2^{(n+1,M)} + u^{(n)} - 2u^{(n)}\|_{\mathcal{H}}^2 \\ &\geq CC''' \|u^{(n+1)} - u^{(n)}\|_{\mathcal{H}}^2. \end{aligned}$$

Therefore, we finally have

$$\|u^{(n)} - u^{(n+1)}\|_{\mathcal{H}} \rightarrow 0, \quad n \rightarrow \infty. \quad (4.82)$$

The rest of the proof follows by analogous arguments to that of Theorem 4.3.16. \square

4.3.6 Domain Decomposition for TV-L²Minimization

In this section we present the application of the illustrated theory and algorithms to the domain decomposition for total variation minimization. In the following we consider the minimization of the functional \mathcal{J} in the setting of Example 4.3.1.1. Specifically, let $\Omega \subset \mathbb{R}^d$, for $d = 1, 2$, be a bounded open set with Lipschitz boundary. We are

4.3 Domain Decomposition for TV Minimization

interested in the case when $\mathcal{H} = L^2(\Omega)$, $\mathcal{H}^\psi = BV(\Omega)$ and $\psi(u) = V(u, \Omega)$. Then the domain decomposition $\Omega = \Omega_1 \cup \Omega_2$, as described in Examples 4.3.2.1, induces the space splitting into $V_i := \{u \in L^2(\Omega) : \text{supp}(u) \subset \Omega_i\}$, and $V_i^\psi = BV(\Omega) \cap V_i$, $i = 1, 2$. In particular, we can consider multiple subspaces, since the algorithms and their analysis presented in the previous sections can be easily generalized to these cases, see [Fo07, Section 6]. As before $u_{\Omega_i} = \pi_{V_i}(u) = 1_{\Omega_i} u$ is the orthogonal projection onto V_i .

To exemplify the kind of difficulties one may encounter in the numerical treatment of the interfaces $\partial\Omega_i \cap \partial\Omega_j$, we present first an approach based on the direct discretization of the subdifferential of \mathcal{J} in this setting. We show that this method can work properly in many cases, but it fails in others, even for simple 1D examples, due to the occurrence of exceptions which cannot be captured by this formulation. Instead of insisting on dealing with these exceptions and strengthening the formulation, we show that the general theory and algorithms presented previously work properly and deal well with interfaces for both $d = 1, 2$.

The “Naive” Direct Approach

In light of (4.55), the first subiteration in (4.56) is given by

$$u_1^{(n+1)} \approx \operatorname{argmin}_{v_1 \in V_1} \|T(v_1 + u_2^{(n)}) - f\|_{L^2(\Omega)}^2 + 2\alpha(|D(v_1)|(\Omega_1) + \int_{\partial\Omega_1 \cap \partial\Omega_2} |v_1^+ - u_2^{(n)-}| d\mathcal{H}_{d-1}).$$

We would like to describe the conditions that characterize subdifferentials of functionals of the type

$$\Gamma(u) = |D(u)|(\Omega) + \underbrace{\int_\theta |u^+ - z| d\mathcal{H}_{d-1}}_{\text{interface condition}},$$

where $\theta \subset \partial\Omega$, in order to handle the boundary conditions that are imposed at the interface. Since we are interested in emphasizing the difficulties of this approach, we do not insist on the details of a rigorous derivation of these conditions, and we limit ourselves to mentioning the main facts.

It is well known [Ve01, Proposition 4.1] that, if no interface condition is present, $\xi \in$

4.3 Domain Decomposition for TV Minimization

$\partial|D(\cdot)|(\Omega)(u)$ implies that

$$\begin{cases} \xi = -\nabla \cdot \left(\frac{\nabla u}{|\nabla u|} \right) & \text{in } \Omega \\ \frac{\nabla u}{|\nabla u|} \cdot \nu = 0 & \text{on } \partial\Omega. \end{cases}$$

The previous conditions fall short of fully characterizing $\xi \in \partial|D(\cdot)|(\Omega)(u)$, additional conditions would be required [AK06, Ve01], but the latter are, unfortunately, hard to implement numerically. This is the source of the failures of this direct method. The presence of the interface further modifies and aggreviates this situation and for $\partial\Gamma(u) \neq \emptyset$ we need to enforce

$$\int_{\partial\Omega} \frac{\nabla u}{|\nabla u|} \cdot \nu w \, d\mathcal{H}_{d-1} + \lim_{s \rightarrow 0} \left(\int_{\theta} \frac{|(u + ws)^+ - z| - |u^+ - z|}{s} \, d\mathcal{H}_{d-1} \right) \geq 0,$$

$\forall w \in C^\infty(\bar{\Omega})$. The latter condition is implied by the following natural boundary conditions:

$$\begin{cases} \frac{\nabla u}{|\nabla u|} \cdot \nu = 0 & \text{on } \partial\Omega \setminus \theta, \\ -\frac{\nabla u}{|\nabla u|} \cdot \nu \in \partial| \cdot |(u^+ - z) & \text{on } \theta. \end{cases} \quad (4.83)$$

Note that the conditions above are again not sufficient to characterize elements in the subdifferential of Γ .

Implementation of the subdifferential approach in TV-L²interpolation Let $D \subset \Omega \subset \mathbb{R}^d$ be open and bounded domains with Lipschitz boundaries. We assume that a function $f \in L^2(\Omega)$ is given only on $\Omega \setminus D$, possibly with noise disturbance. The problem is to reconstruct a function u in the damaged domain $D \subset \Omega$ which nearly coincides with f on $\Omega \setminus D$. In 1D this is a classical interpolation problem, while in 2D it has assumed the name of “inpainting” due to its applications in image restoration. TV-interpolation/inpainting with L^2 fidelity is solved by the minimization of the functional

$$J(u) = \|1_{\Omega \setminus D}(u - f)\|_{L^2(\Omega)}^2 + 2\alpha|D(u)|(\Omega), \quad (4.84)$$

where $1_{\Omega \setminus D}$ denotes the indicator function of $\Omega \setminus D$. Hence, in this case T is the multiplier operator $Tu = 1_{\Omega \setminus D}u$. We consider in the sequel the problem for $d = 1$,

4.3 Domain Decomposition for TV Minimization

so that $\Omega = (a, b)$ is an interval. We may want to minimize (4.84) iteratively by a subgradient descent method,

$$\begin{aligned} \frac{u^{(n+1)} - u^{(n)}}{\tau} &= -\nabla \cdot \left(\frac{\nabla u^{(n+1)}}{|\nabla u^{(n)}|} \right) + 2\lambda(u^{(n)} - f) && \text{in } \Omega \\ \frac{1}{|\nabla u^{(n)}|} \frac{\partial u^{(n+1)}}{\partial n} &= 0 && \text{on } \partial\Omega, \end{aligned} \quad (4.85)$$

where

$$\lambda(x) = \begin{cases} \lambda_0 = \frac{1}{4\alpha} & \Omega \setminus D \\ 0 & D. \end{cases}$$

We can also attempt the minimization by the following domain decomposition algorithm: We split Ω into two intervals $\Omega = \Omega_1 \cup \Omega_2$ and define two alternating minimizations on Ω_1 and Ω_2 with the interface $\theta = \partial\Omega_1 \cap \partial\Omega_2$

$$\begin{aligned} \frac{u_1^{(n+1)} - u_1^{(n)}}{\tau} &= -\nabla \cdot \left(\frac{\nabla u_1^{(n+1)}}{|\nabla u_1^{(n)}|} \right) + 2\lambda_1(u_1^{(n)} - f) && \text{in } \Omega_1 \\ \frac{1}{|\nabla u_1^{(n)}|} \frac{\partial u_1^{(n+1)}}{\partial n} &= 0 && \text{on } \partial\Omega_1 \setminus \theta \\ -\frac{1}{|\nabla u_1^{(n)}|} \frac{\partial u_1^{(n+1)}}{\partial n} &\in \partial |\cdot| (u_1^{(n+1)+} - u_2^{(n)-}) && \text{on } \theta, \end{aligned}$$

and

$$\begin{aligned} \frac{u_2^{(n+1)} - u_2^{(n)}}{\tau} &= -\nabla \cdot \left(\frac{\nabla u_2^{(n+1)}}{|\nabla u_2^{(n)}|} \right) + 2\lambda_2(u_2^{(n)} - f) && \text{in } \Omega_2 \\ \frac{1}{|\nabla u_2^{(n)}|} \frac{\partial u_2^{(n+1)}}{\partial n} &= 0 && \text{on } \partial\Omega_2 \setminus \theta \\ \frac{1}{|\nabla u_2^{(n)}|} \frac{\partial u_2^{(n+1)}}{\partial n} &\in \partial |\cdot| (u_2^{(n+1)+} - u_1^{(n+1)-}) && \text{on } \theta. \end{aligned}$$

In this setting u_i denotes the restriction of $u \in BV(\Omega)$ to Ω_i . The fitting parameter λ is also split accordingly into λ_1 and λ_2 on Ω_1 and Ω_2 respectively. Note that we enforced the interface conditions (4.83), with the hope to match correctly the solution at the internal boundaries.

The discretization in space is done by finite differences. We only explain the details for the first subproblem on Ω_1 because the procedure is analogous for the second one.

4.3 Domain Decomposition for TV Minimization

Let $i = 1, \dots, N$ denote the space nodes supported in Ω_1 . We let $h = \frac{b-a}{N}$ and $u(i) := u(ih)$. The gradient and the divergence operator are discretized by backward differences and forward differences respectively,

$$\begin{aligned}\nabla u(i) &= \frac{1}{h}(u(i) - u(i-1)) \\ \nabla \cdot u(i) &= \frac{1}{h}(u(i+1) - u(i)) \\ |\nabla u|(i) &= \sqrt{\epsilon^2 + \frac{1}{h^2}(u(i) - u(i-1))^2},\end{aligned}$$

for $i = 2, \dots, N-1$ and $\epsilon > 0$. Note that we have replaced the total variation $|\nabla u|$ here by its regularized form $\sqrt{\epsilon^2 + |\nabla u|^2}$. The discretized equation on Ω_1 turns out to be

$$u_1^{(n+1)}(i) = u_1^{(n)}(i) + 2\tau\lambda(i)(u_1^{(n)}(i) - f(i)) + \frac{\tau}{h^2} \left(\frac{u_1^{(n+1)}(i+1) - u_1^{(n+1)}(i)}{c_1^n(i+1)} - \frac{u_1^{(n+1)}(i) - u_1^{(n+1)}(i-1)}{c_1^n(i)} \right),$$

with $c_1^n(i) = \sqrt{\epsilon^2 + (u_1^{(n)}(i) - u_1^{(n)}(i-1))^2/h^2}$ and $i = 2, \dots, N-1$. The Neumann boundary conditions on the external portion of the boundary are enforced by

$$\frac{1}{c_1^n(1)}u_1(1) = \frac{1}{c_2^n(2)}u_1(2).$$

The interface conditions on the internal boundaries are computed by solving the following subdifferential inclusion

$$-(u_1^{(n+1)}(N) - u_1^{(n+1)}(N-1)) \in c_1^n(N) h \cdot \partial| \cdot |(u_2^{(n)}(N) - u_1^{(n+1)}(N)).$$

For the solution of this subdifferential inclusion we recall that the soft-thresholding operator $u = S_\alpha(x)$ that has been defined in (4.54) provides the unique solution of the subdifferential inclusion $0 \in (u - x) + \alpha \partial| \cdot |(u)$. We reformulate our subdifferential inclusion as

$$0 \in \left[v - (u_2^{(n)}(N) - u_1^{(n+1)}(N-1)) \right] + c_1^n(N)h \cdot \partial| \cdot |(v),$$

with $v := u_2^{(n)}(N) - u_1^{(n+1)}(N)$ and get

$$v = S_{c_1^n(N)h}(u_2^{(n)}(N) - u_1^{(n+1)}(N-1)).$$

4.3 Domain Decomposition for TV Minimization

Therefore the interface condition on θ reads $u_1^{(n+1)}(N) = u_2^{(n)}(N) - v$.

In the left column of Figure 4.10 three one dimensional signals are considered. The right column shows the result of the application of the domain decomposition method for total variation minimization described above. The support of the signals is split into two intervals. The interface developed by the two intervals is marked by a red dot. In all three examples we fixed $\lambda_0 = 1$ and $\tau = 1/2$. The first example 4.10(a)-4.10(b) shows a step function which has its step directly at the interface of the two intervals. The total variation minimization (4.85) is applied with $D = \emptyset$. This example confirms that jumps are preserved at the interface of the two domains. The second and third example 4.10(c)-4.10(f) present the behavior of the algorithm when interpolation across the interface is performed, i.e., $D \neq \emptyset$. In the example 4.10(c)-4.10(d) the computation at the interface is correctly performed. But the computation at the interface clearly fails in the last example 4.10(e)-4.10(f), compare the following remark.

Remark 4.3.19. *Evaluating the soft thresholding operator at $u_2^{(n)}(N) - u_1^{(n+1)}(N - 1)$ implies that we are treating implicitly the computation of $u_1^{(n+1)}$ at the interface. Namely, the interface condition can be read as*

$$u_1^{(n+1)}(N) = u_2^{(n)}(N) - \Theta^{(n+1)} \cdot [u_2^{(n)}(N) - u_1^{(n+1)}(N - 1) \\ - \operatorname{sgn}(u_2^{(n)}(N) - u_1^{(n+1)}(N - 1)) \cdot c_1^{(n)}(N)h],$$

where

$$\Theta^{(n+1)} = \begin{cases} 1, & |u_2^{(n)}(N) - u_1^{(n+1)}(N - 1)| - c_1^{(n)}(N)h > 0 \\ 0, & \text{otherwise.} \end{cases}$$

The solution of the implicit problem is not immediate and one may prefer to modify the situation in order to obtain an explicit formulation by computing $S_{c_1^n(N)h}(u_2^{(n)}(N) - u_1^{(n)}(N - 1))$ instead of $S_{c_1^n(N)h}(u_2^{(n)}(N) - u_1^{(n+1)}(N - 1))$. The problem here is that, with this discretization, we cannot capture differences in the steepness of u_1 and u_2 at the interface because $u_1^{(n)}(N) = u_2^{(n)}(N)$ for all n . Indeed the condition $|u_2^{(n)}(N) - u_1^{(n)}(N - 1)| - c_1^{(n)}(N)h > 0$ is never satisfied and the interface becomes always a Dirichlet boundary condition. Even if we change the computation of $c_1^{(n)}(N)$ from

$$\sqrt{\epsilon^2 + (u_1^{(n)}(N) - u_1^{(n)}(N - 1))^2/h^2}$$

to a forward difference

$$\sqrt{\epsilon^2 + (u_1^{(n)}(N + 1) - u_1^{(n)}(N))^2/h^2}$$

4.3 Domain Decomposition for TV Minimization

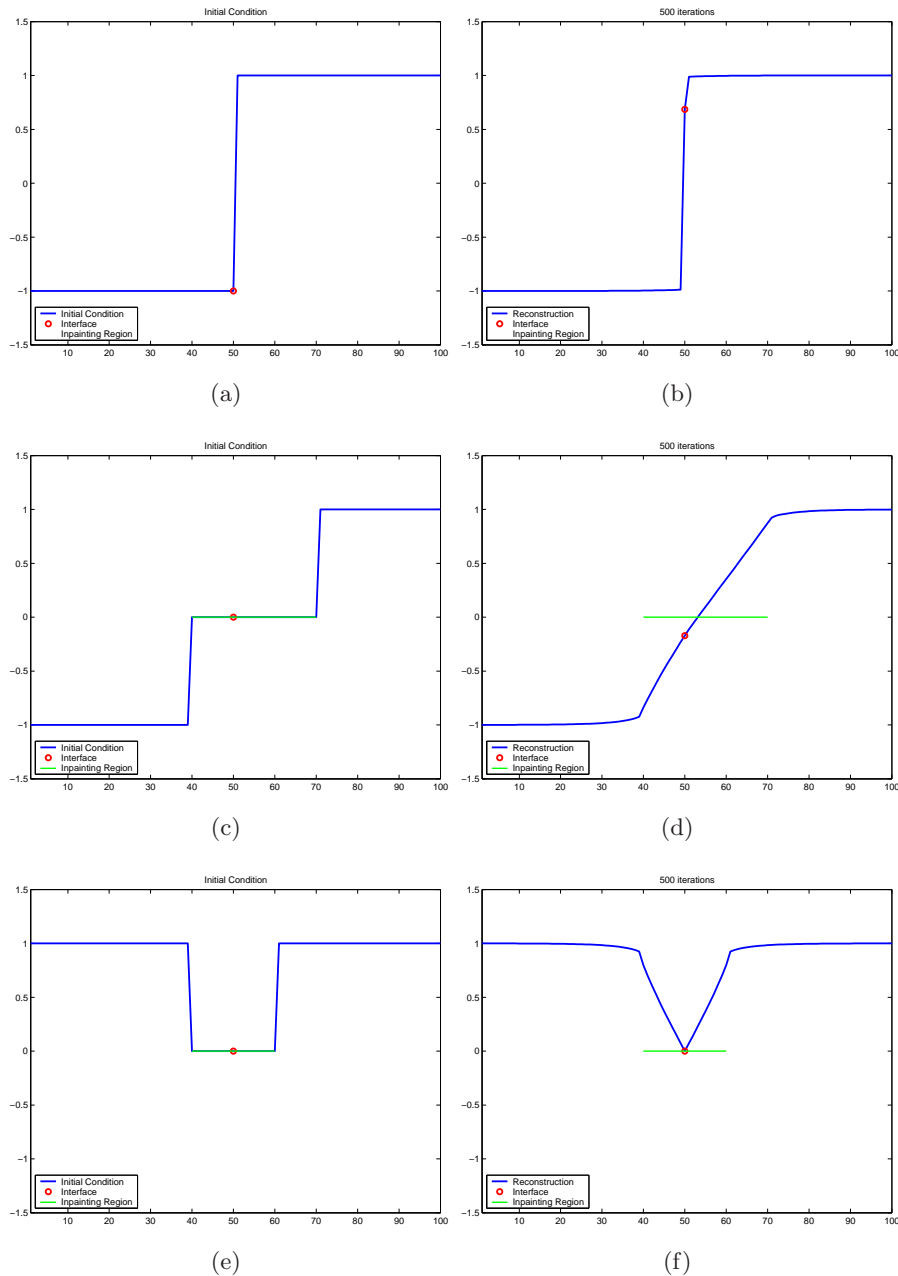


Figure 4.10: Examples of TV-L²inpainting in 1D where the domain was split in two.
(a)-(f): $\lambda = 1$ and $\tau = 1/2$

(as it is indeed done in the numerical examples presented in Figure (4.10)) the method fails when the gradients are equal in absolute value on the left and the right side of the

interface.

We do not insist on trying to capture heuristically all the possible exceptions. We can expect that this approach to the problem may become even more deficient and more complicated to handle in 2D. Instead, we want to develop an algorithm in the spirit of (4.53) which allows to deal with the problem in a transparent way.

The Novel Approach Based on Subspace Corrections and Oblique Thresholding

We want to implement algorithm (4.65) for the minimization of \mathcal{J} . To solve its subiterations we compute the minimizer by means of oblique thresholding. Denote $u_2 = u_2^{(n,M)}$, $u_1 = u_1^{(n+1,\ell+1)}$, and $z = u_1^{(n+1,\ell)} + \pi_{V_1} T^*(f - Tu_2 - Tu_1^{(n+1,\ell)})$. We would like to compute the minimizer

$$u_1 = \operatorname{argmin}_{u \in V_1} \|u - z\|_{L^2(\Omega)}^2 + 2\alpha|D(u + u_2)|(\Omega)$$

by

$$u_1 = (I - \mathbb{P}_{\alpha K_{|D(\cdot)|(\Omega)}})(z + u_2 - \eta) - u_2 = \mathbb{S}_\alpha^{|D(\cdot)|(\Omega)}(z + u_2 - \eta) - u_2,$$

for any $\eta \in V_2$. It is known [Ch04] that $K_{|D(\cdot)|(\Omega)}$ is the closure of the set

$$\left\{ \operatorname{div} \xi : \xi \in [C_c^1(\Omega)]^d, |\xi(x)| \leq 1 \quad \forall x \in \Omega \right\}.$$

The element $\eta \in V_2$ is a limit of the corresponding fixed point iteration (4.63).

In order to guarantee concrete computability and the correctness of this procedure, we need to discretize the problem and approximate it in finite dimensions, compare Examples 4.3.1.2 and Remark 4.3.9.2.

In contrast to the approach of the previous subsection, where we used the discretization of the subdifferential to solve the subiterations, in the following we directly work with discrete approximations of the functional \mathcal{J} . In dimension $d = 1$ we consider vectors $u \in \mathcal{H} := \mathbb{R}^N$, $u = (u_1, u_2, \dots, u_N)$ with gradient $u_x \in \mathbb{R}^N$ given by

$$(u_x)_i = \begin{cases} u_{i+1} - u_i & \text{if } i < N \\ 0 & \text{if } i = N, \end{cases}$$

for $i = 1, \dots, N$. In this setting, instead of minimizing

$$\mathcal{J}(u) := \|Tu - f\|_{L^2(\Omega)}^2 + 2\alpha|D(u)|(\Omega),$$

4.3 Domain Decomposition for TV Minimization

we consider the discretized functional

$$\mathcal{J}^\delta(u) := \sum_{1 \leq i \leq N} ((Tu)_i - g_i)^2 + 2\alpha|(u_x)_i|.$$

As in Section 4.2.2, we assume that T is applied on the piecewise linear interpolant \hat{u} of the vector $(u_i)_{i=1}^N$ (we make a similar assumption for $d = 2$).

To highlight the relationship between continuous and discrete setting we introduce a step-size $h \sim \min\{1/N, 1/M\}$ in the discrete definition of \mathcal{J} by defining a new functional \mathcal{J}_h^δ equal to h times the expression \mathcal{J}^δ above. One can show that as $h \rightarrow 0$, \mathcal{J}_h^δ $\Gamma-$ converges to the continuous functional \mathcal{J} , see [Ch04, Br02]. In particular, piecewise linear interpolants \hat{u}_h of the minimizers of the discrete functional \mathcal{J}_h^δ converge to minimizers of \mathcal{J} . This observation clearly justifies our discretization approach.

For the definition of the set $K_{|D(\cdot)|(\Omega)}$ in finite dimensions we further introduce discrete divergence in one dimension $\nabla \cdot : \mathcal{H} \rightarrow \mathcal{H}$ (resp. $\nabla \cdot : \mathcal{H} \times \mathcal{H} \rightarrow \mathcal{H}$ in two dimensions), defined, by analogy with the continuous setting, by $\nabla \cdot = -\nabla^*$ (∇^* is the adjoint of the gradient ∇). That is, the discrete divergence operator is given by backward differences, in one dimension by

$$(\nabla \cdot p)_i = \begin{cases} p_i - p_{i-1} & \text{if } 1 < i < N \\ p_i & \text{if } i = 1 \\ -p_{i-1} & \text{if } i = N, \end{cases}$$

The discrete setting in dimension $d = 2$ is analogous to the one specified at the beginning of Section 4.2.2, with the only difference being that we have the L^2 norm in the definition of \mathcal{J}^δ instead of the H^{-1} norm.

With these definitions the set $K_{\|\cdot\|_{\ell_1^N}}$ in one dimension is given by

$$\{\nabla \cdot p : p \in \mathcal{H}, |p_i| \leq 1 \forall i = 1, \dots, N\}.$$

and in two dimensions $K_{\|\nabla(\cdot)\|_{\ell_1^{N \times M}}}$ is given by

$$\{\nabla \cdot p : p \in \mathcal{H} \times \mathcal{H}, |p_{i,j}| \leq 1 \forall i = 1, \dots, N \text{ and } j = 1, \dots, M\}.$$

For the computation of the projection in oblique thresholding we use the dual algorithm of Chambolle, which has been presented in Section 4.2.2 for dimension $d = 2$. For $d = 1$ a similar algorithm for the computation of $\mathbb{P}_{\alpha K_{\|\cdot\|_{\ell_1^N}}} (f)$ is given:

4.3 Domain Decomposition for TV Minimization

We choose $\tau > 0$, let $p^{(0)} = 0$ and for any $n \geq 0$,

$$p_i^{(n+1)} = \frac{p_i^{(n)} + \tau((\nabla \cdot p^{(n)} - f/\alpha)_x)_i}{1 + \tau |((\nabla \cdot p^{(n)} - f/\alpha)_x)_i|}, \quad (4.86)$$

for $i = 1, \dots, N$.

In this case the convergence of $\alpha \nabla \cdot p^{(n)}$ to the corresponding projection as $n \rightarrow \infty$ is guaranteed for $\tau \leq 1/4$. In this special setting the oblique thresholding algorithm reads

Oblique Thresholding for TV-L² Minimization

Start with an initial condition $u^0 = 0$, z given as above, and u_j the respective projection of the most recent iterate on $L^2(\Omega_j)$. Then iterate

$$u_i^{k+1} = (Id - \mathbb{P}_{\alpha K_{|D(\cdot)|}(\Omega)})((z + u_j) - \eta) - u_j, \quad i = 1, 2, i \neq j,$$

where η is computed via the fixed point iteration

Let $\eta^0 = 0 \in V_2$ and iterate

$$\eta^{m+1} = \pi_{V_2} [\mathbb{P}_{\alpha K_{|D(\cdot)|}(\Omega)} (\eta^m - (u_j + z))], \quad m \geq 0.$$

Domain decomposition In one dimension the domain $\Omega = [a, b]$ is split into two intervals $\Omega_1 = [a, \lceil \frac{N}{2} \rceil]$ and $\Omega_2 = [\lceil \frac{N}{2} \rceil + 1, b]$. The interface $\partial\Omega_1 \cap \partial\Omega_2$ is located between $i = \lceil N/2 \rceil$ in Ω_1 and $i = \lceil N/2 \rceil + 1$ in Ω_2 . In two dimensions the domain $\Omega = [a, b] \times [c, d]$ is split in an analogous way with respect to its rows. In particular we have $\Omega_1 = [a, \lceil \frac{N}{2} \rceil] \times [c, d]$ and $\Omega_2 = [\lceil \frac{N}{2} \rceil + 1, b] \times [c, d]$, compare Figure 4.11. The splitting in more than two domains is done similarly:

Set $\Omega = \Omega_1 \cup \dots \cup \Omega_N$, the domain Ω decomposed into N disjoint domains Ω_i , $i = 1, \dots, N$. Set $s = \lceil N/N \rceil$. Then

$$\Omega_1 = [1, s] \times [c, d]$$

for $i = 2 : N - 1$

$$\Omega_i = [(i-1)s + 1, is] \times [c, d]$$

end

$$\Omega_N = [(N-1)s + 1, N] \times [c, d].$$

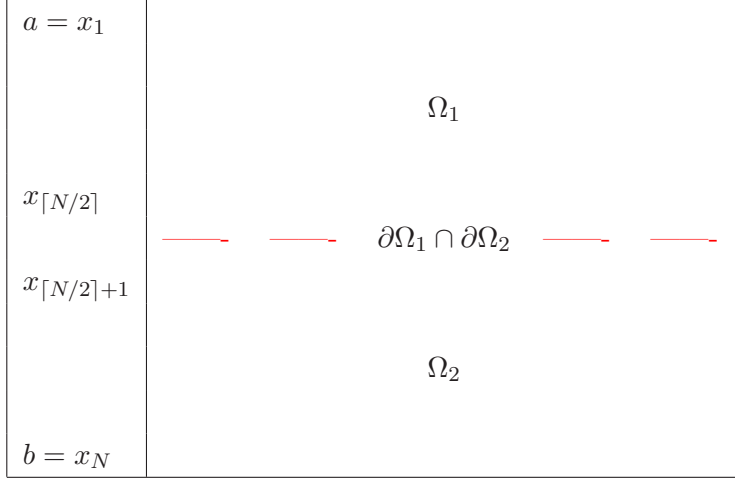


Figure 4.11: Decomposition of the discrete image in two domains Ω_1 and Ω_2 with interface $\partial\Omega_1 \cap \partial\Omega_2$

To compute the fixed point η of (4.62) in an efficient way we make the following considerations, which allow to restrict the computation to a relatively small strip around the interface. For $u_2 \in V_2^\psi$ and $z \in V_1$ a minimizer u_1 is given by

$$u_1 = \operatorname{argmin}_{u \in V_1} \|u - z\|_{L^2(\Omega)}^2 + 2\alpha|D(u + u_2)|(\Omega).$$

We further decompose $\Omega_2 = \hat{\Omega}_2 \cup (\Omega_2 \setminus \hat{\Omega}_2)$ with $\partial\hat{\Omega}_2 \cap \partial\Omega_1 = \partial\Omega_2 \cap \partial\Omega_1$, where $\hat{\Omega}_2 \subset \Omega_2$ is a strip around the interface $\partial\Omega_2 \cap \partial\Omega_1$, as illustrated in Figure 4.12. By using the splitting of the total variation (4.55) we can restrict the problem to an equivalent minimization where the total variation is only computed in $\Omega_1 \cup \hat{\Omega}_2$. In other words, we have

$$u_1 = \operatorname{argmin}_{u \in V_1} \|u - z\|_{L^2(\Omega)}^2 + 2\alpha|D(u + u_2)|(\Omega_1 \cup \hat{\Omega}_2).$$

Hence, for the computation of the fixed point $\eta \in V_2$, we need to carry out the iteration $\eta^{(m+1)} = \pi_{V_2} \mathbb{P}_{\alpha K_{|D(\cdot)|(\Omega)}}(\eta^{(m)} - z + u_2)$ only in $\Omega_1 \cup \hat{\Omega}_2$. By further observing that η will be supported only in Ω_2 , i.e. $\eta(x) = 0$ in Ω_1 , we may additionally restrict the fixed point iteration on the relatively small strip $\hat{\Omega}_1 \cup \hat{\Omega}_2$, where $\hat{\Omega}_1 \subset \Omega_1$ is a neighborhood around the interface from the side of Ω_1 . Although the computation of η restricted to $\hat{\Omega}_1 \cup \hat{\Omega}_2$ is not equivalent to the computation of η on whole $\Omega_1 \cup \hat{\Omega}_2$, the produced errors are practically negligible, because of the Neumann boundary

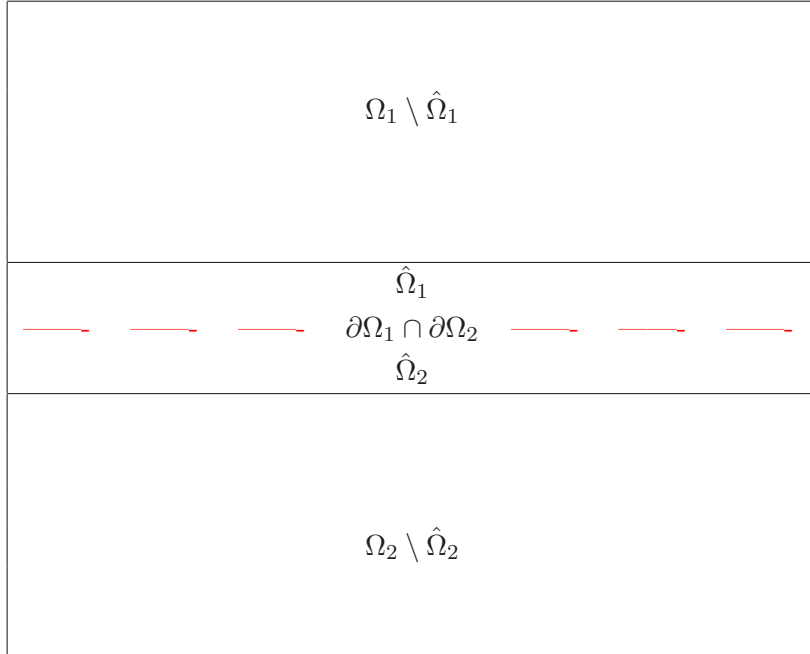


Figure 4.12: Computation of η only in the strip $\hat{\Omega}_1 \cup \hat{\Omega}_2$.

conditions involved in the computation of $\mathbb{P}_{\alpha K_{|\nabla(\cdot)|(\Omega_1 \cup \hat{\Omega}_2)}}$. Analogously, one operates for the minimization on Ω_2 .

Numerical experiments in one and two dimensions We shall present numerical results in one and two dimensions for the algorithm in (4.65), and discuss them with respect to the choice of parameters.

In one dimension we consider the same three signals already discussed for the “naive” approach in Figure 4.10. In the left column of Figure 4.13 we report again the one dimensional signals. The right column shows the result of the application of the domain decomposition method (4.65) for total variation minimization. The support of the signals is split in two intervals. The interface developed by the two intervals is marked by a red dot. In all three examples we fixed $\alpha = 1$ and $\tau = 1/4$. The first example 4.57-4.59 shows a step function, which has its step directly at the interface of the two intervals. The total variation minimization (4.65) is applied with $T = I$. This example confirms that jumps are preserved at the interface of the two domains. The second and third example 4.13(c)-4.13(f) present the behavior of the algorithm when interpolation across the interface is performed. In this case the operator T is given

4.3 Domain Decomposition for TV Minimization

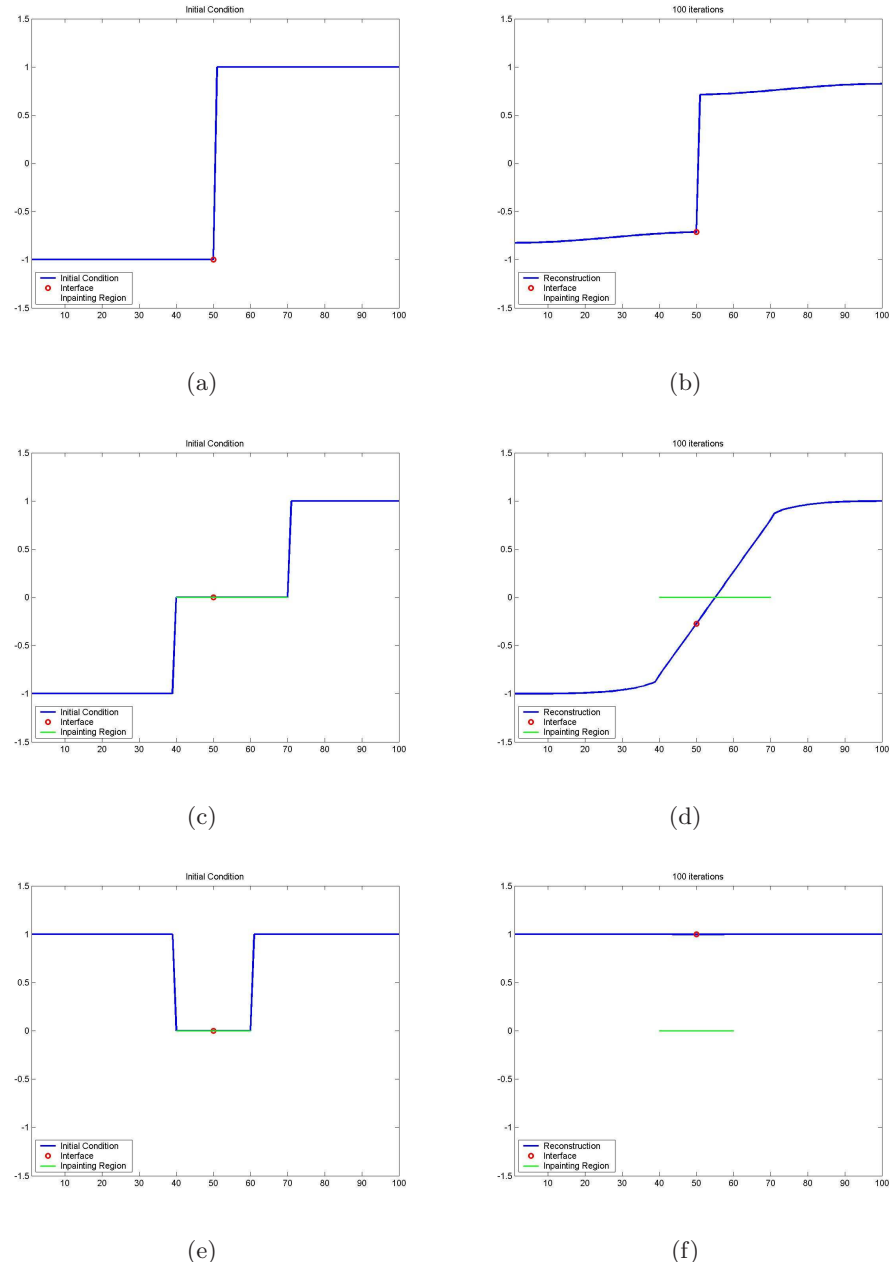


Figure 4.13: (a)-(f): Examples of the domain decomposition method for TV- L^2 denoising/inpainting in 1D where the domain was split in two domains with $\alpha = 1$ and $\tau = 1/4$

4.3 Domain Decomposition for TV Minimization

by the multiplier $T = 1_{\Omega \setminus D}$, where D is an interval containing the interface point. In contrast to the performance of the interpolation of the “naive” approach for the third example, Figure 4.10(e)-4.10(f), the new approach solves the interpolation across the interface correctly, see Figure 4.13(e)-4.13(f).



Figure 4.14: An example of TV- L^2 inpainting in where the domain was split in two with $\alpha = 10^{-2}$ and $\tau = 1/4$

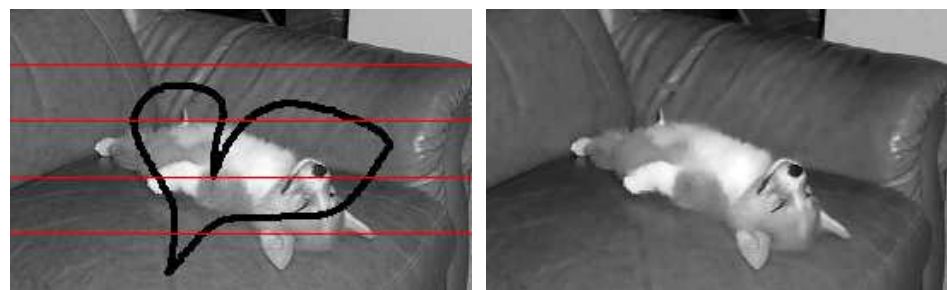


Figure 4.15: An example of TV- L^2 inpainting in where the domain was split in five with $\alpha = 10^{-2}$ and $\tau = 1/4$

Inpainting results for the two dimensional case are shown in Figures 4.14-4.15. The interface is here marked by a red line in the given image. In the first example in Figure

[4.14](#) the domain is split in two subdomains, in the second example in [Figure 4.15](#) the domain is split in five subdomains. The Lagrange multiplier $\alpha > 0$ is chosen equal to 10^{-2} . The time-step for the computation of $\mathbb{P}_{\alpha K_{|\nabla(\cdot)|(\Omega)}}$ is chosen as $\tau = 1/4$. The examples confirm the correct reconstruction of the image at the interface, preserving both continuities and discontinuities as desired. Despite the fact that [Theorem 4.3.16](#) does not guarantee that the algorithm in [\(4.65\)](#) can converge to a minimizer of \mathcal{J} (unless one of the conditions in (iv) holds), it seems that for total variation minimization the result is always rather close to the expected minimizer.

Let us now discuss the choice of the different parameters. As a crucial issue in order to compute the solution at the interface $\partial\Omega_1 \cap \partial\Omega_2$ correctly, one has to pay attention to the accuracy up to which the projection $\mathbb{P}_{\alpha K_{|\nabla(\cdot)|(\Omega)}}$ is approximated and to the width of the strip $\hat{\Omega}_1 \cup \hat{\Omega}_2$ for the computation of η . The alternating iterations [\(4.65\)](#) in practice are carried out with $L = M = 5$ inner iterations. The outer iterations are carried out until the error $|J(u^{(n+1)}) - J(u^{(n)})|$ is of order $\mathcal{O}(10^{-10})$. The fixed point η is computed by iteration [\(4.63\)](#) in at most 10 iterations with initialization $\eta_n^{(0)} = 0$ when $n = 1$ and $\eta_{n+1}^{(0)} = \eta_n$, the η computed in the previous iteration, for $n > 1$. For the computation of the projection $\mathbb{P}_{\alpha K_{|\nabla(\cdot)|(\Omega)}}$ by Chambolle's algorithm [\(4.39\)](#) we choose $\tau = 1/4$. Indeed Chambolle points out in [\[Ch04\]](#) that, in practice, the optimal constant for the stability and convergence of the algorithm is not $1/8$ but $1/4$. Moreover, if the derivative along the interface is high, i.e., if there is a step along the interface, one has to be careful concerning the accuracy of the computation for the projection. The stopping criterion for the iteration [\(4.39\)](#) consists in checking that the maximum variation between $p_{i,j}^n$ and $p_{i,j}^{n+1}$ is less than 10^{-3} . With less accuracy, artifacts on the interface can appear. This error tolerance may need to be further decreased for very large $\alpha > 0$. Furthermore, the size of the strip varies between 6 and 20 pixels, also depending on the size of $\alpha > 0$, and on whether inpainting is carried out via the interface or not (e.g., the second and third example in [Figure 4.13](#) failed in reproducing the interface correctly with a strip of size 6 but computed it correctly with a strip of size 20).

Parallel Implementation The principal reasons to develop domain decomposition algorithms is the formulation of solvers which can be easily parallelized. In [Section 4.3.5](#), equation [\(4.79\)](#), we also propose a parallelized version for the subspace minimization

using oblique thresholding. As for the alternating algorithm, we provide a detailed analysis of the convergence properties of its modification for parallel computation, cf. Theorem 4.3.18.

Based on this, I developed a parallel implementation of the domain decomposition algorithm for total variation minimization in Matlab (using MatlabMPI¹ provided by MIT²). Both the parallel code and the sequential code are available online³. Numerical tests exploring the computational performance of the parallel algorithm are a matter of future research.

4.3.7 Domain Decomposition for TV-H⁻¹Minimization

As already pointed out earlier in this chapter, one of the drawbacks of using TV-H⁻¹minimization in applications is its slow numerical performance. The semi-implicit scheme for TV-H⁻¹inpainting in Section 4.1.3 suffers from a damping of the iterates dependent on the choice of the fidelity parameter; and the new dual algorithm for TV-H⁻¹minimization from Section 4.2.1 , i.e., **Algorithm (P)**, is conditioned to time steps $\tau \leq 1/64$ in order to guarantee convergence. If now, additionally, the data dimension is large, e.g., when we have to process 2D images of high resolution, of sizes 3000×3000 pixels for instance, or even 3D image data, each iteration step itself is computationally expensive and we are far away from real-time computations.

Motivated by this, we wish to apply the theory developed in the previous subsections for the solution of the TV-H⁻¹minimization problem (4.33), i.e., the minimization of

$$\mathcal{J}(u) := \|Tu - f\|_{H^{-1}(\Omega)}^2 + 2\alpha|Du|(\Omega).$$

To do so, we shall use the algorithm developed in Section 4.2.2 for the computation of the oblique thresholding operator. This part of the present work is contained in [Sc09].

We follow the notation from the previous sections and from Section 4.2.2. We are in the same setting as for TV-L²minimization, with the only difference being that the fidelity term in (4.33) is minimized in the weaker H^{-1} norm instead of the norm in $L^2(\Omega)$. However, as it turns out later, we fulfill all the necessary properties, assumed in

¹The author thanks Jahn Müller from the University of Münster for his help with the implementation in MatlabMPI

²see <http://www.ll.mit.edu/mission/isr/matlabmpi/matlabmpi.html>

³http://homepage.univie.ac.at/carola.schoenlieb/webpage_tvdode/tv_dode_numerics.htm

4.3 Domain Decomposition for TV Minimization

Section 4.3.1, in order to apply the general theory to the case of TV-H⁻¹ minimization. Then we want to minimize \mathcal{J} in (4.33) by the alternating algorithm (4.65). As in Section 4.3.3, the subproblem on Ω_1 reads

$$\operatorname{argmin}_{u_1 \in V_1} \left\{ \mathcal{J}(u_1 + u_2) = 2\alpha |D(u_1 + u_2)|(\Omega) + \|Tu_1 - (f - Tu_2)\|_{-1}^2 \right\}. \quad (4.87)$$

Differently to the surrogate functionals suggested in Section 4.3.3, we follow the approach presented in Section 4.2.2, i.e., **Algorithm (P)** and use the slightly different surrogate functionals (4.47). This means that we introduce the following sequence of functionals for this subminimization problem, i.e., let $u^0 = 0$, for $k \geq 0$ let

$$\mathcal{J}_1^s(u_1 + u_2, u_1^k) = |D(u_1 + u_2)|(\Omega) + \frac{1}{2\tau} \|u_1 - u_1^k\|_{-1}^2 + \frac{1}{2\alpha} \|u_1 - (f - Tu_2 + (Id - T)u_1^k)\|_{-1}^2.$$

and realize an approximate solution to (4.87) by using the following algorithm: For $u_1^0 \in BV(\Omega_1)$,

$$u_1^{k+1} = \operatorname{argmin}_{u_1 \in V_1} \mathcal{J}_1^s(u_1 + u_2, u_1^k), \quad k \geq 0. \quad (4.88)$$

As in the general theory in Section 4.3.3, we are going to use Theorem 4.3.7 to solve the subminimization problem (4.88) via its reformulation on Ω , i.e.,

$$u_1^{k+1} = \operatorname{argmin}_{u \in BV(\Omega)} \{F(u), \pi_{V_2}(u) = 0\},$$

with $F(u) = J_1^s(u + u_2, u_1^k)$. Now, since $L^2(\Omega) \subset L^2(\mathbb{R}^2) \subset H^{-1}(\Omega)$ (by zero extensions of functions on Ω to \mathbb{R}^2), our functional F is continuous on $V_1^\psi \subset V_1 = \ker \pi_{V_2}$ in the norm topology of $BV(\Omega)$. Further $\pi_{V_2}|_{BV(\Omega)}$ is a bounded and surjective map with closed range in the norm topology of $BV(\Omega)$, i.e., $(\pi_{V_2}|_{BV(\Omega)})^*$ is injective and $\operatorname{Range}(\pi_{V_2}|_{BV(\Omega)})^* \cong (V_2^\psi)^*$ is closed. By applying Theorem 4.3.7, we know that the optimality of u_1^{k+1} is equivalent to the existence of an $\eta \in \operatorname{Range}(\pi_{V_2}|_{BV(\Omega)})^* \cong (BV(\Omega_2))^*$ such that

$$-\eta \in \partial_{BV(\Omega)} F(u_1^{k+1}).$$

Now

$$\partial_{BV(\Omega)} F(u_1^{k+1}) = \frac{1}{\mu} \Delta^{-1}(u_1^{k+1} - z) + \partial_{BV(\Omega)} |D(u_1^{k+1} + u_2)|(\Omega)$$

where

$$z = \frac{z_1 \alpha + z_2 \tau}{\alpha + \tau}, \quad \mu = \frac{\alpha \tau}{\alpha + \tau}, \quad (4.89)$$

4.3 Domain Decomposition for TV Minimization

with $z_1 = u_1^k$, $z_2 = f - Tu_2 + (Id - T)u_1^k$. Then the optimality of u_1^{k+1} is equivalent to

$$0 \in \frac{1}{\mu} \Delta^{-1}(u_1^{k+1} - z) + \eta + \partial_{BV(\Omega)} |D(u_1^{k+1} + u_2)|(\Omega).$$

The latter is equivalent to

$$u_1^{k+1} + u_2 \in \partial_{BV(\Omega)} |D.|(\Omega)^*(\frac{1}{\mu} \Delta^{-1}(z - u_1^{k+1}) - \eta),$$

i.e.,

$$\frac{u_2 + z}{\mu} \in \frac{z - u_1^{k+1}}{\mu} + \frac{1}{\mu} \partial_{BV(\Omega)} |D.|(\Omega)^*(\frac{1}{\mu} \Delta^{-1}(z - u_1^{k+1}) - \eta).$$

By letting $w = \Delta^{-1}(z - u_1^{k+1})/\mu - \eta$ we have

$$0 \in (-\Delta(w + \eta) - (u_2 + z)/\mu) + \frac{1}{\mu} \partial_{BV(\Omega)} |D.|(\Omega)^*(w),$$

or, in other words, w is a minimizer of

$$\frac{\|w - (\Delta^{-1}(u_2 + z)/\mu - \eta)\|_{H_0^1(\Omega)}^2}{2} + \frac{1}{\mu} |D.|(\Omega)^*(w).$$

Following the same procedure as in Section 4.2.2 we deduce that

$$w = \mathbb{P}_K^1(\Delta^{-1}(u_2 + z)/\mu - \eta),$$

where \mathbb{P}_K^1 denotes the orthogonal projection on K over $H_0^1(\Omega)$ like in Section 4.2.2. Then a minimizer u_1^{k+1} of (4.88) can be computed as

$$u_1^{k+1} = -\Delta(Id - \mathbb{P}_{\mu K}^1)(\Delta^{-1}(z + u_2) - \mu\eta) - u_2.$$

By applying π_{V_2} to both sides of the latter equality we get

$$0 = \mu\Delta\eta + \pi_{V_2} [\Delta\mathbb{P}_{\mu K}^1(\Delta^{-1}(u_2 + z) - \mu\eta)].$$

Assuming necessary zero boundary conditions on $\partial\Omega$, the resulting fixed point equation for η reads

$$\eta = \frac{1}{\mu} \pi_{V_2} [\mathbb{P}_{\mu K}^1(\mu\eta - \Delta^{-1}(u_2 + z))].$$

As before for the general theory, the fixed point can be computed via the iteration

$$\eta^0 \in V_2, \quad \eta^{m+1} = \frac{1}{\mu} \pi_{V_2} [\mathbb{P}_{\mu K}^1(\mu\eta^m - \Delta^{-1}(u_2 + z))], \quad m \geq 0.$$

Oblique Thresholding for TV-H⁻¹ Minimization

Start with an initial condition $u^0 = 0$, z as in (4.89) and u_j the respective projection of the most recent iterate on $L^2(\Omega_j)$. Then iterate

$$u_i^{k+1} = -\Delta (Id - \mathbb{P}_{\mu K}^1) (\Delta^{-1}(z + u_j) - \mu\eta) - u_j, \quad i = 1, 2, i \neq j, \quad (4.90)$$

where η in (4.90) is computed via the fixed point iteration

Let $\eta^0 = 0 \in V_2$ and iterate

$$\eta^{m+1} = \frac{1}{\mu} \pi_{V_2} [\mathbb{P}_{\mu K}^1 (\mu\eta^m - \Delta^{-1}(u_j + z))], \quad m \geq 0. \quad (4.91)$$

In sum we solve (4.33) by the alternating subspace minimizations where each subminimization problem is computed by the oblique thresholding algorithm for TV-H⁻¹ minimization:

As before the projection $\mathbb{P}_{\mu K}^1$ is computed by **Algorithm (P)**.

Unsurprisingly, we are especially interested in the inpainting setting $T = \mathbf{1}_{\Omega \setminus D}$, compare also with (4.48) in Section 4.2.3. In Figures 4.16 and 4.17 the given images have been divided in four subdomains, marked by red lines, and the image is inpainted by TV-H⁻¹ inpainting computed by the sequential algorithm (4.65) by means of oblique thresholding. Note that for these examples we used a different decomposition of the spatial domain Ω , where the four interfaces form a cross and meet in the middle of the domain. Special care has to be taken about this meeting point in the middle, i.e., the solution has to be averaged over the subdomains there.

4.3 Domain Decomposition for TV Minimization

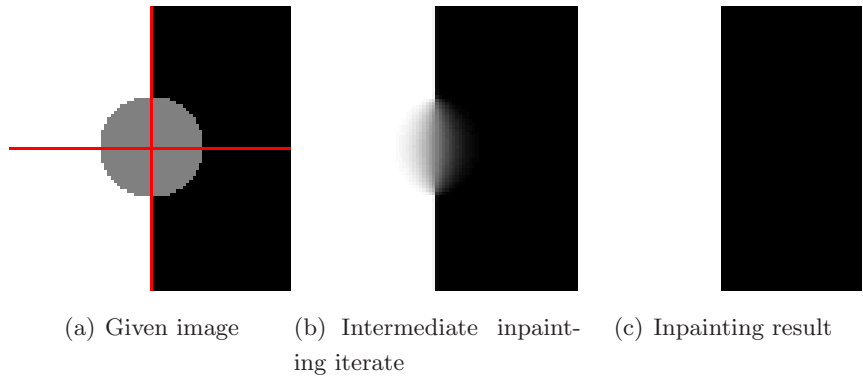


Figure 4.16: $\text{TV}-\mathbf{H}^{-1}$ inpainting computation for a model example on four domains with $\alpha = 0.01$.

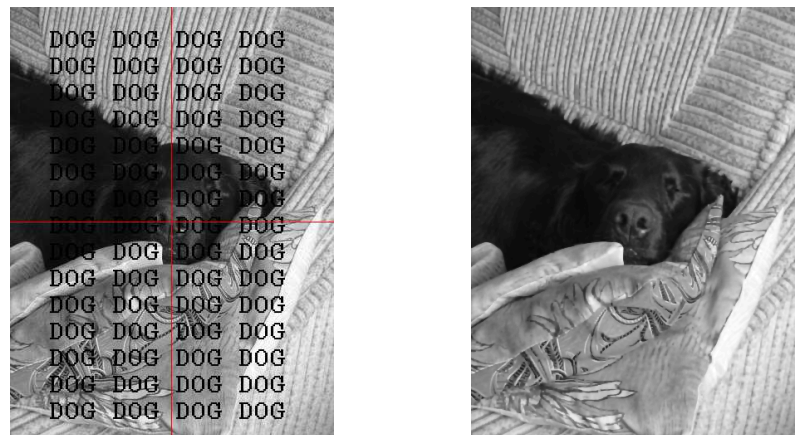


Figure 4.17: $\text{TV}-\mathbf{H}^{-1}$ inpainting computation on four domains with $\alpha = 0.005$.

Chapter 5

Applications

Digital inpainting methods provide an important tool in the restoration of images in a wide range of applications. In my Ph.D. thesis I focus on two special applications. The first is the inpainting of ancient frescoes. In particular we discuss the Cahn-Hilliard equation for the inpainting of binary structure and $\text{TV}-\text{H}^{-1}$ inpainting for the reconstruction of the grayvalues in the recently discovered Neidhart frescoes in Vienna, cf Section 5.1. The second application has originated in a project of Andrea Bertozzi taking place at UCLA (University of California Los Angeles) and is about the inpainting of roads in satellite images. It is presented in Section 5.2.

5.1 Restoration of Medieval Frescoes

In the course of an ongoing interdisciplinary project¹ we aim to use digital inpainting algorithms for the restoration of frescoes. Most of the results presented within this section can be found in [BFMS08].

Particular consideration has been extended to the newly found Neidhart frescoes (Tuchlauben 19, 1010 Vienna). These medieval frescoes from the 14th Century are depicting a cycle of songs of the 13th Century minnesinger Neidhart von Reuelental. Hidden behind a wall over years, the frescoes have been damaged during exposure. Advanced mathematical tools were developed specifically for so-called "mathematical inpainting/retouching" of digital images. To this end, variational methods and third

¹WWTF Five senses-Call 2006, *Mathematical Methods for Image Analysis and Processing in the Visual Arts*

and fourth-order partial differential equations have been investigated. Efficient numerical methods for the solution of the devised partial differential equations have been designed.

In the following we discuss our mathematical inpainting methods and present numerical results from their application to the Neidhart frescoes.

5.1.1 Neidhart Frescoes

Fragments of 14th century wall frescoes found beneath the crumbling plaster of an old apartment in the heart of Vienna depict a popular medieval cycle of songs of the 13th century minnesinger, Neidhart von Reuenthal. In the very late 14th century, Michel Menschein, a wealthy Viennese council member and cloth merchant, commissioned local artists to paint the stories in Neidhart's songs on the walls of his Festsaal (banquet hall). The Neidhart frescoes provide a unique peek into medieval humor, and at the same time, a peek into the taste of a medieval man.



Figure 5.1: Part of the Neidhart frescoes. Image courtesy Andrea Baczyński.

In Figure 5.1 a part of the Neidhart frescoes is shown¹. The white holes in the fresco are due to the wall which covered the fresco until a few years ago. They occurred

¹The author thanks Andrea Baczyński for providing the fresco data.

when the wall was removed. In the following we want to apply digital restoration methods to these frescoes. Thereby the main challenge is to capture the structures in the preserved parts of the fresco and transport them into the damaged parts continuously. Due to their great age and almost 600 years of living by owners and tenants in the apartment, saturation, hue and contrast quality of the colours in the frescoes suffered. Digital grayvalue, i.e., colour interpolation, in the damaged parts of the fresco therefore demands sophisticated algorithms taking these detrimental factors into account.

5.1.2 Methods

In the following we present the mathematical methods we used in order to reconstruct the damaged parts in the fresco. In particular, two inpainting methods based on higher-order partial differential equations, i.e., Cahn-Hilliard- (2.1) and TV-H⁻¹inpainting (2.27), are to be presented. We finalize this section by proposing a possible strategy to adapt these two inpainting approaches to the requirements of the Neidhart frescoes.

Let us start with briefly recalling the Cahn-Hilliard inpainting approach (2.1). The inpainted version $u(x)$ of $f(x) \in L^2(\Omega)$ is constructed by following the evolution equation

$$\begin{cases} u_t = \Delta(-\epsilon\Delta u + \frac{1}{\epsilon}F'(u)) + \lambda(f - u) & \text{in } \Omega, \\ \frac{\partial u}{\partial \nu} = \frac{\partial \Delta u}{\partial \nu} = 0 & \text{on } \partial\Omega, \end{cases}$$

with $F(u)$ a so-called double-well potential, e.g., $F(u) = u^2(u - 1)^2$, while

$$\lambda(x) = \begin{cases} \lambda_0 & \Omega \setminus D \\ 0 & D \end{cases}$$

is the characteristic function of $\Omega \setminus D$ multiplied by a constant $\lambda_0 \gg 1$.

A generalization of the Cahn-Hilliard inpainting approach to an approach for grayvalue images was already presented in Section 2.2 (also cf. [BHS08]). Namely we consider TV-H⁻¹inpainting (2.27): Let $f \in L^2(\Omega)$, $|f| \leq 1$ be the given grayvalue image. The inpainted version $u(x)$ of $f(x)$ evolves in time like

$$u_t = -\Delta \left(\nabla \cdot \left(\frac{\nabla u}{|\nabla u|} \right) \right) + \lambda(f - u), \quad (5.1)$$

where $p \in \partial TV(u)$ was replaced by a relaxed version

$$p \approx \nabla \cdot \left(\frac{\nabla u}{|\nabla u|} \right) = \nabla \cdot \left(\frac{\nabla u}{\sqrt{|\nabla u|^2 + \epsilon}} \right),$$

for an $0 < \epsilon \ll 1$.

As mentioned in Section 5.1.1, the Neidhart frescoes pose a special challenge concerning their digital restoration. We summarize the main issues in the following list:

1. Lack of grayvalue contrast
2. Low colour saturation and hue
3. Damaged parts can be rather large, i.e., the diameter of the damaged domain can be larger than the width of lines which are to be continued into the damaged part

Hence we need an inpainting approach which takes into account these possible difficulties and solves (or circumvents) them. As we have pointed out earlier in this section, the third issue can be solved by using a higher-order inpainting method such as (2.1) and (2.27). Unfortunately difficulties two and three prevent the effective application of these methods. As the contrast between grayvalues is low, the edges (which identify the main structure of an image) are not clearly defined. As inpainting lives and dies with uniqueness of edge continuation (cf. Figure 5.2) we may run into trouble if we do not preprocess the digital images of the fresco in an adequate manner.

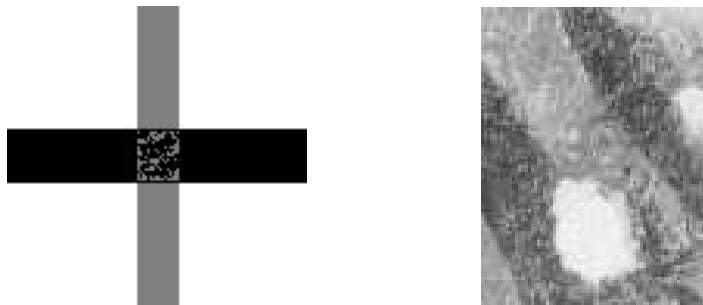


Figure 5.2: (l.) What is the right solution? (r.) Part of the Neidhart fresco: How should the inpainting algorithm decide in this case?

Specifically we follow two strategies:

- **Strategy 1:** Structure inpainting on binary images with the Cahn-Hilliard equation. Based on the recovered binary structure, the fresco is colourized. We discuss the recolourization, i.e., the filling in of grayvalues based on the given binary structure, in more detail in Section 5.1.2. Also compare [Fo06] for a similar approach.

- **Strategy 2:** Apply TV-H⁻¹inpainting in two steps. First with a small λ_0 , e.g., $\lambda_0 = 1$, to merge together fine artifacts in the fresco by diffusion. In the second step we choose a large $\lambda_0 \gg 1$, e.g., $\lambda_0 = 10^3$, to reconstruct the fresco inside the damaged parts.

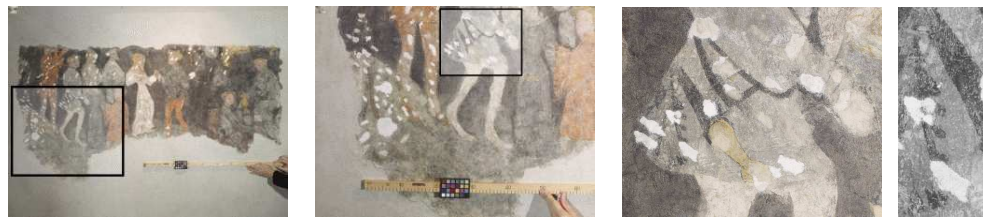


Figure 5.3: Part of the Neidhart frescoes

In the following we present first numerical results following these two strategies. For both inpainting methods (2.1) and (2.27) we used the convexity splitting algorithms presented in Section 4.1 for their discretization in time.

Strategy 1 - Binary based fresco inpainting

We begin with the inpainting of the binary structure of the frescoes by means of (2.1), cf. Figure 5.4–5.5. In our numerical examples we applied (2.1) in two steps (cf. [BEG07b]). In the first few time steps we solve (2.1) with a rather big ϵ , e.g., $\epsilon = 3$. We stop when we are sufficiently close to a steady state. Then we switch the ϵ value to a smaller one, e.g., $\epsilon = 0.01$. Using the steady state from the first few time steps of (2.1) with a large ϵ as an initial condition, we apply the iteration now for the switched ϵ . Again we stop when we are sufficiently close to the steady state.

The next step is to recolourize the damaged parts by using the recovered binary structure as underlying information. This can be done in the following way.

Motivated by previous work, Fornasier [Fo06], and Fornasier and March [FM07], we propose an inpainting model for grayvalue images which uses a given (or previously obtained) binary structure inside the missing domain D . Thereby the binary structure of the image is usually obtained by a preprocessing step with Cahn-Hilliard inpainting [BEG07a, BEG07b]. Let us describe this method in more detail.



Figure 5.4: Cahn-Hilliard inpainting with $\lambda_0 = 10^7$ f.l.t.r.: Part of the fresco; binary selection in red; binary selection in black and white; initial condition for the inpainting algorithm where the inpainting region is marked with a gray rectangle; inpainting result after 200 time steps with $\epsilon = 3$; inpainting result after additional 800 time steps with $\epsilon = 0.01$.

Let $f \in L^2(\Omega)$ be a given image which grayvalue in $\Omega \setminus D$ and binary in D . We wish to recover the grayvalue information in D based on the binary structure given by f by means of the following minimization problem:

$$\begin{aligned} u^* = \operatorname{argmin} \left\{ & \frac{\mu}{2} \int_{\Omega \setminus D} |u(x) - f(x)|^2 \, dx \right. \\ & + \frac{\lambda}{2} \int_D |\mathcal{L}_{bin}(u(x)) - f(x)|^2 \, dx \\ & \left. + |Du|(\Omega), \, u \in L^2(\Omega)(\Omega, \mathbb{R}_+) \right\}. \end{aligned} \quad (5.2)$$

In our case \mathcal{L}_{bin} is a transformation which projects the grayvalue range of u , e.g., $[0, 1]$, on the binary range $\{0, 1\}$.

The corresponding Euler-Lagrange equation of (5.2) then reads

$$0 = p + \mu \cdot \chi_{\Omega \setminus D}(u - f) + \lambda \cdot \chi_D(\mathcal{L}_{bin}(u) - f) \frac{\partial \mathcal{L}_{bin}}{\partial u}(u), \quad p \in \partial |Du|(\Omega), \quad (5.3)$$

where $\chi_{\Omega \setminus D}$ and χ_D are the characteristic functions of $\Omega \setminus D$ and D respectively. In (5.3) we approximate the subgradient of the total variation by a relaxed version $p \approx -\nabla \cdot (\nabla u / |\nabla u|_\epsilon)$, where $|\nabla u|_\epsilon := \sqrt{|\nabla u|^2 + \epsilon}$. The relaxed version of (5.3) then reads

$$0 = -\nabla \cdot \left(\frac{\nabla u}{|\nabla u|_\epsilon} \right) + \mu \cdot \chi_{\Omega \setminus D}(u - f) + \lambda \cdot \chi_D(\mathcal{L}_{bin}(u) - f) \frac{\partial \mathcal{L}_{bin}}{\partial u}(u).$$



Figure 5.5: Cahn-Hilliard inpainting with $\lambda_0 = 10^6$ f.l.t.r.: Part of the fresco; binary selection in red; binary selection in black and white; initial condition for the inpainting algorithm where the inpainting region is marked with a gray rectangle; inpainting result after 200 time steps with $\epsilon = 4$; inpainting result after additional 800 time steps with $\epsilon = 0.01$.

For our purpose \mathcal{L}_{bin} is modeled by a relaxed version of the Heaviside function depending on a (presumably) given threshold τ . Recall that the Heaviside function is given by

$$H(x) = \begin{cases} 1 & x \geq 0, \\ 0 & x < 0. \end{cases}$$

In order to have a differentiable transformation, we approximate H by H^δ with

$$H^\delta(x) = \frac{1}{2} \left(1 + \frac{2}{\pi} \arctan \left(\frac{x}{\delta} \right) \right), \quad 0 < \delta \ll 1.$$

Let us assume now that the binary part of f in D was obtained such that it is 1 where the lost grayvalue information $f_g \geq \tau$ and 0 otherwise, i.e., for $x \in D$ we assume

$$f(x) = \begin{cases} 1 & f_g(x) \geq \tau, \\ 0 & f_g(x) < \tau. \end{cases}$$

Then we want the binarization \mathcal{L}_{bin} of u to be modeled subject to the same assumption and we finally define

$$\mathcal{L}_{bin}(u) := H^\delta(u - \tau) \approx \begin{cases} 1 & u \geq \tau, \\ 0 & u < \tau. \end{cases} \quad (5.4)$$

The derivative of \mathcal{L}_{bin} is then a smooth approximation of the Dirac δ -function in $u = \tau$, i.e.,

$$\frac{dH^\delta}{dx}(x) = \delta^\delta(x) = \frac{1}{\pi\delta} \frac{1}{1 + (x/\delta)^2}, \quad 0 < \delta \ll 1,$$

and

$$\frac{\partial \mathcal{L}_{bin}}{\partial x}(u) = \delta^\delta(u - \tau). \quad (5.5)$$

In Figure 5.1.2 two numerical examples for the binary based grayvalue inpainting are shown.

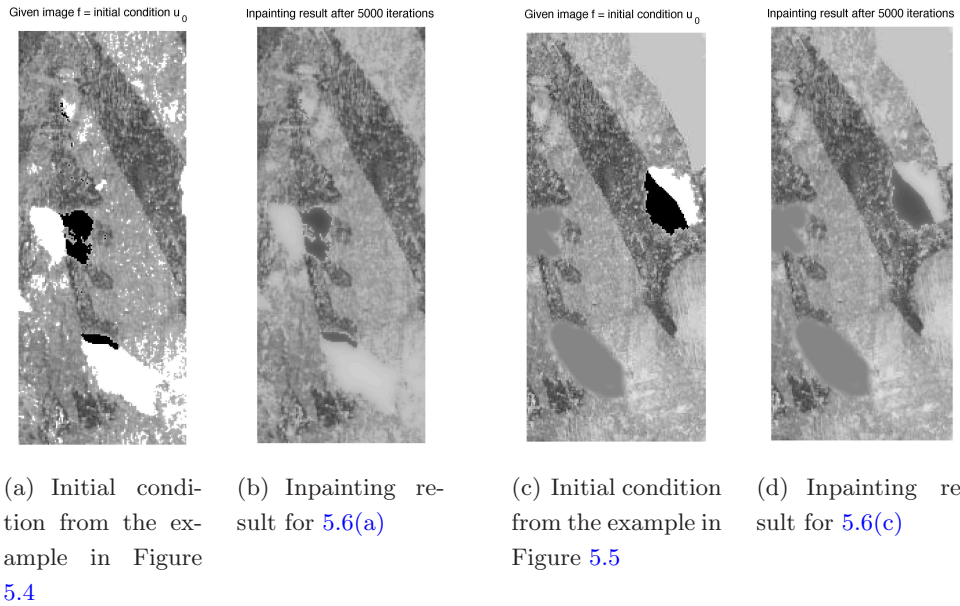


Figure 5.6: Two examples for binary based grayvalue inpainting with $\mu = \lambda = 10^2$ and 5000 time steps. The grayvalues inside of the inpainting domain are initialized with the results from Cahn-Hilliard inpainting in Figure 5.4–5.5, cf. 5.6(a) and 5.6(c). Solving (5.2) via a steepest descent approach constitutes 5.6(b) and 5.6(d)

Strategy 2 - Grayvalue fresco inpainting

We consider (5.1) and apply it for the grayvalue inpainting of the Neidhart frescoes.

In Figure 5.7 the algorithm (5.1) has been applied to a small part of the Neidhart frescoes. In this particular case we did not even have to preprocess the image because only plain grayvalue information was to be imported into the inpainting domain, whereas in Figure 5.8 we acted on strategy 2. Namely, we primarily denoised the image by (5.1) with $\lambda(x) = \lambda_0$ on the whole image domain and applied the inpainting algorithm ((5.1) with $\lambda(x) = 0$ inside the inpainting domain D) on the "cleaned" image in

a second step. Clearly our binary based approach in Figure 5.1.2-5.8 produces superior visual results in the presence of edges.



Figure 5.7: $\text{TV}-\text{H}^{-1}$ inpainting applied to a part of the Neidhart fresco

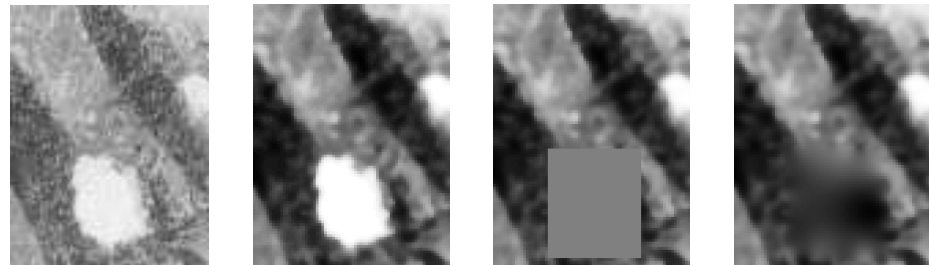


Figure 5.8: $\text{TV}-\text{H}^{-1}$ inpainting following strategy 2. **f.l.t.r.** part of the Neidhart fresco; preprocessed image; initial condition for the inpainting algorithm where the inpainting domain is marked as a gray rectangle; preliminary inpainting result (algorithm carried out until $err \approx 10^{-4}$). Inpainting difficulties due to the reasons indicated in Figure 5.2 are clearly visible.

Conclusion

We succeeded in developing methods for the restoration of digital images using mathematical concepts of partial differential equations. We showed the reconstruction of the grayvalue information in the Neidhart frescoes using basically two strategies. In the first strategy Cahn-Hilliard inpainting was used to reconstruct the binary structure in the frescoes. Then the grayvalues were filled into the missing parts based on the binary information available from the Cahn-Hilliard reconstruction. The main idea of this strategy is to exploit the good reconstruction qualities of Cahn-Hilliard inpainting

(smooth connection of edges even across large distances) as much as possible. This approach turned out to be the method of choice in the presence of edges in the neighborhood of the missing parts and when the gaps in the frescoes are large. The second strategy uses $\text{TV}-\text{H}^{-1}$ inpainting for the reconstruction of the grayvalue information in the frescoes. This approach produced fairly good results for the inpainting of homogeneous areas in the frescoes. As one immediately observes, parts of the surface of the Neidhart frescoes are more texture-like. Since the inpainting methods we used cannot reproduce texture, they can only deliver visually good results to a limited extent.

In Figure 5.9 a part of the fully restored frescoes is shown¹. A direct comparison between the restorated frescoes and our digital results defines the next step within this project.



Figure 5.9: The restored fresco. Image courtesy Wolfgang Baatz.

5.2 Road Reconstruction

This project is about the continuation of roads in aerial images and takes place in Andrea Bertozzi's group at UCLA² (cf. also [DB08]). The roads are partially occluded, e.g., by trees, cf. Figure 5.10, and now the challenge is to reconstruct the roads such that one is able to follow them in aerial images.

¹The author thanks Wolfgang Baatz for providing this data.

²I would like to thank the UCLA Mathematics Department, and Alan Van Nevel and Gary Hewer from the Naval Air Weapons Station in China Lake, CA for providing the data.



Figure 5.10: Road data from Los Angeles

Our first approach is to binarize the road data and apply Cahn-Hilliard inpainting (cf. (2.1) in Section 2.1) to the binary roads¹. In Figure 5.11 two examples for Cahn-Hilliard inpainting of binary roads are shown. Note that the Cahn-Hilliard inpainting approach is applied to the corrupted road images in two steps. First the large gap(s) in the road are filled by choosing rather large parameter ϵ in (2.1) and letting the inpainting algorithm run until it reaches a steady state. Using the result from this first step, Cahn-Hilliard inpainting is applied again with a small ϵ in order to sharpen the edges in the image.



Figure 5.11: Cahn-Hilliard inpainting in two steps, namely with $\epsilon = 0.1$ and $\epsilon = 0.01$ in the first row, and $\epsilon = 1.6$ and $\epsilon = 0.01$ in the second row of the Figure

5.2.1 Bitwise Cahn-Hilliard Inpainting

In a second approach we shall reconstruct the roads with a bitwise Cahn-Hilliard inpainting approach. Specifically, one possible generalization of Cahn-Hilliard inpainting

¹Thanks to Shao-Ching Huang (UCLA) for the preparation of the data

5.2 Road Reconstruction

for grayscale images is to split the grayscale image bit-wise into channels

$$u(x) \sim \sum_{k=1}^K u_k(x) 2^{-(k-1)},$$

where $K > 0$. The Cahn-Hilliard inpainting approach is then applied to each binary channel u_k separately, compare Figure 5.12. At the end of the inpainting process the channels are assembled again and the result is the inpainted grayvalue image in lower grayvalue resolution, cf. Figure 5.13. In Figure 5.12 and 5.13 the application of bitwise Cahn-Hilliard inpainting for the restoration of satellite images of roads is demonstrated. One can imagine that the black dots in the first picture in Figure 5.13 represent trees that cover parts of the road. The idea of bitwise Cahn-Hilliard inpainting was proposed in [DB08] for inpainting with wavelets based on Allen-Cahn energy.

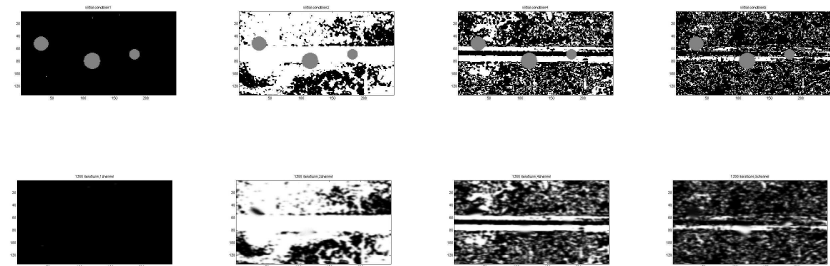


Figure 5.12: What is going on in the channels? The given image (first row) and the Cahn-Hilliard inpainting result (second row) for the 1st, 3rd, 4th, and 5th channel

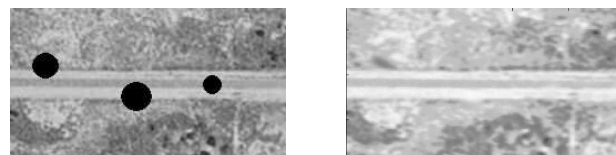


Figure 5.13: Bitwise Cahn-Hilliard inpainting with $K = 8$ binary channels applied to road restoration: (l.) given distorted aerial image of a road; (r.) result of the inpainting process with the assembled binary channels of Figure 5.12.

Chapter 6

Conclusion

My PhD thesis is mainly concerned with higher-order partial differential equations in image inpainting. The analysis and numerical realization of Cahn-Hilliard inpainting and TV-H⁻¹inpaiting have been of particular interest. I could extend the understanding of these inpainting approaches by, among other things, giving answers about stationary solutions of the underlying equations, by an analysis for the inpainting error, and by giving an interpretation of these inpainting approaches in terms of a mechanism based on transport and diffusion. Moreover, I presented reliable and efficient numerical solvers for higher-order inpainting approaches concluding with a domain decomposition approach for TV-based inpainting methods. In addition, the applicability of the discussed inpainting approaches was brought to the test for the restoration of ancient frescoes and the inpainting of satellite images of roads.

In the following I would like to address some open problems that I consider to be interesting for the understanding of higher-order inpainting schemes:

- The advantage of fourth-order inpainting models over models of second differential order is in the smooth continuation of image contents even across large gaps in the image. A motivation for the reasonability of this claim was already given in the Introduction of this thesis. Briefly we can imagine that a fourth-order partial differential equation requires one boundary condition more than a second-order equation. In [BEG07b] the authors showed that, in the limit $\lambda_0 \rightarrow \infty$, a stationary solution u of the Cahn-Hilliard equation fulfills two conditions on the boundary of the inpainting domain, i.e., $u = f$ and $\nabla u = \nabla f$ on ∂D , cf. also (2.2) in Section 2.1. Hence during the inpainting process, in addition, to the value

of the image function, its gradient is continued into the missing domain. This is also true for our other two inpainting approaches, i.e., TV- H^{-1} inpainting and inpainting with LCIS, and is motivated by the numerical results in Figures 2.8 and 2.4. A rigorous derivation of this phenomenon, as the one for Cahn-Hilliard inpainting in [BEG07b], is a matter for future research.

- Besides the fact that rigorous results for fourth-order partial differential equations are rare in general, an asymptotic analysis of our three inpainting models would be of high (even practical) interest. More precisely the convergence of a solution of the evolution equations (2.1), (2.27), and (2.42), to a stationary state is still open. Since the inpainted image is the stationary solution of those evolution equations, the asymptotic behavior is of course an issue. Also in practice, the numerical schemes are solved to steady state (up to an approximational error). Note that additionally to the fourth differential order, a difficulty in the convergence analysis of (2.1) and (2.27) is that they do not follow a variational principle.

Moreover, regularity results for solutions of higher-order inpainting approaches are mostly missing. For the proofs of Theorem 4.1.16 and Theorem 4.1.21, for instance, we had to assume that the exact solution is bounded on a finite time interval in a certain Sobolev norm. As we already argued in the remarks after the statement of the theorems, these assumptions seem to be heuristically reasonable, considering earlier results in [BGOV05, BG04]. Nevertheless, a rigorous derivation of such bounds is still missing.

- Fast numerical solvers for inpainting with higher-order equations is still a mostly open issue, cf. the introductory Section 1.3.3 and Chapter 4. Let me list two promising approaches, whose applicability for inpainting has to be tested still.
 - As already pointed out in Section 1.3.3, the work in [GBO09], i.e., the so-called Bregman split method, promises very small computation times for ℓ_1 regularized optimization problems in the context of surface reconstruction with missing data points. A future project could be to check the possible effectiveness of the algorithm in [GBO09] for the higher-order TV- H^{-1} inpainting approach and inpainting with LCIS.

-
- In [WAB] Weiss et al. propose an efficient numerical algorithm for constrained total variation minimization, which is based on a recent advance in convex optimization proposed by Nesterov [Ne05]. They show that their scheme allows to obtain a solution of precision ϵ in $O(1/\epsilon)$ iterations, i.e., in the case of a strongly convex constraint even in only $O(1/\sqrt{\epsilon})$ iterations. An idea, is to speed up the computation for TV-H⁻¹inpainting, combining this new method from [WAB] with my approach in Section 4.2, where TV-H⁻¹inpainting is computed iteratively via the minimization of surrogate functionals (4.47).

Appendix A

Mathematical Preliminaries

A.1 Distributional Derivatives

Take $\Omega \subset \mathbb{R}^d$, $d \geq 1$, to be an open set. We define $\mathcal{D}(\Omega) := C_c^\infty(\Omega)$, where $C_c^\infty(\Omega)$ is the set of C^∞ functions with compact support in Ω . Then $\mathcal{D}'(\Omega)$ denotes the set of real continuous linear functionals on $\mathcal{D}(\Omega)$ which we call **the space of distributions** on Ω . We will denote the pairing of $\mathcal{D}'(\Omega)$ and $\mathcal{D}(\Omega)$ by $\langle \cdot, \cdot \rangle_{\mathcal{D}', \mathcal{D}}$. In the following we define partial derivatives of a distribution.

Definition A.1.1. ($\partial^\alpha u$) For $u \in \mathcal{D}'(\Omega)$ and for any multi-index α we define $\partial^\alpha u$ by

$$\langle \partial^\alpha u, \phi \rangle_{\mathcal{D}', \mathcal{D}} := (-1)^{|\alpha|} \langle u, \partial^\alpha \phi \rangle_{\mathcal{D}', \mathcal{D}} \quad \text{for all } \phi \in \mathcal{D}(\Omega).$$

Compare [Fo99] for more details on distribution theory.

A.2 Subgradients and Subdifferentials

Let H be a real Hilbert space with norm $\|\cdot\|$ and inner product (\cdot, \cdot) . Given $\mathcal{J} : H \rightarrow \mathbb{R}$ and $u \in H$ we say that \mathcal{J} is **Fréchet-differentiable** at $u \in H$ if

$$\nabla \mathcal{J}(u) = \lim_{t=0} \frac{d}{dt} \mathcal{J}(u + tv) < \infty.$$

Then $\nabla \mathcal{J}(u)$ is called the Fréchet derivative (or first variation) of \mathcal{J} .

In some cases the above limit does not exist, i.e., the function \mathcal{J} is not differentiable. Then we introduce the notion of the subdifferential of a function (cf. [Ev98]).

Definition A.2.1. Let X be a locally convex space, X' its dual, $\langle \cdot, \cdot \rangle$ the bilinear pairing over $X \times X'$ and \mathcal{J} a mapping of X into \mathbb{R} . The **subdifferential** of \mathcal{J} at $u \in X$ is defined as

$$\partial\mathcal{J}(u) = \{p \in X' | \langle v - u, p \rangle \leq \mathcal{J}(v) - \mathcal{J}(u), \forall v \in X\}.$$

A.3 Functional Analysis

Theorem A.3.1. (Rellich-Kondrachov Compactness Theorem) cf. [Al92], Theorem 8.7, p. 243

Assume that Ω is a bounded and open subset of \mathbb{R}^d with Lipschitz boundary. Suppose that $1 \leq r < d$. Then

$$W^{1,r}(\Omega) \hookrightarrow L^q(\Omega),$$

for each $1 \leq q < \frac{dr}{d-r}$.

Theorem A.3.2. (Fatou's Lemma) If f_1, f_2, \dots is a sequence of non-negative measurable functions defined on a measure space (S, Σ, μ) , then

$$\int_S \liminf_{n \rightarrow \infty} f_n d\mu \leq \liminf_{n \rightarrow \infty} \int_S f_n d\mu.$$

Let X denote a real Banach space.

Definition A.3.3. A set $K \subset X$ is convex if for all $u, v \in K$ and constants $0 \leq \lambda \leq 1$, $\lambda u + (1 - \lambda)v \in K$.

Theorem A.3.4. (Characterization of compact sets) A closed subset K of a Banach space X is compact if and only if there is a sequence (x_n) in X such that $\|x_n\| \rightarrow 0$ and K is a subset of the closed convex hull of (x_n) .

Theorem A.3.5. (Schauder's fixed point theorem). Suppose that $K \subset X$ is compact and convex, and assume also $A : K \rightarrow K$ is continuous. Then A has a fixed point.

Proof. cf. [Ev98] Section 9.2.2. page 502-507. □

A.4 The Space H^{-1} and the Inverse Laplacian Δ^{-1}

We denote by $H^{-1}(\Omega)$ the dual space of $H_0^1(\Omega)$ with corresponding norm $\|\cdot\|_{-1}$. For a function $f \in H^{-1}(\Omega)$ the norm is defined as

$$\|f\|_{-1}^2 = \|\nabla \Delta^{-1} f\|_2^2 = \int_{\Omega} (\nabla \Delta^{-1} f)^2 dx.$$

Thereafter the operator Δ^{-1} denotes the inverse to the negative Dirichlet Laplacian, i.e., $u = \Delta^{-1}f$ is the unique solution to

$$\begin{aligned} -\Delta u &= f && \text{in } \Omega \\ u &= 0 && \text{on } \partial\Omega. \end{aligned}$$

A.5 Functions of Bounded Variation

The following results can be found in [AFP00], see also [Gi84], and [EG92]. Let $\Omega \subset \mathbb{R}^2$ be an open and bounded Lipschitz domain. As in [AFP00] the space of functions of bounded variation $BV(\Omega)$ in two space dimensions is defined as follows:

Definition A.5.1. ($BV(\Omega)$) *Let $u \in L^1(\Omega)$. We say that u is a **function of bounded variation in Ω** if the distributional derivative of u is representable by a finite Radon measure in Ω , i.e., if*

$$\int_{\Omega} u \frac{\partial \phi}{\partial x_i} dx = - \int_{\Omega} \phi dD_i u \quad \forall \phi \in C_c^{\infty}(\Omega), i = 1, 2,$$

for some \mathbb{R}^2 -valued measure $Du = (D_1 u, D_2 u)$ in Ω . The vector space of all functions of bounded variation in Ω is denoted by $BV(\Omega)$.

Further, the space $BV(\Omega)$ can be characterized by the total variation of Du . For this we first define the so-called variation $V(u, \Omega)$ of a function $u \in L^1_{loc}(\Omega)$.

Definition A.5.2. (*Variation*) *Let $u \in L^1_{loc}(\Omega)$. The **variation** $V(u, \Omega)$ of u in Ω is defined by*

$$V(u, \Omega) := \sup \left\{ \int_{\Omega} u \operatorname{div} \phi dx : \phi \in (C_c^1(\Omega))^2, \|\phi\|_{L^\infty(\Omega)} \leq 1 \right\}.$$

A simple integration by parts proves that

$$V(u, \Omega) = \int_{\Omega} |\nabla u| dx$$

if $u \in C^1(\Omega)$. By a standard density argument this is also true for functions $u \in W^{1,1}(\Omega)$. Before we proceed with the characterization of $BV(\Omega)$ let us recall the definition of the total variation of a measure:

Definition A.5.3. (*Total variation of a measure*) Let (X, \mathcal{E}) be a measure space. If μ is a measure, we define its **total variation** $|\mu|$ as follows:

$$|\mu|(E) := \sup \left\{ \sum_{h=0}^{\infty} |\mu(E_h)| : E_h \in \mathcal{E} \text{ pairwise disjoint}, E = \bigcup_{h=0}^{\infty} E_h \right\}, \forall E \subset \mathcal{E}.$$

With Definition A.5.2 the space $BV(\Omega)$ can be characterized as follows

Theorem A.5.4. Let $u \in L^1(\Omega)$. Then u belongs to $BV(\Omega)$ if and only if $V(u, \Omega) < \infty$. In addition, $V(u, \Omega)$ coincides with $|Du|(\Omega)$, the total variation of Du , for any $u \in BV(\Omega)$ and $u \mapsto |Du|(\Omega)$ is lower semicontinuous in $BV(\Omega)$ with respect to the $L^1_{loc}(\Omega)$ topology.

Note that $BV(\Omega)$ is a Banach space with respect to the norm

$$\|u\|_{BV(\Omega)} = \|u\|_{L^1(\Omega)} + |Du|(\Omega).$$

Now we introduce so-called weak* convergence in $BV(\Omega)$ which is useful for its compactness properties. Note that this convergence is much weaker than the norm convergence.

Definition A.5.5. (*Weak* convergence*) Let $u, u_h \in BV(\Omega)$. We say that (u_h) **weakly*** converges in $BV(\Omega)$ to u (denoted by $u_h \xrightarrow{*} u$) if (u_h) converges to u in $L^1(\Omega)$ and (Du_h) weakly* converges to Du in all (Ω) , i.e.,

$$\lim_{h \rightarrow \infty} \int_{\Omega} \phi \, dDu_h = \int_{\Omega} \phi \, dDu \quad \forall \phi \in C_0(\Omega).$$

A simple criterion for weak* convergence is the following:

Theorem A.5.6. Let $(u_h) \subset BV(\Omega)$. Then (u_h) weakly* converges to u in $BV(\Omega)$ if and only if (u_h) is bounded in $BV(\Omega)$ and converges to u in $L^1(\Omega)$.

Further we have the following compactness theorem:

Theorem A.5.7. (*Compactness for $BV(\Omega)$*)

- Let Ω be a bounded domain with compact Lipschitz boundary. Every sequence $(u_h) \subset BV_{loc}(\Omega)$ satisfying

$$\sup \left\{ \int_A |u_h| \, dx + |Du_h|(A) : h \in \mathbb{N} \right\} < \infty \quad \forall A \subset \subset \Omega \text{ open},$$

admits a subsequence (u_{h_k}) converging in $L^1_{loc}(\Omega)$ to $u \in BV_{loc}(\Omega)$. If the sequence is further bounded in $BV(\Omega)$ then $u \in BV(\Omega)$ and a subsequence converges weakly* to u .

- Let Ω be a bounded domain in \mathbb{R}^d with Lipschitz boundary. Then every uniformly bounded sequence $(u_k)_{k \geq 0}$ in $BV(\Omega)$ is relatively compact in $L^r(\Omega)$ for $1 \leq r < \frac{d}{d-1}$, $d \geq 1$. Moreover, there exists a subsequence u_{k_j} and u in $BV(\Omega)$ such that $u_{k_j} \rightharpoonup u$ weakly* in $BV(\Omega)$. In particular for $d = 2$ this compact embedding holds for $1 \leq r < 2$.

Let $u \in L^1(\Omega)$. We introduce the mean value u_Ω of u as

$$u_\Omega := \frac{1}{|\Omega|} \int_\Omega u(x) dx.$$

A generalization of the Poincare inequality gives the so-called Poincare-Wirtinger inequality for functions in $BV(\Omega)$.

Theorem A.5.8. (*Poincare-Wirtinger inequality*) If $\Omega \subset \mathbb{R}^2$ is a bounded, open and connected domain with compact Lipschitz boundary, we have

$$\|u - u_\Omega\|_{L^p(\Omega)} \leq C |Du|(\Omega) \quad \forall u \in BV(\Omega), \quad 1 \leq p \leq 2$$

for some constant C depending only on Ω .

Finally, since every normed vector space is a locally convex space, the theory of subdifferentials from Section A.2 applies to the framework where $X = BV(\Omega)$. For a characterization of elements in the subdifferential $\partial |Du|(\Omega)$ we refer to the very detailed analysis of L. Vese in [Ve01].

References

- [AV94] R. Acar, and C.R. Vogel, *Analysis of bounded variation penalty method for ill-posed problems*, Inverse Problems, Vol. 10, No. 6, pp.1217-1229, 1994. [136](#)
- [ABC94] N. Alikakos, P.W. Bates, and X. Chen, *Convergence of the Cahn-Hilliard equation to the Hele-Shaw model*, Arch. Rat. Mech. Anal. 128, No. 2, pp. 165-205, 1994. [43](#)
- [ABF91] N. Alikakos, P.W. Bates, and G. Fusco, *Slow motion for the Cahn-Hilliard equation in one space dimension*, J. Differ. Equations, 90, 1, 81-135, 1991. [72](#), [76](#), [81](#), [82](#)
- [AF94] N. Alikakos, and G. Fusco, *Slow dynamics for the Cahn-Hilliard equation in higher space dimensions. I: Spectral estimates*, Commun. Partial Differ. Equations, 19, 9-10, 1397-1447, 1994. [72](#), [76](#), [82](#), [83](#)
- [Al92] H.W. Alt, *Linear Funktionalanalysis*, Springer Verlag, 1992. [218](#)
- [AFP00] L. Ambrosio, N. Fusco, and D. Pallara, *Functions of bounded variation and free discontinuity problems.*, Oxford Mathematical Monographs. Oxford: Clarendon Press. xviii, 2000. [42](#), [161](#), [162](#), [164](#), [219](#)
- [AMRT08] F. Andreu, J. M. Mazon, J.D. Rossi, J. Toledo, *The Neumann problem for nonlocal nonlinear diffusion equations*. J. Evol. Eqns., 8(1), pp. 189–215, 2008. [95](#)
- [AKR97] S. Armstrong, A. Kokaram, P. J. W. Rayner, *Nonlinear interpolation of missing data using min-max functions*, IEEE Int. Conf. Nonlinear Signal and Image Processing, 1997. [7](#)

REFERENCES

- [AK06] G. Aubert, and P. Kornprobst, *Mathematical Problems in Image Processing. Partial Differential Equations and the Calculus of Variations*, Springer, Applied Mathematical Sciences, Vol 147, 2006. [4](#), [8](#), [52](#), [184](#)
- [AV97] G. Aubert and L. Vese, *A variational method in image recovery.*, SIAM J. Numer. Anal. **34**, no. 5, pp. 1948–1979, 1997. [42](#)
- [BFMS08] W. Baatz, M. Fornasier, P. Markowich, C.-B. Schönlieb, *Inpainting of ancient Austrian frescoes*, Conference proceedings of Bridges 2008, Leeuwarden, pp.150-156, 2008. [6](#), [23](#), [202](#)
- [BBCSV01] C. Ballester, M. Bertalmio, V. Caselles, G. Sapiro, and J. Verdera, *Filling-in by joint interpolation of vector fields and grey levels*, IEEE Transactions on Image Processing, vol. 10, no. 8, pp. 1200-1211, 2001. [6](#), [11](#), [13](#)
- [Ba07] R. Baraniuk, *Compressive sensing*, Lecture Notes in IEEE Signal Processing Magazine, Vol. 24, July 2007. [159](#)
- [BP96] V. Barbu and T. Precupanu, *Convexity and Optimization in Banach Spaces*, 1996. [167](#)
- [BB97] J. W. Barrett, and J. F. Blowey, *Finite element approximation of a model for phase separation of a multi-component alloy with non-smooth free energy*, Numer. Math. 77, Nr. 1, pp.1-34, 1997. [106](#)
- [BB98] J. W. Barrett, and J. F. Blowey, *Finite element approximation of a model for phase separation of a multi-component alloy with a concentration-dependent mobility matrix*, IMA J. Numer. Anal. 18, Nr. 2, pp. 287-328, 1998. [19](#)
- [BB99a] J. W. Barrett, and J. F. Blowey, *Finite element approximation of a model for phase separation of a multi-component alloy with nonsmooth free energy and a concentration dependent mobility matrix*, Math. Models Methods Appl. Sci. 9, Nr. 5, pp. 627-663, 1999. [19](#)
- [BB99b] J. W. Barrett, and J. F. Blowey, *Finite element approximation of the Cahn-Hilliard equation with concentration dependent mobility*, Math. Comp. 68, Nr. 226, pp. 487-517, 1999. [19](#)

REFERENCES

- [BCC05] P. Bates, X. Chen, A. Chmaj, *Heteroclinic solutions of a van der Waals model with indefinite nonlocal interactions*, Calc. Var. 24, 261–281, (2005). [94](#)
- [BFRW97] P. Bates, P. Fife, X. Ren and X. Wang, *Travelling waves in a convolution model for phase transitions*. Arch. Rat. Mech. Anal., 138, 105–136, (1997). [94](#)
- [BX94] P.W. Bates, and J. Xun, *Metastable patterns for the Cahn-Hilliard equation.* I., J. Differ. Equations, 111, 2, 421-457, 1994. [72](#)
- [BDHP03] H. H. Bauschke, F. Deutsch, H. Hundal, and S-H. Park, *Accelerating the convergence of the method of alternating projections*, Trans. Americ. Math. Soc. **355**, no. 9, pp. 3433–3461, 2003. [153](#)
- [BBL97] H. H. Bauschke, J. M Borwein, and A. S. Lewis, *The method of cyclic projections for closed convex sets in Hilbert space. Recent developments in optimization theory and nonlinear analysis*, (Jerusalem, 1995), 1–38, Contemp. Math., 204, Amer. Math. Soc., Providence, RI, 1997 [170](#)
- [BGLR02] J. Becker, G. Grün, M. Lenz, and M. Rumpf, *Numerical methods for fourth order nonlinear diffusion problems*, Applications of Mathematics, Vol. 47, pp. 517–543, 2002. [19](#)
- [BBAC04] J. Bect, L. Blanc-Féraud, G. Aubert, and A. Chambolle, *A ℓ^1 -unified variational framework for image restoration*. In T. Pajdla and J. Matas, editors, Proceedings of the 8th European Conference o Computer Vision, vol. IV, Prague, Czech Republic, 2004. Springer Verlag. [21](#), [136](#), [148](#)
- [BBS01] M. Bertalmio, A.L. Bertozzi, and G. Sapiro, *Navier-Stokes, fluid dynamics, and image and video inpainting*, Proceedings of the 2001 IEEE Computer Society Conference on Computer Vision and Pattern Recognition, 1, pp. 355-362, 2001. [11](#)
- [BSCB00] M. Bertalmio, G. Sapiro, V. Caselles, and C. Ballester, *Image Inpainting*, Siggraph 2000, Computer Graphics Proceedings, pp.417–424, 2000. [6](#), [7](#), [11](#), [13](#), [14](#), [18](#), [19](#), [44](#), [62](#), [64](#)

REFERENCES

- [BVS03] M. Bertalmio, L. Vese, G. Sapiro, and S. Osher, *Simultaneous structure and texture image inpainting*, IEEE Trans. Image Process., Vol. 12, Nr. 8, pp. 882-889, 2003. [16](#), [44](#)
- [BEG07a] A. Bertozzi, S. Esedoglu, and A. Gillette, *Inpainting of Binary Images Using the Cahn-Hilliard Equation*. IEEE Trans. Image Proc. 16(1) pp. 285-291, 2007. [15](#), [18](#), [19](#), [20](#), [21](#), [22](#), [24](#), [25](#), [37](#), [95](#), [110](#), [118](#), [120](#), [206](#)
- [BEG07b] A. Bertozzi, S. Esedoglu, and A. Gillette, *Analysis of a two-scale Cahn-Hilliard model for image inpainting*, Multiscale Modeling and Simulation, vol. 6, no. 3, pages 913-936, 2007. [15](#), [17](#), [18](#), [19](#), [20](#), [21](#), [22](#), [25](#), [26](#), [27](#), [34](#), [37](#), [59](#), [95](#), [110](#), [118](#), [206](#), [214](#), [215](#)
- [BG04] A. Bertozzi, J.B. Greer, *Low-Curvature Image Simplifiers: Global Regularity of Smooth Solutions and Laplacian Limiting Schemes*, Communications on Pure and Applied Mathematics, Vol.LVII, p. 764-790, 2004. [60](#), [61](#), [130](#), [215](#)
- [BGOV05] A. Bertozzi, J. Greer, S. Osher, and K. Vixie, *Nonlinear regularizations of TV based PDEs for image processing*, AMS Series of Contemporary Mathematics, vol. 371, pages 29-40, Gui-Qiang Chen, George Gasper, and Joseph Jerome eds, 2005. [120](#), [122](#), [123](#), [215](#)
- [BE92] J.F. Blowey, and C.M. Elliott, *The Cahn-Hilliard gradient theory for phase separation with non-smooth free energy. II: Numerical analysis*, Eur. J. Appl. Math., 3, 2, 147-179, 1992. [85](#)
- [BM07] F. Bornemann and T. M  rz, *Fast Image Inpainting Based on Coherence Transport*, J. Math. Imaging Vis. 28, pp.259-278, 2007. [15](#), [20](#)
- [Br02] A. Braides, *Gamma-Convergence for Beginners*. Nr. 22 in Oxford Lecture Series in Mathematics and its Applications. Oxford University Press, 2002. [190](#)
- [BPWX91] J. H. Bramble, J. E. Pasciak, J. Wang, and J. Xu, *Convergence estimates for product iterative methods with applications to domain decomposition*, Math. Comp. **57**, no. 195, pp.1–21, 1991. [153](#)
- [Br98] P. Bremaud, *Markov Chains: Gibbs Fields, Monte Carlo Simulation, and Queues*, Springer-Verlag, New York, 1998. [9](#)

REFERENCES

- [BC08] C. Brito-Loeza, and K. Chen, *Multigrid method for a modified curvature driven diffusion model for image inpainting*, Journal of Computational Mathematics, Vol.26, No.6, pp. 856875, 2008. [20](#)
- [BH92] L. Bronsard, and D. Hilhorst, *On the slow dynamics for the Cahn-Hilliard equation in one space dimension*, Proc. R. Soc. Lond., Ser. A, 439, 1907, 669-682, 1992. [72](#)
- [BK90] L. Bronsard, and R.V. Kohn, *On the slowness of phase boundary motion in one space dimension*, Commun. Pure Appl. Math., 43, 8, 983-997, 1990. [72](#)
- [BR77] R. E. Bruck and S. Reich, *Nonexpansive projections and resolvents of accretive operators in Banach spaces*. Houston J. Math. 3, no. 4, pp. 459–470, 1977. [170](#)
- [BCM05] A. Buades, B. Coll, and J-M. Morel, *On image denoising methods*. SIAM Multiscale Modeling and Simulation, 4(2), 490-530, (2005). [94](#)
- [BCMS08] M.Burger, S.-Y.Chu, P.Markowich, C.-B. Schönlieb, *The Willmore Functional and Instabilities in the Cahn-Hilliard equation*, Communications in Mathematical Sciences, Volume 6, Issue 2 (June 2008), pp 309-329, 2008. [23](#), [70](#), [74](#)
- [BHS08] M. Burger, L. He, C. Schönlieb, *Cahn-Hilliard inpainting and a generalization for grayvalue images*, UCLA CAM report 08-41, June 2008. [15](#), [18](#), [19](#), [20](#), [21](#), [22](#), [24](#), [26](#), [37](#), [42](#), [58](#), [151](#), [204](#)
- [BO05] M. Burger, and S. Osher, *Convergence rates of convex variational regularization*, Inverse Problems, Vol. 20, Nr. 5, pp. 1411-1421(11), 2005. [54](#)
- [BRH07] M. Burger, E. Resmerita, L. He, *Error Estimation for Bregman Iterations and Inverse Scale Space Methods in Image Restoration*, Computing, Vol. 81, pp. 109-135, 2007. [51](#), [54](#), [55](#)
- [CH58] J.W. Cahn, and J.E. Hilliard, *Free energy of a non-uniform system. I. Interfacial free energy*, J. Chem. Phys., 28, 258-267, 1958. [71](#)
- [Ca06] E. J. Candès, *Compressive sampling*, Int. Congress of Mathematics, 3, pp. 1433-1452, Madrid, Spain, 2006 [159](#)

REFERENCES

- [Ca88] S.Carlsson, *Sketch Based Coding of Grey Level Images*, Signal Processing, 15, 57- 83, 1988. [7](#)
- [CGS84] J. Carr, M.E. Gurtin, and M. Slemrod, *Structured phase transitions on a finite interval*, Archive for Rational Mechanics and Analysis, 86, 317-351, 1984. [82](#)
- [Ca97] C. Carstensen, *Domain decomposition for a non-smooth convex minimization problems and its application to plasticity*, Numerical Linear Algebra with Applications, 4, 177–190, 1997. [157](#), [158](#)
- [Ca96] J. R. Casas, *Image Compression based on Perceptual Coding Techniques*, PhD Thesis, Dept. Signal Theory Commun., UPC, Barcelona, Spain, March 1996. [7](#)
- [CT94] J. R. Casas and L. Torres, *Coding of Details in Very Low Bit-rate Video Systems*, IEEE Trans. CSVT, vo1.4, pp. 317-327, June, 1994. [7](#)
- [CMS98] V. Caselles, J.-M. Morel, and C. Sbert, *An axiomatic approach to image interpolation*, IEEE Trans. Image Processing, 7(3):376386, 1998. [7](#), [12](#)
- [Ch04] A. Chambolle, *An Algorithm for Total Variation Minimization and Applications*, J. Math. Imaging Vis. 20, 1-2, pp. 89-97, 2004. [21](#), [42](#), [104](#), [136](#), [140](#), [142](#), [144](#), [145](#), [158](#), [159](#), [163](#), [189](#), [190](#), [196](#)
- [CD08] A. Chambolle, J. Darbon, *On total variation minimization and surface evolution using parametric maximum flows*, UCLA CAM report 08-19, 2008. [22](#)
- [CL97] A. Chambolle and P.-L. Lions, *Image recovery via total variation minimization and related problems.*, Numer. Math. **76**, no. 2, pp. 167–188, 1997. [9](#), [42](#), [162](#)
- [CK06] T.F. Chan, and S.H. Kang, *Error Analysis for Image Inpainting*, J. Math. Imaging Vis. 26, 1-2, 85-103, 2006. [54](#), [55](#), [57](#)
- [CKS02] T.F. Chan, S.H. Kang, and J. Shen, *Euler's elastica and curvature-based inpainting*, SIAM J. Appl. Math., Vol. 63, Nr.2, pp.564–592, 2002. [13](#), [14](#), [18](#), [19](#), [20](#), [22](#), [23](#), [24](#), [62](#), [63](#), [64](#)
- [CM94] T. F. Chan and T. P. Mathew, *Domain decomposition algorithms*, Acta Numerica, pp. 61–143, 1994. [153](#)

REFERENCES

- [CS05] T.F. Chan and J. Shen, *Variational Image Inpainting*, Comm. Pure Applied Math, Vol. 58, pp. 579-619, 2005. [6](#), [9](#), [16](#), [17](#), [19](#)
- [CS01a] T. F. Chan and J. Shen, *Mathematical models for local non-texture inpaintings*, SIAM J. Appl. Math., 62(3):10191043, 2001. [6](#), [7](#), [9](#), [10](#), [13](#), [15](#)
- [CS01b] T.F. Chan, and J. Shen, *Morphologically invariant PDE inpaintings*, CAM report 01-15. [14](#)
- [CS01c] T. F. Chan and J. Shen, *Non-texture inpainting by curvature driven diffusions (CDD)*, J. Visual Comm. Image Rep., 12(4):436449, 2001. [6](#), [10](#), [13](#), [14](#), [18](#), [19](#), [20](#), [62](#), [64](#)
- [CS01d] T. F. Chan and J. Shen, *Variational restoration of non-flat image features: models and algorithms*, SIAM J. Appl. Math., 61(4):13381361, 2001. [13](#)
- [CSZ06] T.F. Chan, J.-H. Shen, and H.-M. Zhou, *Total variation wavelet inpainting*, J. Math. Imaging Vis., 25:1, pp. 107-125, 2006. [15](#)
- [CCB03] L. Chanas, J. P. Cocquerez, and J. Blanc-Talon, *Simultaneous inpainting and motion estimation of highly degraded video-sequences*, Lecture Notes in Computer Science, Vol 2749, pp. 11-23, 2003. [6](#)
- [CCR06] E. Chasseigne, M. Chaves and J. D. Rossi, *Asymptotic behaviour for nonlocal diffusion equations*. J. Math. Pures Appl., 86, 271–291, (2006). [95](#), [96](#)
- [Ch96] X. Chen, *Global asymptotic limit of solutions of the Cahn-Hilliard equation*, J. Differ. Geom., 44, 2, 262-311, 1996. [74](#)
- [CK96] X. Chen, and M. Kowalczyk, *Existence of equilibria for the Cahn-Hilliard equation via local minimizers of the perimeter*, Commun. Partial Differ. Equations, 21, 7-8, 1207-1233, 1996. [72](#)
- [CW05] P. L. Combettes and V. R. Wajs, *Signal recovery by proximal forward-backward splitting*, Multiscale Model. Simul., 4, no. 4, pp. 1168–1200, 2005. [158](#), [162](#), [163](#), [167](#), [171](#), [172](#), [174](#)

REFERENCES

- [CCEM07] C. Cortázar, J. Coville, M. Elgueta, S. Martínez, *A non local inhomogeneous dispersal process*, Journal of Differential Equations Vol. 241, Iss. 2, pp. 332–358, 2007. [95](#)
- [CER05] C. Cortázar, M. Elgueta and J. D. Rossi, *A non-local diffusion equation whose solutions develop a free boundary*. Annales Henri Poincaré, 6(2), 269–281, 2005. [95](#)
- [CERW07] C. Cortazar, M. Elgueta, J.D. Rossi and N. Wolanski, *Boundary fluxes for non-local diffusion*. J. Differential Equations, 234, 360–390, 2007. [95](#)
- [CERW08] C. Cortazar, M. Elgueta, J.D. Rossi and N. Wolanski, *How to approximate the heat equation with Neumann boundary conditions by nonlocal diffusion problems*. Arch. Rat. Mech. Anal., 187(1), 137–156, 2008. [95](#), [97](#)
- [Co06] J. Coville, *On uniqueness and monotonicity of solutions on non-local reaction diffusion equations*. Ann. Mat. Pura Appl. 185, 461–485, 2006. [94](#)
- [Co07] J. Coville, *Maximum principles, sliding techniques and applications to nonlocal equations*. Electron. J. Diff. Eqns. 2007, no. 68, 1–23, 2007. [94](#)
- [CDM08] J. Coville, J. Dávila, S. Martínez, *Existence and uniqueness of solutions to a nonlocal equation with monostable nonlinearity*, Siam Journal on Mathematical Analysis, 39 (5), pp. 1693–1709, 2008. [94](#)
- [CD05] J. Coville, L. Dupaigne, *Propagation speed of travelling fronts in nonlocal reaction diffusion equations*. Nonl. Anal. 60, 797–819, 2005. [94](#)
- [CD07] J. Coville, L. Dupaigne, *On a nonlocal equation arising in population dynamics*. Proc. Roy. Soc. Edinburgh 137, 1–29, 2007. [94](#)
- [CH93] M.C. Cross, and P.C. Hohenberg, *Pattern formation outside of equilibrium*. Rev. Mod. Phys., Vol. 65(3), 1993. [95](#)
- [DS05] J. Darbon, and M. Sigelle, *A fast and exact algorithm for total variation minimization*, IbPRIA 2005, 3522(1), pp. 351–359, 2005. [22](#)

REFERENCES

- [DDD04] I. Daubechies, M. Defrise, and C. DeMol, *An iterative thresholding algorithm for linear inverse problems*, Comm. Pure Appl. Math. **57**, no. 11, pp. 1413–1457, 2004. [158](#), [163](#), [167](#), [172](#), [173](#)
- [DFL08] I. Daubechies, M. Fornasier, and I. Loris, *Acceleration of the projected gradient method for linear inverse problems with sparsity constraints*, J. Fourier Anal. Appl., Vol. 14, No. 5-6, pp. 764–792, 2008. [159](#), [163](#), [167](#)
- [DTV07] I. Daubechies, G. Teschke, and L. Vese, *Iteratively solving linear inverse problems under general convex constraints*, Inverse Probl. Imaging **1**, no. 1, pp. 29–46, 2007. [148](#), [159](#), [163](#), [167](#), [174](#)
- [DL88] R. Dautray, and J.L. Lions, *Mathematical Analysis and Numerical Methods for Science and Technology*. Vol.2, Springer-Verlag, 1988. [139](#)
- [DSC03] L. Demanet, B. Song, T. Chan, *Image inpainting by correspondance maps: a deterministic approach*, Proc. VLSM Conf., Nice, October 2003. [15](#)
- [DB08] J. A. Dobrosotskaya, and A. L. Bertozzi, *A Wavelet-Laplace Variational Technique for Image Deconvolution and Inpainting*, IEEE Trans. Imag. Proc., **17**(5), pp. 657–663, 2008. [211](#), [213](#)
- [DV97] D. C. Dobson and C. R. Vogel, *Convergence of an iterative method for total variation denoising*, SIAM J. Numer. Anal. **34**, no. 5, 1779–1791, 1997. [42](#)
- [DD71] J. Jr. Douglas, and T. Dupont T, *Alternating-direction Galerkin methods on rectangles Numerical Solution of Partial Differential Equations*, II (SYNSPADE 1970) (Proc. Symp., University of Maryland, College Park, Md. 1970) (New York: Academic) pp. 133214, 1971. [19](#)
- [DLRW05] Q. Du, C. Liu, R. Ryham, and X. Wang, *A phase field formulation of the Willmore problem*, Nonlinearity, **18**, 3, pp. 1249–1267, 2005. [73](#)
- [ET76] I. Ekeland and R. Temam, *Convex analysis and variational problems. Translated by Minerva Translations, Ltd., London.*, Studies in Mathematics and its Applications. Vol. 1. Amsterdam - Oxford: North-Holland Publishing Company; New York: American Elsevier Publishing Company, Inc., 1976. [52](#), [163](#), [167](#), [168](#), [171](#)

REFERENCES

- [ESQD05] M. Elad, J.-L. Starck, P. Querre, and D. Donoho, *Simultaneous cartoon and texture image inpainting using morphological component analysis*, Applied and Computational Harmonic Analysis, Vol. 19, No. 3, pp. 340-358, November 2005. [16](#)
- [EF87] C.M. Elliott, and D.A. French, *Numerical Studies of the Cahn-Hilliard Equation for Phase Separation*, IMA J Appl Math, 38, 97-128, 1987. [71](#)
- [ES07] C. M. Elliott, and S. A. Smetheman, *Analysis of the TV regularization and H^{-1} fidelity model for decomposing an image into cartoon plus texture*, Communications on Pure and Applied Analysis, Vol. 6, Nr. 4, pp. 917-936, 2007. [21](#)
- [ES08] C. M. Elliott, and S. A. Smetheman, *Numerical analysis of the TV regularization and H^{-1} fidelity model for decomposing an image into cartoon plus texture*, IMA Journal of Numerical Analysis, pp. 1-39, 2008. [21](#)
- [Em76] G. Emile-Male, *The Restorer's Handbook for Easel Painting*, Van Nostrand Reinhold, New York, 1976. [6](#)
- [ES02] S. Esedoglu, and J.-H. Shen, *Digital inpainting based on the Mumford-Shah-Euler image model*, Eur. J. Appl. Math., 13:4, pp. 353-370, 2002. [15](#), [106](#)
- [Ev98] L.C. Evans, *Partial differential equations*, Graduate Studies in Mathematics 19, American Mathematical Society, Providence, RI, 1998. [12](#), [31](#), [217](#), [218](#)
- [EG92] L. C. Evans and R. F. Gariepy, *Measure Theory and Fine Properties of Functions.*, CRC Press, 1992. [42](#), [219](#)
- [Eyre98] D. Eyre, *An Unconditionally Stable One-Step Scheme for Gradient Systems*, Jun. 1998, unpublished. [85](#), [105](#), [107](#), [108](#)
- [FP03] X. Feng, and A. Prohl, *Analysis of total variation flow and its finite element approximations*, M2AN, 37, pp. 533-556, 2003. [21](#)
- [FP04] X. Feng, and A. Prohl, *Error analysis of a mixed finite element method for the Cahn-Hilliard equation*, Numer. Math., 99, 1, 47-84, 2004. [19](#), [77](#)

REFERENCES

- [FP05] X. Feng, and A. Prohl, *Numerical analysis of the Cahn-Hilliard equation and approximation for the Hele-Shaw problem*, Interfaces Free Bound., 7, 1, 1-28, 2005. [19](#), [71](#), [77](#)
- [Fi00] P.C. Fife, *Models for phase separation and their mathematics*, Electronic Journal of Differential Equations, 2000, 48, 1-26, 2000. [71](#), [95](#)
- [Fi03] P. Fife, *Some nonclassical trends in parabolic and parabolic-like evolutions*. Trends in nonlinear analysis, pp. 153–191, Springer, Berlin, (2003). [94](#)
- [FKMW97] P.C. Fife, H. Kielhoefer, S. Maier-Paape, and T. Wanner, *Perturbation of doubly periodic solution branches with applications to the Cahn-Hilliard equation*, Physica D, 100, 1-4, 257-278, 1997. [72](#)
- [FL96] H. Le Floch, and C. Labit, *Irregular image sub-sampling and reconstruction by adaptive sampling*, in Proc. Int. Conf. Image Processing ICIP-96, Sept. 1996, Lausanne, Switzerland, vol. III, pp. 379-382, 1996. [7](#)
- [Fo99] G. B. Folland, *Real Analysis: Modern Techniques and Their Applications*, Wiley, New York, 1999. [217](#)
- [Fo07] M. Fornasier, *Domain decomposition methods for linear inverse problems with sparsity constraints*, Inverse Problems **23** (2007), 2505–2526. [159](#), [163](#), [165](#), [167](#), [169](#), [183](#)
- [Fo06] M. Fornasier, *Nonlinear projection recovery in digital inpainting for color image restoration*, J. Math. Imaging Vis. Vol. 24, No. 3, pp. 359-373, 2006. [205](#), [206](#)
- [FM07] M. Fornasier, and R. March, *Restoration of color images by vector valued BV functions and variational calculus*, SIAM J. Appl. Math., Vol. 68 No. 2, pp. 437-460, 2007. [206](#)
- [FS07] M. Fornasier, C.-B. Schönlieb, *Subspace correction methods for total variation and l_1 - minimization*, submitted to SIAM J. Numer. Anal., December 2007, 33 pp. [21](#), [23](#), [105](#), [153](#), [157](#), [159](#), [179](#)
- [GG84] S. Geman, and D. Geman, *Stochastic relaxation, Gibbs distributions, and the Bayesian restoration of images*, IEEE Trans. Pattern Anal. Machine Intell. 6 (1984), pp. 721-741. [9](#)

REFERENCES

- [GO07] G. Gilboa and S. Osher, *Nonlocal linear image regularization and supervised segmentation*, SIAM Multiscale Modeling and Simulation (MMS), Vol. 6, No. 2, pp. 595-630, 2007. [15](#), [70](#), [94](#)
- [Gi84] E. Giusti, *Minimal Surfaces and Functions of Bounded Variation*, Birkhäuser Boston 1984. [219](#)
- [Gl03] K. Glasner, *A Diffuse Interface Approach to Hele-Shaw Flow*, Nonlinearity , Vol. 16, pp. 1-18, 2003. [19](#), [133](#)
- [GBO09] T. Goldstein, X. Bresson, S. Osher, *Geometric Applications of the Split Bregman Method: Segmentation and Surface Reconstruction*, UCLA CAM Report 09-06, 2009. [21](#), [215](#)
- [GO08] T. Goldstein, S. Osher, *The Split Bregman Method for L1 Regularized Problems*, UCLA CAM Report 08-29, 2008. [21](#)
- [Gr95] C.P. Grant, *Slow motion in one-dimensional Cahn-Morral systems*, SIAM J. Math. Anal., 26, 1, 21-34, 1995. [72](#)
- [GB04a] J.B. Greer, and A. Bertozzi, *H^1 solutions of a class of fourth order nonlinear equations for image processing*, Discrete Contin. Dyn. Syst., Vol.10, Nr.1-2, pp.349-366, 2004. [60](#)
- [GB04b] J.B. Greer, and A. Bertozzi, *Traveling wave solutions of fourth order PDEs for image processing*, SIAM J. Math. Anal., Vol.36, Nr.1, pp.38-68, 2004. [60](#)
- [GN95] M. Grinfeld, and A. Novick-Cohen, *Counting stationary solutions of the Cahn-Hilliard equation by transversality arguments*, Proc. R. Soc. Edinb., Sect. A, 125, 2, 351-370, 1995. [72](#)
- [GN99] M. Grinfeld, and A. Novick-Cohen, *The viscous Cahn-Hilliard equation: Morse decomposition and structure of the global attractor*, Trans. Am. Math. Soc., 351, 6, 2375-2406, 1999. [72](#)
- [GS03] H. Grossauer, and O. Scherzer, *Using the complex Ginzburg-Landau equation for digital inpainting in 2D and 3D*, Scale Space Methods in Computer Vision, 2695, pp. 225-236, 2003. [15](#), [20](#)

REFERENCES

- [GR00] G. Grün, and M. Rumpf, *Nonnegativity preserving convergent schemes for the thin film equation*, Num. Math., Vol. 87, pp. 113-152, 2000. [19](#)
- [GZYXC06] J.-W. Gu, L. Zhang, G.-Q. Yu, Y.-X. Xing, and Z.-Q. Chen, *X-ray CT metal artifacts reduction through curvature based sinogram inpainting*, Journal of X-Ray Science and Technology, 14:2, pp. 73-82, 2006. [6](#)
- [Gu88] M.E. Gurtin, *Toward a nonequilibrium thermodynamics of two-phase materials*, Archive for Rational Mechanics and Analysis, 100, 3, 275-312, 1988. [71](#)
- [Ha88] J.K. Hale, *Asymptotic behavior of dissipative systems*, Mathematical Surveys and Monographs, A.M.S., 25, 1988. [72](#)
- [Ha04] J. Han, *The Cauchy problem and steady state solutions for a nonlocal Cahn-Hilliard equation*. Electronic J. Differential Equations, Vol. 2004 (113), 1-9, (2004). [95](#)
- [IP97] H. Igehy, and L. Pereira, *Image replacement through texture synthesis*, in Proceedings of the 1997 IEEE International Conference on Image Processing. [7](#)
- [IR07] L. I. Ignat, J. D. Rossi, *A nonlocal convection-diffusion equation*. J. Funct. Anal. 251, 399–437, (2007). [95, 97](#)
- [IR08] L. I. Ignat, J. D. Rossi, *Refined asymptotic expansions for nonlocal evolution equations*, Journal of Evolution Equations. Vol. 8, pp. 617–629, 2008. [95](#)
- [JHC98] E. Jonsson, S.-C. Huang, and T. Chan, *Total Variation Regularization in Positron Emission Tomography*, CAM report 98-58, UCLA, November 1998. [135](#)
- [JCL94] K.-H. Jung, J.-H. Chang, and C. W. Lee, *Error concealment technique using data for block-based image coding*, SPIE, 2308, pp. 1466-1477, 1994. [7](#)
- [KCS02] S. H. Kang, T. F. Chan, and S. Soatto, *Inpainting from multiple views*, IEEE Proceedings of First International Symposium on 3D Data Processing Visualization Transmission, pp. 622-625, 2002. [15](#)
- [Ka96] G. Kanizsa, *Grammaire du Voir*, Diderot, 1996 [12](#)

REFERENCES

- [KOJ05] S. Kindermann, S. Osher, and P. Jones, *Deblurring and denoising of images by nonlocal functionals*. SIAM Multiscale Modeling and Simulation, 4(4), 1091-1115, 2005. [94](#)
- [KMFR95a] A. C. Kokaram, R. D. Morris, W. J. Fitzgerald, and P. J. W. Rayner, *Detection of missing data in sequences I*, IEEE Transactions on Image Processing, vo. 11, no. 4, pp. 1496-1508, 1995. [7](#)
- [KMFR95b] A. C. Kokaram, R. D. Morris, W. J. Fitzgerald, and P. J. W. Rayner, *Interpolation of missing data in image sequences II*, IEEE Trans. Image Process., 11, no.4, pp. 1509-1519, 1995. [6](#), [7](#)
- [KS93] W. Kwok, and H. Sun, *Multidirectional interpolation for spatial error concealment*, IEEE Trans. Consumer Electronics, 39, 1993. [7](#)
- [LXZ03] Y-J. Lee, J. Xu, and L. Zikatanov, *Successive subspace correction method for singular system of equations*, Fourteenth International Conference on Domain Decomposition Methods (I. Herrera, D. E. Keyes, O. B. Widlund, and R. Yates, eds.), UNAM, pp. 315–321, 2003. [153](#)
- [LV08] L. Lieu and L. Vese, *Image restoration and decomposition via bounded total variation and negative Hilbert-Sobolev spaces*, Applied Mathematics & Optimization, Vol. 58, pp. 167-193, 2008. [9](#), [44](#), [136](#), [138](#), [139](#), [140](#), [150](#)
- [Li88] P. L. Lions, *On the Schwarz alternating method*, Proc. First Internat. Sympos. on Domain Decomposition Methods for Partial Differential Equations (R. Glowinski, G. H. Golub, G. A. Meurant, and J. P閞iaux, eds.), SIAM, Philadelphia, PA, 1988. [153](#)
- [Lo93] S. Lojasiewicz, *On semi- and subanalytic geometry. (Sur la gomtrie semi- et sous-analytique)*, Ann. Inst. Fourier, 43, 5, 1575-1595, 1993. [74](#)
- [Lo27] A. E. H. Love, *A Treatise on the Mathematical Theory of Elasticity*, 4th ed., Dover, New York, 1927. [12](#)
- [LT06] O. M. Lysaker and Xue-C. Tai, *Iterative image restoration combining total variation minimization and a second-order functional*, International Journal of Computer Vision, Vol.66, Nr.1, pp.5-18, 2006. [18](#)

REFERENCES

- [Ma00] F. Malgouyres, *Increase in the resolution of digital images: variational theory and applications*, PhD Thesis, Ecole Normale Supérieure de Cachan, France, 2000. [6](#)
- [MG01] F. Malgouyres, and F. Guichard, *Edge direction preserving image zooming: a mathematical and numerical analysis*, SIAM J. Num. Anal., Vol. 39, No.1, pp.1-37, 2001. [6](#)
- [MO00] A. Marquina, and S. Osher, *Explicit algorithms for a new time dependent model based on level set motion for nonlinear deblurring and noise removal*, SIAM J. Sci. Comput. Vol. 22, Nr. 2, pp. 387-405, 2000. [20](#)
- [Ma82] D. Marr, *Vision*, New York: Freeman, 1982. [7](#)
- [MM98] S. Masnou and J. Morel, *Level Lines based Disocclusion*, 5th IEEE Int'l Conf. on Image Processing, Chicago, IL, Oct. 4-7, 1998, pp.259–263, 1998. [6](#), [7](#), [12](#), [13](#), [14](#), [18](#)
- [Ma02] S. Masnou, *Disocclusion: a variational approach using level lines*, IEEE Trans. Image Process. 11(2), pp. 68-76, 2002. [13](#)
- [Ma93] G. Dal Maso, *An introduction to Gamma-convergence*, Birkhäuser, Boston, 1993. [46](#), [47](#)
- [MF05] E.V.L. de Mello, and O.T. da Silveira Filho, *Numerical study of the Cahn-Hilliard equation in one, two and three dimensions*, Physica A, 347, 429-443, 2005. [71](#)
- [Me01] Y. Meyer, *Oscillating Patterns in Image Processing and Nonlinear Evolution Equations*, The Fifteenth Dean Jacqueline B. Lewis Memorial Lectures. American Mathematical Society, Boston, MA, USA, 2001. [9](#), [137](#)
- [Mi86] D. Michelson, *Steady Solutions of the Kuramoto-Sivashinsky Equation*. Physica D 19, 89–111, (1986). [95](#)
- [MM77a] L. Modica and S. Mortola, *Il limite nella Γ -convergenza di una famiglia di funzionali ellittici*, Boll. Unione Mat. Ital., V. Ser., A 14, pp.526-529, 1977. [43](#), [47](#)

REFERENCES

- [MM77b] L. Modica, S. Mortola, *Un esempio di Γ^- -convergenza*, Boll. Unione Mat. Ital., V. Ser., B 14, pp.285-299, 1977. [43](#), [47](#)
- [MS95] J.-M. Morel, and S. Solimini, *Variational methods in image segmentation*. Progress in Nonlinear Differential Equations and Their Applications, Vol. 14, Birkhäuser, Boston, 1995. [14](#)
- [Mu08] J. Müller, *Parallel Total Variation Minimization*, Diploma thesis, WWU Münster, 2008. [158](#)
- [MS63] W. W. Mullins, R. F. Sekerka, *Morphological Stability of a Particle Growing by Diffusion or Heat Flow*, J. Appl. Phys. 34, 323, 1963. [43](#)
- [Mu94] D. Mumford, *Elastica and computer vision*, in Algebraic Geometry and Its Applications, C. L. Bajaj, ed., Springer-Verlag, New York, pp. 491-506, 1994. [8](#), [9](#), [12](#)
- [MG01] D. Mumford, and B. Gidas, *Stochastic models for generic images*, Quart. Appl. Math., 59, pp. 85-111, 2001. [138](#)
- [MS89] D. Mumford, and J. Shah, *Optimal approximations by piecewise smooth functions and associated variational problems*, Comm. Pure Applied Math. 42, pp. 577-685, 1989. [9](#), [15](#)
- [NS05] R. Nabben and D.B. Szyld, *Schwarz iterations for symmetric positive semidefinite problems*, Research Report 05-11-03, Department of Mathematics, Temple University, 2005. [153](#)
- [Ne05] Y. Nesterov, *Smooth minimization of non-smooth functions*, Math. Program. 103, 1, pp. 127-152, 2005. [216](#)
- [NST89] B. Nicolaenko, B. Scheurer, and R. Temam, *Some global dynamical properties of a class of pattern formation equations*, Commun. Partial Differ. Equations, 14, 2, pp. 245-297, 1989. [72](#)
- [NMS93] M. Nitzberg, D. Mumford, and T. Shiota, *Filtering, Segmentation, and Depth*, Springer-Verlag, Lecture Notes in Computer Science, 662, 1993. [6](#), [7](#), [12](#)

REFERENCES

- [NO95] Y. Nishiura, and I. Ohnishi, *Some Mathematical Aspects of the Micro-phase Separation in Diblock Copolymers*. Physica D 84, pp. 31–39, 1995. [95](#)
- [OK86] T. Ohta, and K. Kawasaki, *Equilibrium Morphology of Block Copolymer Melts*. Macromolecules 19, 2621–2632, 1986. [95](#)
- [Op67] Z. Opial, *Weak convergence of the sequence of successive approximations for nonexpansive mappings*, Bull. Amer. Math. Soc. **73** (1967), 591–597. [172](#)
- [OSV03] S. Osher, A. Sole, and L. Vese. *Image decomposition and restoration using total variation minimization and the H^{-1} norm*, Multiscale Modeling and Simulation: A SIAM Interdisciplinary Journal, Vol. 1, Nr. 3, pp. 349-370, 2003. [9](#), [44](#), [120](#), [138](#)
- [Pe89] R.L. Pego, *Front migration in the nonlinear Cahn-Hilliard equation*, Proc. Roy. Soc. London Ser. A, 422, 261-278, 1989. [43](#), [71](#)
- [PF90] O. Penrose, and P.C. Fife, *Thermodynamically consistent models of phase-field type for the kinetics of phase transitions*, Physica D, 43, 44-62, 1990. [71](#)
- [PM90] P. Perona, and J. Malik, *Scale-space and Edge Detection Using Anisotropic Diffusion*, IEEE Transactions on Pattern Analysis and Machine Intelligence, 12(7), pp.629-639, July 1990. [14](#), [60](#)
- [QV99] A. Quarteroni and A. Valli, *Domain decomposition methods for partial differential equations*, Numerical Mathematics and Scientific Computation, The Clarendon Press Oxford University Press, New York, 1999, Oxford Science Publications. [153](#)
- [RF95] X. Ran, and N. Favardin, *A Perceptually Motivated Three-Component Image Model. Part II: Applications to image compression*, IEEE Trans. Image Processing, vol. 4, pp. 430-447, 1995. [7](#)
- [RW98] R.T. Rockafellar and R.J.B. Wets, *Variational analysis*, Grundlehren der Mathematischen Wissenschaften, vol. 317, Springer-Verlag, Berlin, 1998. [167](#), [179](#)
- [RS06] M. Röger, and R. Schätzle, *On a modified conjecture of De Giorgi*, Math. Z., 254, 4, 675-714, 2006. [73](#)

REFERENCES

- [RT07] M. Röger, and M.Y. Tonegawa, *Convergence of phase-field approximations to the Gibbs-Thomson law*, Calc. Var. Partial Differ. Equat., 2007. [74](#)
- [RS09] J.-D. Rossi, C.-B. Schönlieb, *Nonlocal higher order evolution equations*, 12p., submitted. [23](#), [70](#), [93](#)
- [RO94] L. Rudin and S. Osher, *Total variation based image restoration with free local constraints*, Proc. 1st IEEE ICIP, 1, pp. 3135, 1994. [13](#)
- [ROF92] L. I. Rudin, S. Osher, and E. Fatemi, *Nonlinear total variation based noise removal algorithms*, Physica D 60, pp. 259-268, 1992. [9](#), [13](#), [42](#), [60](#), [61](#), [137](#), [150](#)
- [RH99] P. Rybka, and K.H. Hoffmann, *Convergence of solutions to Cahn-Hilliard equation*, Commun. Partial Differ. Equations, 24, 5-6, pp. 1055-1077, 1999. [72](#), [74](#)
- [SW00] E. Sander, and T. Wanner, *Unexpectedly linear behavior for the Cahn-Hilliard equation*, SIAM J. Appl. Math., 60, 6, 2182-2202, 2000. [75](#), [76](#)
- [Sc09] C.-B. Schönlieb, *Total variation minimization with an H^{-1} constraint*, CRM Series 9, Singularities in Nonlinear Evolution Phenomena and Applications proceedings, Scuola Normale Superiore Pisa, pp. 201-232, 2009. [21](#), [23](#), [104](#), [159](#), [197](#)
- [SB09] C.-B. Schönlieb, and A. Bertozzi, *Unconditionally stable schemes for higher order inpainting*, in preparation. [18](#), [21](#), [22](#), [23](#), [24](#), [37](#), [58](#), [60](#), [61](#), [104](#)
- [Si83] L. Simon, *Asymptotics for a class of non-linear evolution equations, with applications to geometric problems*, Ann. of Math., 118, 525-571, 1983. [74](#)
- [Sm03] P. Smereka, *Semi-implicit level set methods for curvature and surface diffusion motion*, Special issue in honor of the sixtieth birthday of Stanley Osher, J. Sci. Comput. 19, no. 1-3, pp. 439-456, 2003. [19](#)
- [SCD02] J.-L. Starck, E. J. Candès, D. L. Donoho, *The curvelet transform for image denoising*, IEEE Trans. Image Process. 11, no. 6, pp. 670–684, 2002. [163](#)
- [St96] B. E. Stoth, *Convergence of the Cahn-Hilliard Equation to the Mullins-Sekerka Problem in Spherical Symmetry*, J. Diff. Equ. 125, pp. 154-183, 1996. [43](#)

REFERENCES

- [SH94] A.M. Stuart, and A.R. Humphries, *Model problems in numerical stability theory for initial value problems*, SIAM Rev. 36, 2, pp. 226-257, 1994. [107](#)
- [TT98] X.-C. Tai and P. Tseng, *Convergence rate analysis of an asynchronous space decomposition method for convex minimization*, Math. Comp. 1998. [156, 157](#)
- [TX02] X.-C. Tai and J. Xu, *Global convergence of subspace correction methods for convex optimization problems*, Mathematics of Computation, 71(237), 105–124, 2002 [156, 157](#)
- [Te04] A. Telea, *An image inpainting technique based on the fast marching method*, J. Graph. Tools, 9(1), pp. 23-34, 2004. [20](#)
- [Te88] R. Temam, *Infinite-Dimensional Dynamical Systems in Mechanics and Physics*, Applied Mathematical Sciences, Vol. 68, Springer, New York, 1988. [119](#)
- [Ti96] R. Tibshirani, *Regression shrinkage and selection via the lasso*, J. Roy. Statist. Soc. Ser. B **58**, no. 1, pp. 267–288, 1996. [163](#)
- [Tr08] J. A. Tropp, *On the conditioning of random subdictionaries*, Appl. Comput. Harmonic Anal., vol. 25, pp. 1–24, 2008. [165](#)
- [TT99] J. Tumblin, and G. Turk, *LCIS: A Boundary Hierarchy for Detail-Preserving Contrast Reduction*, Siggraph 1999, Computer Graphics Proceedings, pp.83-90, 1999. [60](#)
- [TYW01] A. Tsai, Jr. A. Yezzi, and A. S. Willsky, *Curve evolution implementation of the Mumford-Shah functional for image segmentation, denoising, interpolation and magnification*, IEEE Trans. Image Process., 10(8), pp. 1169-1186, 2001. [6, 15](#)
- [Ve01] L. Vese, *A study in the BV space of a denoising-deblurring variational problem*, Applied Mathematics and Optimization, 44 (2), pp. 131-161, 2001. [42, 52, 162, 183, 184, 221](#)
- [VO03] L. Vese, and S. Osher, *Modeling textures with total variation minimization and oscillating patterns in image processing*, J. Sci. Comput., Vol. 19, Nr. 1-3, pp. 553-572, 2003. [44](#)

REFERENCES

- [VO04] L. Vese, S. Osher, *Image Denoising and Decomposition with Total Variation Minimization and Oscillatory Functions*, J. Math. Imaging Vision, 20 (2004), pp.7-18. [138](#)
- [VR03] B. P. Vollmayr-Lee and A. D. Rutenberg, *Fast and accurate coarsening simulation with an unconditionally stable time step*, Phys. Rev. E, vol. 68, no. 0066703, pp. 113, 2003. [133](#)
- [Wa85] S. Walden, *The Ravished Image*, St. Martin's Press, New York, 1985. [6](#)
- [WZ98] Y. Wang, and Q. F. Zhu, *Error control and concealment for video communication: A review*, Proc. IEEE, Vol. 86, No. 5, pp. 974-997, 1998. [6](#)
- [WL00] L.-Y. Wei, and M. Levoy, *Fast texture synthesis using tree-structured vector quantization*, in Proceedings of SIGGRAPH 2000. [7](#)
- [WW98a] J. Wei, and M. Winter, *On the stationary Cahn-Hilliard equation: Interior spike solutions*, J. Differ. Equations, 148, 2, 231-267, 1998. [72](#)
- [WW98b] J. Wei, and M. Winter, *On the stationary Cahn-Hilliard equation: bubble solutions*, SIAM J. Math. Anal., 29, 6, 1492-1518, 1998. [72](#)
- [WW98c] J. Wei, and M. Winter, *Stationary solutions for the Cahn-Hilliard equation*, Annales de l'institut Henri Poincar (C) Analyse non linéaire, 15, 4, 459-492, 1998. [72](#)
- [WAB] P. Weiss, L. Blanc-Féraud, and G. Aubert, *Efficient schemes for total variation minimization under constraints in image processing*, Rapport de recherche 6260, July 2007. [216](#)
- [Wi93] T.J. Willmore, *Riemannian geometry*, Oxford Science Publications, Oxford: Clarendon Press. xi, 1993. [73](#)
- [Xu92] J. Xu, *Iterative methods by space decomposition and subspace correction*, SIAM Rev. **34**, no. 4, pp. 581–613, 1992. [153](#)
- [XZ02] J. Xu and L. Zikatanov, *The method of alternating projections and the method of subspace corrections in Hilbert space*, Journal of The American Mathematical Society 15, 573–597, 2002. [153](#)

REFERENCES

- [YR03] A.L. Yuille, and A. Rangarajan, *The Concave-Convex Procedure (CCCP)*, Neural Computation, Vol. 15, No. 4, pp. 915-936, April 2003. [106](#)
- [Zh04] L. Zhang, *Existence, uniqueness and exponential stability of traveling wave solutions of some integral differential equations arising from neuronal networks*. J. Differential Equations 197(1), 162–196, (2004). [94](#)
- [Zh86] S. Zheng, *Asymptotic behavior of solution to the Cahn-Hilliard equation*, Appl. Anal., 23, 165-184, 1986. [72](#)